STUDIES ON PHOTOIONISATION

A thesis presented by

CHRISTOPHER RICHARD BRUNDLE

for the degree of

DOCTOR OF PHILOSOPHY

FACULTY OF SCIENCE

UNIVERSITY OF LONDON

Chemistry Department,

Imperial College,

London.

September 1968

ABSTRACT

Extensive modifications to an existing one meter normal incidence vacuum ultraviolet monochromator, coupled to a time-of-flight mass spectrometer are described. The improvements are such as to increase both the sensitivity and resolving power of the apparatus by an order of magnitude.

A survey has been made of suitable ionising lines (in three grating orders) of the low pressure flashing light source over the spectral range used(10 - 25 eV). Oxygen, Nitrogen, Helium, Hydrogen, Carbon Dioxide, Argon, Nitrous Oxide and Ethylene were all used as light source gases.

Photoionisation studies using this apparatus have been carried out on acetone, nitrous oxide, formaldehyde and deuterformaldehyde. Ionisation efficiency curves have been constructed for the parent and fragment ions.

Photoionisation studies using the method of Photoelectron Spectroscopy have also been carried out on an existing apparatus (127° electrostatic electron velocity analyser). The electronic states of the positive ions lying below 21·23 ev have been studied for H_2O, D_2O, H_2CO, D_2CO and the series N_2O, COS, CS_2 and CO_2. Previously unknown vibrational frequencies in many ionic electronic states have been found, and others confirmed. Experimental vibrational Franck-Condon factors have been measured, and the results compared with calculated values where possible. For H_2O and D_2O the

Franck-Condon factors of the ground state of the ion have been used to estimate the geometry of this state. Attempts have been made to correlate ionic energy levels and the shapes of photoelectron bands with the bonding characteristics of the orbital from which the electron is ejected, with reference to theoretical calculations. Possible fragmentation processes are suggested in some cases. The spectra of NH_2HCO, $NH(CH_3)CHO$, $N(CH_3)_2CHO$ and H COOH have been studied briefly.

ACKNOWLEDGEMENTS

The author expresses his thanks to Dr. D. W. Turner for his guidance in this work, and the constant encouragement he has provided throughout it.

He would also like to thank Professor D. H. R. Barton, F. R. S. for providing the opportunity to work in the Organic Chemistry Department at Imperial College, Professor R. E. Richards F. R. S. for a similar provision at the Physical Chemistry Department at Oxford, and finally, the Science Research Council for a Research Studentship.

C. R. Brundle.

Publications

Some of the work described in this thesis is also included in a number of publications. :-

(1) "The Carbonyl π-Ionisation Potential of Formaldehyde." By C. R. Brundle and D. W. Turner, Chem. Comm. 314 (1967).

(2) "High Resolution Photoelectron Spectroscopy. II. Water and Deuterium Oxide. By C. R. Brundle and D. W. Turner, Proc. Roy. Soc. 307 27 (1968)

(3) "The Electronic Structure of Methane, Ethane, Ethylene , and Formaldehyde studied by High Resolution Photoelectron Spectroscopy." By A. D. Baker C. Baker, C. R. Brundle, and D. W. Turner, J. Mass Spec. and Ion Phys. 1968. In the press.

(4) "The Interpretation of Photoelectron Spectra – Especially those of Benzene and Water." By A. D. Baker, C. R. Brundle, and D. W. Turner, J. Mass Spec. and Ion Phys. 1968. In the press.

(5) "Studies on the Photoionisation of the Linear Triatomic Molecules :- N_2O, COS, CS_2, CO_2, Using High Resolution Photoelectron Spectroscopy." C. R. Brundle and D. W. Turner, J. Mass Spec. and Ion Phys. 1968. In the press.

CONTENTS

CHAPTER 1.

INTRODUCTION AND SOME BACKGROUND THEORY.

1.1. The importance of Excitation Phenomena. 8
1.2. The General Scope of the Thesis. 9
1.3. Historical Background of Photoionisation Processes in Gases.... ..9
1.4. Theoretical Considerations and Practical Measurements of Excitation Processes. 10
(a) Possible Excitation Processes. 10
(b) The Franck-Condon Principle in Electronic Excitation... ... 11
(c) Correlations between F-C factors, changes in vibrational frequencies and the bonding type of the electron excited in transitions.. 15
(d) Processes occuring after initial excitation. 17
(e) Kinetic Energy of Fragment Species. 19
(f) Dissociation Energies of excited States. 20
(g) The relation of the Electronic Energy Levels Of Molecular Ions to the Electronic Structure of the Molecule. 21
(h) The Geometry of excited states. 22

CHAPTER 2.

EXPERIMENTAL METHODS OF OBTAINING INFORMATION ON EXCITATION PROCESSES.

2.1. Absorption Spectroscopy in the Vacuum Ultraviolet. 24
2.2. Measurements of Absorption and Ionisation Cross-sections ... 26
2.3. Total Ionisation Efficiency Measurements. 28
2.4. Electron Spectroscopy 30
(a) Photoelectron Spectroscopy. 30
(b) Electron Spectroscopy using Metastable Atom Source. 37
2.5. Ion Impact Spectroscopy. 38
2.6 (a) Electron Impact Efficiency Curves with Mass Analysis.. ... 38
2.6 (b) Electron Impact Energy Loss Spectroscopy. 43
2.7. Photon Impact Efficiency Curves with Mass Analysis. 45
2.8. Fluorescence Spectroscopy. 47
2.9. Emission Spectroscopy. 49
2.10. K.E. of Fragments. 49

CHAPTER 3

EXPERIMENTAL

3.1. The 127° Electrostatic Analyser Photoelectron Spectrometer. ... 57
3.2. The Development and Use of Time-of-Flight Mass Specrometers .. 65
3.3. Design and Construction of a T.O.F.M.S. with a vacuum U.V. Ionising Source. 70
3.3.A. Vacuum U.V. Monochromator and Light Source... 70
3.3.B. T.O.F.M.S. Section. 75
3.4. Limitations in Performance of the Original Spectrometer.. .. 78
3.5. Improvements made in the Design and Construction of the Mass Spectrometer. 79

3.6. Preparation and Purification of Materials. 94

CHAPTER 4

ANALYSIS OF THE ULTRAVIOLET RADIATION OBTAINABLE FROM THE LIGHT SOURCE OF THE U.V. MONOCHROMATOR. 96

CHAPTER 5

RESULTS AND DISCUSSION

5.1 H_2O and D_2O. 109
5.2. H_2CO and D_2CO 131
5.2.1. The Photoelectron Spectra of H_2CO and D_2CO. 131
5.2.2. The T.O.F.M.S. of H_2CO and D_2CO. 139
5.3.3. Some Estimates of Bond Dissociation Energies and Some Possible Fragmentation Processes. 143
5.3. N_2O, COS, CS_2, CO_2. 149
5.3.1. Photoelectron Spectra of the Compounds. 149
5.3.2. Discussion of Results. 168
5.3.3. T.O.F.M.S. of N_2O 185
5.4. Formamide, N,Methyl Formamide, and N,N,Dimethyl Formamide.... .. 191
5.5. Preliminary T.O.F.M.S. Study of Acetone.... 200

BIBLIOGRAPHY. 209

CHAPTER 1.

INTRODUCTION AND SOME BACKGROUND THEORY

1.1. The Importance of Excitation Phenomena

Information relating to excitation, dissociation, and ionisation phenomena has great practical importance in branches of applied physics, theoretical chemistry, biochemistry, and recently in certain aspects of analytical chemistry. Examples of this importance can be found in work on the following subjects :-

1) Gaseous Electronics[1]
2) Upper Atmosphere Studies[2-4]
3) Astrophysics[5]
4) Plasma spectroscopy - e.g. the measurement of very high temperatures[6]
5) The study of atomic structure[7]
6) The study of molecular bonding[8], with particular reference to molecular orbital theoretical calculations[9,10]
7) Polypeptide Chemistry - e.g. the study of polypeptide bonding by relating the optical properties of constituent amides to the polypeptides[11,12]
8) Chemical Analysis. Organic[13,14] and Metallurgical[6]
9) Photochemical Reactions[15]

1.2. The General Scope of the Thesis

The experimental work in this thesis is concerned entirely with the study of photon impact in the gas phase, over the energy range of 10—25 eV. Information is directly obtained on the ground and excited electronic states of ions, the nature of the vibrational modes excited in these states, and the relative transition probabilities (Franck-Condon Factors) to the excited vibrational levels. Information on fragmentation processes can be obtained in some cases, and this is of particular interest since though the mechanisms involved in the dissociation of diatomic ions are fairly well understood[16], much less is known in the case of polyatomic ions (see Section 2.10)

1.3. Historical Background of Photoionisation Processes in Gases

The experimental study of photoionisation processes requires quite sophisticated techniques and no reliable quantitative data concerning the ionisation of gases was obtained till 1925. The main reason for this is that in general, light of wavelength shorter than 2,000 Å is required to produce ionisation, and such short wavelengths require high vacuum techniques and the use of special window materials, photographic plates etc. to avoid absorption in the apparatus. Lenard[17], and Hughes[18] had done some early work which indicated that Ultraviolet light was capable of ionising gases, and Schumann[19] and Lyman[20] pioneered the first vacuum U.V. spectrographs. They were able to study and identify emission lines from several gases, but it was not until the work of Mohler[21-23], in 1925 that absorption coefficients and ionisation efficiencies of gases were at all understood. Much of the early work

in the vacuum U.V. is reviewed by Tousey,[6] as well as later developments. From 1925 - 1940's the study of molecular spectra by emission and absorption expanded but the photoionisation field in general did not really gain momentum till the 1950's, since when a considerable amount of work has been in progress. Reviews by Weissler[24] (up to 1955) and Samson[25] (up to 1967) give references to the most important work, much of which is mentioned in this introduction or referred to later in this thesis.

1.4. Theoretical Considerations and Practical Measurements of Excitation Processes

1.4. (a) Possible Excitation Processes

Though the work in this thesis is concerned primarily with photon impact phenomena, and mainly ionising processes, this is only one part of a large field of work investigating excitation phenomena (dominated until very recently by electron impact work), and it will be necessary to consider other excitation processes in some detail for a proper perspective to be achieved.

Below is given a list of some of the more important excitation processes which can occur when a molecule absorbs energy sufficient to cause an electronic transition. The number of possibilities for different types of excitation, and combinations of types, is large, particularly for polyatomic molecules, and has been dealt with more thoroughly elsewhere.[8,24]

Ionising Processes :-

1) $AB + \text{Energy, } E \longrightarrow AB^{+} + e$ (with or without vibrational energy) — Direct Ionisation

2) $AB + E \longrightarrow A^{+} + B^{-}$ — Direct dissociative ionisation

3) $AB + E \longrightarrow A^{+} + B + e$ — Direct dissociative ionisation

4) $AB + E \longrightarrow AB^{*}$ (excited neutral species)

$AB^{*} \longrightarrow AB^{+} + e$ — Auto-Ionisation

$\longrightarrow A^{+} + B + e$ — Auto-ionisation

OR $\longrightarrow A^{+} + B^{-} + \blacksquare$ and pre-dissociation

5) $AB + E \longrightarrow AB^{++} + 2e$ — Double ionisation

6) $AB + E \longrightarrow A^{+} + B^{+}$ (both possessing K.E.) + 2e — Dissociative ionisation

Non Ionising Processes :-

7) $AB + E \longrightarrow AB^{*}$ — Direct Excitation

8) $AB + E \longrightarrow AB^{*} \longrightarrow A + B$ — Pre-dissociation

9) $AB + E \longrightarrow A + B$ — Direct dissociation

1.4. (b) The Franck-Condon Principle in Electronic Excitation

The Franck- Condon Principle states that the transfer of energy, in an electronic transition, occurs in a time which is short compared with the time of a vibration of the molecule. Thus no change in internuclear co-ordinates occurs, and the principle governs the relative transition probabilities to the various vibrational levels of an excited electronic state.

In the approximation of a transition moment varying slowly with respect to the internuclear co-ordinate, and the separability of

electronic, vibrational, and rotational parts of the wavefunction, the transition probabilities are proportional to the square of the vibrational overlap integrals, $\int \psi_v \psi_{v'} dr$ between the initial and final states. The actual probability is given by the Born-Oppenheimer[26] equation :-

$$P_{v'v} = [G e'e(r)]^2 [\int \psi_{v'} \psi_v dr]^2$$

where $G\ e'e$ = electronic transition moment

r = internuclear co-ordinate

$[\int \psi_{v'} \psi_v dr]^2$ is called the Franck-Condon factor (more correctly $[\int \psi_{v'} \psi_v dr]^2$ is the F-C Factor squared) and may be compared directly to observed transition probabilities which may be termed Experimental F-C factors.

F - C factors have been calculated, using modern computational methods for a number of molecular vibronic transitions. The early work on H_2, N_2, O_2, CO and NO has been reviewed by Halmann and Laulicht[26] and compared with new calculations. Sharp and Rosenstock[27] have formulated a more general method of calculating F-C factors for transitions in polyatomic molecules.

To see exactly how the F-C principle and the Born-Oppenheimer approximation affect electronic transitions one must refer to figure 1. Transitions are all taken as originating from the zeroth vibrational level of the initial electronic state. In this vibrational level ψ_v has its maximum at the equilibrium position, so the maximum probability for transition occurs in the centre of the Franck-Condon region (marked in figure 1 by shading). Significant transitions cannot occur outside the F-C region (ψ_v approaches zero), and how far away from the centre they can

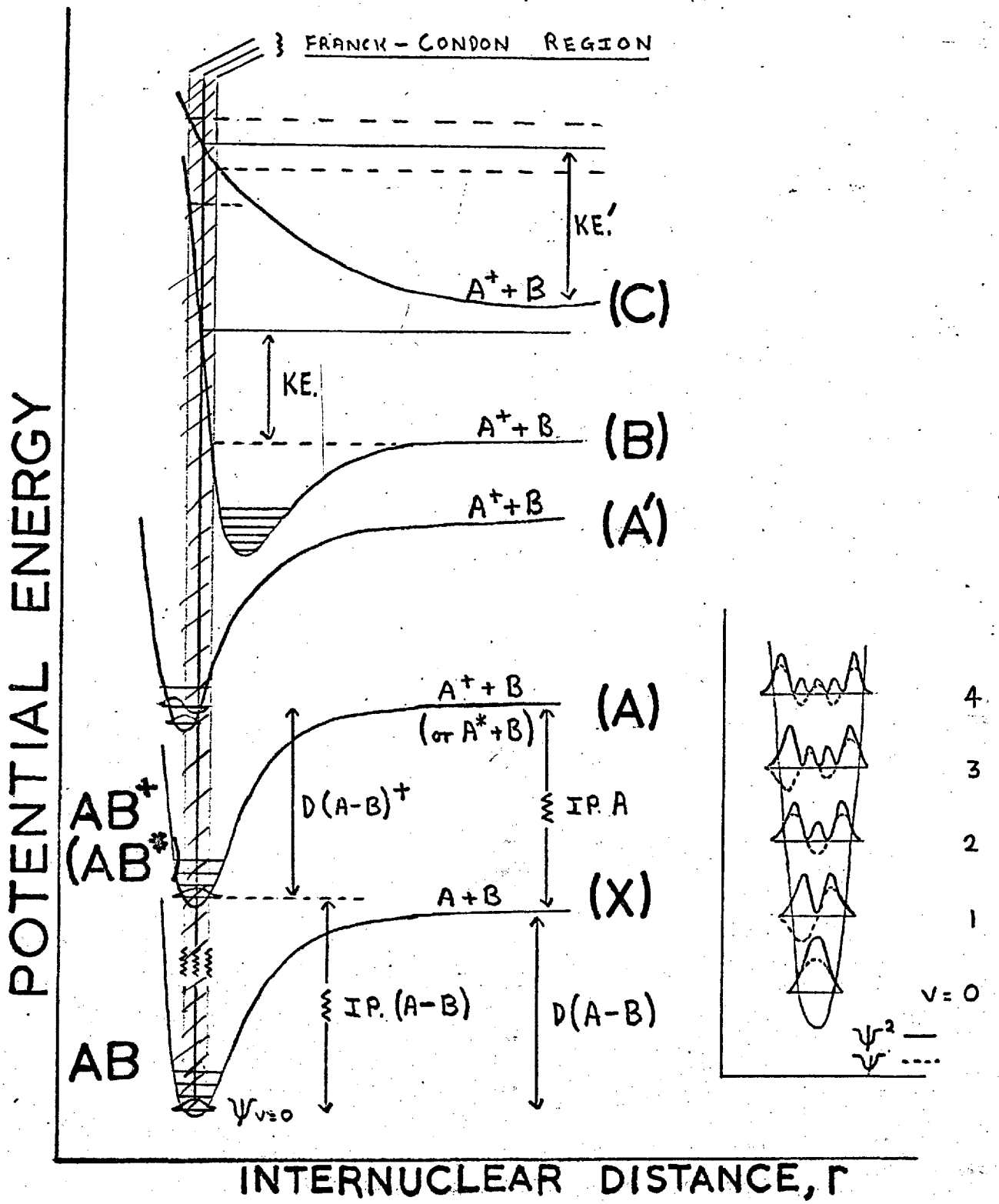

FIG. 1 — Franck-Condon Transitions for a diatomic molecule AB.

Inset : Form of wave-function ψ and probability distribution ψ^2 for the vibrational levels of the molecule.

be detected depends on the sensitivity of measurement.

Excitation to the electronic state (A), where the equilibrium internuclear distance, r_e', is the same or very nearly the same as that in the ground state, (X), requires by the F-C principle that the most probable transition is to the V = 0 level of state (A). Transitions to other vibrational levels will have a very low probability which decreases as V increases. Transitions to the V = 0 level are termed ADIABATIC TRANSITIONS.

Excitation (X) $\longrightarrow$ (A $'$) corresponds to the case where r_e' is slightly less than r_e. From the diagram it can be seen that the maximum overlap of wave-functions occurs at $V' = 1$ and thus the maximum transition probability occurs at this level. Transitions will occur to other levels, the probability of which depends on $[\int \psi_{v'} \psi_v dr]^2$ The transition of maximum probability is termed a VERTICAL TRANSITION. In the case of excitation (X) $\longrightarrow$ (A) the adiabatic and vertical transitions are identical. In the case of (X) $\longrightarrow$ (A$'$) they are not. The adiabatic transition is strictly to the $V' = 0$ level, but transitions to this level may be of a very low probability if the difference between r_e' and r_e is large (e.g. excitation (X) $\longrightarrow$ (B)). Hence the experimental adiabatic transition is then the one of lowest energy which is detectable.

Both transitions (X) $\longrightarrow$ (A), and (X) $\longrightarrow$ (A $'$) represent a case (1) excitation process (Section 1.4. (a)), and could equally well represent case (7), if the transitions were to molecular, not ionic levels.

Transition (X) $\longrightarrow$ (B) shows the situation where there is a very

large change in r e. Here transitions occur to the level of the continuum and the ion fragments into $A^+ + B$. The fragments will possess kinetic energy but there will be a spread in this energy reflecting the shape of $\psi V = 0$. This transition represents a case (3) ionisation, and case (9) excitation if to a molecular, not ionic, level.

Transition (X)—(C) represents a transition to an unstable state and fragments possessing kinetic energy will again result. This transition is also included in a case (3) or (9) process.

Transition (X)⟶(J), (shown in figure 2) is a direct double ionisation, yielding two ionised fragments A^+ and B^+, as in case (6). Such ionisations usually require energy > 25 e V.

Thus all these types of <u>direct</u> transition are possible in a molecule A B, the transitions being governed by the F-C principle.

1. 4. (c) <u>Correlations Between F-C factors, changes in vibrational frequencies, and the bonding type of the electron excited in transitions.</u>

It is interesting to see how the vibrational frequencies change on transition to each of the states (A), (A′), (B) and (C)

The energies of the vibrational levels are given by

$$E_v = (v + \tfrac{1}{2})hw - (v + \tfrac{1}{2})^2 hxw$$

where v = vibrational quantum number

h = Planck's Constant

x = anharmonicity constant.

$w = \frac{1}{2\pi}\sqrt{\frac{k}{u}}$ the vibrational frequency

k = force constant of the vibration

μ = reduced mass of the system

Now k is a measure of the strength of the bond. If a non-bonding electron is removed on ionisation, the bond strength will alter little, and so k, and hence w and the energy separation between vibrational levels, will remain almost unchanged. r_e will also be unaffected. On removing a bonding electron, k and w will decrease, and r_e will increase as there is less bonding strength holding together the nuclei. Conversely, on removing an anti-bonding electron, k and w increase and r_e decreases. Similar effects occur when the electron is just excited to a higher molecular level and not ionised off.

Thus in general, from figure 1., it can be said that :-

1) (X)$\rightarrow$(A) transitions correspond to the excitation of a non-bonding electron, with vibrational frequency, w', in state (A) essentially the same as w in state (X)

2) (X)$\rightarrow$(A') corresponds to the removal of an anti-bonding electron, and the vibrational frequency in state (A') is increased somewhat.

3) (X)$\rightarrow$(B) results from the removal of a very strongly bonding electron, the vibrational frequency being greatly reduced.

Since the values of the F-C factors are dependent on r_e (Section 1.4 (b)), they will also be characteristic of the bonding type of electron removed. Removal of non-bonding electrons lead to transitions essentially to the V'=0 level, while bonding or anti-bonding electrons will significantly populate higher V' levels, so that the maximum F-C factor may not be at V'=0. The argument above can be extended to polyatomic systems but in practice it becomes complex because even for linear triatomic molecules

three vibrational modes are involved and a three dimensional potential surface is required to describe correctly the vibrational motion of the molecule.

1.4. (d) Processes Occuring After Initial Excitation

The simple direct ionisation and excitation processes have been dealt with, but what can happen afterwards is also important. Some of the possibilities are illustrated in figure 2.

Here the terms "Autoionisation" (also called pre-ionisation), and "Pre-dissociation" are used. Autoionisation is defined as an ionisation which occurs by a means other than a direct transition to an ionic state. Transitions to neutral state (H) (Figure 2), followed by a radiationless decay to the ground ionic state (D) with the ejection of an electron of energy E, is an example of autoionisation. The F - C region for the decay is different from that of the excitation, and may significantly populate the higher vibrational levels of AB^{+}(D), (see figure 2), a situation which could not arise by direct ionisation. A similar enhancement could occur by a radiative decay from ionic level (I) (lifetime $\simeq 10^{-8}$ sec) to ground ionic level (D), if allowed, though this is not an auto-ionising process. The curve crossing of neutral state (H) with state (F) is also an example of autoionisation, but since it results in an ionised fragment the process also qualifies as a pre-dissociation. A further example of pre-dissociation is given by the crossing of state (H) with (G). The scope of such curve-crossings is large since there will be numerous potential surfaces, particularly for polyatomic molecules.

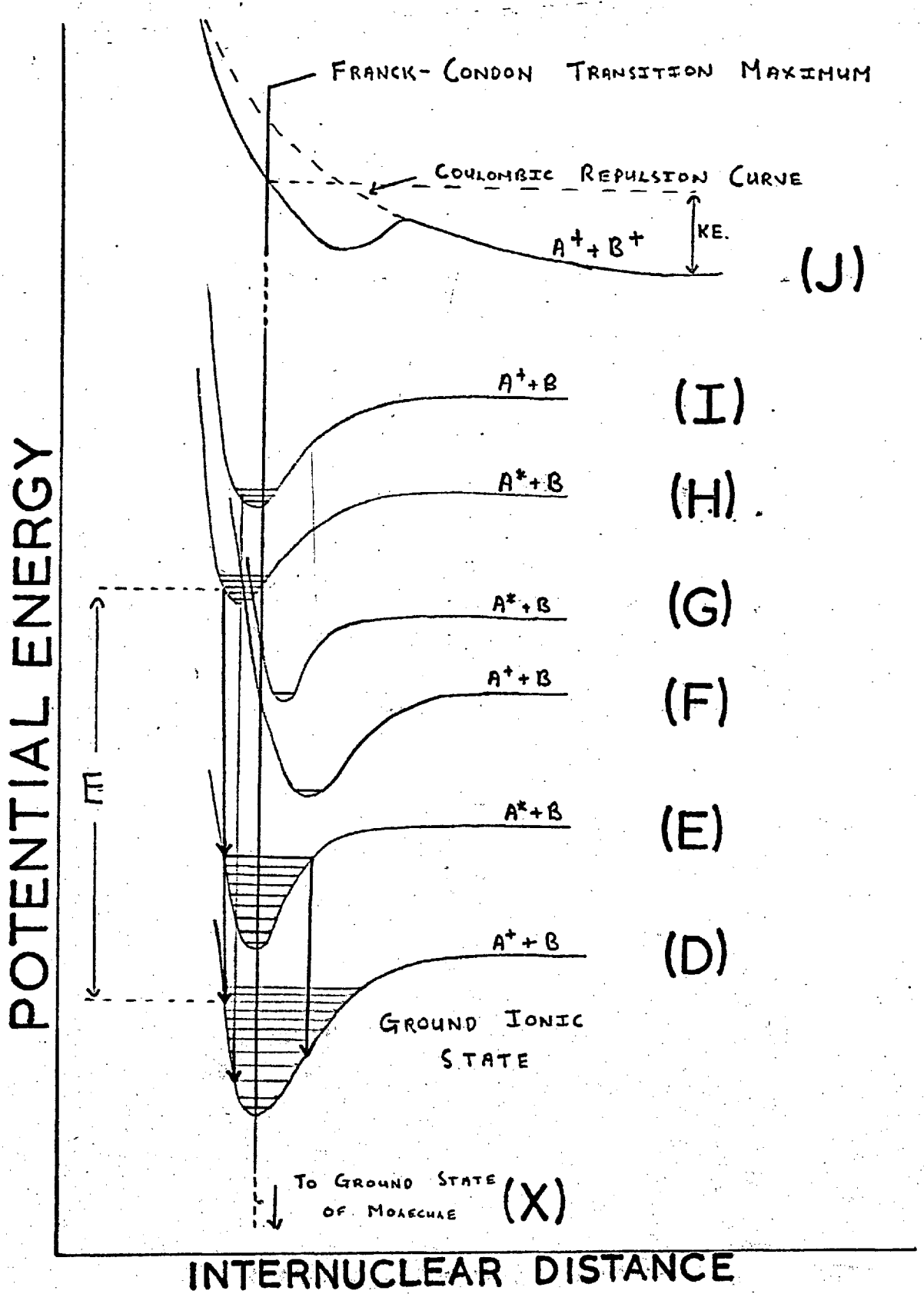

FIG. 2 Complex transitions for a diatomic molecule AB.

They can play an important role in fragmentation processes as is indicated in section 2.10. Lempka, Passmore, and Price[28] have recently discussed crossing of potential energy curves for the halogen acids, in relation to their observed photoelectron spectra.

As a final example a combination of radiative decay from neutral state (H) to neutral state (E), followed by autoionisation to the ground level ionic state (D) is a further possibility.

All the processes described here have to be taken into account when considering the interaction of vacuum U.V. light with molecules.

1.4. (e) Kinetic Energy of Fragment Species

In figure 1 transitions to states (B) + (C) result in dissociative ionisation where the fragments possess total kinetic energy, KE. The partition of the kinetic energy between fragments will be inversely proportional to their masses (conservation of momentum), and so if two fragments are formed and the energy and identity of one of them found, the total K.E. possessed by the fragments may be obtained, yielding in turn information about the potential energy curves and dissociation limits.

Polyatomic molecules are more difficult to treat effectively because of the large number of potential surfaces and the number of fragments that may be formed. The whole subject of K.E. of fragments and their measurement, is dealt with more fully in section 2.10.

1.4. (f). Dissociation Energies of Excited States

Referring again to figure 1., the dissociation energy D(A-B) in the ground state of the molecule can sometimes be measured by conventional techniques (e.g. U.V. & Optical. Electronic - Vibrational Spectra). Obviously one would like information on the dissociation energies of excited states.

The fundamental energetic equation relating to a dissociation process such as

$$A\,B + E \longrightarrow A^{+} + B + e$$

is $$A.P.\ A^{+} = D\,(A\text{-}B) + I.P\ A\cdot$$

where A.P A^{+} represents the excitation energy required to produce fragment A^{+}. This equation has been widely used in calculating dissociation energies, but even if I.P A· is accurately known (measurement is often difficult[29]), D (A-B) calculated in this fashion is only an unambiguous quantity if it is known that the fragments possess no kinetic energy, and are formed in their ground electronic states.

$$D\,(A\text{-}B)^{+} = I.P\ A\cdot + D\,(A\text{-}B) - I.P\,(A\,B)$$

From the above equation $D\,(A\text{-}B)^{+}$ may be found, subject to the same ambiguities, and from the following equation it is possible to deduce heats of formation of ions or radicals[30].

$$D\,(A\text{-}B)^{+} + I\,P\,(A\,B) = \Delta H_f(A) + \Delta H_f(B) - \Delta H_f(A\,B)$$

When these quantities are already known, such relationships may be used to ascertain the nature and structure of the fragment produced.

1.4. (g) The relationship of the Electronic Energy Levels of Molecular ions to the Electronic Structure of the Molecule

Since Mulliken's original work[31], the concepts of molecular orbital theory have been developed rapidly, and with the application of modern computer techniques many sophisticated molecular orbital calculations[32-37] have been carried out, yielding information on orbital energies and bonding characteristics. Experimental data to test the accuracy of the calculations has been less forthcoming.

A Molecule has as many ionisation potentials as it has occupied orbitals of different energies, and if one has a reliable method of determining these "inner" or "higher" ionisation potentials it is possible to correlate experimental ionisation potentials with the orbital energies of the ground state of the molecule through the use of Koopmans' Theorem.

Koopmans' Theorem[9] states that the energy required to ionise an electron from an orbital (i.e. the I.P. of the resultant ionic state) is equal to the binding energy of that orbital. This is illustrated schematically in figure 3. The theorem is in fact only an approximation since the re-orientation energy of the remaining electrons is ignored. Thus the energy required to remove an electron, (I), will in general be less than the orbital energy, (ε). It is often assumed that the re-orientation energy is similar for the removal of all electrons, so that the correct spacing between orbital energies can still be obtained from the differences between ionisation potentials. One has to be cautious about this assumption, since there is some recent evidence[11-12] that re-orientation energies can differ by as much as 1.5 eV, causing

a reversal of the ordering of experimental I.P's compared to the energies of the orbitals concerned.

The re-orientation energy may be calculated theoretically as the difference between the Self Consistent Field (S.C.F.) total energy of the ion, and the energy of the ion calculated using the orbital obtained in the original S.C.F. calculation of the neutral molecule. Since this involves obtaining a small difference between two large values, it may not be a very reliable technique.

Experimental information about the bonding characteristics of the orbital from which an electron is removed can be obtained by studying the vibrational frequencies and F - C factors of the resulting ionic state, as explained in sections 1.4. (b) and 1.4. (c). This information can also be used to test the accuracy of the theoretical M.O. predictions.

1.4. (h) The Geometry of Excited States

Calculating F - C factors depends on knowing the geometry of the excited state produced by the transition. Where the geometry of the excited state is unknown, the F - C factors can be calculated for a range of geometries, and compared to the experimental values. In this manner it should be possible to obtain an estimate of the geometry involved, of comparable accuracy to conventional techniques. This has been done in the case of H_2O^+ and D_2O^+ in their ground ionic states [38-39], and for a Rydberg state of acetylene [38] but the field is new and the experimental accuracy required for useful results quite high.

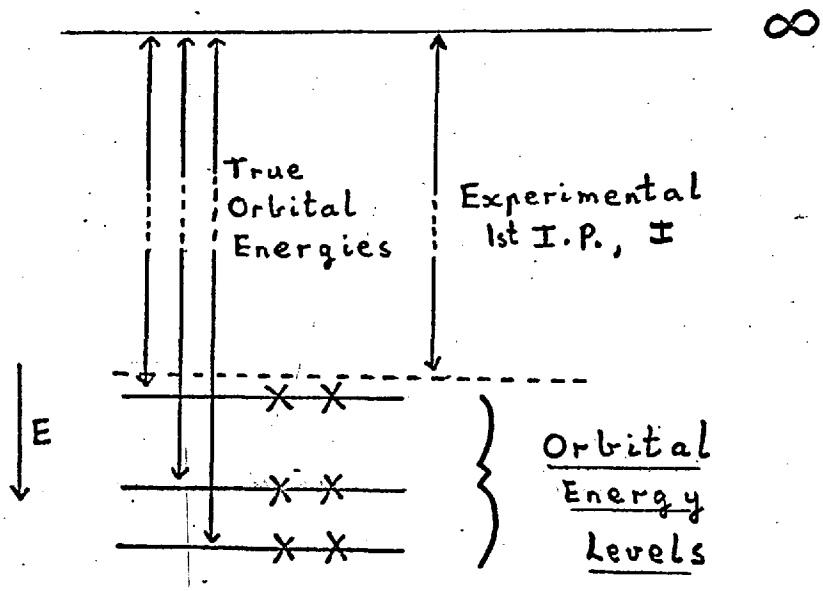

FIG.3 Koopmans' Theorem Diagram.

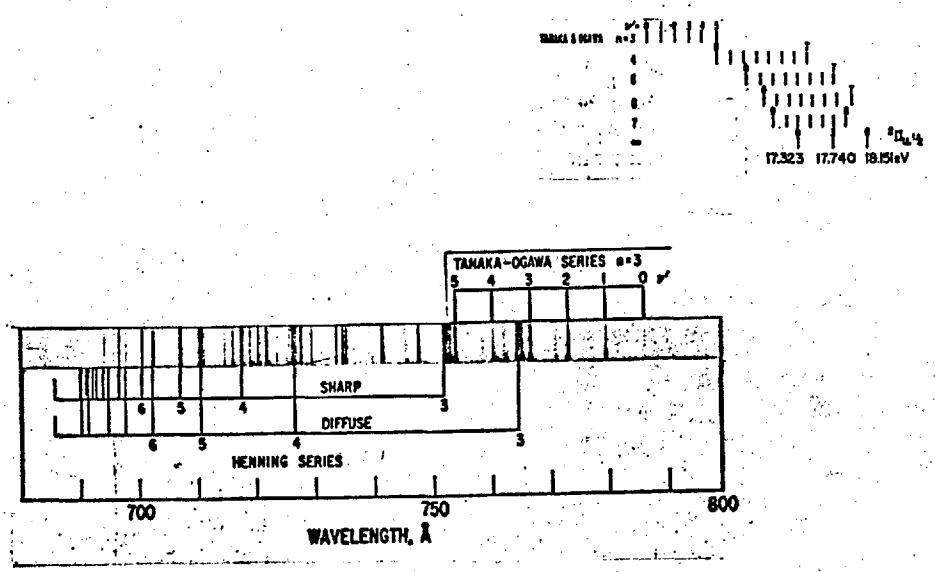

FIG.4 Absorption Spectrum of CO_2 from Reference 43
Inset : Schematic Representation of Tanaka-Ogawa Absorption Series in CO_2 (Reference 40)

CHAPTER 2

EXPERIMENTAL METHODS OF OBTAINING INFORMATION ON EXCITATION PROCESSES

Having dealt with the types of trnsitions which can occur, and the different types of information which, in theory, are available, we now consider some of the experimental methods utilised in obtaining such information.

Since high energies are required, the investigation of electronic excitation phenomena relies largely on the transfer of energy by the impact of photons (U.V.), electrons emitted from a heated filament, or occasionally ions and metastable atoms. The information yielded can be divided up into two categories, information on the initial excitation proces (cf. section 1.4 (b)) and that on subsequent processes (cf. section 1.4. (d)), but the experimental techniques cannot, since usually some of both types is obtained. However the techniques described are given in such an order that those coming first are more closely related to initial processes, and those later to subsequent processes. Since the experimental work in this thesis is concerned primarily with ionisation, this side of the work is stressed.

2.1. Absorption Spectroscopy in the Vacuum Ultraviolet

The oldest of the techniques for studying direct excitation processes, absorption spectroscopy still yields the most accurate energy data in favourable cases. Spectrally dispersed vacuum ultraviolet light is

passed through the vapour of the molecule being examined, and then impinges on a photographic plate. Light is absorbed in exciting or ionising processes, and at positions on the plate corresponding to the wavelengths at which absorption occurs, exposure is reduced.

A typical plate is shown in figure 4. It is possible that all the processes (1) to (9) (section 1.4. (a)) may be occurring so the spectrum could be very complex. However, excitations to outer unfilled molecular orbitals can be considered equivalent to the Rydberg transitions in atoms, which result in the well-known converging series of absorption lines culminating in a continuum when an ionisation limit is reached. In favourable cases these series can be picked out and fitted to the general Rydberg expression.

$$\nu_n = \text{I.P.} - \frac{R}{(n-\Delta)^2}$$

where R = Rydberg Constant

$(n-\Delta)$ = effective quantum number

ν_n = frequency of absorption line.

If enough members of the series can be identified it enables the I.P to be evaluated to an accuracy of $\pm \cdot 0\,1$ ev.

Many first I.P's have been evaluated by this method, and several higher ones also. The major defficiences of the technique can be listed as :-

(1) The skill required in picking out, correctly, Rydberg series among the many other discrete and continuum absorptions occuring. Wrong identifications are sometimes made, leading to false I.P.'s.

(2) The continuous absorption above the first I.P usually makes it

more difficult for discrete absorptions to be observed above this value.

(3) The method is in general only successful when non-bonding or weakly bonding electrons are ionised. For ionisation of bonding electrons, where vibrational levels of the ion are significantly populated, the absorption spectrum comprises a very complex system (see inset figure 4). Since the absorption is no longer concentrated into the $V' = 0$ levels and since the closeness of the vibrational structure gives added complexity, the series may often be missed altogether. Analysis has been achieved in some cases[40], and from the separation of vibrational components of each Rydberg level the frequencies of each excited vibrational mode, may be found.

(4) Autoionisation is possible at energies higher than the first I.P. This may broaden the absorption lines as a consequence of the Heisenberg Uncertainty Principle, and may thus hinder interpretation.

Experimental details of photographic U.V. absorption spectroscopy can be found in individual papers, and in reviews by Herzberg[8c], Price[41], and Wilkinson[42].

2.2. Measurement of Absorption and Ionisation Cross-Sections

Absorption of light follows the Beer-Lambert Law

$$I = I_o e^{-n\sigma x}$$

where I_o = incident light

I = transmitted light

σ is the absorption cross section, a constant for a particular gas at a particular wavelength

x = path length traversed by the light

n = number of molecules / cc

It is convenient to reduce all measurements to N.T.P

when $I = I_o e^{-n_o \sigma x}$

and $n_o = 2.69 \times 10^{19}$ mols / cm^3

The equation is sometimes presented as

$$I = I_o e^{-k_o x}$$

where absorption coefficient $k_o = n_o \sigma$ (or $k_\rho = n k$)

can be found from the gradient of a graph of $\ln I_o/I$ against pressure using an absorption spectrometer similer to that in section 2.1, and recording the light intensities photoelectrically. Only relative values of I_o and I are required.

σ can be split into two parts :-

$$\sigma_{Total} = \sigma_i + \sigma_d$$

ionisation dissociation + excitation

Now the light being absorbed per second is $\phi_o - \phi$ (where ϕ is the absolute value of light intensity, as compared to the relative values I_o and I) and the number of ions produced per second is

$$N = \frac{\sigma_i}{\sigma} (\phi_o - \phi)$$

or current $i = e \frac{\sigma_i}{\sigma} \phi_o (1 - e^{-n \sigma x})$

Therefore from measurements of the current produced σ_i can be determined. Rather than measure the absolute light intensities directly, it is usual to calibrate a photonmultiplier by applying the equation to a gas of known $\frac{\sigma_i}{\sigma}$, thereby establishing ϕ_o.

Combined measurements of absorption and ionisation cross-sections can be made by introducing a pair of parallel plates into the absorption chamber to monitor the ionisation produced. Cook, Metzger and Ogawa[43] have adopted this procedure for a number of gases. Plots of σ_i and σ (or k_i and k) against wavelength are constructed (see figure 5). The σ curve is essentially of similar nature to the photographic plates of absorption spectroscopy in section 2.1., except that the resolution is lower and the intensity of absorption has been recorded.

Apart from the need for absolute measurements, which is satisfied by this technique, information on the percentage autoionisation and dissociation of each discrete absorption process is available, studies of the underlying ionisation and dissociation continua can be made[44], and first and sometimes high ionisation potentials can be observed from the σ_i curves.

2.3. Total Ionisation Efficiency Measurements

Watanabe[45] developed a simple method of obtaining first ionisation potentials using apparatus similar to that described above, and at an earlier date, where the ionisation current, i, produced in the absorption chamber was measured while the relative intensity of incident and transmitted light was monitored.

$$\text{Ionisation Efficiency } \eta = \frac{\sigma_i}{\sigma} = \frac{i}{K(I_0 - I)}$$

where K is an apparatus constant.

A graph of η versus wavelength of incident light rises sharply at the first I.P. yielding an accurate value (Figure 6). Higher

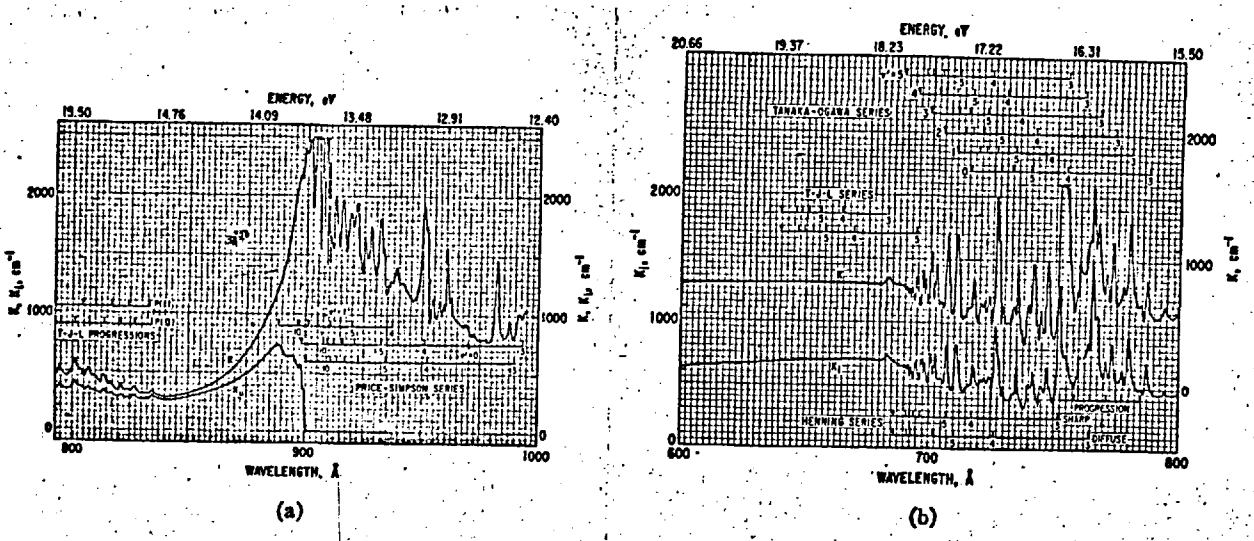

FIG. 5 Absorption, k, and ionisation, k_i, coefficients of CO_2. Known positions of Rydberg series are marked. (a) 800 – 1000 Å region (b) 600 – 800 Å region.

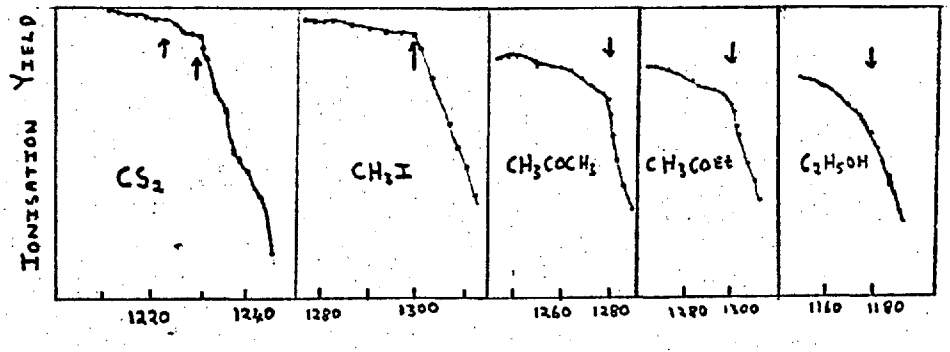

FIG. 6 Watanabe Total Ionisation Efficiency Method

c.f. K. Watanabe J. Chem. Phys 22, 1564, 1954

ionisation potentials and occasionally vibrational structure on the first I.P. can sometimes be observed, but this is made difficult by the formation of ions by numerous autoionisation processes. W.C. Price et al[46]. have also measured a number of first ionisation potentials by this method.

2.4. Electron Spectroscopy

This technique entails the measurement of kinetic energies of electrons ejected in ionisation processes induced by collision with mono-energetic photons or metastable atoms. It is the most recent technique to be adopted in studying ionisation processes, and most of the work has been done using He 584 Å (21·23 eV) incident radiation.

The energy of an electron ejected when a molecule absorbs a photon in a direct ionisation process is given by

$$K.E. = h\nu - Ij$$

where $h\nu$ is the energy of the impacting photon and Ij the ionisation potential of the j^{th} excited state of the ion. The electrons possess all the significant K.E., and the resulting ion none, since from the law of conservation of momentum the ratio of their kinetic energies is the inverse ratio of their masses. The above equation applies equally well when metastable atoms are used, $h\nu$ being replaced by the energy of the metastable.

2.4. (a) Photoelectron Spectroscopy

The application of the technique using photon impact is termed "Photoelectron Spectroscopy", and since a lot of the experimental results in this thesis are obtained by photoelectron spectroscopy, it will be dealt with in some detail.

The technique was first described by Vilesov et Al[47] and later, independently, by Turner and Al-Joboury[48]. Vilesov used incident wavelength down to 1040 Å (LiF window cut off), provided via a monochromator, and studied the electron spectra as a function of wavelength for a number of organic compounds. Lately other groups[49-52] have continued this line of study, for small molecules, using fast pumping systems which enable the windows to be removed and wavelengths below 1040 Å to be used.

Turner has used an helium resonance lamp giving a " pure " He(I) resonance line at 584 Å (21·21 ev). The advantage of this system is the much greater photon intensity available compared to that in the use of a monochromator, and the sureness of the monochromatic nature of the radiation. The use of undispersed resonance lines has been adopted by several other groups[28, 53-56]. Price has succeeded in utilising the He(II) 304 Å line and the Ne(II) 735 Å and 744 Å lines. Argon 1048 Å and 1067 Å, and Hydrogen 1215 Å and 1026 Å lines have been used occasionally in this laboratory.

Many types of electron analysers have been used, and a comprehensive coverage is given in a review by Turner[57]. Electrostatic analysers have provided the best resolution so far, but grid types give greater signal intensity and so can be used for compounds of a lower vapour pressure. Limits to resolving power are discussed by Turner[58], and general reviews of photoelectron spectroscopy are given by Turner[58,59], and by W.C. Price[60]. A description of a 127° electrostatic selector photoelectron spectrometer is given in section 3.1.

Information available from a Photoelectron Spectrum

A typical high resolution spectrum of a small molecule is shown in figure 7. The spectrum is discussed in detail in the results section of this thesis (Section 5. 3.), and only a brief description of the information available is given here.

The important difference between this technique and the methods described in sections 2.1. ; 2.2 ; 2.3 ; 2.6 and 2.7 is that it is not a "threshold" technique, and so ionisations processes which can only occur at discrete impacting energies (see Threshold Laws section 2.6.a.) do not occur unless the discrete energy of the process coincides with the energy of the impacting light.

For He 584 Å spectra this removes all autoionising processes except any occuring at 584 Å (21·2# ev). Autoionising levels are usually abundant only at much lower energies, and there is no evidence that they have every been observed in a He 584 Å spectrum for the molecules studied. They have been observed at lower impacting energies, and the effect is discussed briefly a little later.

Thus in general the only processes observed are direct ionisations to the various configuration states of the ion, which follow the Franck-Condon principles stated in Chapter 1. The first band in the spectrum (figure 7) corresponds to the removal of an electron from the highest filled Molecular Orbital of CO_2 yielding the adiabatic first I.P. This information is usually easily obtained by the earlier methods described in this chapter. The remaining three bands correspond to removal of electrons from the remaining three orbitals of energy less than 21·23 ev , and yield three "inner"ionisation potentials. Immediately we have in our possession the experimental information

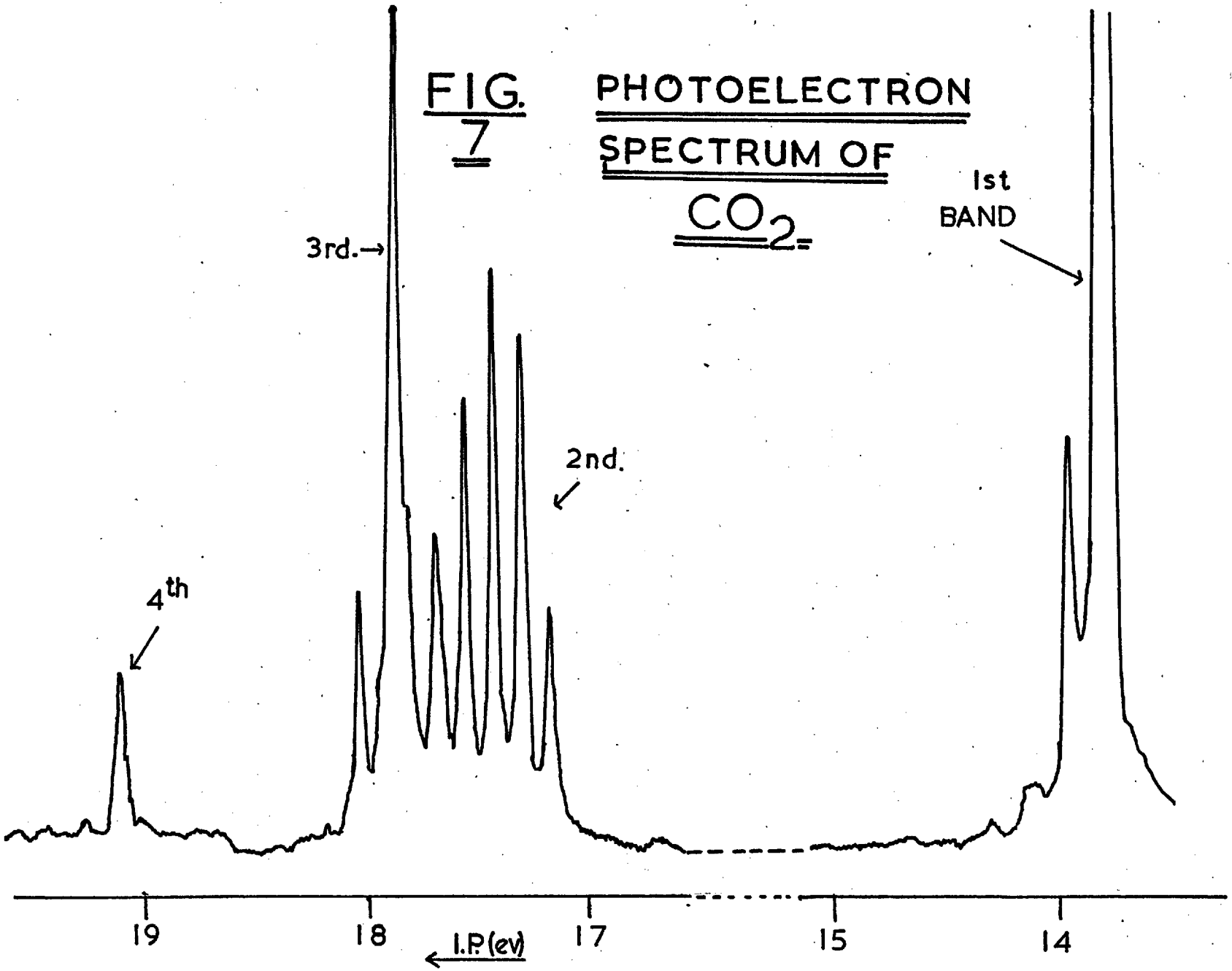

FIG. 7 PHOTOELECTRON SPECTRUM OF CO_2

necessary to test the accuracy of molecular orbital calculations on CO_2 (see section 1.4. (g)). Also in our possession are the experimental F-C factors of the vibrationally excited levels of each ionic state and the vibrational frequencies, both of which help to indicate the bonding nature of the orbital from which the electron has been removed, (see section 1.4. (b), (c) and (g)). If theoretical F-C factors have been calculated comparisons can be made, and in some cases previously unknown geometries established (section 1.4. (h)). The experimental F-C factors are also important in considering possible fragmentation processes, for it is obvious that fragmentation by direct ionisation is not possible if the vibrationally excited levels at the dissociation limit are not significantly populated. For the fullest information on fragmentation, results on initial ionisation, such as are obtained from photoelectron spectroscopy, should be correlated with information on processes occuring after ionisation.

Information of a more general chemical nature may be obtained for larger molecules, where the electronic structure and hence the photoelectron spectrum of the molecule are complex. Examples of this can be found in a paper by Baker, May and Turner[61], where a large number of benzene compounds have been studied. The effects of substitution in the ring on the degeneracy of the π levels, and hence a measure of the mesomeric action of the substituent can be observed in the photoelectron spectra. The substitution of halogens onto the ring produces sharp peaks in the spectrum (non-bonding halogen orbitals), and the relative positions of these peaks in different

compounds can yield information on inductive and mesomeric effects.

Detailed interpretations of photoelectron spectra can be found in Chapter 5 of this thesis, and also in reference 62.

Effects of Autoionisation on Photoelectron Spectra

As already stated autoionisation has not been observed in spectra obtained with a He 584 Å source, though it has been observed at lower energies [63,64,52]. A "normal" autoionising process can only produce photoelectrons of an energy already detectable by direct ionisation (see figure 8a). What can occur, however, is a drastic change in the Franck-Condon factors (figure 8 (b)) since the Franck-Condon region for the ionisation step can be very different from that of the initial excitation step (figure 8 (c) and also section 1.4. (d)). The possibility of "Fluorescent autoionisation" cannot be ruled out either (figure 8 (d)). This is discussed by Blake and Carver [52], where they claim to observe it for oxygen. In this case a new band in the spectrum is possible, but for the scheme proposed by Blake and Carver the energy of the ejected electrons should not alter as the energy of the impacting photons is changed.

Recent Developments in Photoelectron Spectroscopy

A development of photoelectron spectroscopy recently to emerge is Coincidence Spectroscopy [56]. By utilising electronic coincidence techniques , and a mass spectrometer to detect the ionic species formed (parent and fragment ions), the electron spectrum in coincidence with each ion species can be determined. Such a system is potentially

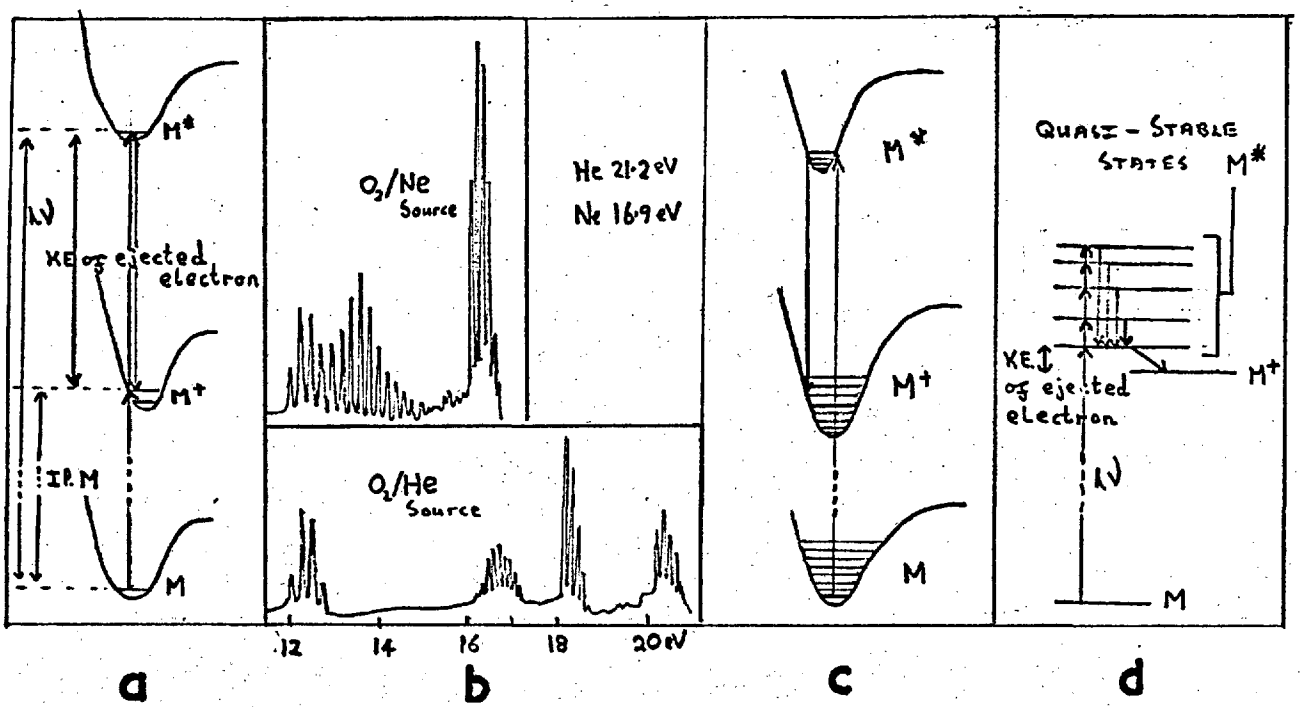

FIG. 8 – Effect of Autoionisation on Photoelectron Spectra

a "Normal Autoionisation" – No change in F-C factors

b Enhancement of high F-C factors by Autoionisation (Reference 63)

c Schematic representation of Enhancement of F-C factors.

d Schematic representation of Fluorescent Autoionisation

very useful, since direct information on fragmentation processes is obtained. However the severe experimental restrictions, especially the need for a low number of collisions to avoid stray coincidences, giving a very low count rate, have limited the studies so far to preliminary work on NH_3 and CH_4[56].

The angular distribution of ejected photoelectrons is of theoretical and practical interest. Cooper and Zare[65] have done some theoretical calculations on this problem, and their results appear to agree with some work done by Hall and Siegel[66] on the detachment of electrons from negative ions by Laser photons. Angular dependence measurements have also been carried out by Berkowitz et Al[67,68]. Though they found small angular dependences, it is too early yet to attempt significant correlations with the type of electron being ejected. There is no evidence that photoelectron peaks could be completely "missed" because of unfavourable angular dependence.

Siegbahn[13], and many of his associates at Uppsala University, have been working on electron spectroscopy over the past few years using X ray sources, and also more recently the He resonance lines. Much of their work has been geared towards the use of electron spectroscopy for chemical analysis, and of course with X ray sources they are able to obtain I.P.'s greater than 21·2 ev.

2.4. (b) Electron Spectroscopy using a Metastable Atom source

The term " Penning Ionisation " is generally used for ionisation induced in this fashion. Čermák[69,70] has done much work in this field

using He (2^1s 20·61 ev, 2^3s 19·81 ev) and Ne (16·71 ev, 16·61 ev) metastables. Penning ionisation is important for two reasons.

1) Collision is between uncharged particles, which differs from other types of ionisation involving particles.

2) The collision time is increased compared to photon impact (10^{-13} sec cf 10^{-18} sec), which may partially invalidate the Franck-Condon Principle, and also allow collision complexes to be formed [70]. There is no evidence as yet to suggest the F - C principle does not operate, but the resolution obtained by Penning ionisation is far too low at the moment to test the theory properly.

2.5. Ion impact Spectroscopy

Ion-Molecule reactions and charge transfer processes can be studied by collision between a beam of ions and a target gas of neutral molecules. Lindholm et Al [71] have done much work using ion beams in a mass spectrometer. Ionisation by charge exchange will only occur when the recombination energy of the ion is close to the I.P. of the neutral molecule. A few inner ionisation potentials have been obtained in this manner by Lindholm [72].

2.6.(a) Electron Impact Efficiency Curves with Mass Analysis

The Mass Spectrometer incorporating an electron beam ionisation source has been in existence for many years. It has been used primarily as an analytical tool and a method by which chemical breakdown routes, re-arrangements etc. can be studied. As such it has been highly

successful, but of course it lends itself to the study of physical processes occuring in ionisation by measurements of ionisation cross-sections, σ_i or efficiencies, γ , in a similar manner to methods described in 2.2. and 2.3. The great advantage here is the division of the total σ_i into the individual components for each ion formed, affording information on fragmentation processes, and in particular the energies at which fragments first appear (A.P. - Appearance Potential).

Curves are usually plotted as σ_i or γ against the electron energy of the ionising beam (figure 9a).* The parent ion curve starts at the first I.P. and may or may not show recognisable "breaks" at higher energies corresponding to further I.P's. As in Watanabe's Total Ionisation method (section 2.3.) there is a strong interference from autoionising processes. Fragment ion curves usually show no further interpretable features after their initial onset.

The electron impact efficiency curves do, in fact, show very little detail for the large number of complex processes which occur. There are two main reasons for this :-

(1) The electron beams are not properly monoenergetic, since electrons from a heated filament have a Boltzmann distribution of energy, and the fine details of the ionisation processes are smeared out by the resulting lack of resolution. The energy spread of the beam can be reduced either by Fox's Retarding Potential Difference method, or by the use of an

---

*$\gamma = \dfrac{i}{K(I_o - I)}$ see section 2.3.

In practice ~~it is far more usual to plot just~~ ion current, i, plotted against electron energy, which is not a true efficiency curve.

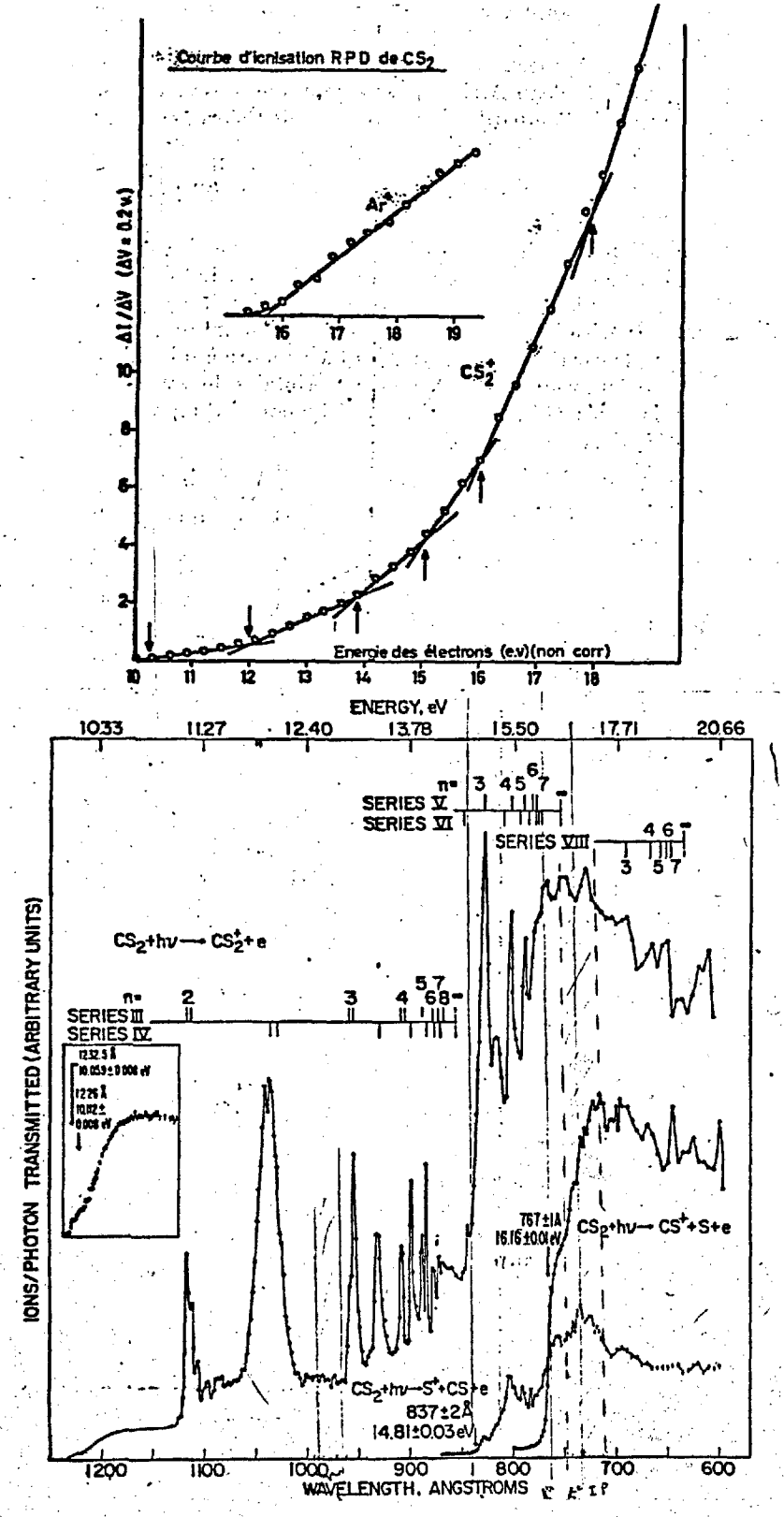

FIG. 9

(a) Electron Impact r.p.d. Mass Spectrum of CS_2 (ref. 112)

(b) Photon Impact Mass Spectrum of CS_2 (ref. 82)

electon energy analyser. These methods are reviewed by Morrison[73], and by Kieffer and Dunn[74].

(2) The threshold laws for processes involving photon and electron impact are different. A theoretical quantum mechanical treatment has been developed by Geltmann[75] and others. The general result of this is that the probability of ionisation is given by

$$P(E) \propto \Delta E^{n-1}$$

where n = Number of electrons leaving the collision complex

E = Energy of the excitation beam (electron or photon)

ΔE = the excess energy above threshold for the process concerned.

From this equation it is obvious that for single direct ionisation by electron impact, and double direct ionisation by photon impact, where $n=2$, the probability of ionisation is a first order function of excess energy. Thus the efficiency curve increases linearly as the electron energy increases above an I.P. For $n = 1$, i.e. simple ionisation by photon impact, autoionisation by electron impact, a zero order law holds and a step-function occurs in the curve. The experimental evidence is in general agreement with the equation (see figure 10).

It is worth noting that ionisation cannot always be described in terms of "auto-ionisation" or "direct", since the main difference is in the time scale of the events as far as threshold laws are concerned. An auto-ionised electron leaves the complex after a time of 10^{-12} - 10^{-13} sec, a directly ionised electron after 10^{-15} sec or less. In the

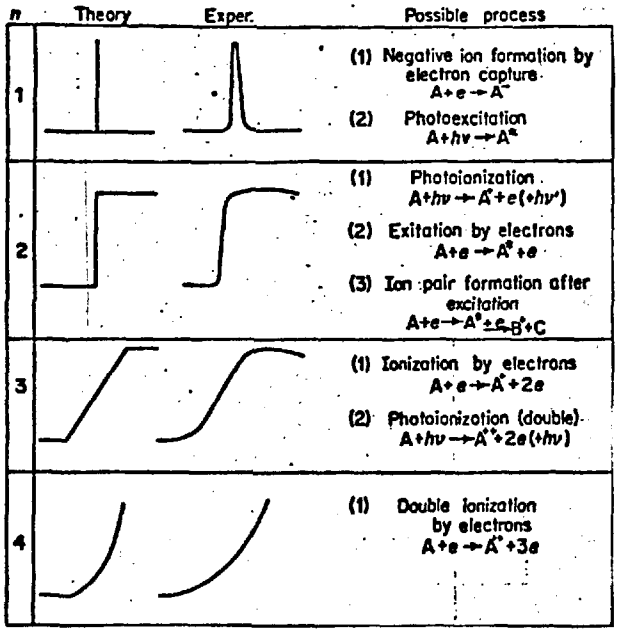

FIG. 10

Theoretical and Experimental Threshold Laws for The Different Classes of Electron-Molecule and Photon-Molecule Interactions.

If the autoionising process has a lifetime approaching that of direct ionisation, then an intermediate threshold law might hold.

Because of the two reasons given above the electron impact study of ionisation phenomena, though being the most generally applicable and easiest of techniques, is often the least reliable. Many inaccurate I.P's have been quoted (up to ·5 ev errors) owing to the difficulty of establishing the exact A.P's or breaks in a curve, and often higher I.P's are not observable at all. Autoionising levels are commonly designated as ionisation potentials. Vibrational structure has been claimed on several occasions, only to be refuted at a later date, but a recent paper by Carette[76] on CO_2 and N_2O shows that it is possible to obtain reliable data concerning vibrationally excited states.

In addition to the two reviews already mentioned, and one by McDowell[77], many aspects of electron impact work are described in Field & Franklin's book "Electron Impact Phenomena"[30].

2.6 (b) "Electron Impact Energy Loss Spectroscopy"

Lassettre[78] has developed a method whereby the kinetic energy of the impacting electrons is examined after having been scattered by collision with target molecules. For a non-ionising (or autoionising) level at energy Ec, the scattered electrons will have an energy

$$E = E_I - E_c$$

where E_I is the energy of the impacting electrons.

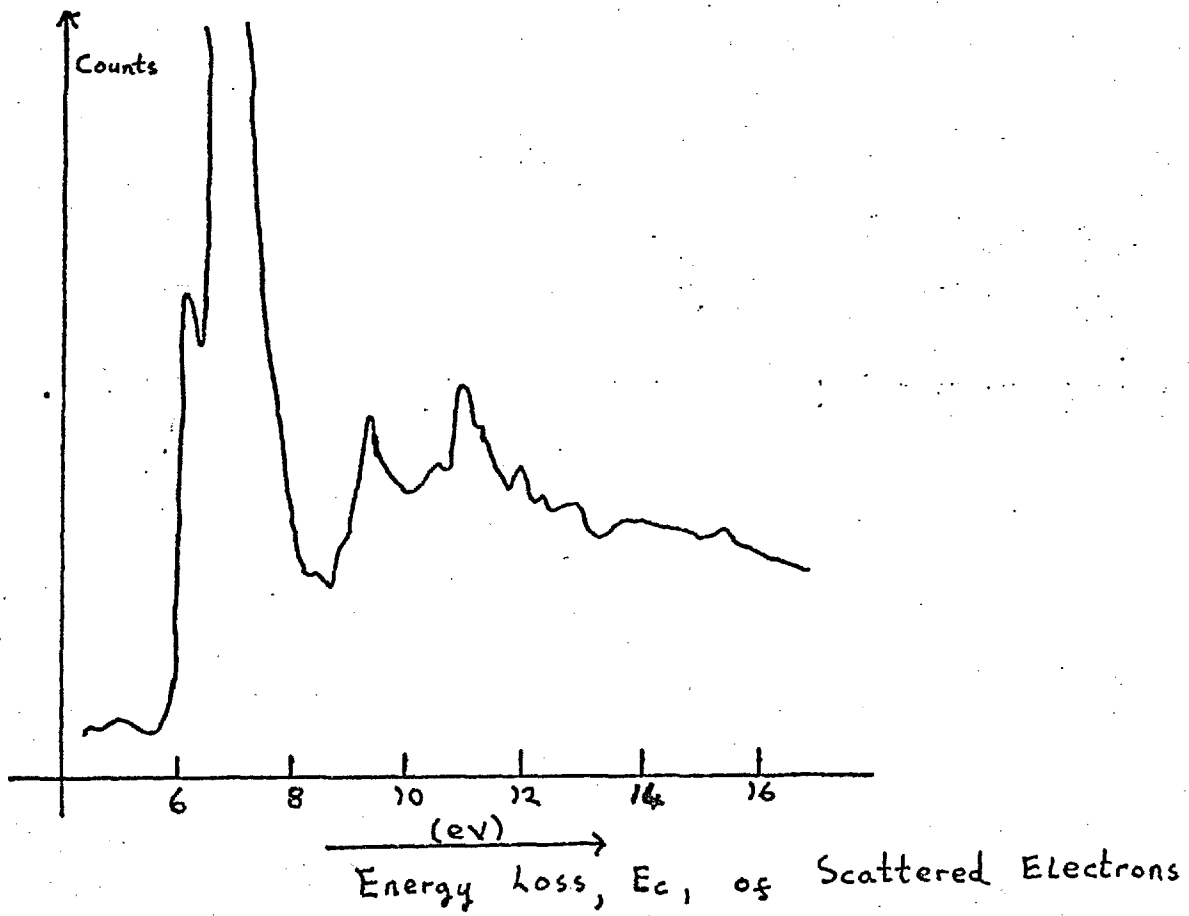

ELECTRON IMPACT ENERGY LOSS SPECTRUM OF BENZENE (A. Skerbele & E.N. Lassettre, J. Chem. Phys. 42. 395. (1965))

A peak will appear in the energy spectrum of the scattered electrons at value E. For an ionising process scattered electrons will have energy

$$E = E_I - E_c - E_e$$

where E_e represents the energy of the ejected electron. This results in an approximation to a step function occuring at energy $E_I - E_c$ in the spectrum. The whole spectrum is thus similar in nature to the absorption cross-section / wavelength curves for photon impact such as is obtained in section 2.2. Experimental limitations (very poor resolution) and the predominance of autoionising processes etc. have meant that so far little useful information at energies higher than the first I.P. have been obtained.

2.7. Photon Impact Efficiency Curves with Mass Analysis

This technique is analagous to the previous one, except that a monochromatic photon beam is used as the ionising source. It is a logical extension of Watanabe's Total Ionisation technique (Section 2.3.) which was used primarily for obtaining first I.P's. In 1958 Hurzeler, Inghram, and Morrison[79] were the first to successfully combine a vacuum monochromator and mass spectrometer. They used Li F windows to separate the residual monochromator gases from those to be studied in the mass spectrometer, and so were limited to wavelengths greater than 1040 Å. Since then a number of people[80-87] have done work to lower wavelengths using fast pumping systems and no windows. The difficulty in this technique is not the energy spread

of the photon beam (<1 Å at 1000 Å may be obtained), but the provision of sufficient light intensity over the required range of wavelengths (1300 Å $\longrightarrow$ 600 Å). This can be done by utilising suitable emission continua and molecular many lined spectra[81], or by providing a distribution of intense lines from a low pressure spark source using a variety of gases, as was done by Weissler et Al[80], and also for some of the results in this thesis.

The advantages that the photon impact experiment has over electron impact are the increased resolution, and the favourable threshold laws which give step functions for direct ionisations and Delta functions for autoionisation. The two processes are generally more easily distinguishable in photon impact curves than in electron impact (figure 9 (a) and (b)), though intense autoionisation can still often obscure the underlying step-functions of direct ionisations. First I.P's can be obtained with an accuracy approaching that of any other technique, often with reliable vibrational and spin-orbit coupling structure[81]. Higher I.P's can often be detected and besides the A.P.'s of fragment ions, meaningful structure can also sometimes be detected on the curves[81]. Chupka[84] has recently been able to detect rotational structure in the ground ionic state of H_2^+.

It ought to be noted that the selection rules for allowed processes are not necessarily the same for photon and electron impact, and would be expected to be less restrictive for electron impact because of the additional electron available for spin and orbital angular momentum transfer. It is an interesting fact that sometimes electron impact

curves, for all their poor resolution and unfavourable threshold laws, do seem sometimes to identify I.P.'s and vibrational structure that is not apparent in the photon impact curves (compare references 77 and 82).

A review of some of the differences between photon and electron impact has been published by Collin[88].

2.8. Fluorescence Spectroscopy

Electronic states excited by the absorption of U.V. light may be identified by observing the fluorescent radiation emitted during the decay of these states. Figure 11 shows a hypothetical diagram for an absorption where fluorescence can occur after excitation. The fluorescence can be detected and analysed by the use of a monochromator and photographic or photoelectric recording techniques. Very high resolution can be obtained by photographic recording (e.g. absorption spectroscopy 2·1), allowing analysis of rotational and vibrational structure. Judge et Al[89] identified the $B^2\Sigma u^+ \longrightarrow X^2\Sigma g$ transition of N_2^+ in this manner.

A simple method of recording the vibrational F - C factors of the upper electronic state is to detect the fluorescence undispersed as a function of incident photon wavelength. Figure 12 shows such a case for N_2O, recorded by Cook et Al[90]. They have done similar work for other molecules[43,90]. The superimposition, or lack of it, of peaks corresponding to autoionising levels on such fluorescence curves (see figure 12) can indicate to which ionic levels the autoioisation

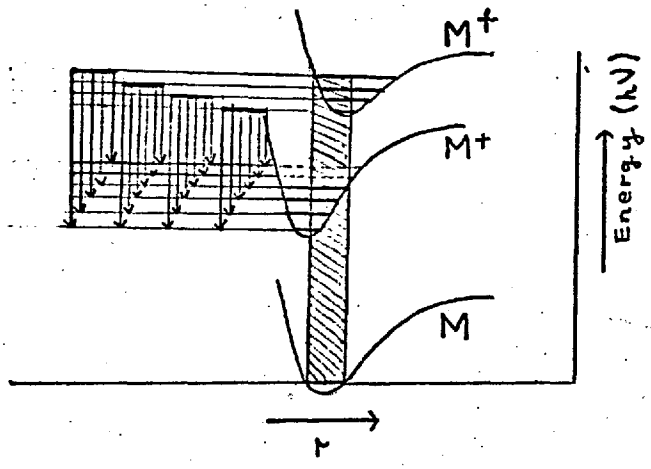

FIG. 11

Potential Energy Curves for a Hypothetical Molecule Showing Fluorescence after absorption of Ultraviolet Light (Reference 25)

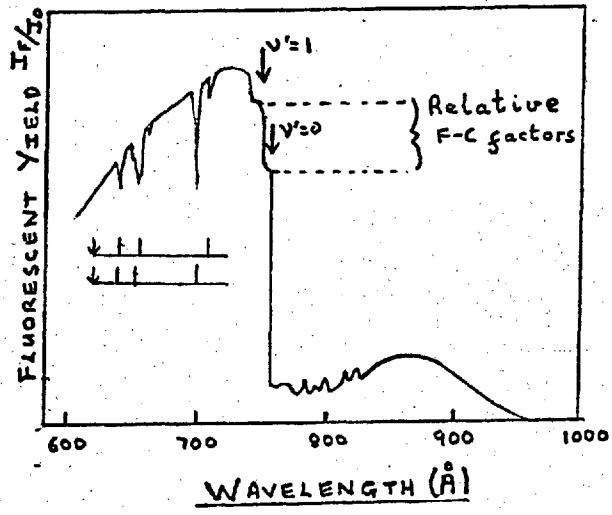

FIG. 12

Undispersed Fluorescent Yield for N_2O plotted against Incident Wavelength (c.f. Reference 90)

is occuring.

In addition to providing information on ionising processes, fluorescence studies can also be useful for observing excited molecular levels. In fact in figure 12, the fluorescence to long wavelengths is from a dissociative molecular level. Other examples have been provided by Becker and Welge[91], and Beyer and Welge[92].

2.9. Emission Spectroscopy

This is a similar technique to the previous one, except that the excited species are not produced by absorption of U.V. light, but usually by a gas discharge. The populated levels may be very numerous, and the vibrational populations are no longer governed by the F - C principle. The emission spectrum is recorded photographically, but emission from unwanted species (dissociation products produced in the discharge etc.) often interfere. Some of the earliest work was done on CO_2 by Mrozowski[93], and recently Callomon[94,95], and Horani and Leach[96] have studied other small molecules. Excited ionic levels have been unambiguously identified and often geometric parameters of the ions obtained.

2.10. K.E. of Fragment Ions

Fragments sometimes possess considerable kinetic energy. The initial energy is of interest for two reasons. It must be taken into account in calculating heats of formation from A.P. measurements (see section 1.4. (f)). In this case K.E. is measured at threshold and the very reason for measuring it is to eliminate it as a source of error.

On the other hand K.E. is itself of interest, and this section is treated in some detail, with specific examples, because of its relevence to such subjects as the Franck- Condon Principle, the meaning of observed appearance potentials, and the mechanism of fragmentation processes.

2. 10 (a). Measurement of K.E. of Ions

In mass spectrometry we would like to know the identity of the fragments produced, their A.P.'s and also the K.E. distribution. Conventionally only the first two are measured, but several techniques have been adopted for measuring simultaneously the K.E. These techniques are highly subjective, the information given often only being of qualitative value, and the correlation of such information with possible excitation processes can be tenuous once one moves away from simple diatomic molecules.

The first and most widely used method of measuring K.E., is the R.P.D. method, in which the ion current at the collector is plotted against an ion retarding potential appled to an electrode immediately before the collector. Hagstrum[97] constructed such an apparatus, based on the original technique of Lozier[98], and used it to study several diatomic gases. The instrumental effect common to all conventional slit system mass spectrometers is that there is always discrimination against collection of ions with high K.E., and so experimental intensities are far below their true value.

Deflection methods[99] have also been successfully applied. In the conventional mass spectrometer, ions of high K.E. are observed as satellites to the high mass side of the zero K.E. peak.[100] It can be shown[101] that ions with K.E. in a small range produce these peaks, while ions with a large range of K.E. produce a broadening of the zero K.E. peak to high mass. These effects have been discussed at some length by Hagstrum and Tate[102].

Much work has been done using these techniques, of which that on the Hydrogen system is an instructive example. Dunn and Kieffer[16] using a spectrometer designed to focus H^+ ions from 0 to 20 ev K.E., showed that the distribution was in good agreement with that calculated for transitions to the $^2\Sigma_g^+$ and $^2\Sigma_u^+$ states of H_2^+ (Figure 13) using the Franck - Condon Principle. Some discrepancies were later cleared up by Rosenstock et Al[103] (see page 56) who showed that H^+ with high K.E. could also be formed by dissociation of H_2^{++}.

Mohler, Dibeler and Reese[100] showed that ions possessing high K.E. in the mass spectra of some polyatomic molecules were consistent with a doubly charged fragment breaking into two singly charged fragments (A.P.'s approximately right, K.E. observed in agreement with calculated Coulombic repulsion energy). This work supplemented the original studies of Hustrulid et Al[101].

Having given some examples where simple correlation with theory is possible, we now turn to cases where interpretation of K.E. and the real meaning of A.P.'s is more uncertain. Chupka[104] has given an excellent account

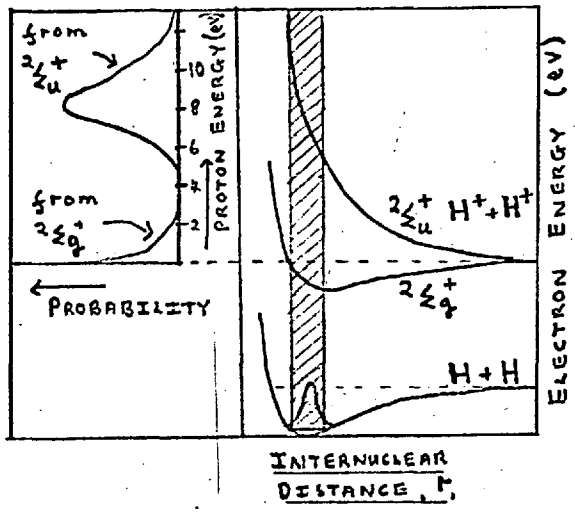

FIG.13

F–C Transitions in H_2 and the Kinetic Energy Distribution of the Resultant H^+ ions
c.f. Dunn & Kieffer
Phys Rev 132, 2109, 1963

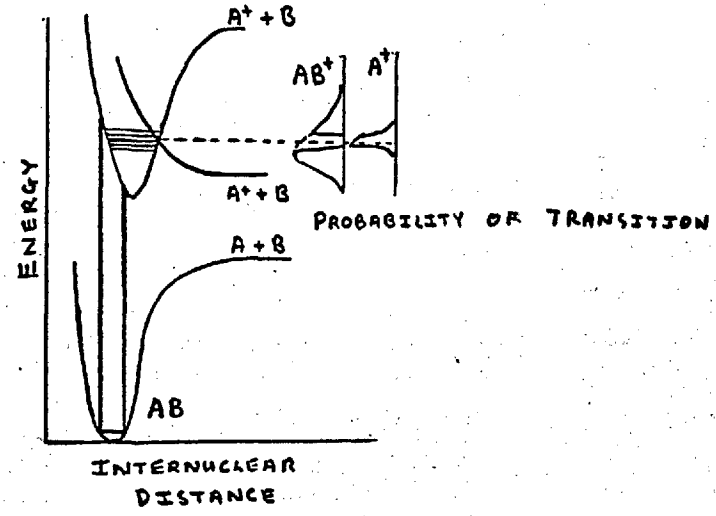

FIG.14 — Pre-dissociation by Curve Crossing and Kinetic Energy Distribution of the Ions formed (cf. Ref. 104)

of the difference between simple "diatomic like" cases, such as described above, and polyatomic systems where the data cannot always be interpreted successfully in terms of direct F ← C transitions to the repulsive portion of potential surfaces.

Several possibilities exist, even for "diatomic like" cases, of fragment K.E.'s which do not fit in with the simple theory. The first is where pre-disociation by curve crossing can yield fragments with considerable K.E. Also the A.P. of the fragment could be quite sharp, a feature often associated with fragments having zero K.E. (see figure 14). Secondly some of the "excess energy" of an A.P. of a fragment above the dissociation limit may appear as K.E. of an electron , ejected in an auto-ionisation, or as radiation emitted by an excited ion as it makes a transition (lifetime $\sim 10^{-8}$ sec) to a lower dissociating or pre-dissociating level (e.g. section 1.4. (d) and figure 2).

As soon as polyatomic molecules are considered there is the possibility that fragments may carry away some of the excess energy as vibrational energy.

Considering these possibilities it is not surprising that the K.E. results of some diatomic and simple polyatomic molecules do not fit the simple theory.

For large polyatomic molecules it becomes impracticable to try to explain fragmentation in terms of detailed potential surfaces. The alternative is to use the statistical theory of mass spectra[105], in which the main hypothesis is that the molecular ion formed by F ← C transitions, possessing electronic and vibrational energy, does

not dissociate within a vibration but rapidly and randomly re-distributes its energy into the vibrational modes of the ground state of the ion. The predominant method of re-distribution is by a large number of curve crossings of closely spaced potential surfaces, and dissociation occurs by the ion attaining certain configurations with sufficient vibrational energy concentrated in the proper modes.

How does such a theory, if correct, affect the A.P's and K.E.'s of fragments measured by electron or photon impact? If a fragment ion is not produced immediately (i.e. within one vibration - 10^{-14}sec) it is at least necessary for it to be produced within 10^{-5} sec to enable detection as a fragment in the mass spectrometer. Normal kinetic considerations will govern the dissociation rate of parent ions, which will increase with the excess energy supplied above the nominal A.P. This excess energy required to give a detectable amount of fragment may be several tenths of a volt for large molecules, and will increase with the complexity of the molecule. Thus the observed A.P. may be as much as 1 volt above the "true A.P."

The theory also requires that no ions should be formed with large amounts of K.E., since this implies dissociation from repulsive surfaces of discrete excited states.

What is the evidence for or against this theory compared to the "diatomic like" treatment? Chupka[104] found that for many larger polyatomic molecules all the fragment ions formed had a low K.E. ($\frac{1}{10}$ eV) with a Maxwellian distribution, and that metastable peaks were detected

for the fragmentation processes concerned, indicating lifetimes of the order of 10^{-5} sec for the dissociating parent ions.

The conclusions that Chupka, and others[106] came to, were that in general there are insufficient potential energy surfaces, too widely spaced, for the statistical theory to be quantitatively correct, but that dissociation does not often occur by a simple "diatomic like" process.

One of the few cases where such a process is indicated is the fragmentation of CH_3^+ from $CH_3CH_2CH_3$ and other compounds.

2. 10. (b) Recent advances in the measurements of K.E. of ions

Two methods of avoiding the large discrimination effects against ions possessing K.E. have been described recently.

Rapp et Al[107] have adopted a system originally used by Bleakney[108] whereby the ionisation chamber of the mass spectrometer is used as a total ionisation tube, the ions being collected on a flat plate instead of drawing them through slits. The percentage of ions possessing K.E can be found by reversing the draw out field, ions thus having to traverse a potential gradient to reach the positive plate. Many simple gases were studied and it was estimated that from 7% (H_2) to 25% (N_2O) of the total ionisation is dissociative with K.E. $>$ ·25 ev.

Green and Ryan[109] used a radio-frequency spectrometer capable of detecting all ions with excess K.E. They detected some ions (e.g. CH_2OH^+ from CH_3CH_2OH) which had discrete K.E. values, suggesting

a specific curve crossing process (e.g. figure 12), and other (e.g. CH_3^+ from ethanol and other alcohols) where the "diatomic like" process is in operation. They analysed their results in general as indicating that the statistical theory was not in operation for the compounds studied.

McCulloh, Sharp and Rosenstock[110], in their entirely novel co-incidence apparatus, have provided evidence that a significant number of the high K.E. ions found in CO_2 and CH_4 come from dissociative double ionisation, yielding positive ion pairs. For CO_2, O^+ and CO^+, C^+ and O^+ ion pairs were verified (2% of total ionisation at 1 K ev ionising energy)

In 1968 they applied another coincidence technique[103] designed specifically for the process

$$H_2^{++} \longrightarrow H^+ + H^+$$

such that pair count versus K.E. could be plotted. The resulting distribution fitted exactly that calculated for the process from the F - C Principle and the K.E. of H^+ produced in this manner was estimated as $9{\cdot}4 \pm 0{\cdot}15$ ev.

CHAPTER 3

EXPERIMENTAL

3. 1. The 127° Electrostatic Analyser Photoelectron Spectrometer

A large portion of the results in this thesis were obtained by photoelectron spectroscopy, the general principles of which have been given in Section 2.4.a. The photoelectron spectrometer described by Turner[112] was used for these studies. A brief description is given here.

3. 1.a. Vacuum system of the spectrometer.

The principal features of the spectrometer are shown, in schematic form, in figure 15. A pressure of approximately 10^{-6} torr could be maintained. Under operating conditions the helium pressure was approximately 0·1 torr in the light source, the sample inlet pressure between ·04 and ·3 torr, and the pressure in the main chamber not above 2×10^{-4} torr (highest allowable operating pressure for the electron multiplier detector). These pressure differentials were maintained by the fast pumping system and the narrow bore inlet tubes used (see figure 15). The pressure in the ionisation chamber was intermediate between that of the sample inlet and the main chamber. For samples with low vapour pressures a direct attachment at point X (figure 15), by-passing the inlet manifold system, was necessary to provide sufficient vapour pressure for a reasonable signal intensity to be obtained.

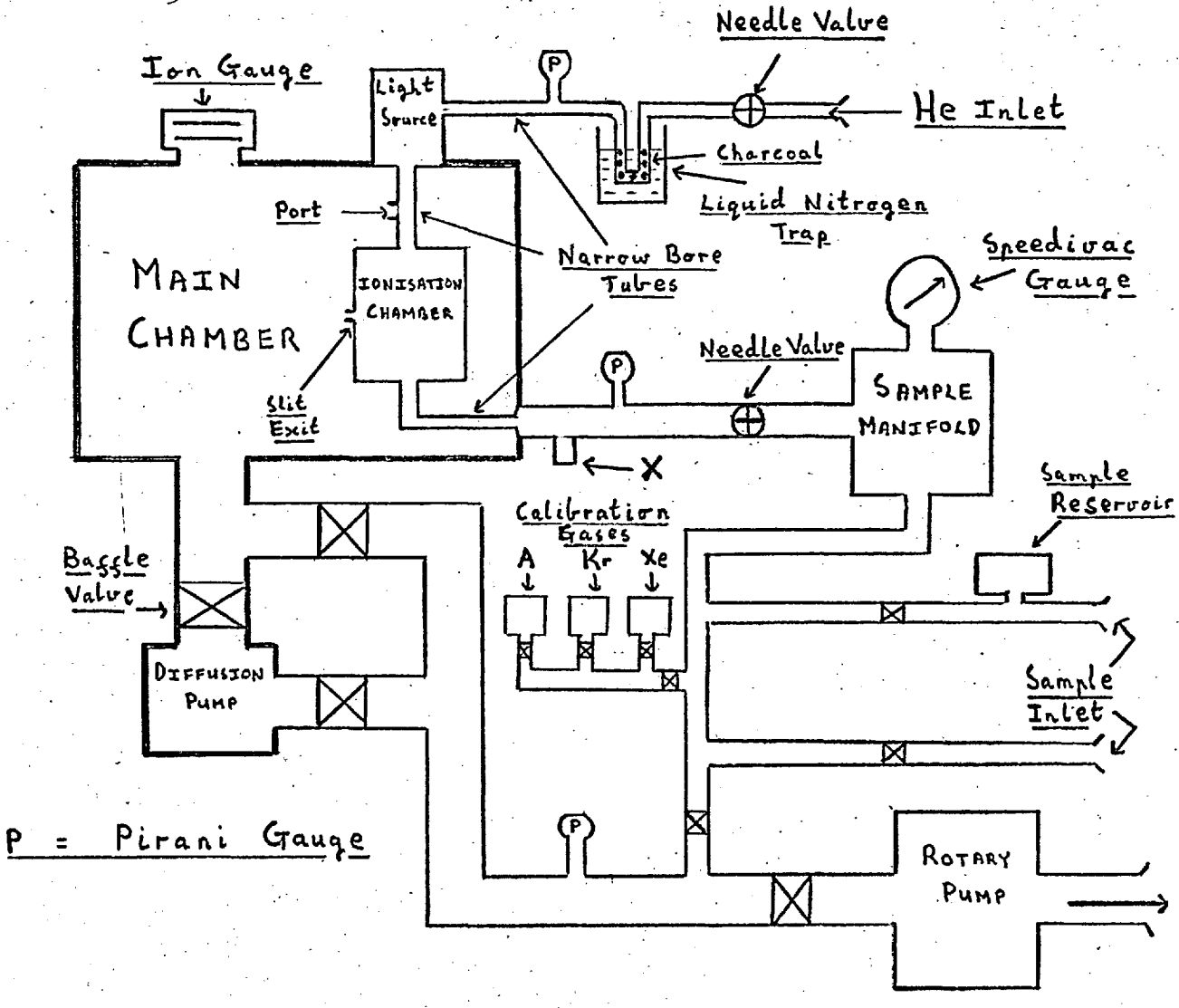

FIG.15

PUMPING SYSTEM OF THE PHOTOELECTRON SPECTROMETER — SCHEMATIC FORM

3. 1.b. The light-scource and ionisation chamber assembly

A plasma discharge was induced in the light source quartz capillary tube (figure 16) by connecting a 2,000 volt power supply in series with a stabilising resistance across electrodes Z - Z'. To obtain a "pure" He I discharge , emitting the 2 P ⟶ 1 S line, the helium was purified by passage through a charcoal trap cooled in liquid nitrogen and the pressure adjusted till the characteristic peach colour was obtained. The photon flux, after travelling down the capillary tube, entered the target gas in the ionisation chamber, I. Most of the helium was pumped away through an exit port, P, in the side of the capillary. Ejected electrons escaped from the ionisation chamber through a narrow slit, S, where they passed into the electrostatic analyser, E (figures 16, 17 and 18).

3. 1.c. The electron detection and recording system.

For optimum performance of the instrument in terms of resolution, the vertical and horizontal components of the Earth's magnetic field were cancelled out by opposing fields from Helmholtz coils surrounding the main chamber.

Electrons leaving the analyser were detected by an electron multiplier, M, which passed through an O-ring seal in the side of the main chamber. After amplification (figure 17) the signal was displayed on an X - Y recorder, enabling a spectrum of the K.E. of ejected ions versus their intensity to be plotted directly. The spectrum could be recorded in two ways, the circuit diagrams for which are

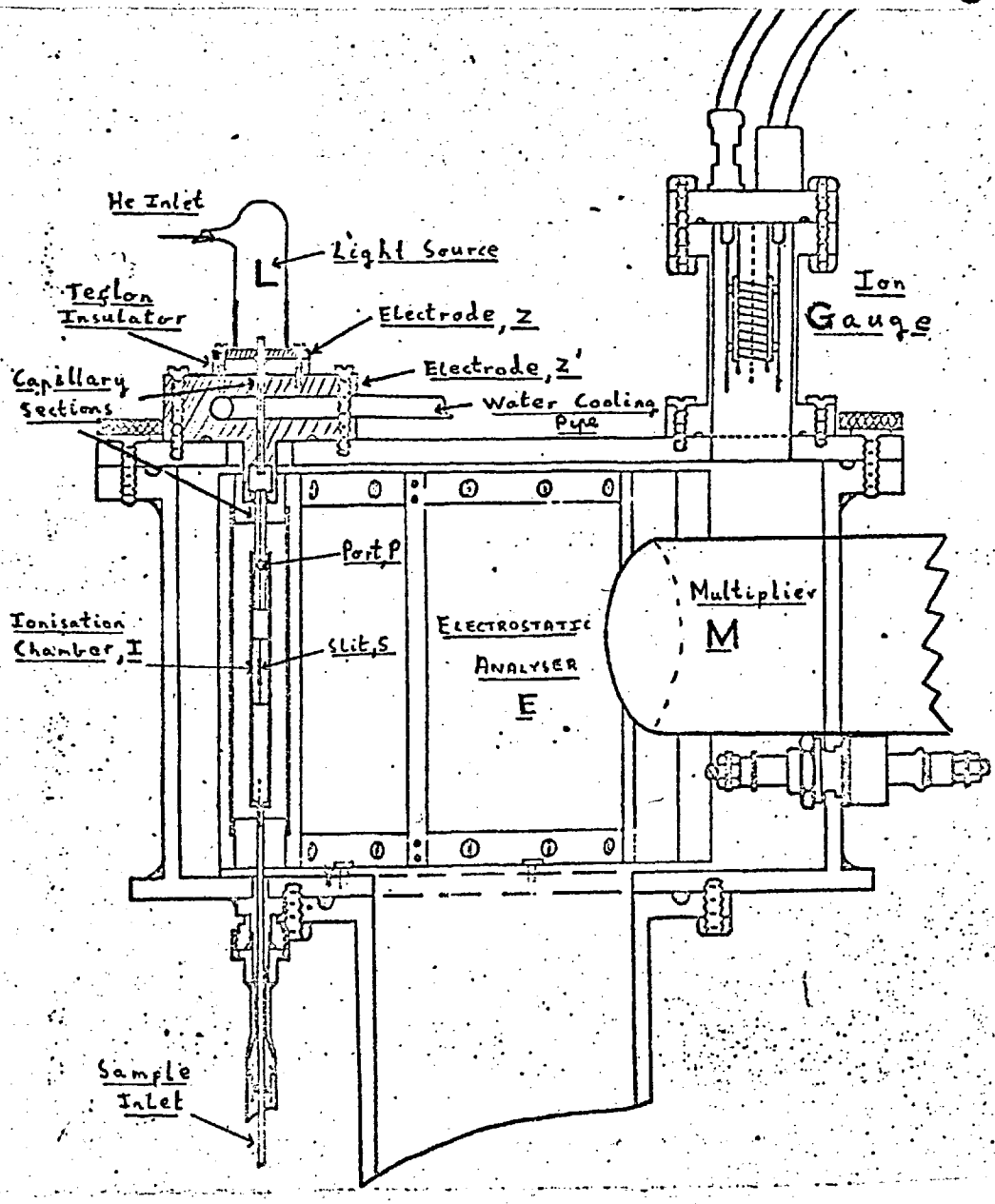

FIG.16 VERTICAL SECTIONAL DRAWING THROUGH MAIN CHAMBER

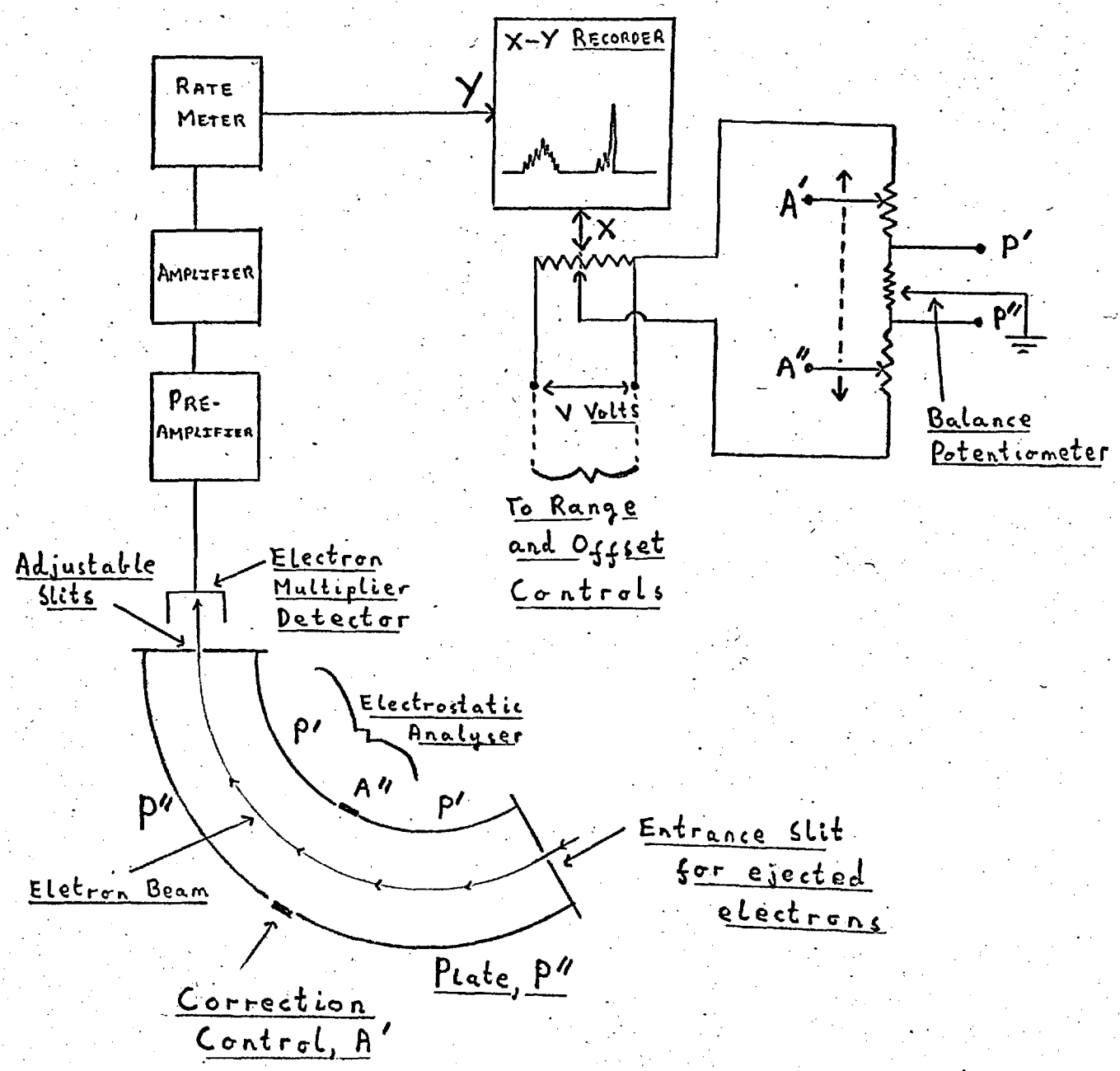

FIG.17

127° ELECTROSTATIC ANALYSER, DETECTION AND RECORDING SYSTEM OF THE PHOTOELECTRON SPECTROMETER

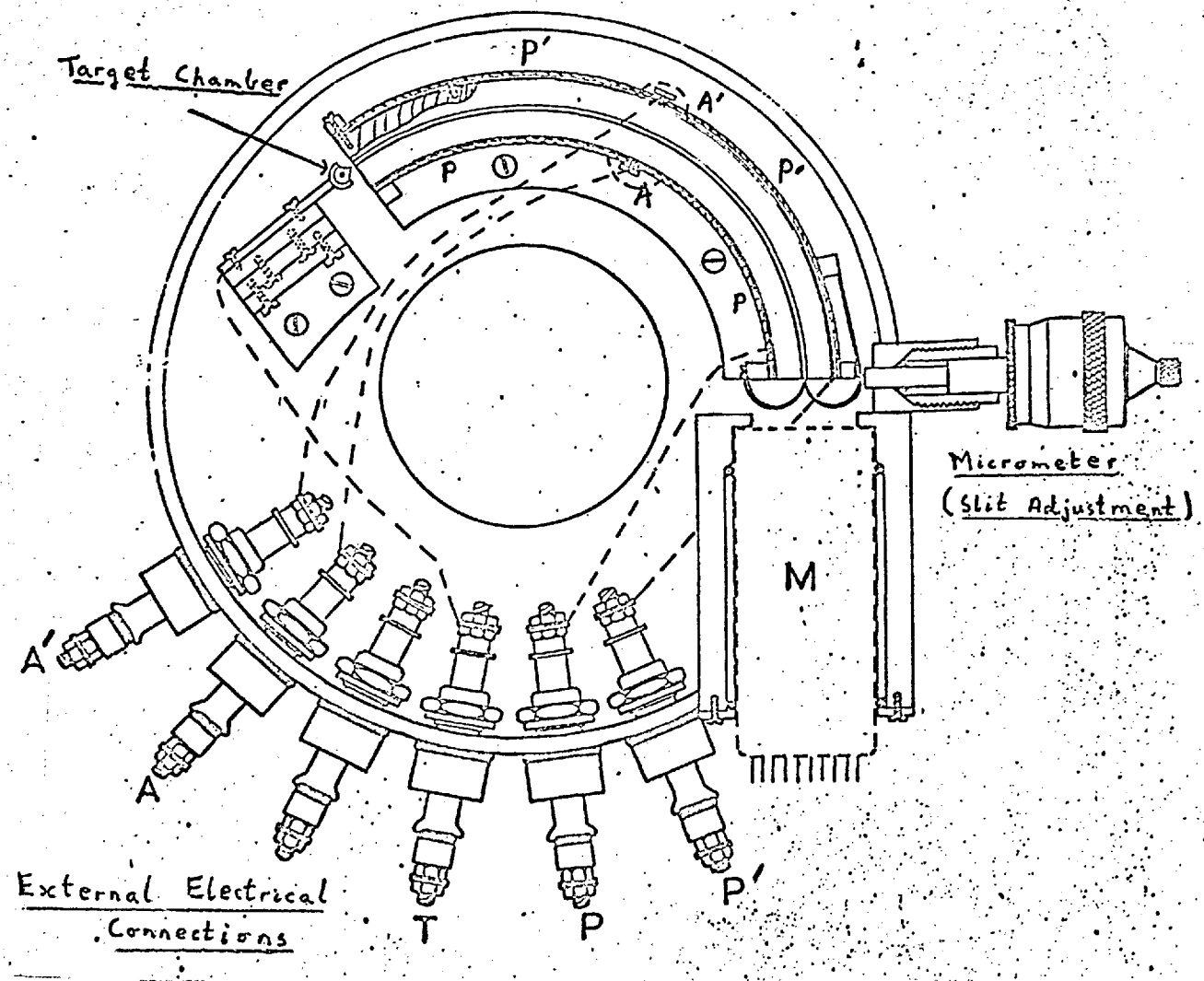

FIG.18

HORIZONTAL SECTIONAL DRAWING THROUGH MAIN CHAMBER

given in figure 19. In the first method the voltage across the deflecting plates P' and P'' was increased, allowing collection of ejected electron having increasing K.E. The voltage applied across the correction plates A' and A'' increased in phase with P' and P'', but was somewhat larger (see figure 19 (a)). This control had the effect of re-focusing electrons which deviated from the optimum path because of their finite angle spread at the entrance slit of the analyser. The balance potentiometer related the plate voltages to earth potential, and provided an additional focusing action. In the second method (figure 19 (b)) the deflection plate and correction voltages were fixed to collect electrons of a known K.E. (set at approximately 6 e V), and the ejected electrons were accelerated by a voltage applied to a repeller plate in the target chamber. By increasing this accelerating voltage the electrons were thus brought to the required energy for collection. The advantage of this system was that all collected electrons had the same band-width, enabling those which were ejected with an energy approaching 0 e.V. to be observed with a much greater intensity than in the first method.

The resolution obtainable was ·02 e.V. (half-width at half-height for Argon), sufficient to resolve much vibrational structure in small molecules.

Mathematical treatments of the electron optics relevant to this type of analyser, and to others, can be found in reference 112.

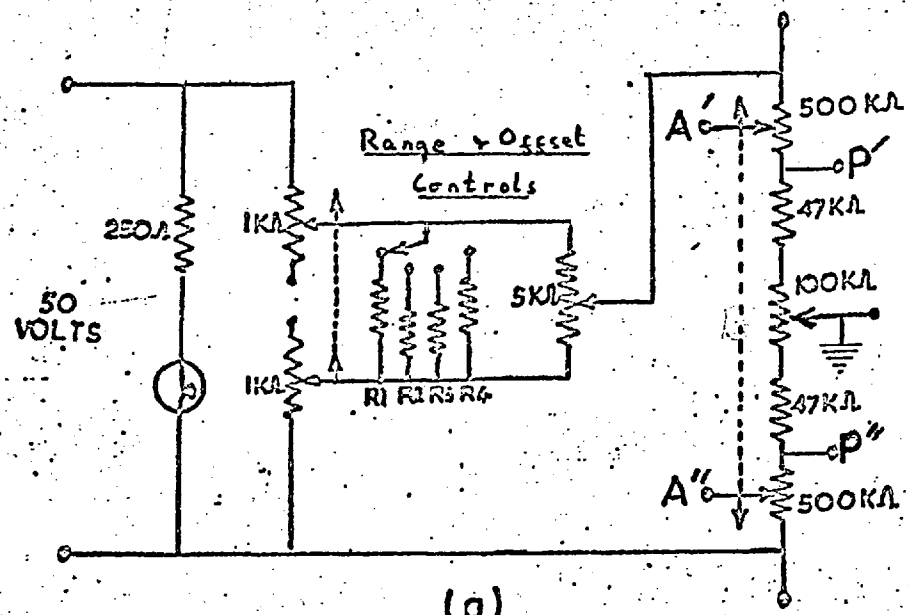

(a)

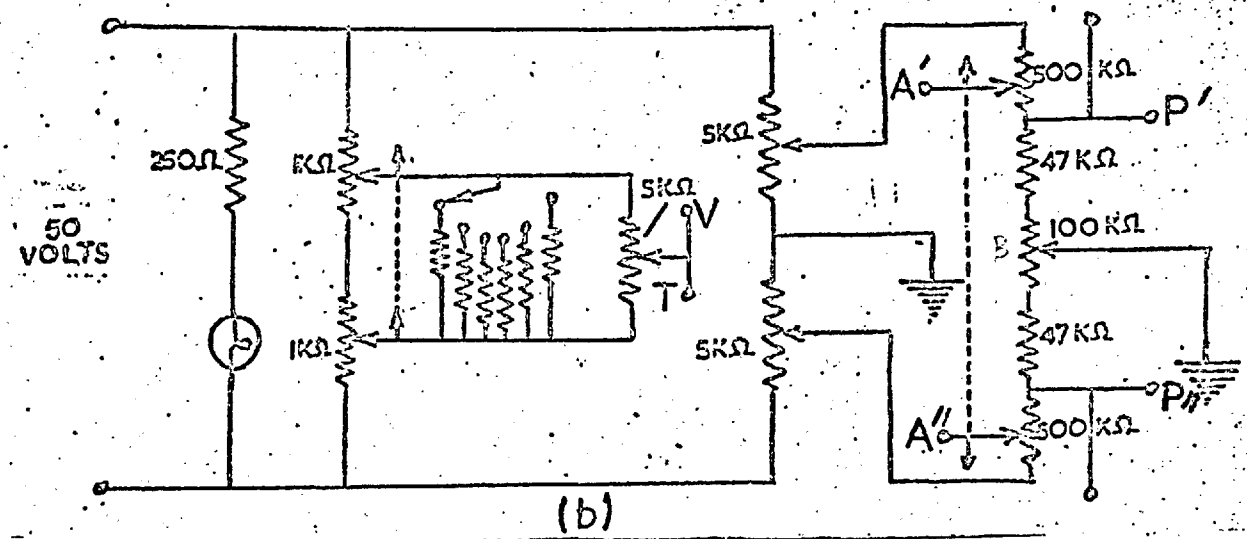

(b)

FIG 19

(a) Sweep/Offset Circuit Used for Obtaining Spectra by Increasing Voltage on Deflector Plates

(b) Sweep/Offset Circuit Used for Obtaining Spectra by Changing Voltage Applied to Target Chamber Repeller Plate

R1 – R4 are the range switch resistors allowing sweep widths of 10 eV, 5 eV, 2 eV, and 1 eV to be used. In (b), two additional sweep widths (15 eV and 0.5 eV) are provided for.

A : Connection to Correction Control T : Connection to Target Chamber
P : Connection to Deflector Plates V: Test point for Target Chamber Voltage

3.2. The Development and Use of Time-of-Flight Mass Spectrometers

3. 2.a. Historical Development

The conventional method of recording the mass spectra of ions is to observe their trajectory in an electrostatic or magnetic field, or in a combination of the two.

In 1946 Stephens[114] first reported a method of measuring mass-to-charge ratio. ($^{m}/_{e}$) using a field--free drift tube. This work was taken up by Cameron and Eggers[115] who produced the first workable Time-of-Flight (T-O-F) Mass Spectrometer. The mass resolution of their device was very poor, but their work encouraged further study of the technique, which has now become well established in the field of mass spectroscopy. The most important general developments were due to Katzenstein and Friedland[116], and Wiley and McLaren[117].

3. 2.b. Operating Principles of a T-O-F Mass Spectrometer(T.O.F.M.S.).

The mass of the ion is determined from the time it takes to travel a known distance under known conditions of acceleration. The essential features of such an instrument (figure 20) are :-

1) An ion source region, ionisation being achieved either by an electron or a photon beam.

2) An ion accelerating region.

3) A field-free drift tube.

4) A detector, amplification, and display system.

Either the ionising beam, or the accelerating voltage must be pulsed, or both. The resulting accelerated ions of different masses

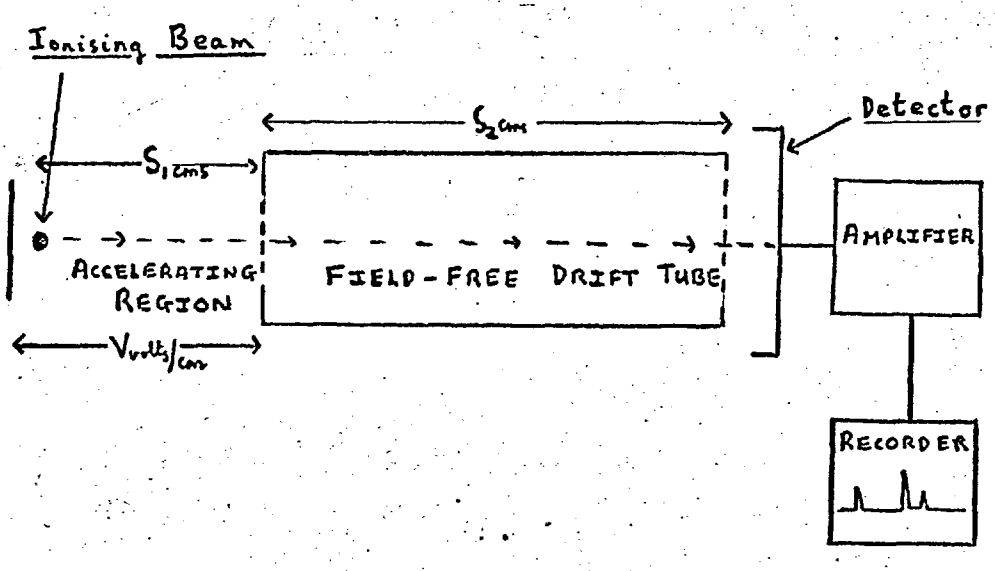

FIG. 20

ESSENTIAL FEATURES OF A T.O.F. MASS SPECTROMETER

will take different times to reach the end of the tube, the low mass ones being detected first. The output signal after amplification may be fed to an oscilloscope, or, by suitable gating techniques, to a recording system. The oscilloscope display represents the whole mass spectrum produced by the ionising beam. The time of transit can be measured directly from the oscilloscope, and the corresponding mass of that ion found. Assuming equality of response of the detecting system to all masses (i.e. velocities), the ion abundances may be estimated from the area under the peaks.

If the ionising beam is pulsed, two methods of mass analysis may be adopted which are generally termed The Constant Ion Energy condition, and The Constant Ion Momentum condition.

Constant Ion Energy. A steady ion accelerating potential, V volts/cm, is applied until the ion reaches the field-free drift-tube.

Now from the equations :-

$$P = mf = Ve \quad \ldots\ldots\ldots\ldots\ldots\ldots\ldots\ldots 1$$

$$v^2 - u^2 = 2fs \quad \ldots\ldots\ldots\ldots\ldots\ldots\ldots\ldots 2$$

where P = force applied, v = final velocity of ion

m = mass of the ion, u = initial velocity of ion

e = electronic charge, f = acceleration of ion

we get :- $\frac{1}{2} mv = Ves \quad \ldots\ldots\ldots\ldots\ldots\ldots\ldots\ldots 3$

i.e. all the ions leaving the accelerating region have the same K.E. Hence Constant Ion Energy.

Using Newton's Equations of Motion, it can be shown that :-

$$T = t_1 + t_2 = \left(\frac{m}{e}\right)^{\frac{1}{2}} \left[\left(\frac{2s_1}{V}\right)^{\frac{1}{2}} + \left(\frac{s_2}{2Vs_1}\right)^{\frac{1}{2}} \right] \quad \ldots\ldots\ldots\ldots\ldots\ldots 4$$

where T = total time-of-flight of ion

t_1 = time of acceleration

t_2 = time-of-flight down drift tube

s_1 = length of accelerating region

s_2 = length of drift tube.

As can be seen $m \propto T^2$, and the mass scale is a square-root one.

Space Focusing Condition. The bunch of ions formed in the ion source will have a finite width, and so ions at different positions in the bunch will be accelerated over different distances.

Consider an ion starting at a position $s_1 + \Delta s_1$ from the field-free drift tube.

$$t_1 + \Delta t_1 > t_1$$

$$v + \Delta v > v$$

$$\therefore \quad t_2 + \Delta t_2 < t_2$$

For a re-focusing effect,

$$t_1 + t_2 = (t_1 + \Delta t_1) + (t_2 + \Delta t_2)$$

i.e. T remains unchanged, therefore $\frac{dT}{ds_1} = 0$ and $\underline{\underline{s_2 = 2 s_1}}$

This is known as the space focusing condition.

Constant Ion Momentum. In this mode of operation an accelerating pulse of width, t, and voltage V, is applied to the ions. Thus all ions are accelerated for the same time, but over different distances. It can be shown that.

$$\underline{\underline{mv = Vte}} \quad \ldots\ldots\ldots\ldots\ldots\ldots\ldots\ldots 5$$

Thus ions of all masses have a constant momentum. The Total time-of-flight, T, of the ions is given by :-

$$T = \frac{m}{e}\frac{(s_1+s_2)}{Vt} + \frac{t}{2} \quad \text{.....6}$$

and the mass scale is in this case linear.

3. 2.c. Advantages and Disadvantages of a T O F M S

Advantages :- 1) An entire spectrum is obtained for each accelerating pulse, and the whole spectrum may be displayed. A conventional spectrometer detects only one mass peak at a time.

2) The operation depends upon the electronics of the system, rather than stable magnetic fields and mechanical alignments.

3) A T O F M S has a higher transmission than a conventional spectrometer, and also discriminates less against ions possessing K.E.

4) A T O F M S should be very suitable, by its pulsed nature, for studying the K.E. of fragments and processes occuring over the range 10^{-7} - 10^{-2} sec. after ionisation.

Disadvantages :- The overriding disadvantage is poor resolution. Resolution is defined as $\frac{M}{\Delta M}$, which equals $\frac{T}{\Delta T}$ for constant momentum conditions.

A value of $\frac{M}{\Delta M} = 300$ is the maximum that can be obtained, which is very poor compared to the values of 25000 obtainable with conventional spectrometers.

3. 3. Design and Construction of a T O F M S with a Vacuum Ultraviolet ionising source

The original form of the present apparatus was designed and constructed by M.A. Hourieh and D.W. Turner, and a full description is given in reference 118, together with the preliminary results obtained using it.

3. 3.A. Vacuum Ultraviolet Monochromator and Light Source

The ionising source is a photon beam, supplied from a flashing gas discharge light source via a monochromator.

3. 3.A.(a) Optical Design of Monochromator. The monochromator was of the normal incidence type, using a Bausch and Lamb precision 0 ·99454 meter concave grating. It was a "tripartate" blazed grating, ruled at 600 lines/mm., with its highest efficiency at 1500 Å in the first order, 750 Å in the second order.

The scanning mechanism (shown in figure 21) consisted of a simple rotary motion about the vertical axis of the grating, coupled with a fine translation along the axis bisecting the entrance and exit slits of the monochromator. The grating and slits were mounted on the Rowland Circle, the translatory motion keeping the exit slit in good focus. The whole system was enclosed in a brass tube, and the scanning mechanism was driven by a geared down electric motor driving a shaft through an O-ring seal.

From figures 21 and 22 it can be shown that [118] :-

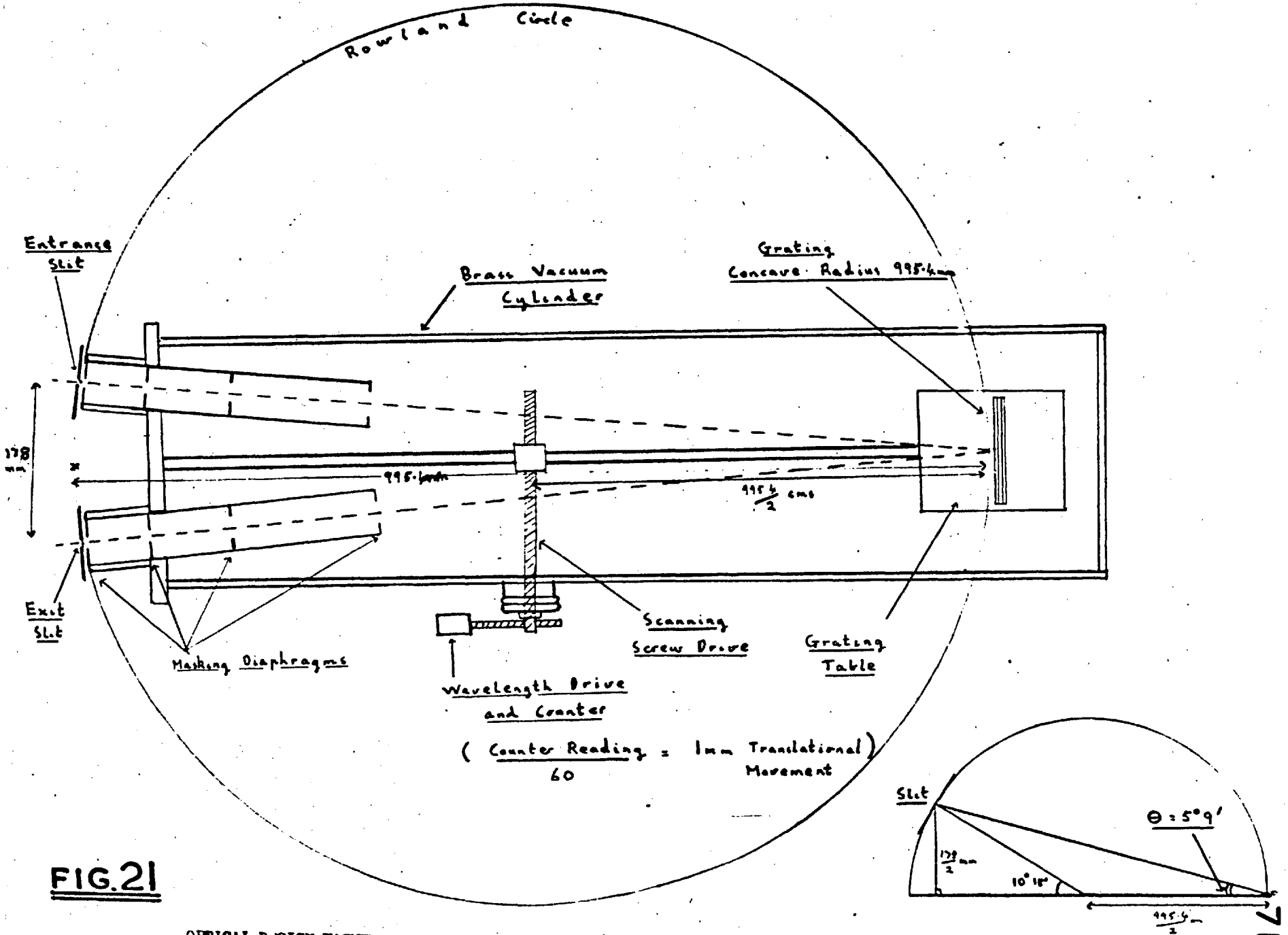

FIG.21

OPTICAL DESIGN VACUUM MONOCHROMATOR

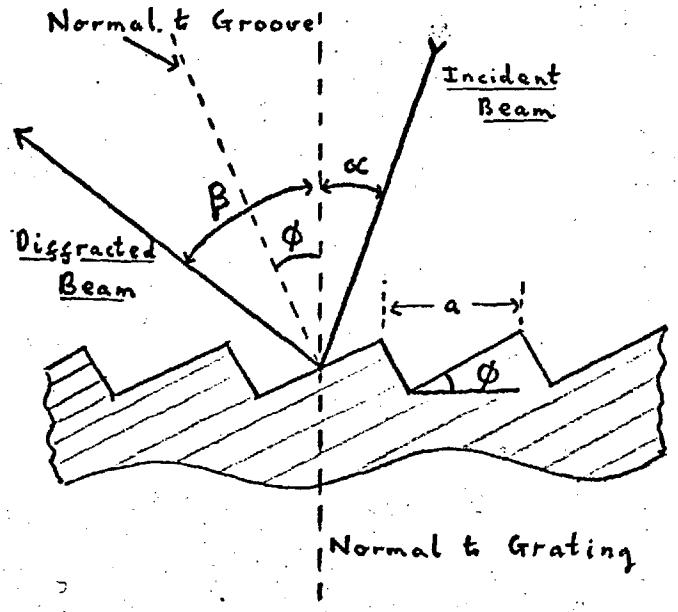

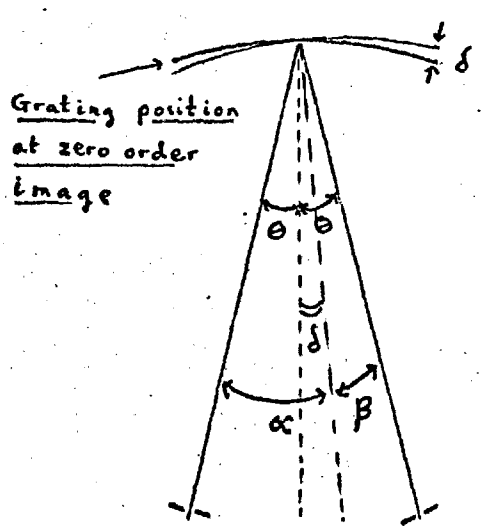

α = angle of incidence

β = angle of diffraction

φ = Blaze angle

a = Grating spacing $\frac{1}{600}$ cms.

δ = angle of rotation

FIG.22

OPERATION OF THE DIFFRACTION GRATING

$$n \lambda_{\text{Å}}^{\circ} = 1.112\ N \qquad \ldots\ldots\ldots\ldots\ldots\ldots\ 7$$

where n = spectral order of grating

$\lambda_{\text{Å}}^{\circ}$ = wavelength of diffracted light passing through the exit slit

N = Counter number of scanning drive motor (0 at zero order position)

The two slit assemblies were bolted (O-ring seals) to the end of the main cylinder in a number of sections, enabling easy dismantling. Secondary masking diaphragms were used to reduce stray light and reflections. The slit widths can be adjusted by a micrometer through a range of ·01 mm to 1 mm

3.3.A (b) The Light Source. A triggered capacitor discharge source, which was used for all the work done on the apparatus in this thesis, was one of the two originally designed to be used in the apparatus [118].

Gaseous flash discharges have been used for many years in photolysis studies [119], and in work on short lived species [120], but it is only within the last ten years that they have been developed for use below 1600 Å [121]. The source described here is similar to one described by Weissler et Al [80].

The construction and triggering arrangements of the discharge tube are shown in figure 23 (a). The gas pressure required for stable operation was approximately 200 microns, and the power dissipated ·18 joule per flash. The repetition frequency was approximately 20 cycles/sec, and the duration of the light flash was approximately ·25 μsec. The discharge gas was introduced through a capillary section to prevent

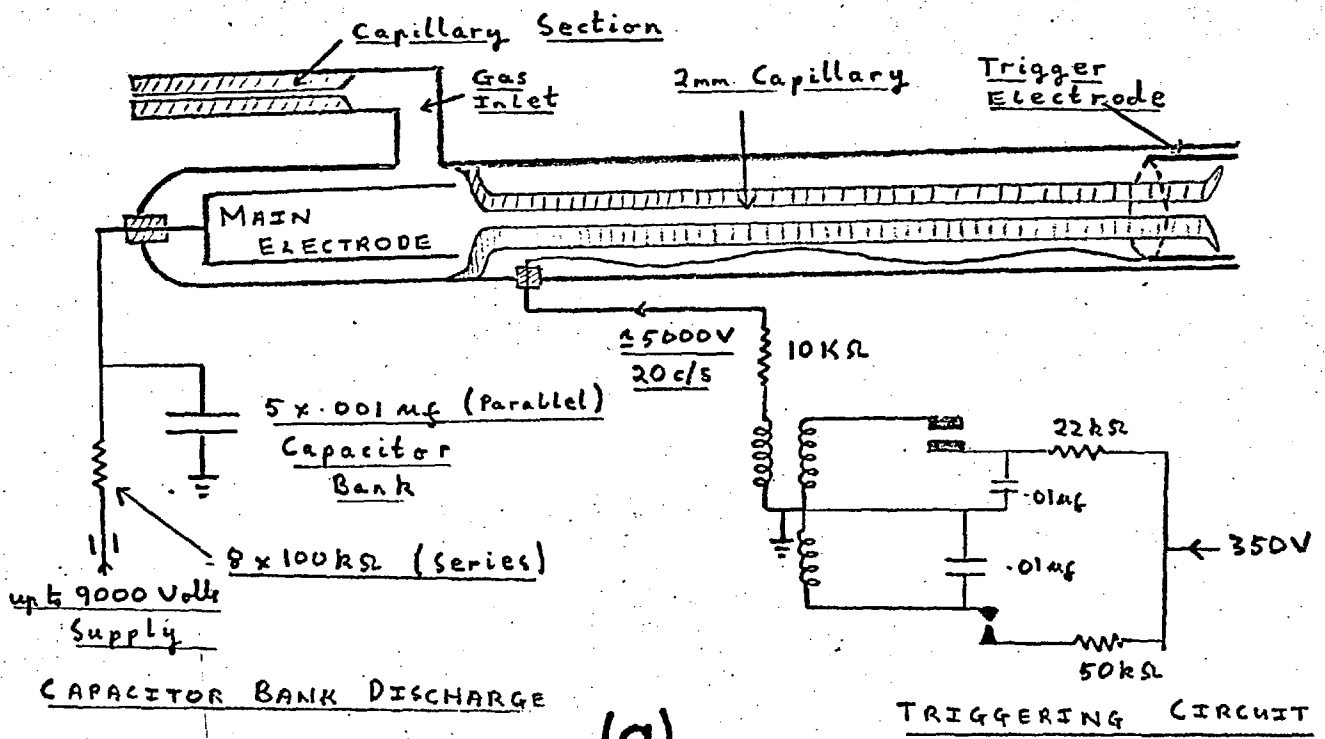

(a)

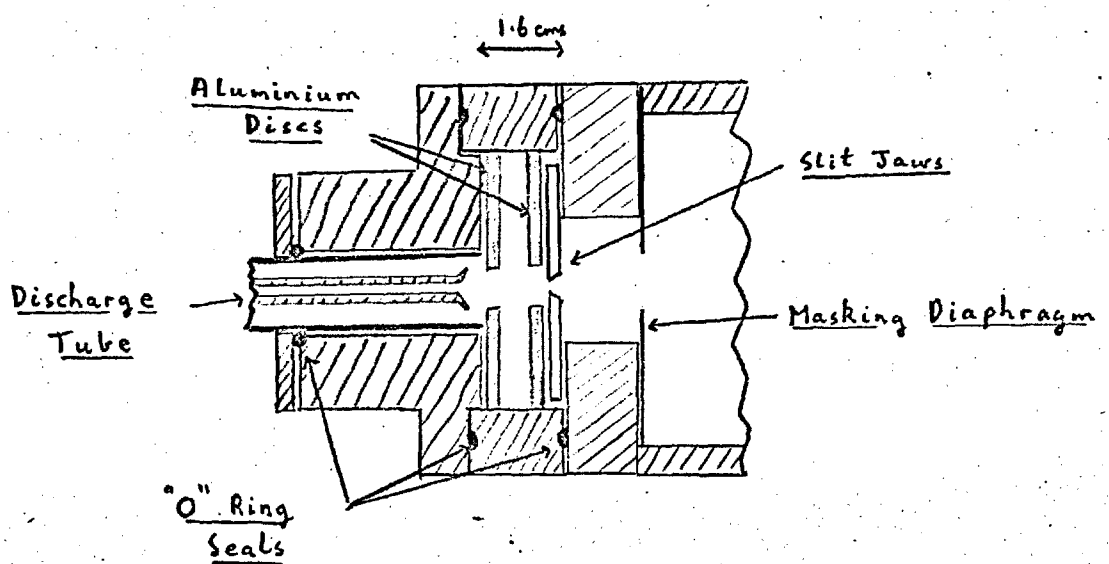

(b)

FIG.23 (a)— CAPACITOR DISCHARGE LIGHT SOURCE AND ORIGINAL TRIGGERING CIRCUIT

(b)— SECTION THROUGH DISCHARGE AND SLIT ASSEMBLY

the discharge striking back down the gas line. The discharge tube was separated from the entrance slit by two aluminium diaphragms, the first of which acted as the ground electrode for the discharge (figure 23 (b)).

3. 3.A(c) Detection. The ultra-Violet detector used was a photonmultiplier (E.M.I. 6256B), with its end window coated with a fine layer of sodium salicylate. It could be placed directly after the exit slit, or, in operation with the T O F M S, after the ionisation chamber (figure 24). Amplification and recording were achieved as in figure 28 to give a spectrum of the intensity of U.V. light against wavelength.

3. 3.A(d) Pumping System. A block diagram of the original system is shown in figure 25. A pressure of 10^{-6} torr could be maintained in the main chamber when no gas was flowing. The fast pumping and subsiduary diaphragm systems enabled a pressure of 5×10^{-5} torr to be maintained in the main chamber when the light source gas was flowing (200 microns). A pressure of several microns of target gas in the T O F M S section did not cause an increase of the pressure in the main chamber.

3. 3.B. T O F M S Section

3.3.B(a) Ionisation Chamber and Drift Tube (figure 25). The chamber consisted of a small brass chamber placed behind the exit slit of the

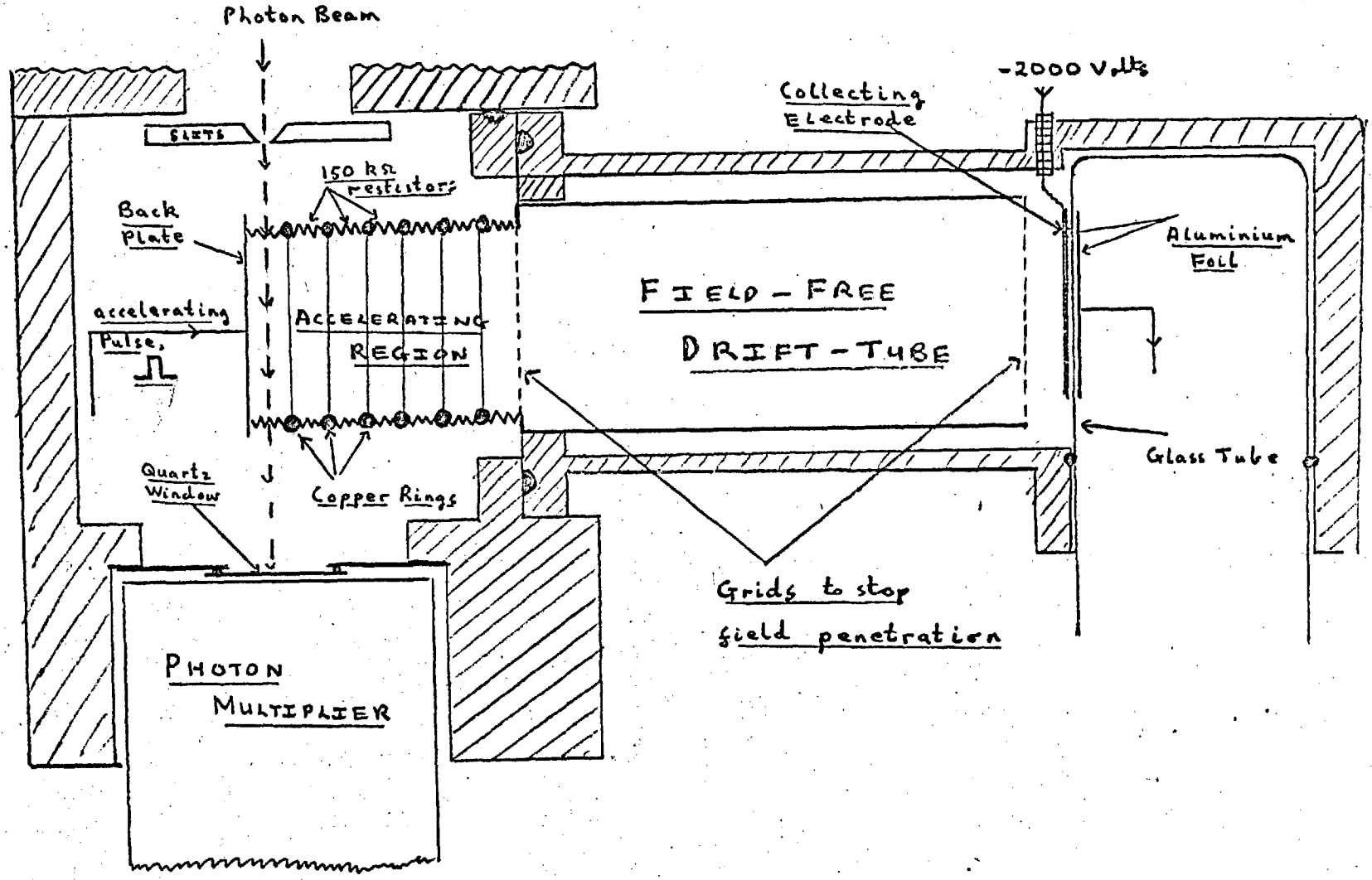

FIG.24

VERTICAL SECTION THROUGH THE ORIGINAL VERSION OF THE T.O.F.M.S. — ACTUAL SIZE

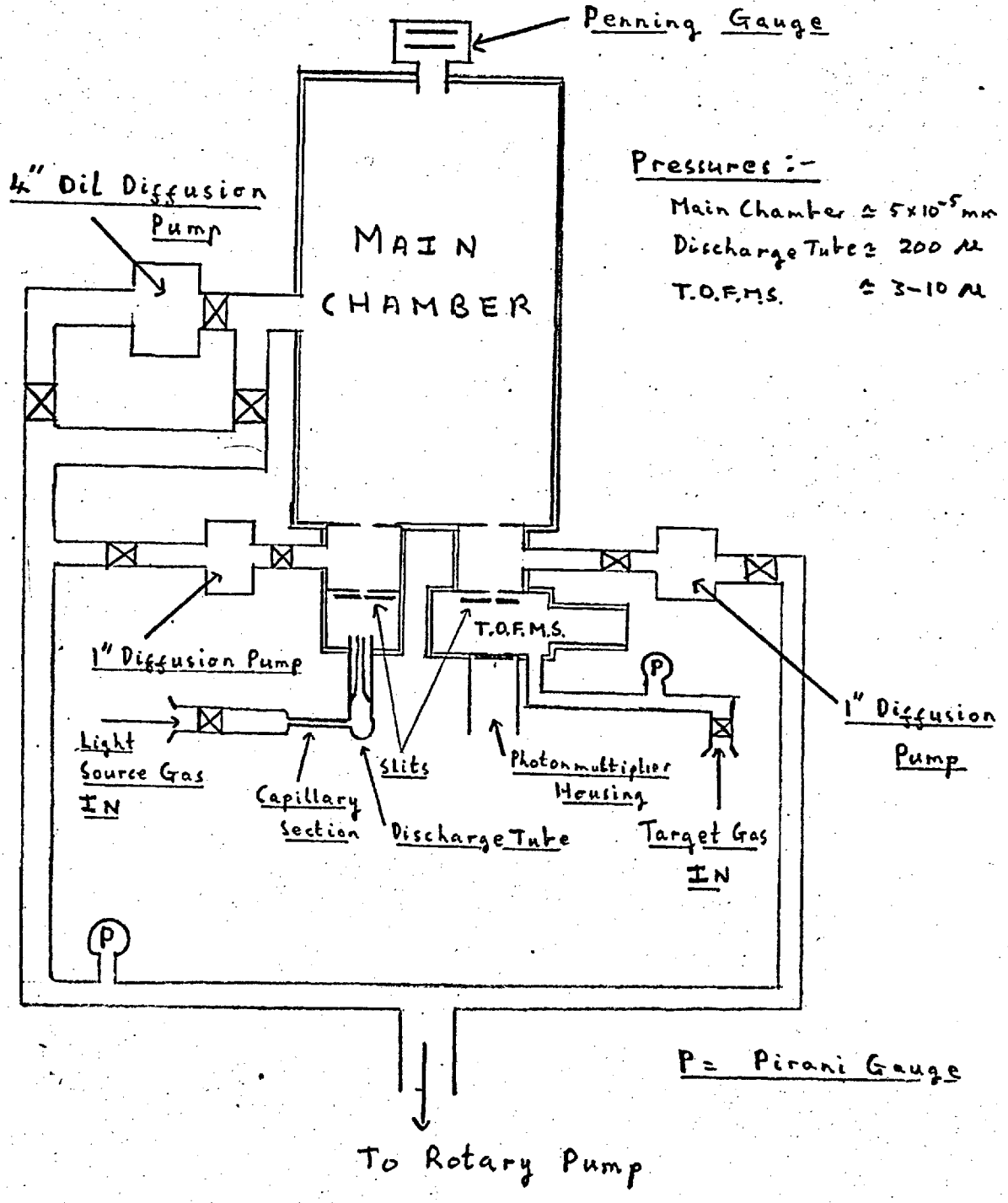

FIG. 25

PUMPING SYSTEM OF THE MONOCHROMATOR AND T.O.F.M.S. APPARATUS

monochromator. It contained the ion accelerating region which was formed by a repeller plate and some rectangular copper rings separated from each other by 300 K Ω resistors. Ionisation occured along the photon beam which passed 3-4 mm in front of the repeller plate. Acceleration of the ions towards the drift tube was achieved either by applying a pulse (constant momentum), or a steady voltage (constant energy) to the repeller plate and ring assembly. In the case of pulse acceleration, the pulse could be applied simultaneously with ionisation or after a time delay. The circuitry supplying the pulse is shown in figure 26. The Drift Tube was separated from the accelerating region and the detector by fine wire mesh grids to help define the field-free region.

3. 3.B(b) Detection and display region of ion signal. Detection was performed by a simple capacitance arrangement (figures 25 and 27) consisting of two aluminium foils on either side of a glass tube. An integrated spectrum was obtained, which was amplified and differentiated as shown in figure 27, and finally displayed on an oscilloscope. Measurements were made directly from the oscilloscope, or from photographs of the oscilloscope trace.

A block diagram of the complete apparatus, showing connections to all the associated electronic circuitry is given in figure 28.

3. 4 Limitations in Performance of the Original Spectrometer

(a) Resolution. A typical spectrum of acetone under constant

momentum conditions is shown in figure 29. As can be seen the resolution is very poor, the peak at 58 a.m.u. only just being separated from that at 43 a.m.u.

(b) Noise Level. The general noise/signal ratio was quite high and for the portion of the spectrum up to approximately 30 a.m.u. it was so high that small peaks would not be detected.

(c) Signal Intensity was low. It was estimated[118] that 6×10^3 ions per pulse were needed for detection. High target gas pressures were required for reasonable signal intensity.

(d) Mass Range. It was found that under constant momentum conditions the $m \propto T$ relation was not obeyed above 70 a.m.u., where the ion peaks became very broad.

(e) Instrumental Effects. Some of the results obtained using the apparatus[118] have since been found to be erroneous and due to instrumental defficiences (see Results section 5.5).

(f) The spectra could not be recorded directly but had to be photographed on an oscilloscope screen.

(g) Target Gas Pressures. The target gas pressures used were high (approximately 5 microns), with the resulting possibility of ion molecule collisions occuring.

3. 5 Improvements made in the Design and Construction of the Mass Spectrometer.

Many changes in the original design have been made in an attempt to increase the resolution, sensitivity, and reliability of the apparatus.

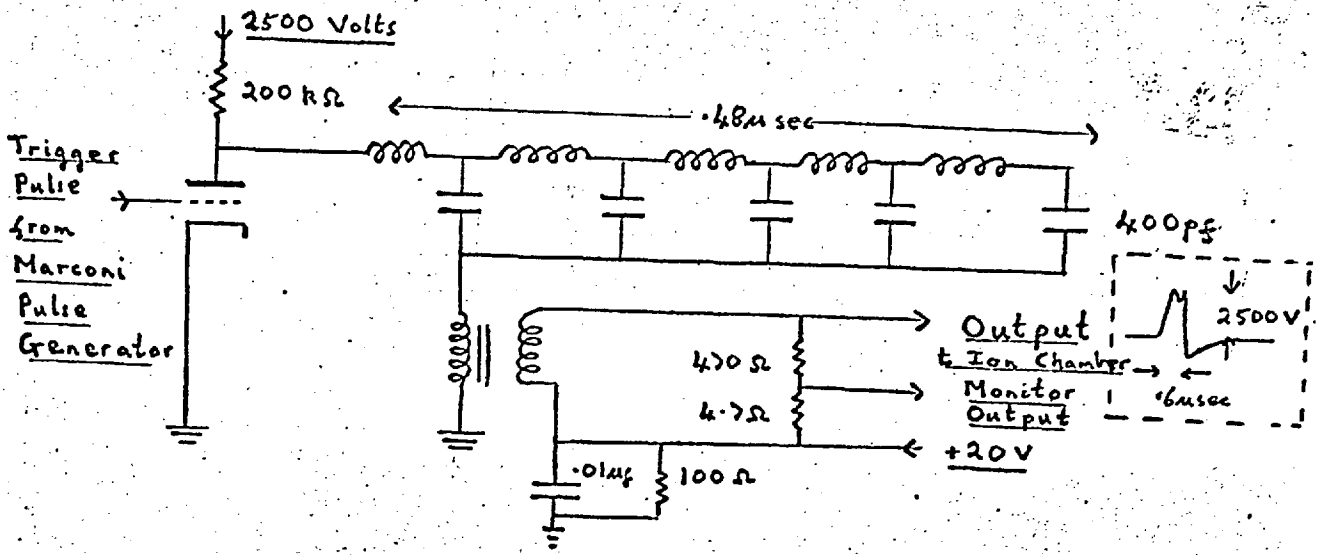

FIG.26 CIRCUIT DIAGRAM OF THE ION ACCELERATING PULSE GENERATOR ——ORIGINAL VERSION

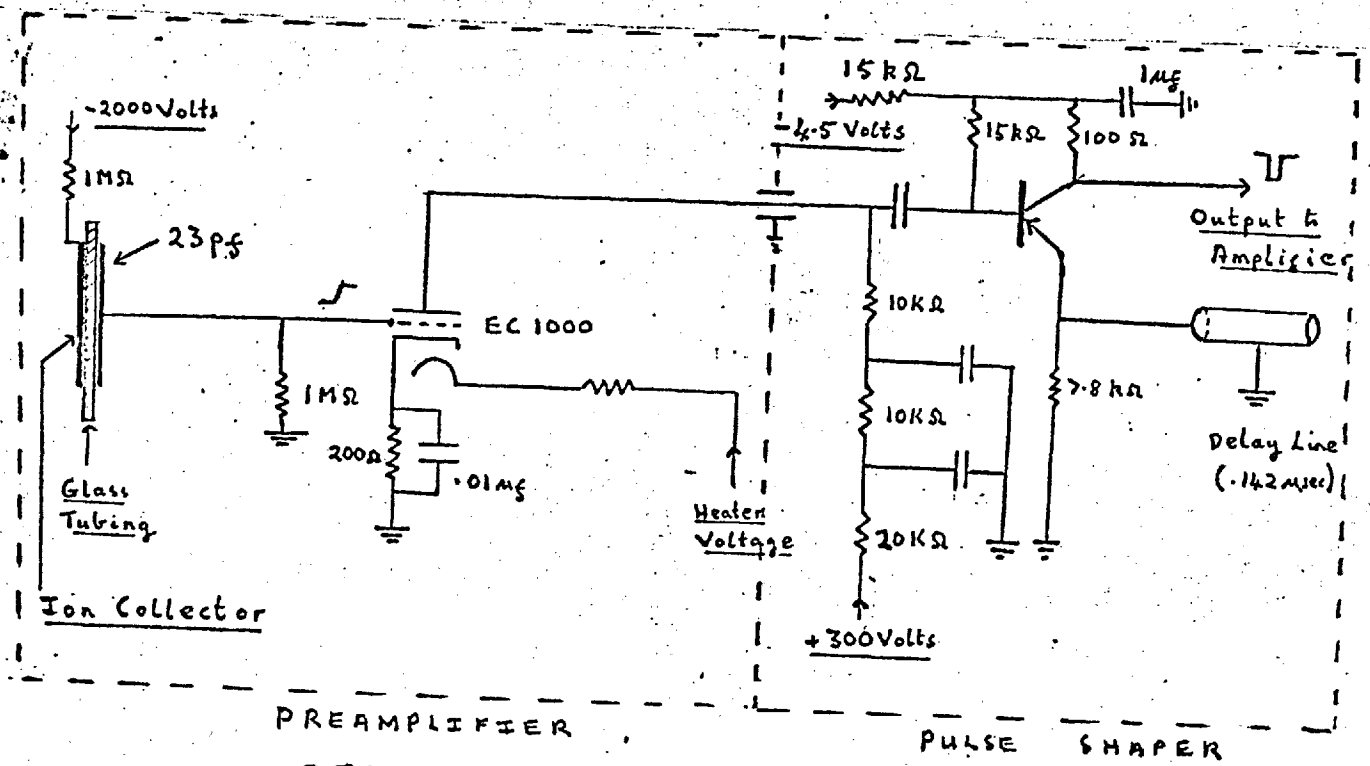

FIG.27 CIRCUIT DIAGRAM OF THE PRE-AMPLIFIER AND PULSE SHAPING UNIT OF THE ION DETECTION AND DISPLAY SYSTEM——ORIGINAL VERSION

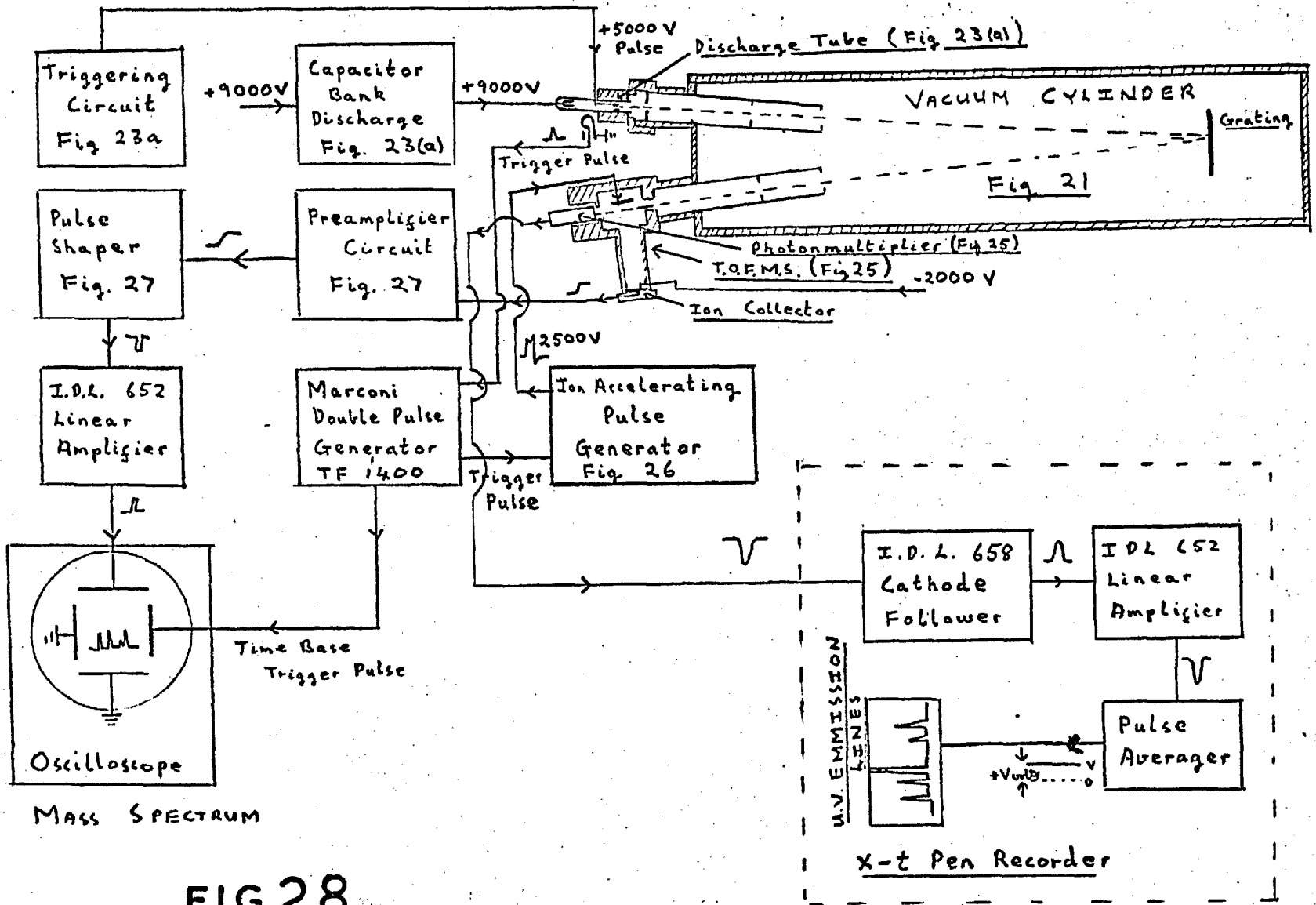

FIG.28

BLOCK DIAGRAM OF VACUUM U.V. T.O.F.M.S. SPECTROMETER COMBINATION and ASSOCIATED ELECTRONIC CIRCUITRY

FIG. 29 (a)

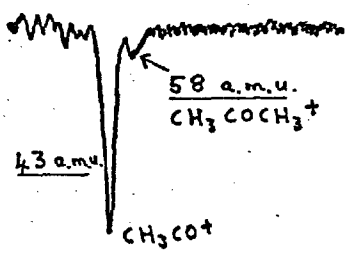

Oscillogram of the mass specrum of acetone using an impacting photon beam of energy 14.89 eV.
— Constant Momentum condition,
Original version of T.O.F.M.S.

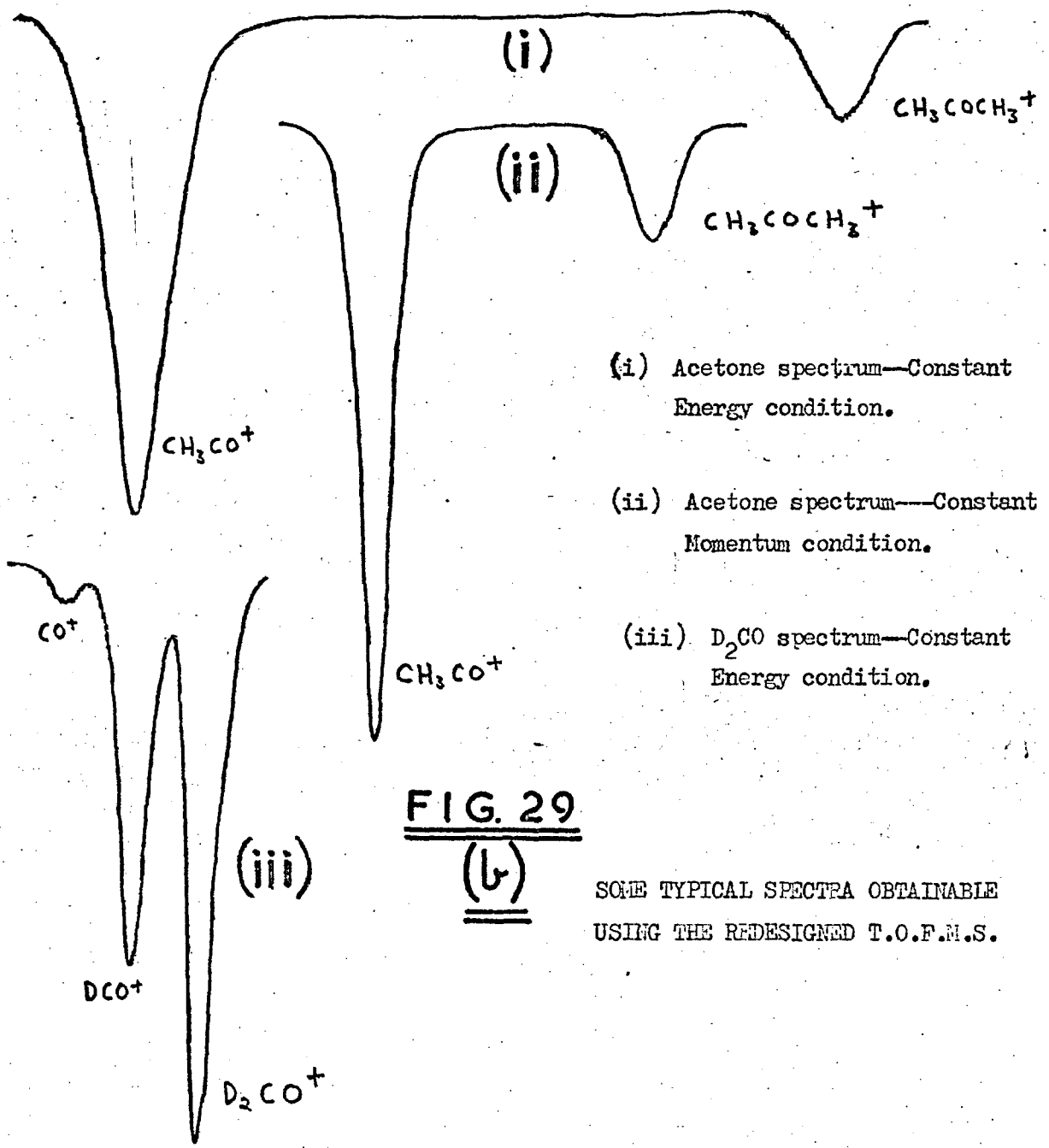

(i) Acetone spectrum—Constant Energy condition.

(ii) Acetone spectrum—Constant Momentum condition.

(iii) D_2CO spectrum—Constant Energy condition.

FIG. 29 (b)

SOME TYPICAL SPECTRA OBTAINABLE USING THE REDESIGNED T.O.F.M.S.

3. 5.A. Vacuum Monochromator and Light source section.

The original triggering circuit (figure 23(a)) of the light source had the disadvantage that it ran at the relaxation frequency of the relay which could not be controlled, and was not completely regular. The circuit also generated noise which was picked up in the ion signal amplification and recording stages (see section 3. 5.B.), making reliable recording impossible. A more sophisticated circuit was constructed (figure 30) enabling the frequency of discharge to be varied. The noise generated was suppressed by isolating the relay section of the triggering circuit in a screened container with suitable noise filtering systems on the input leads, and by synchronising the initial multivibrator in the circuit with mains frequency by tying the grid of the E C C 83 valve to the heater circuit through a .001 capacitor. The repetition frequency of the triggering circuit was thus locked to $50/4$ cycles per second.

The lightsource itself was left unchanged as it was found that several design alterations only worsened its performance. The vacuum monochromator likewise remaind unmodified, apart from a re-alignment of the optics.

3. 5.B. T O F M S Section

Virtually the whole section has been re-designed.

3. 5.B.(a) Re-construction of the Accelerating Region and Drift Tube.

Figure 31 shows the final rebuilt form. The geometry of the

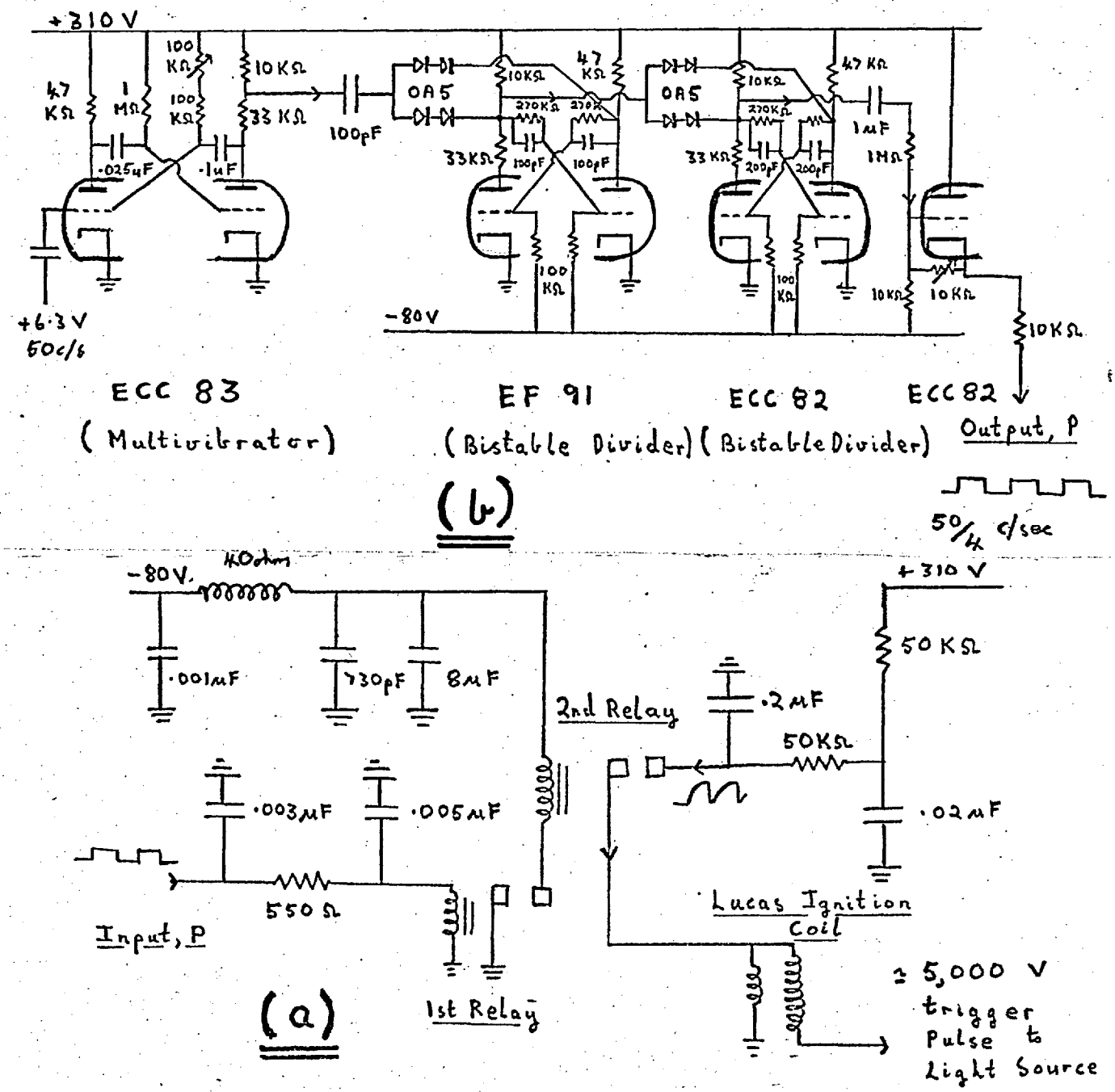

(a)—REDESIGNED LIGHT SOURCE TRIGGER CIRCUIT
50/4 CYCLES PER SEC. OUTPUT.

FIG.30

(b)—SQUARE WAVE GENERATOR AND DIVIDER CIRCUIT
56/4 cycles sec output triggers 1st relay
in the trigger circuit above.

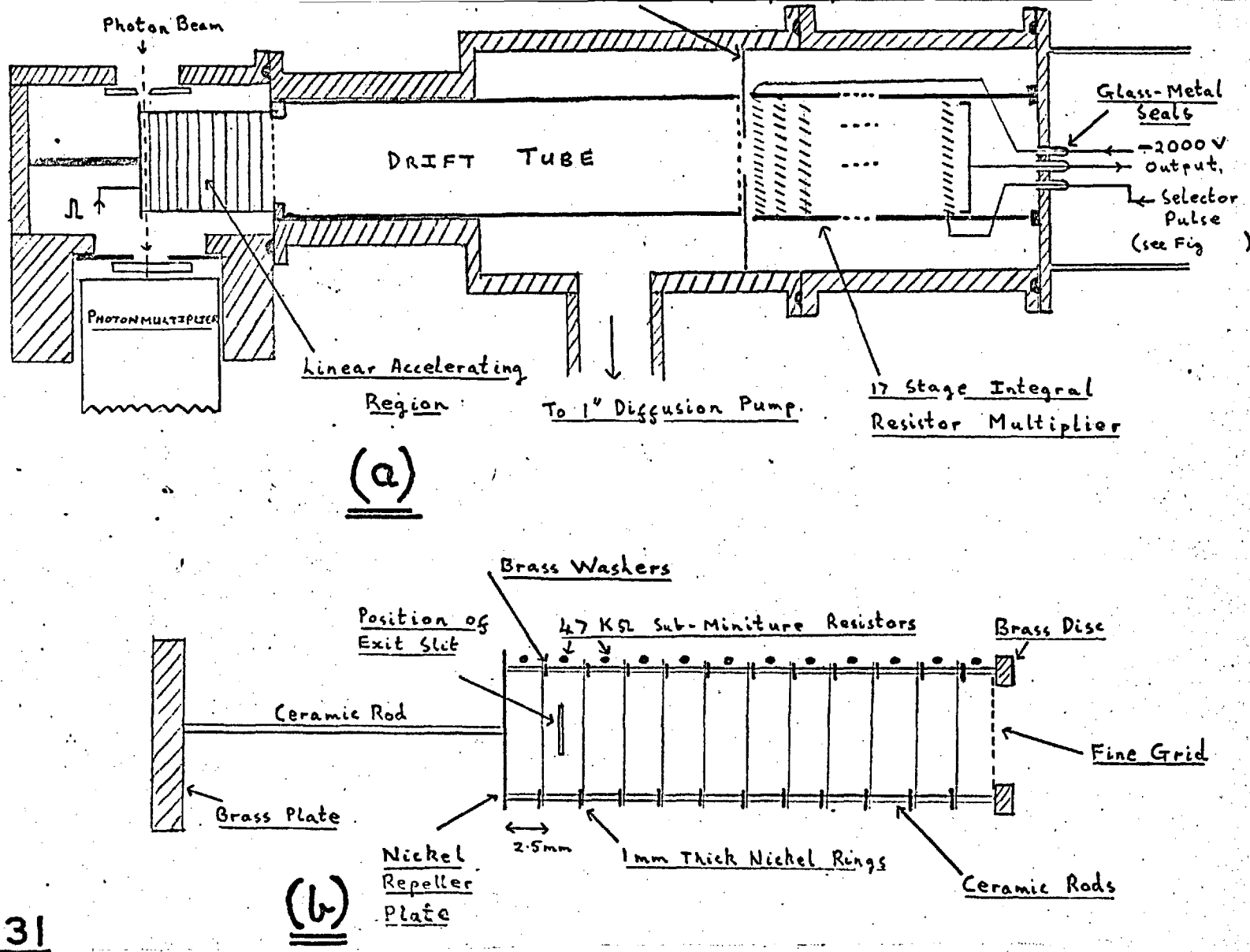

FIG. 31

(a)–VERTICAL SECTON THROUGH THE RECONSTRUCTED T.OF.M.S. —— HALF ACTUAL SIZE

(b)–EXPANDED SECTON OF THE LINEAR ACCELERATING REGION

accelerating region was improved considerably to provide a more uniform accelerating field, and the whole ionisation chamber was coated with soot from a benzene/coal gas flame to reduce light reflection and the formation of photoelectrons by impact of the photon beam on the metal surfaces. The drift tube was lengthened to provide a longer ion time-of-flight. This was necessary because it was found that the mass resolution was being limited with a shorter flight-path (see section 3. 5.B.(b) and (c)).

Detection was performed by an electron multiplier allowing a far greater sensitivity than in the original capacitance type detector.

An additional 1 inch diffusion pump was added to the field-free drift tube section, and a Penning gauge fitted to the ionisation chamber so that the target pressure could be accurately monitored.

3. 5.B.(b) Amplification and Recording System One of the major faults with the original apparatus was that a spectrum could only be recorded by photographing the oscilloscope trace. Also the action of the signal pulse shaping circuit (figure 27), and amplification by the main amplifier and the oscilloscope broaden the signal pulses considerably, decreasing the resolution obtainable. A system was designed whereby the spectrum could be recorded on a pen recorder and in which any pulse broadening after detection did not affect the resolution. A gating circuit was used so that detection of the signal was suppressed except at the point in time, $0 + \Delta t$ when it coincided with a selector pulse (figure 32). The selector pulse scanned the

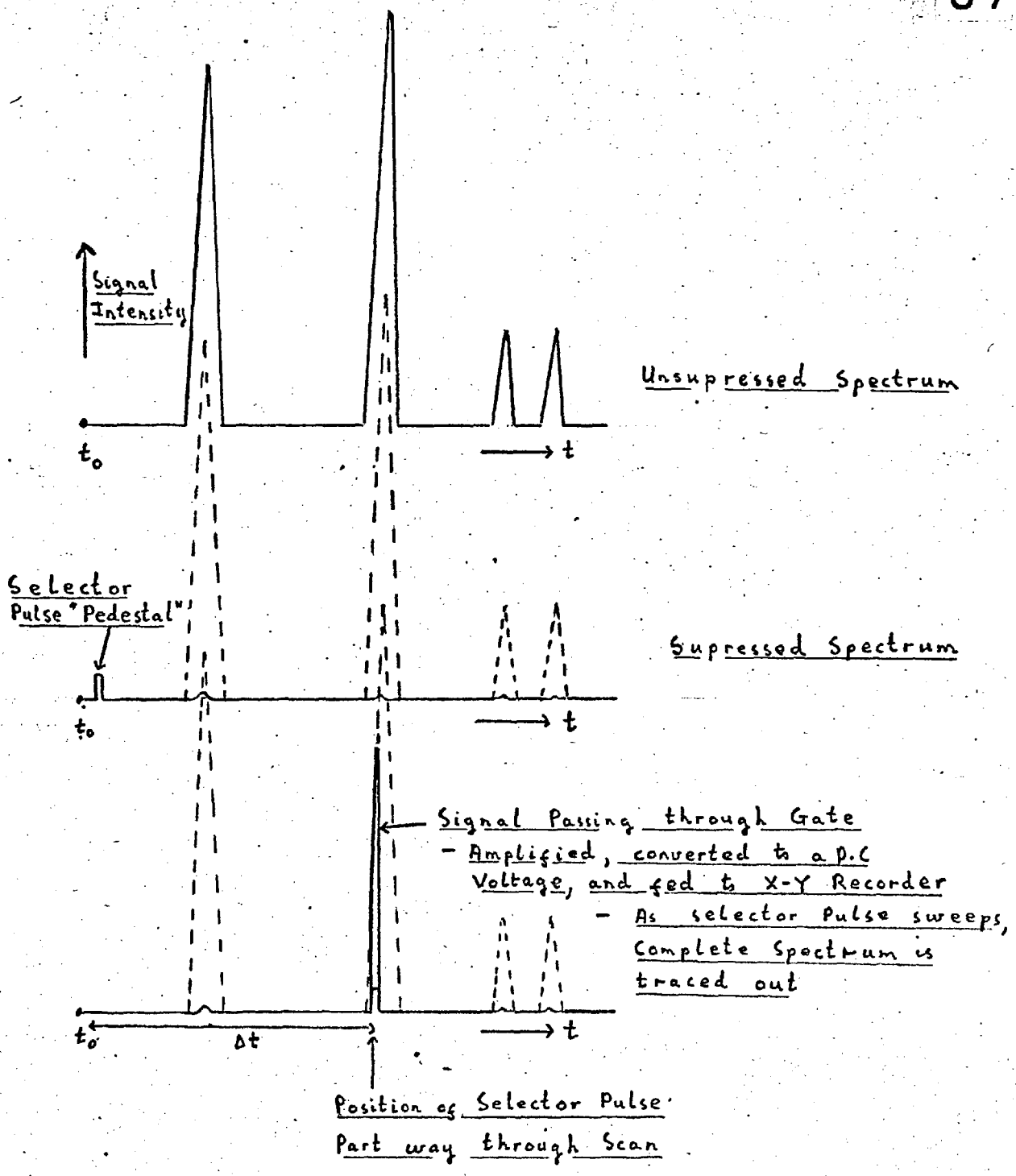

FIG. 32 OPERATION OF GATING SYSTEM ON THE HYPOTHETICAL SPECTRUM

spectrum, and the signal pulse detected was amplified, converted to a steady Voltage, and its amplitude recorded on an X - Y recorder. In this way a copy of the oscilloscope display was obtained on chart paper without the broadening due to shaping and amplification. The only thing which directly affected the resolution was the duration of the selector pulse. A signal shorter in duration than the selector pulse would be degraded.

The general technique of electronic tracing of repetetive oscilloscope displays is quite well established, and some specific examples of its use can be found in references 122 - 129.

Several systems of gating the signal after the multiplier were tried, the simplest and most successful being a single diode gate[126] (figure 33). Even this was not entirely suitable however, since the signal breakthrough at positions not in co-incidence with the selector pulse was too large and so was the Selector Pulse "pedestal" (see figure 32). It was abandoned in favour of gating the multiplier itself. Two methods were developed, the circuit diagrams of which are given in figure 34. The thyratron discharge system produced a slightly narrower selector pulse (·13 μsec) of greater voltage, and resulted in a better shaped selector pulse "pedestal", and so was preferred. There was little to choose between the two systems in terms of signal resolution.

Figure 29(b) shows some typical spectra obtainable using the re-designed spectrometer. Those of CH_3COCH_3 may be compared with the oscilloscope photograph obtained by Hourieh shown in figure 29(a).

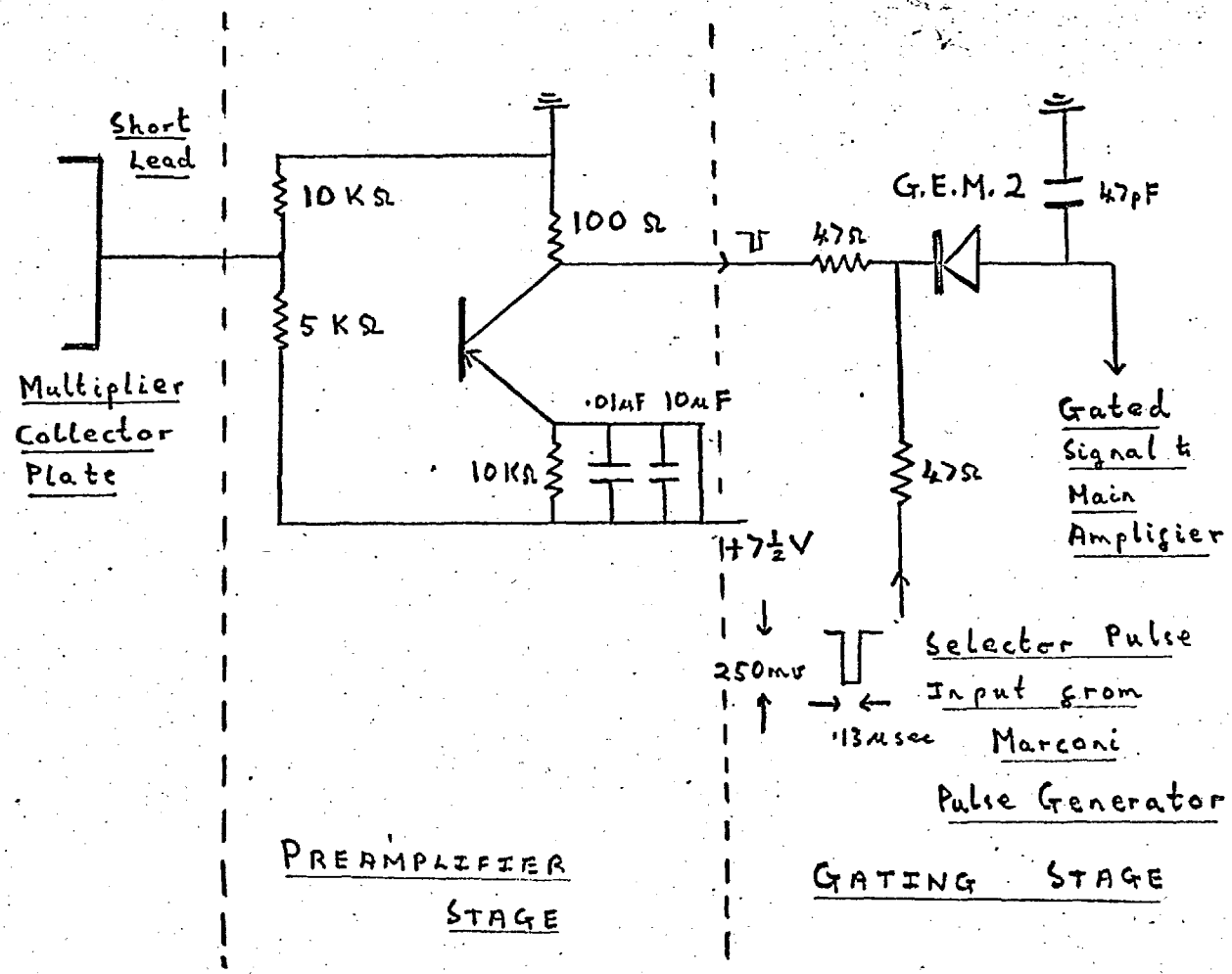

FIG. 33

SINGLE DIODE GATING SYSTEM
(cf. R. Sugarman Rev. Sci. Instr. 28 11 933)

— The back bias of the diode holds it open against the signal, but not the signal plus selector pulse.

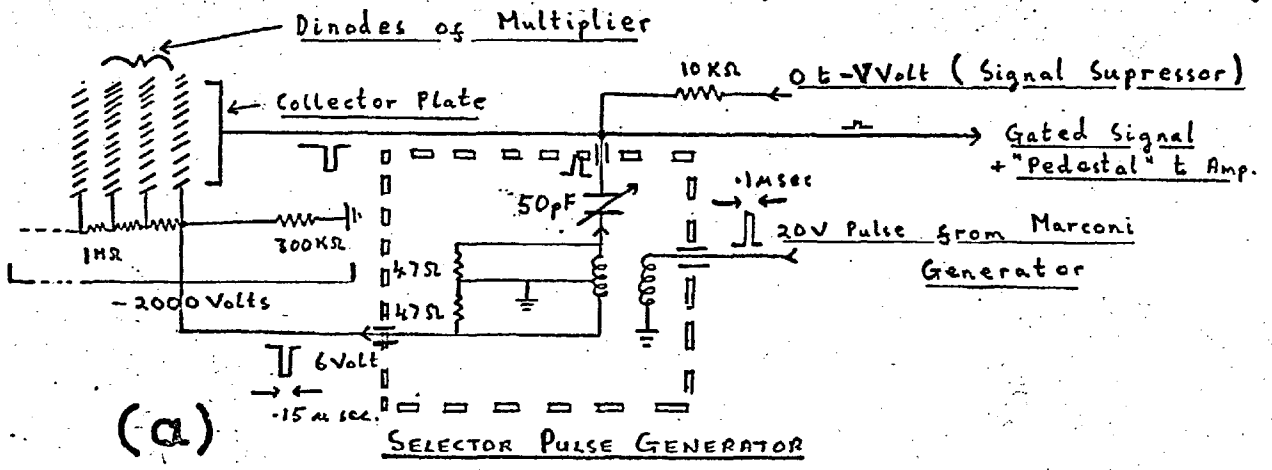

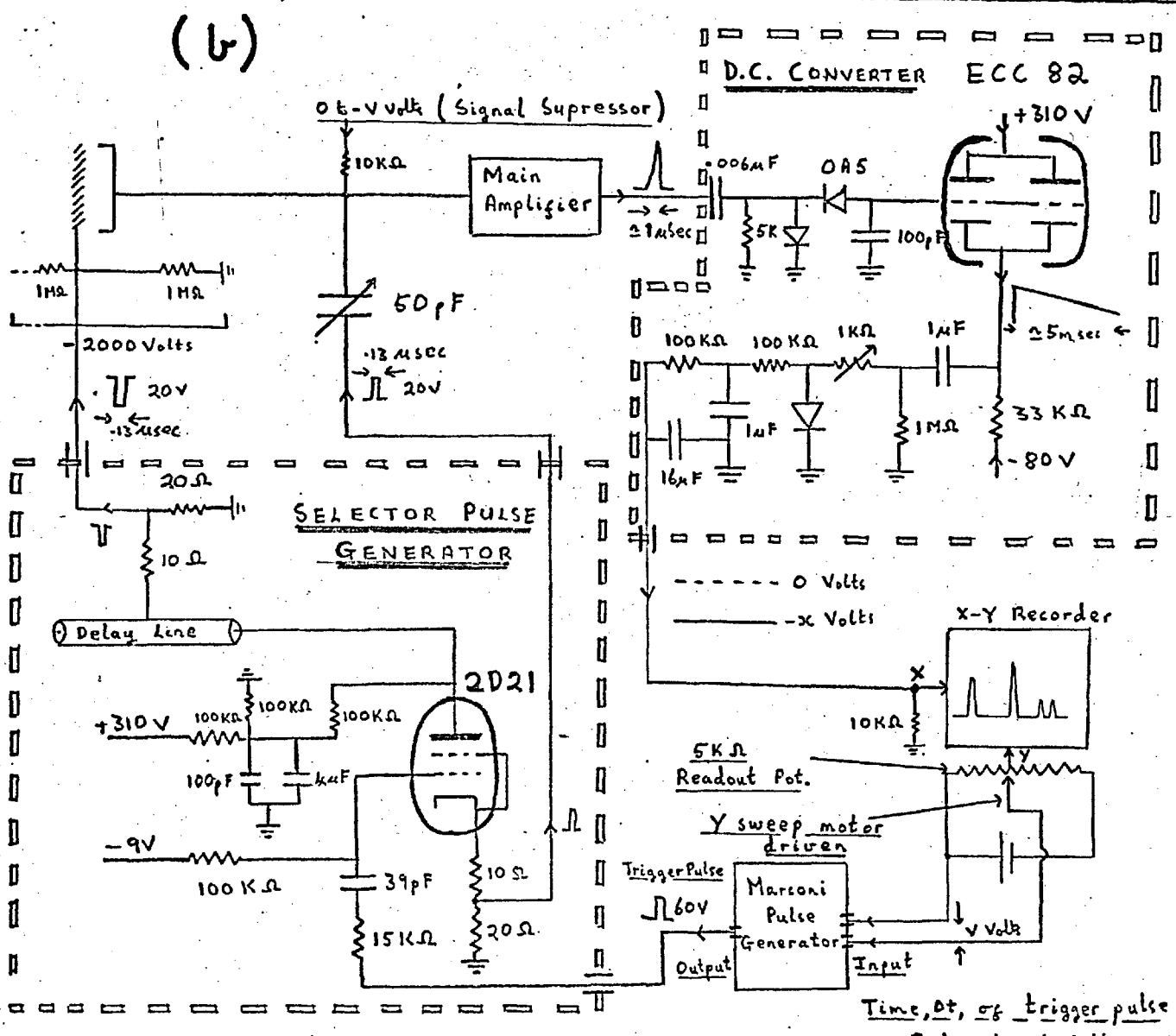

FIG. 34

(a)— ION GATING SYSTEM using TRANSFORMER PULSE GENERATOR.

(b)— GATING SYSTEM using THYRATRON DISCHARGE — Plus details of the recording system.

3. 5.B.(c) The ion accelerating Pulse (Constant Momentum Acceleration)

Although the resolution using the re-designed spectrometer was considerably improved compared to the original system, at high masses under constant momentum acceleration conditions, ion peaks were still broadened and occurred at a later time than would be expected for their masses. A typical spectrum of a mixture of Xenon and Krypton is shown in figure 35(a). This behaviour was found to be due to the poor shape of the positive accelerating pulse, which possessed a large negative tail (see figure 26). The circuit generating the pulse was modified from that shown in figure 26 to that shown in figure 36, and a much better pulse shape was obtained. In the resulting spectrum of the Xenon and Krypton mixture (figure 35 (b)) the peaks were of the correct shape and width and occurred at the predicted positions in the spectrum, showing that the scale was linear ($m \propto t$) up to a mass of at least 132 a.m.u.

As mentioned in section 3. 5.B.(b) with this method of detection and recording only the width of the selector pulse could degrade the mass resolution of the apparatus. Under constant momentum acceleration conditions, the flight times of the ions were short enough, and hence each mass peak narrow enough, for this to occur. By reducing the accelerating pulse height, the flight time of the ions was increased and the difficulty overcome. This is demonstrated in figure 37 where two spectra of a Nitrogen and Oxygen mixture are shown, one obtained with an accelerating pulse of 2KV, and one with 1KV. It can clearly be seen that the separation between the peaks has increased using a

FIG. 35

MASS SPECTRUM OF Xe/Kr MIXTURE
(a)— ORIGINAL ACCELERATING PULSE CIRCUIT.
(b)— MODIFIED ACCELERATING PULSE CIRCUIT.

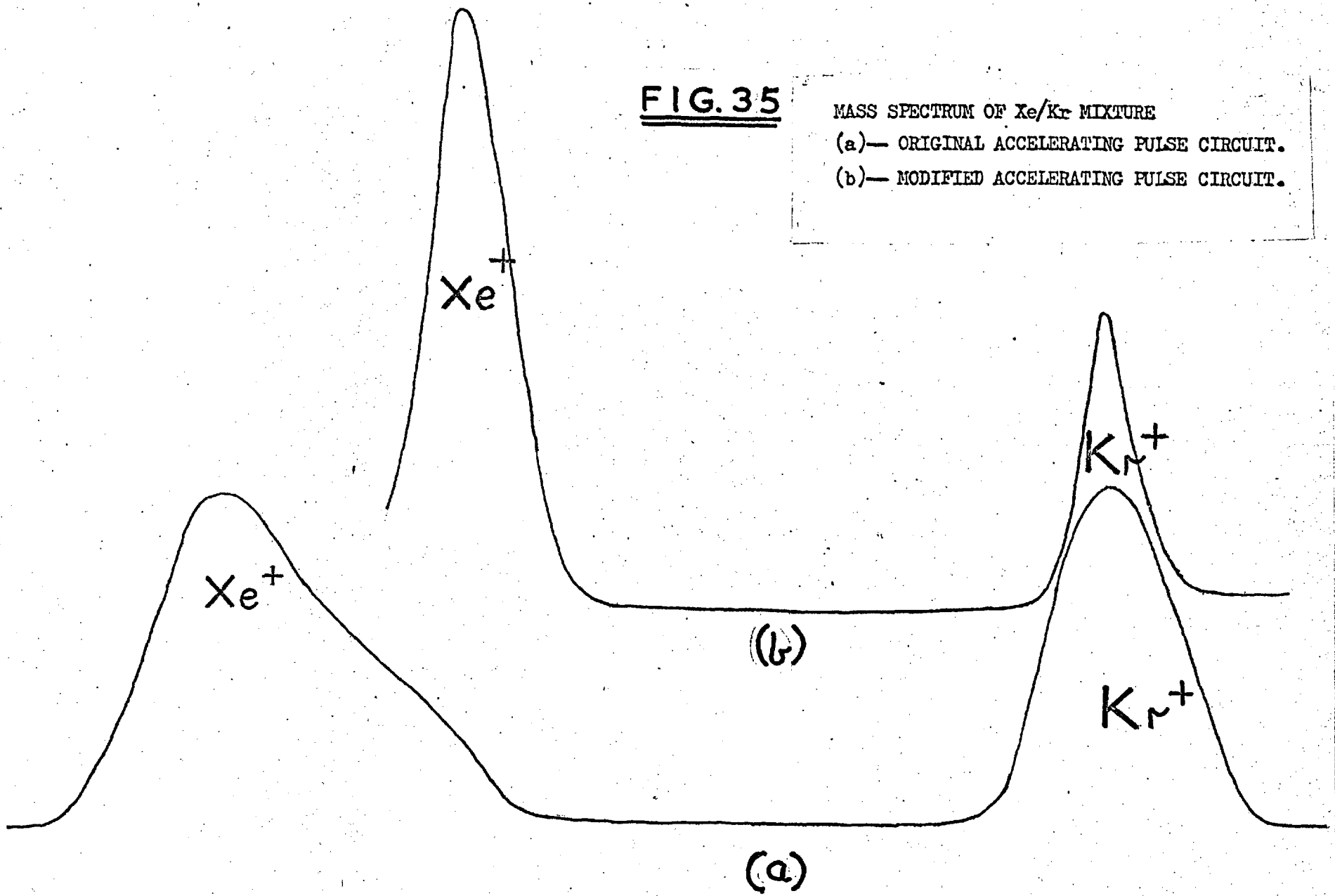

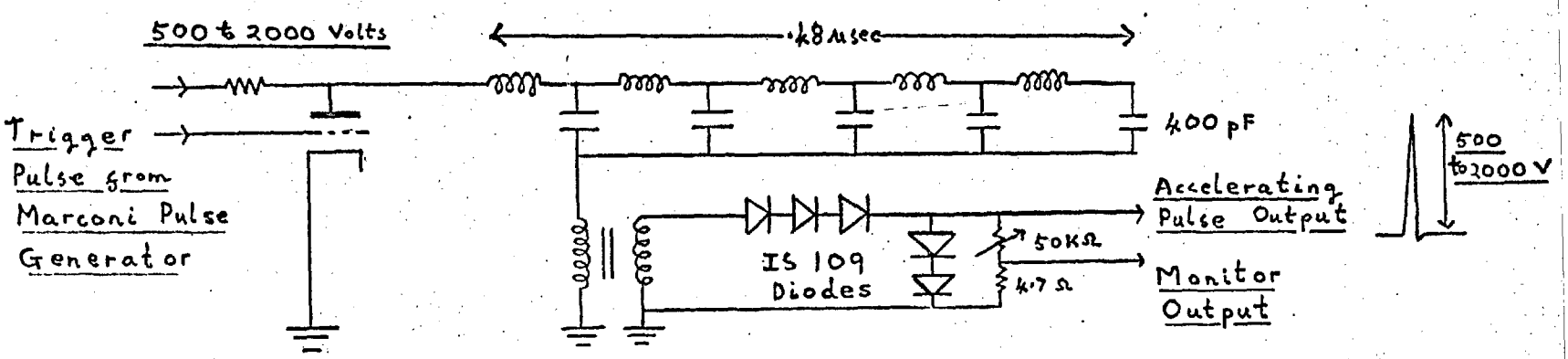

FIG. 36 MODIFIED CIRCUIT DIAGRAM OF ION ACCELERATING PULSE GENERATOR

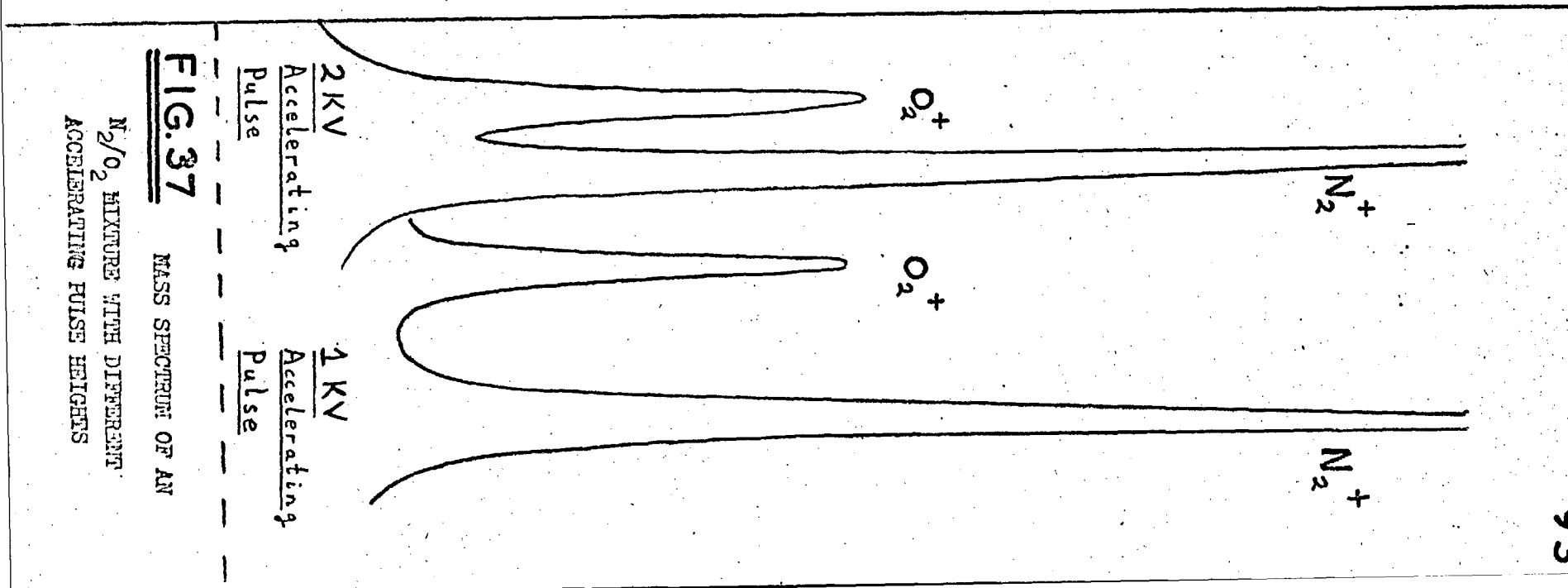

FIG. 37 MASS SPECTRUM OF AN N_2/O_2 MIXTURE WITH DIFFERENT ACCELERATING PULSE HEIGHTS

1 KV pulse, while the peak width remains unchanged.

3. 5.B.(d) Ion Accelerating Constant Voltage (Constant Energy Acceleration)

The accelerating voltage was originally supplied by a battery. Apart from the disadvantage of not being able to introduce a time delay between ionisation and ion acceleration (for K.E. studies), it was noted that ion peaks were broadened on the high mass side. On using a 60 volt 30 μsec pulse from the Marconi Generator, the peaks were symmetrical and narrower. The difference was attributed to the finite width and the shape of the light source flash :-

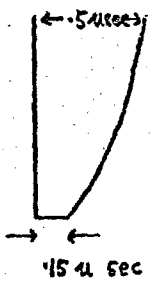

When a battery voltage is supplied, ions are starting their acceleration throughout the duration of the flash, and a broadening of the ion signal occurs, reflecting the shape of the light flash. The 60 Volt 30 μsec pulse is applied after a variable delay of at least 1.25 μ sec after the light flash. Consequently all the ions are accelerated from the same point in time, and the light source spread is not reproduced.

3. 6. Preparation and Purifaction of Materials

(a) Gases. The following commercially available gases were obtained from cylinders :- Oxygen, Nitrogen, Hydrogen, Carbon Dioxide,

Nitrous Oxide, Ethylene, Argon and Helium. When used in the light source they were taken directly from the cylinders, whilst those used as target gases in the mass spectrometer and the photoelectron spectrometer were subjected to freezing (liquid Nitrogen) and pumping cycles, when their freezing point made this possible.

H_2CO was generated by heating paraformaldehyde. The vapour produced was dried by passing through calcium chloride and sodium sulphate, and subjected to trap-to-trap distillation.

D_2CO was generated in a similar manner from a sample of d_2 - paraformaldehyde kindly provided by Dr.J.H. Callomon. The purity of both D_2CO and H_2CO was checked by mass spectrometery.(M.S.9)

COS was prepared by the action of 50% H_2SO_4 on a concentrated aqueous solution of potassium thiocyanate.[127] The gas was passed through 30% KOH solution to remove CO_2, through animal charcoal to remove CS_2, and dried by passing through calcium chloride and sodium sulphate. The purified sample was then subjected to trap-to-trap distillation.

(b) Liquids. Commercial Acetone, carbon disulphide, formamide and N - methyl formamide were used, all being subjected to freezing and pumping cycles, as was a purified sample of N - N dimethyl formamide, kindly provided by Dr. J. Jones. Distilled H_2O was boiled to remove any CO_2. D_2O was commercially available ($>$ 98% purity). Both were subjected to freezing and pumping cycles.

CHAPTER 4.

ANALYSIS OF THE ULTRAVIOLET RADIATION OBTAINABLE FROM THE LIGHT SOURCE OF THE VACUUM U.V. MONOCHROMATOR

To be able to use the monochromator / T O F M S assembly effectively for the study of photoionisation, it is necessary to have available emission lines which are reasonably intense, well characterised, and spaced over the energy range required (10 - 25 eV). These were supplied by using a variety of gases in the light source discharge tube, but very careful analysis of the resulting lines was required to ensure that :-

(a) The spectral order of each line had been correctly identified.

(b) The wavelength ascribed to it was accurate.

(c) There was no contribution from an underlying line of a different spectral order, and hence energy, present.

Only when these conditions were satisfied was the photoionisation data obtained using the lines of any significance.

In section 3.3.A.a. it was shown that the wavelength of the diffracted light passing through the exit slit of the monochromator should be given by equation 7 . In practice it was found that if this equation were used, the experimental wavelengths found were not in agreement with the known values for some lines. This was ascribed to an error in the zero order position of the grating rotation counter, such that the correct equation should be :-

$$n\lambda_{\text{Å}} = 1{\cdot}112\,N + 18\ \text{Å} \qquad \ldots\ldots\ldots\ldots\ldots\ldots\ 8$$

The wavelengths of the emission lines were ascribed accordingly.

In fact equation 8 was also incorrect, and from the known wavelengths of the Lyman α and β emission lines of H_2[128], the correct expression was shown to be

$$n \lambda_{\text{Å}} = 1{\cdot}112 \frac{N}{1{\cdot}018} \quad \ldots\ldots\ldots\ldots\ldots\ldots 9$$

the deviation from the theoretical equation 7 being due to an error in the nominal value of the number of turns per cm. of the screw thread driving the scanning mechanism.

The spectral order of an emission line was established by studying the ionising effect of each line on a number of gases of known I.P. Tn this manner the wavelength of most of the lines produced in the discharge of O_2, N_2, A, CO_2, $CH_2 = CH_2$, N_2O, and H_2, of sufficient intensity to be useful in photoionisation studies, were identified. The wavelengths of many of these lines were confirmed from Kelly 's " A Table of Emission Lines in the Vacuum Ultraviolet[129]", Moore's " Atomic Energy Levels Tables[130]", and work done with a light source of a similar type[80]. Agreement was usually within experimental limits.

An additional check on the correctness of the spectral order was provided by identification of each line in at least two, and sometimes three orders. It was usually possible to confirm or disprove the presence of suspected underlying lines of a different order by looking for them in other spectral orders. The use of suitable filters, placed between the exit slit of the monochromator and the light detector would probably help establish the wavelengths of the few remaining lines. A thin Aluminium film (1000 Å) could be used since it is known that

the transmission through such films increases steeply from 0 to 40% at wavelengths shorter than 800 Å [132]. A gas filter might also prove useful. Neon at a pressure of ·1 torr has negligible absorption at wavelengths between 1000 - 600 Å but it rises rapidly below 575 Å [131].

In Tables I -VII are listed all the usable ultraviolet lines for each gas for which no ambiguity occurs.

Delayed Emission Lines

During the light source line survey the time dependences of a number of lines were observed, using an oscilloscope, to have a form different from the normal. An example is shown in figure 38 (a). The ionising effect of these lines was observed using both a battery accelerating voltage (60 volts), and a 60 volt, 30 μsec pulse from the Marconi pulse generator, with a 1.25 μ sec delay between light source discharge and ion acceleration.

Using the 30 μ sec pulse, one ion peak corresponding to O_2^+ appeared in the mass spectrum. For the battery accelerating voltage two peaks were observed for some of the abnormal light source lines, and only one for others. A typical example of the mass spectrum resulting from ionisation by one of the abnormal lines, under each condition of acceleration, is shown in figure 38 (b). The separation between the two ion peaks was independent of accelerating voltage, the first having the theoretical flight time, t, for an O_2^+ ion, the second appearing at time, Δt, later. That Δt did not change with a change in accelerating voltage indicated that the second peak was also O_2^+.

This implied that two ionising light source lines were present, one of which was " normal " (i.e. reaches a maximum intensity within $\cdot 1\,\mu$sec of the discharge), and another which has a maximum at time, Δt, after the discharge. One ion peak only was expected and observed using a $30\,\mu$sec ion accelerating pulse delayed $1\cdot 25\,\mu$sec after discharge, since ions formed by both "normal" and "late" lines were in this case accelerated together. This behaviour is illustrated diagramatically in figure 38 (c).

In the cases where a "late" line did not produce a "late" O_2^+ ion peak, the line was first order and of insufficient energy to cause ionisation.

The "late" O_2^+ peak was usually broader than the "normal" one, indicating that the "late" light source line had a greater time duration than the "normal" one.

Table VIII gives a list of the lines which have been identified as "late" lines, together with an estimate of the time, Δt, by which they are delayed.

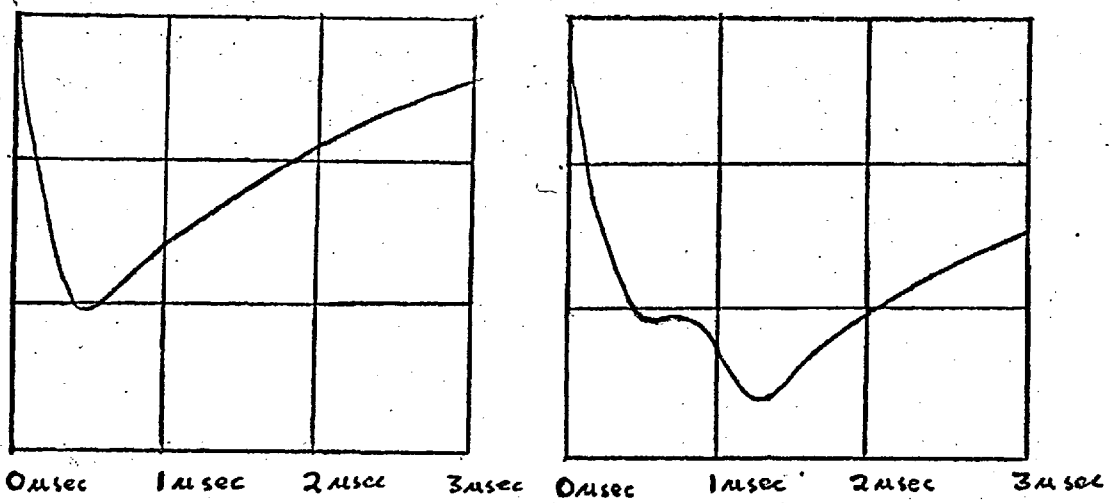

"normal" light source line (a) "late" light-source line

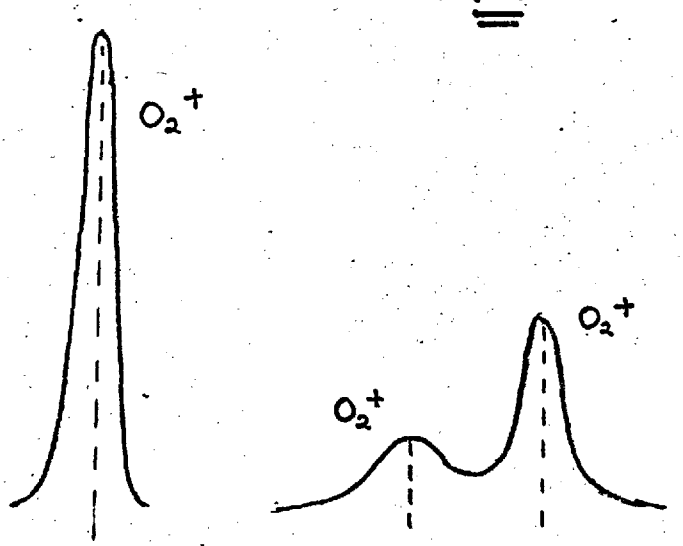

(b)

60 V, 30μsec Accelerating Pulse (1·25μsec Delay)

60 V Battery Acceleration

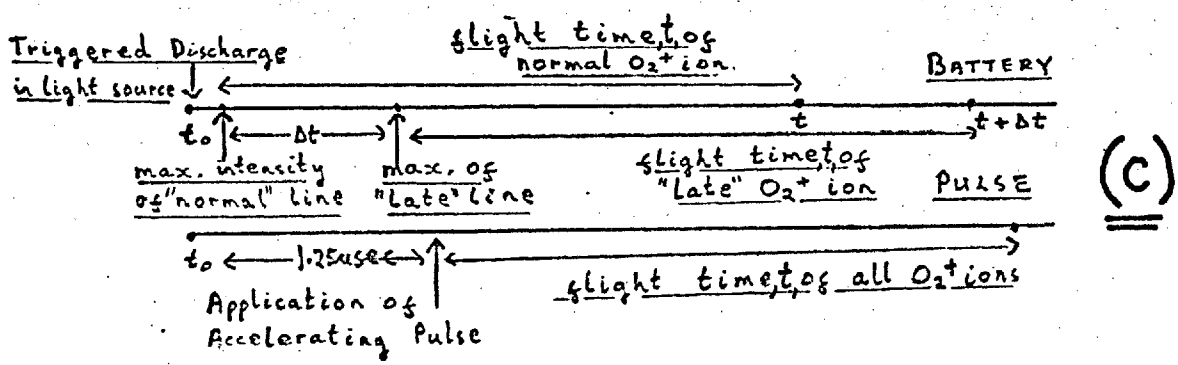

(c)

FIG 38

(a)— OSCILLOSCOPE TRACE OF LIGHT SOURCE PULSES

(b)— MASS SPECTRUM OF O_2 FROM AN " ABNORMAL LINE "

(c)— SCHEMATIC REPRESENTATION OF THE LIGHT PULSES, &ION DETECTION DELAY, RELATIVE TO INITIAL DISCHARGE.

TABLE I

OXYGEN EMISSION LINES OBTAINABLE FROM THE VACUUM U. V. MONOCHROMATOR LIGHT SOURCE - RECORDED IN THREE ORDERS

EXPERIMENTAL WAVELENGTH (A)			EMISSION LINES INCLUDED IN AN APPROXIMATELY 4A (1st. Order) RESOLUTION OF THE MONOCHROMATOR.	ENERGY (E.V.)
1st. Ord.	2nd. Ord	3rd. Ord		
—	539*	538	II 537·8 538·3 539·1 539·1	23·01
—	552	553*	IV 553·3 554·5 555·3	22·47
—	579	579	II 580·4 581·0	21·39
—	598	599*	III 597·8 599·6 II 600·6	20·71
—	615	615	II 616·3 616·4 IV 617·0	20·14
—	643	643	II 644·1	19·26
—	670	672	II 672·9 673·8	18·43
685	684	685	N III See Nitrogen	18·11
702	701	702	III 702·3 702·8 702·9 703·8	17·67
718	718	717	II 718·6	17·28
—	738	739	(II 739·9 ? — Weak Line)	16·81
786	787	—	IV 787·7 790·1 790·2	15·78
796	794	—	II 796·6 (Cu 788·0 & 793·1)	15·58
833	833*	—	II 832·8 833·3 834·5	14·89
			III 832·9 833·7 835·3	14·89
901	902*	—	III 899·0 (Cu 899·8 901·1)	13·78
915	914	—	N II See Nitrogen (Cu II 914·2)	13·56
972	975	—	I 971·7 973·2 973·8 976·5	12·73
989	990	—	I 988·8 990·2 N III See Nitrogen	12·53
1036	1036	—	I 1039·2 1037·6 1041·0	11·95
1084*	1084*	—	N II See Nitrogen	11·44
1153	1153	—	I 1152·2 III 1153·7	10·76
1217	1217	—	I 1217·6	10·19

* Indicates lines which lie near lines of a differing order.

TABLE II

NITROGEN EMISSION LINES OBTAINABLE FROM THE VACUUM U. V. MONOCHROMATOR LIGHT SOURCE – RECORDED IN THREE ORDERS

EXPERIMENTAL WAVELENGTH (A)			EMISSION LINES INCLUDED IN AN APPROXIMATELY 4A (1st. Order) RESOLUTION OF THE MONOCHROMATOR.	ENERGY (E.V.)
1st. Ord.	2nd. Ord	3rd. Ord		
—	580	581	II 582.2 O II See Oxygen	21.31
—	627	628	II 629.2 629.4	19.72
—	635	635	II 635.2	19.53
—	643	643	II 644.6 644.8 645.1	19.26
—	659	660*	II 660.2	18.79
670	670	670*	II 671.0 671.4 671.6 672.0	18.49
685	684	685	III 685.0 685.5 685.8 686.3	18.08
745	745	746	II 745.8 747.0	16.63
—	762	763	III 764.4 IV 765.1	16.24
769	770	771	III 771.9 772.4 772.8 773.0	16.07
—	775	776	II 776.0	15.98
796	794	—	(Cu III 788.0 & 793.1) O II 796.6	15.60
833	833	—	O II + III See Oxygen	14.89
901	901	—	(Cu II 899.8 901.1)	13.77
917	917	—	II 915.6 916.0 IV 922.0 922.2	13.53
		—	922.7 (Cu III 914.2)	13.[illegible]
962	—	—	I 964.0 964.6 – 965.1	12.87
976	976*	—	III 979.8 979.9	12.71
989	990*	—	III 989.8 991.5 991.6	12.54
1003	1003*	—	III 1006.0	12.33
1084	1084	—	II 1084.0 1084.6 1085.4	11.44
11			1085.7	
1131	—	—	I 1134.2 1134.4 1135.0	10.97
			(Si IV 1128.4)	

* Indicates lines which lie near lines of a differing order.

TABLE III

ARGON EMISSION LINES OBTAINABLE FROM THE VACUUM U. V. MONOCHROMATOR LIGHT SOURCE - RECORDED IN THREE ORDERS

EXPERIMENTAL WAVELENGTH (A)			EMISSION LINES INCLUDED IN AN APPROXIMATELY 4A (1st. Order) RESOLUTION OF THE MONOCHROMATOR.	ENERGY (E.V.)
1st. Ord.	2nd. Ord	3rd. Ord		
—	538*	538	III 536·8 537·5 538·8	23·06
—	555	554	III 553·5	22·39
		556	II 556·8 556·9 III 558·5	22·27
—	603	603*	II 602·9 III 604·2	20·57
—	640	636	III 637·3	19·47
		642	III 641·8 643·3	19·32
—	662	661	II 661·9	18·74
—	669	671	II 671·0 671·8	18·49
685	687	688*	IV 688·4 689·0 690·2	18·00
698	698	698	II 698·8 IV 699·4 700·3	17·77
—	716	716	V 715·6	17·32
769	767	769	III 769·2	16·13
803	799	—	IV 800·6 801·1 801·4 801	15·49
847	841	—	IV 840·0	14·77
	850	—	IV 850·6	14·59
881	877	—	III 875·1 I 876·1 III 878·8	14·14
	885	—	III 883·2 887·4	14·02
898	901*	—	IV 901·2 901·8	13·77
918	919	—	II 919·8	13·48
928	929	—	II 932·0	13·31
948	948	—	(Cu II 946·0)	13·11
1033	1033*	—	(Cu II 1036·2)	12·01
1084*	1084*	—	NI See Nitrogen	11·44

* Indicates lines which lie near lines of a differing order.

TABLE IV

CARBON DIOXIDE EMISSION LINES OBTAINABLE FROM THE VACUUM U. V. MONOCHROMATOR LIGHT SOURCE - RECORDED IN THREE ORDERS

EXPERIMENTAL WAVELENGTH (A)			EMISSION LINES INCLUDED IN AN APPROXIMATELY 4A (1st. Order) RESOLUTION OF THE MONOCHROMATOR.	ENERGY (E.V.)
1st. Ord.	2nd. Ord	3rd. Ord		
—	538	538	See $CH_2=CH_2$ and Oxygen	23.06
—	552	553*	Oxygen	24.47
—	579	579*	"	21.39
—	598	598	"	20.71
—	608	609	O III 609.7 610.8 IX 608.4 609.8	20.37
—	615	615	Oxygen	20.14
—	643	642	Carbon	19.26
—	650	650	Carbon	19.05
—	670	673*	Oxygen	18.43
685	686	685	Carbon	18.05
698	701	702	Oxygen	17.67
718	716	717	(Cu III 715.5)	17.32
800	796	—	Oxygen	15.58
833	833*	—	Oxygen	14.89
857	857*	—	Carbon	14.46
901	902	—	"	13.72
948	945	—	"	13.13
976	975	—	"	12.70
990	989	—	Nitrogen & Oxygen	12.53
1009*	1009*	—	Carbon	12.28
1036	1034	—	"	11.96
1064	1064	—	"	11.64
1084	1084	—	"	11.44
1128	1128	—	Nitrogen	10.97

* Indicates lines which lie near lines of a differing order.

TABLE V

ETHYLENE EMISSION LINES OBTAINABLE FROM THE VACUUM U. V. MONOCHROMATOR LIGHT SOURCE – RECORDED IN THREE ORDERS

EXPERIMENTAL WAVELENGTH (A)			EMISSION LINES INCLUDED IN AN APPROXIMATELY 4A (1st. Order) RESOLUTION OF THE MONOCHROMATOR.	ENERGY (E.V.)
1st. Ord.	2nd. Ord	3rd. Ord		
—	537	537*	III 535.3 538.1 538.2 538.3	23.06
—	574	571*	III 574.3	21.61
—	650	651*	II 651.2 651.2 651.3	19.08
688	686	—	II 686.5 687.1 687.4	18.05
715	718	—	III 714.9 (Cu III 715.5)	17.32
745	747	—	—	16.60
766	762	—	—	16.24
803	806*	—	II 806.4 806.4 806.9	15.38
857	857*	—	II 858.1 858.6	14.46
901	902	—	II 903.7 904.0 904.5	13.72
916	914	—	(H I 915.3 916.4)	13.56
942	943	—	I 945.3 945.6 (Cu 943.3)	13.13
976	977*	—	III 977.1	12.70
1006	1007*	—	II 1009.8 1010.1 1010.4	12.28
1033	1036	—	II 1037.0	11.97
1064	1064	—	II 1065.9 1066.1	11.64
1084	1084	—	N II See Nitrogen	11.44

* Indicates lines which lie near lines of a differing order.

TABLE VI

N_2O &— EMISSION LINES OBTAINABLE FROM THE VACUUM U. V. MONOCHROMATOR LIGHT SOURCE – RECORDED IN THREE ORDERS

EXPERIMENTAL WAVELENGTH (A)			EMISSION LINES INCLUDED IN AN APPROXIMATELY 4A (1st. Order) RESOLUTION OF THE MONOCHROMATOR.	ENERGY (E.V.)
1st. Ord.	2nd. Ord	3rd. Ord		
—	615	—	O III See Oxygen	12.66
898	898	—	O III "	13.81
980	980	—	N III See Nitrogen	20.71

TABLE VII

HYDROGEN EMISSION LINES OBTAINABLE FROM THE VACUUM U. V. MONOCHROMATOR LIGHT SOURCE – RECORDED IN THREE ORDERS

EXPERIMENTAL WAVELENGTH (A)			EMISSION LINES INCLUDED IN AN APPROXIMATELY 4A (1st. Order) RESOLUTION OF THE MONOCHROMATOR.	ENERGY (E.V.)
1st. Ord.	2nd. Ord	3rd. Ord		
1026	1026	—	H Lyman α 1025.7	12.09
1216	—	—	H Lyman β 1215.7	10.20
1575	—	—	} Molecular Lines	7.88
1605	—	—		7.73
1636	—	—		7.58

&— Only lines which are more intense than the corresponing lines in Nitrogen or Oxygen are indicated

* Indicates lines which lie near lines of a differing order.

TABLE VIII

OXYGEN " IATE " LINES IDENTIFIED IN THE T.O.F.M.S. LIGHT SOURCE

1st.Ord. line	2nd.Ord. line	3rd.Ord. line	Time delay, t, of late line.	Time between "normal" and "late" O_2^+ ion mass peaks.
——	670 Å	672 Å	1 μ sec.	.8 μ sec.
——	615 Å	615 Å	1 μ sec.	.8 μ sec.
1747 Å	——	——	2 μ sec.	no ion
1490 Å	——	——	2 μ sec.	no ion
1300 Å	——	——	2 μ sec.	no ion
1217 Å	——	——	2 μ sec.	no ion

CHAPTER 5

RESULTS AND DISCUSSION

In this chapter photoelectron spectroscopic results are presented for a number of molecules. In the cases of H_2CO, D_2CO and N_2O, relevant mass spectrometric results obtained using the TOFMS are included. In some cases the photoelectron spectra have been examined at an earlier date under lower resolution, and comparisons are made. The results are discussed in relation to the electronic energy levels of the molecules concerned, and the theoretical calculations concerning them. Previously unknown vibrational frequencies in many ionic electronic states have been found, and others confirmed. Some F - C factors have been measured, and where possible the values compared to those calculated. In an effort to obtain as much information as possible on the ionising processes concerned it is necessary to correlate the results with those of related work in the field of photoionisation.

Section 5. 5. covers a brief mass spectrometric study of acetone using the T O F M S, which was made primarily in an attempt to assess the usefulness of the spectrometer for studying the K.E. of ions and the processes occurring after initial ionisation (or excitation). The results are compared to some made using the original version of the spectrometer[118].

5. 1. H_2O and D_2O

The 584 Å He resonance photoelectron spectrum of H_2O (figure 39) exhibits three bands, indicating three orbital levels of energy greater than - 21·2 eV, and not four as reported earlier from electron impact studies[133,134]. The values of the three adiabatic ionisation potentials deduced from these bands are 12·61(6) eV, 13.7 eV, and 17·22 eV, and the corresponding vertical ionisation potentials (from the strongest peaks) are 12·61(6) eV, 14·73(6) eV, and 18.55 eV. The first is in close agreement with the spectroscopic value 12·61 eV[135], whereas the ionisation energies corresponding to the maxima of the very broad second and third bands (14·73(6) eV, 18·55 eV) can be compared with the figures 14·35 eV[134] and 18·1 eV[136] obtained by electron impact measurements. Al - Joboury and Turner[137] obtained values of 12·61 eV, 14·23 eV, and 18·02 eV for the adiabatic ionisation potentials from a low resolution photoelectron spectrum, using a grid analyser photoelectron spectrometer.

Deuterium Oxide gives a spectrum whose overall form is very similar to that of water, adiabatic ionisation potentials being 12·62(4) eV, 13·7 eV, and 17·26 eV, vertical ionisation potentials 12·62(4) eV, 14·67(3) eV, and approximately 18·5 eV.

Ellison and Shull[138], from their molecular orbital calculations on the water molecule, found the ground state configuration and orbital energies to be :-

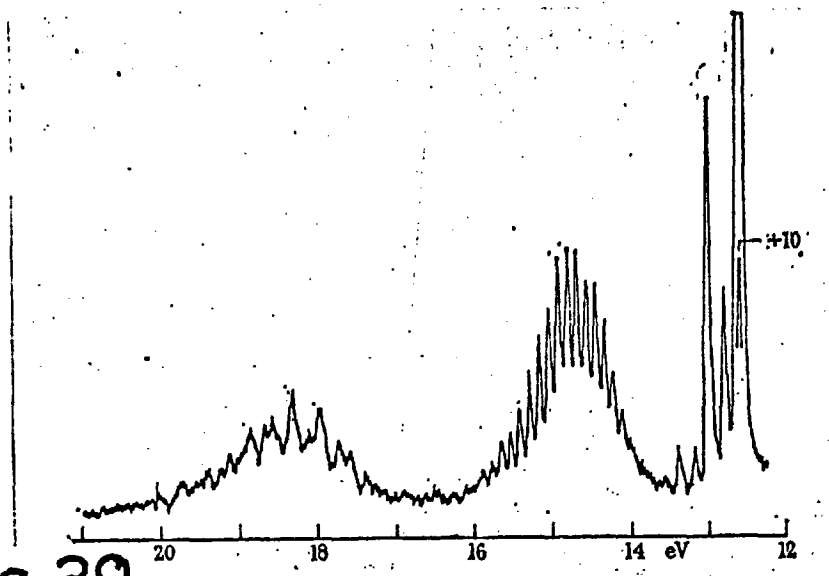

FIG. 39 The photoelectron spectrum of H_2O using the helium 584 Å line.

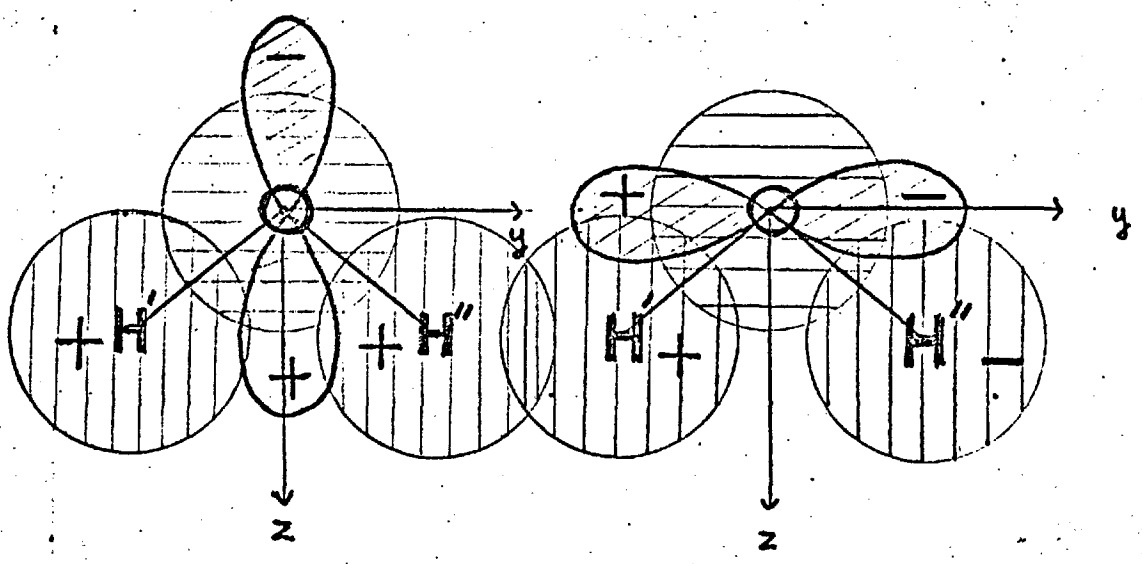

$\psi(3a_1)$ $\psi(1b_2)$

FIG. 40 SCHEMATIC REPRESENTATION OF THE $3a_1$ AND $1b_2$ MOLECULAR ORBITALS OF H_2O. — x axis perpendicular to plane of paper.

H_2O $(1a_1)^2$ $(2a_1)^2$ $(1b_2)^2$ $(3a_1)^2$ $(1b_1)^2$ $^1A_1$

$\left[\cong (1s_O)^2 (2s_O)^2 (1b_2)^2 (3a_1)^2 (2px_O)^2\right]$

Orbital Energies 577eV 36eV 18·55eV 13·2eV 11.79eV

where $\psi(3a_1) = C_{31}\sigma_1 + C_{32}\,1s_O + C_{33}\,2s_O + C_{34}\,2pz_O$

$\psi(1b_2) = C_{55}\sigma_5 + C_{56}\,2py_O$

$\sigma_1 = 2^{-\frac{1}{2}}(1S_{H'} + 1S_{H''})$

$\sigma_5 = 2^{-\frac{1}{2}}(1S_{H'} - 1S_{H''})$

Thus, on this basis, orbital $3a_1$ can be described as possessing H - H bonding character, and the orbital $1b_2$, H - H antibonding character. These orbitals are illustrated schematically in figure 40.

Each band in the spectrum shows a different vibrational fine structure which will now be considered in detail

First Band (Adiabatic Ionisation Potential H_2O 12.61(6)eV D_2O 12·62(4)eV

Figs. 41 & 42 show on an expanded energy scale this region of the spectrum, which relates to the ion in its ground electronic state. Several vibrational states of the ion are clearly discerned, and analysis of the spectra lead to the values for ν_1 and ν_2 given in Table IX. The similarity of the vibrational frequencies of the ion to those in the molecular ground state and Rydberg levels leading to this state of the ion, demonstrates clearly that the first band corresponds to the removal of an essentially non-bonding electron from the oxygen atom, with little resultant change

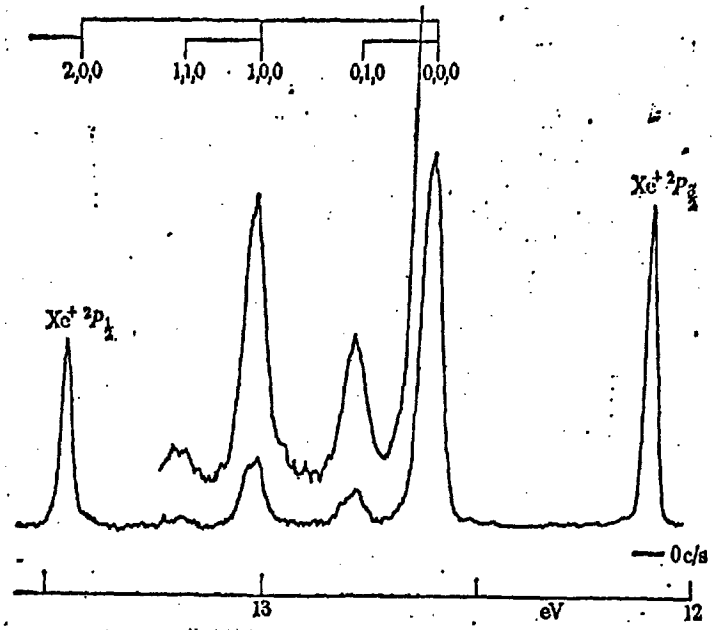

FIG.41

The photoelectron spectrum of H_2O using the helium 584 Å line; first band, expanded scale. Some added xenon provides accurate calibration.

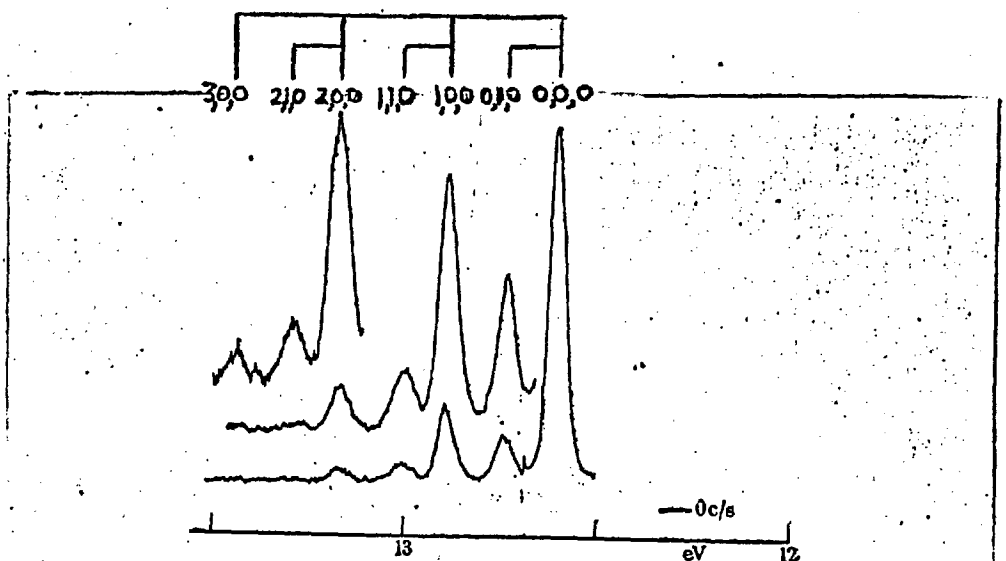

FIG.42

The photoelectron spectrum of D_2O using the helium 584 Å line.

TABLE IX

VIBRATIONAL FREQUENCIES OF H_2O AND D_2O

		ν_1(cms^{-1})	ν_2(cms^{-1})	ν_1/ν_2	$\frac{\nu_1 D_2O \ \nu_2 D_2O}{\nu_1 H_2O \ \nu_2 H_2O}$
Molecular Ground State ($^1A_1$) (Herzberg [8b])	H_2O	3652	1595	2.29	.538
	D_2O	2666	1178	2.26	
Rydberg State $\tilde{C}$ ($^1B_1$) (Herzberg [8b])	H_2O	3170	1422	2.23	.527
	D_2O	2290	1038	2.20	
Ionic Ground State* ($^1B_1$) (present results)	H_2O	3200±50	1380±50	2.32	.513
	D_2O	2310±50	980±50	2.36	

in molecular dimensions,

$$H_2O^+ , \ldots\ldots (1b_1)^1 , {}^2B_1 \longleftarrow H_2O , \ldots\ldots (1b_1)^2 , {}^1A_1$$

Supporting evidence is supplied by the relatively strong $(0,0,0) \longleftarrow (0,0,0)$ transition.

The Franck-Condon factors which are deduced from the relative electron fluxes for the various vibrational states of the ion are recorded in table X .

Botter and Rosenstock[139] have calculated the F - C factors as a function of both bond distance and angle using the Rydberg $\tilde{C}\ {}^2B_1$ state vibrational frequencies. There is a close correspondence between the ground state frequencies and those of the Rydberg $\tilde{C}$ state for both isotopic species, as can be seen from table IX , and this leads to the expectation of very similar geometry for the two states.

They then used the very approximate experimental Franck-Condon factors for the 0,1,0; 1,0,0 vibrational levels of the H_2O^+ ion found from the steps in photoionisation efficiency curves[140], to estimate the parameters of the H_2O^+ ion in its ground state (see Introduction - Section 1. 4(h)). Similarly the experimental Franck-Condon factors of the D_2O molecule in its Rydberg $^1B_1\ \tilde{C}$ state[141] were used to estimate the parameters of the molecule in this state.

From our results, it is apparent that the experimental Franck- Condon factors for the vibrationally excited states found by Dibeler et al[140], are too large, possibly due to the unrecognised contribution from auto - ionisation. Brehm[85] has measured the photoionisation efficiencies of both H_2O and D_2O, and an estimate of the experimental Franck-Condon factors

TABLE X

EXPERIMENTAL FRANCK-CONDON FACTORS OF THE $^2B_1$ IONIC LEVELS OF H_2O AND D_2O

ν_1	ν_2	ν_3	H_2O	D_2O
0	0	0	0.757 ± .005	0.702 ± .005
0	1	0	0.069 "	0.087 "
1	0	0	.143 "	0.148 "
1	1	0	0.013 ± .002	0.034 ± .002
2	0	0	0.018 "	0.025 "
2	1	0	$\leqslant$ 0.002	0.004 "
3	0	0	$\leqslant$ 0.008	$\leqslant$ 0.002
3	1	0	——	$\leqslant$ 0.002

TABLE XI

EXPERIMENTAL FRANCK- CONDON FACTORS AND THE PARAMETERS OBTAINABLE FROM THEM. — (After Botter and Rosenstock)

	← H_2O →					← D_2O →				
	Experimental Franck-Condon factors for the Ground Ionic State Vibrational Levels.			Parameters		Experimental normalised Franck-Condon factors for the Ground Ionic State Vibrational Levels.			Parameters	
	0,0,0	0,1,0	1,0,0	r_{eq}(Å)	θ_{eq} (°)	0,0,0	0,1,0	1,0,0	r_{eq}(Å)	θ_{eq}(°)
Present Results	100	9.1	18.9	.999	110.3	100	12.4	21.1	.996	110.0
Dibeler et al [140]	100	18±2	30±10	≃1.01	≃ 112	—	—	—	—	—
Brehm [85]	100	≃ 11	≃ 17	≃1.00	≃ 111	100	≃ 13	≃ 13	≃ 1.01	≃ 110
		$^1B_1$ Rydberg level		1.016	106.9				1.009	107.6
		$^1A_1$ Ground Molecular State		.956	105.2				.957	104.9

may be obtained from his curves. All three sets of experimental results are given, (in Table XI), as percentages relative to the 0,0,0 transition, together with the ionic parameters derived by fitting them to the calculated curves of Franck-Condon factors versus bond angle and distance, due to Botter and Rosenstock. Though the calculated curves do not yield a unique solution, only one of the possible solutions is consistent with the idea of an ion formed by removal of a largely non-bonding electron possessing some weakly bonding character. This solution is the one given in table XI . Also included in Table XI are the molecular ground state parameters, and the parameters of the $^1B_1$ Rydberg state deduced from a rotational analysis[142].

The results are in disagreement with the calculations of Krauss[143], who obtained a bond angle of 119° for the H_2O ion using an SCF - Gaussian basis method. Such a large increase in bond angle is certainly not what would be expected on removal of a non-bonding electron.

Very recently Botter and Rosenstock[144] have extended their calculations of F - C factors for H_2O and D_2O to include the effects of anharmonicity on the calculated values. The F.C. factors were calculated for both molecules as a function of both bond distance and angle. Figure 43 shows graphically their latest results, excluding anharmonicity effects, in the region of interest, for a larger number of transitions than in their earlier work[139]. The tenfold difference in ordinate scale for both the 0,0,0 and 1,0,0 values should be kept in mind. Marked on the curves are the photoelectron experimental values of the F - C factors of table X . The measure of agreement is whether all the points lie on the same vertical line. There is obviously a

major discrepancy in both cases for the 0,0,0 ⟶ 2,0,0 transition, when no estimate of anharmonicity is included in the F - C calculations, but a geometry estimate of 1·0(0) Å and approximately 110° has been clearly established.

As there is no direct indication of the magnitude of the anharmonicity in the water ion, Botter and Rosenstock carried out a simple one dimensional perturbed harmonic oscillator calculation corresponding to a cubic term in the potential for the symmetric stretching mode. Their results (figure 44) give the F - C factors as a function of the square root of the anharmonic constant x_e. They are shown for a geometry of 1·00 Å and 110°. A reasonable value for the anharmonicity constant accounts entirely for the intensity discrepancy in the 0,0,0 - 2,0,0 transition. Further if r_{eq} is reduced to ·955 Å the 0,0,0, - 0,0,0, 0,0,0, - 1,0,0, 0,0,0 - 2,0,0,0 transitions can all be brought into accord with a value of x_e 0·0 0 8 - 0·0 0 9.

A similar parameterised calculation for the bending mode indicates that for increasing anharmonicity, the same F - C factor is obtained for a decreasing bond angle. A reasonable estimate of the anharmonicity is thought to be x_e = ·01, which reduces the calculated bond angle from 110° to 109°.

It is obvious from these latest calculations that the precision to which the geometry of the ion was established, from the original calculations, is too great, and that now a reasonable estimate for the geometry of both ions would be :-

$$\underline{r_{eq.} = \cdot 995 \pm \cdot 005 \text{ Å}}$$

$$\underline{\theta_{eq.} = 109^\circ}$$

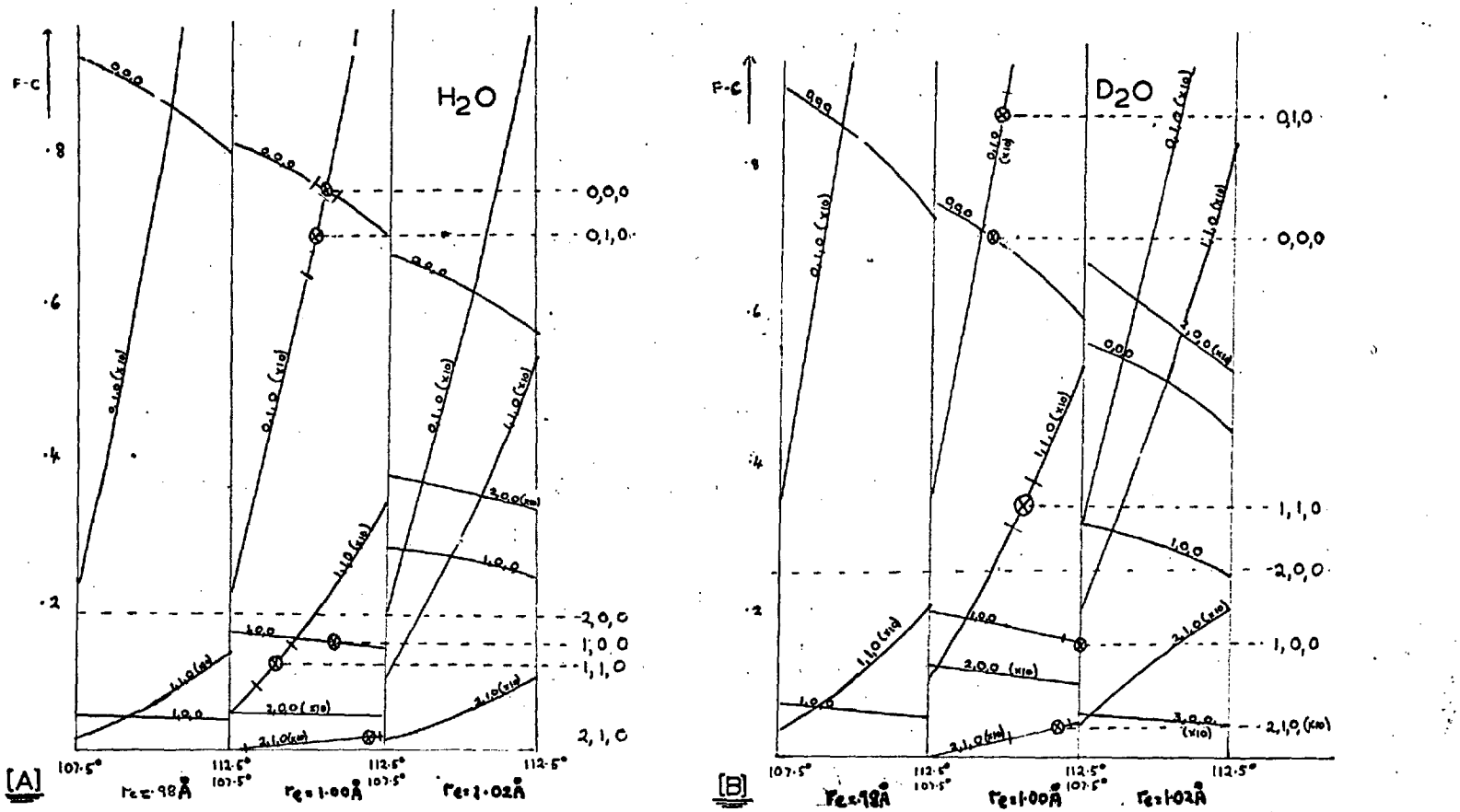

FIG. 43

Calculated Franck-Condon Factors for [A] H_2O, and [B] D_2O, as a function of bond angle and bond length (after Botter and Rosenstock)

—⊗ Experimental F-C values from photoelectron spectroscopy

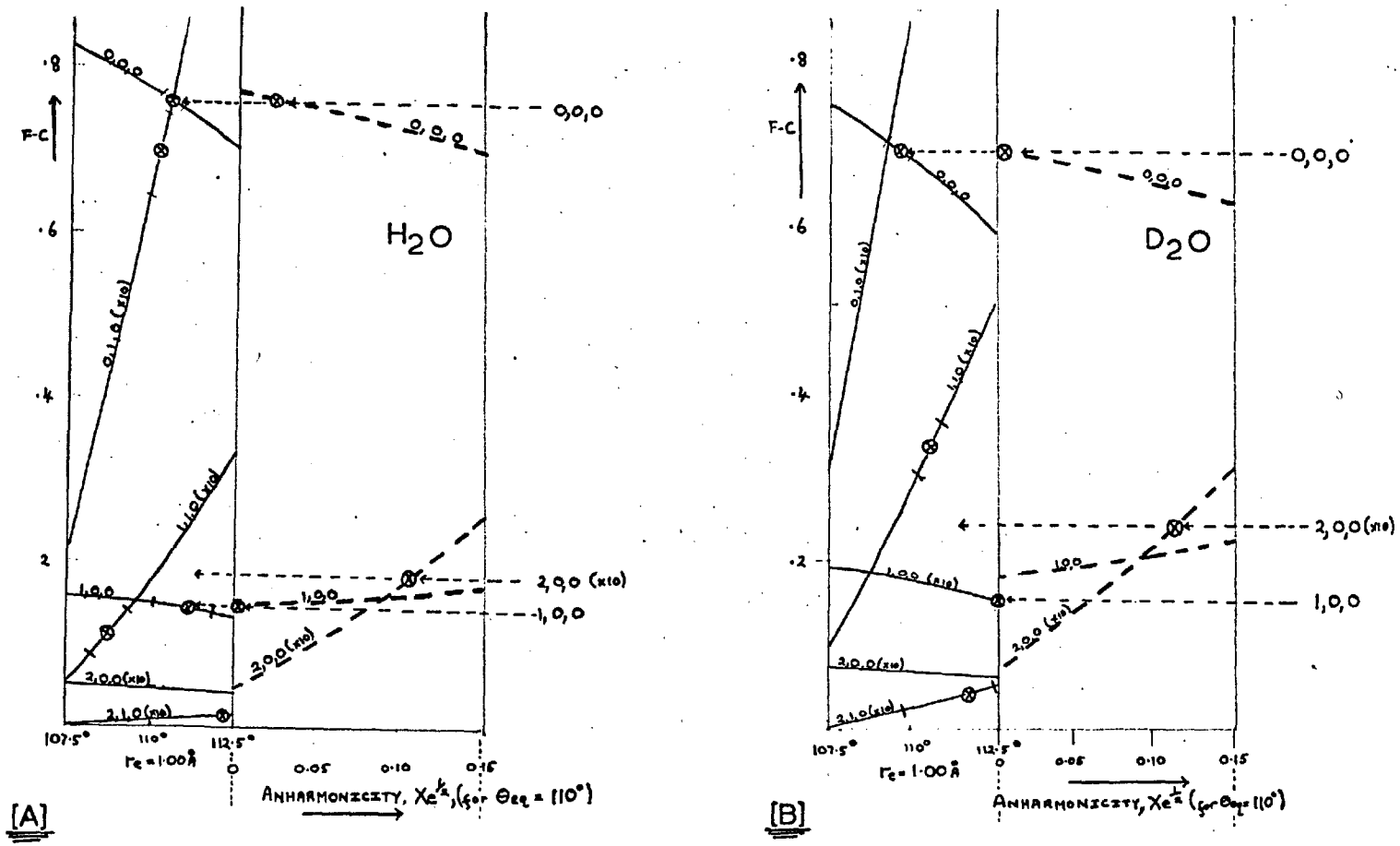

FIG. 44

Calculated F-C factors for [A] H_2O, and [B] D_2O for $r_{eq} = 1.00$ Å and $\theta_{eq} = 110°$ (after Botter and Rosenstock).

⊗ Experimental F-C factors

The bond angle estimate is of only moderate value, an improved estimate resting upon improved knowledge of the anharmonicity of the bending vibration.

Second Band (Adiabatic Ionisation Potentials H_2O = 13·7 eV, D_2O = 13·7 eV)

This band (figures 45 and 46) appears to be a long series of almost equally spaced peaks, the mean separation (·120 eV (H_2O), ·089 eV (D_2O)) corresponding to a vibrational frequency of 975 ± 50 cm^{-1} in water, and 715 ± 50 cm^{-1} in deuterium oxide. Comparison with the frequency of ν_2 in the ground state of the H_2O molecule (1595 cm^{-1}), and in the $B(^1A_1)$ Rydberg state (800 cm^{-1}) shows ν_2, the bending mode, to be the only reasonable assignment here.

The length of the series (the transition H_2O^+ A; 0,8,0 ← H_2O , 0,0,0 being the most probable), and the reduction in the magnitude of ν_2 with respect to that observed in the ground state of the molecule, indicates that an electron has been removed from a strongly bonding level. That the magnitude of ν_2 in the Rydberg level is reduced even further than in the ion may indicate that the Rydberg orbital, to which the electron is promoted, has some anti-bonding character.

Since only the bending mode is excited, the major dimensional change on ionisation must be in a bond angle. This is consistent with the removal of an electron from an orbital possessing strong H - H bonding character, as is suggested by the calculations of Ellison and Shull[138] for the $\psi 3a_1$ orbital of water.

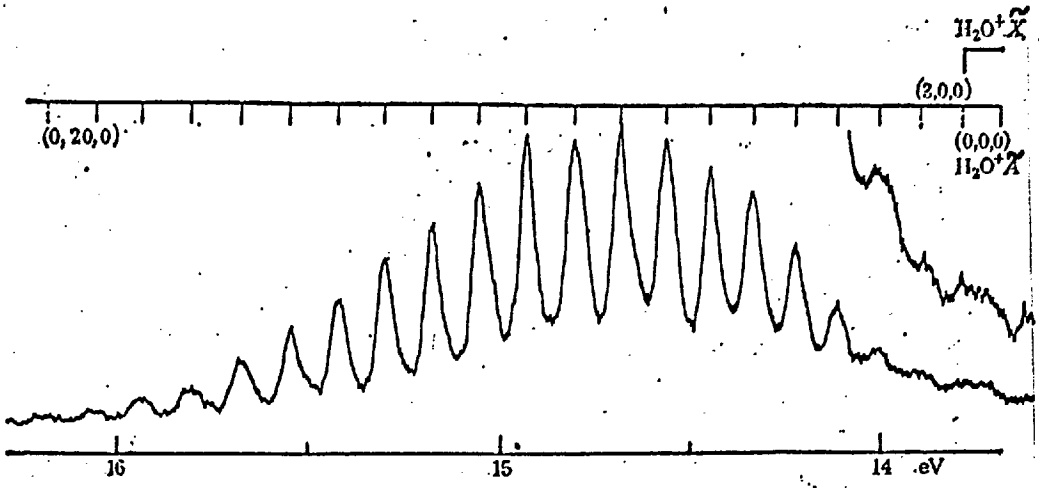

FIG. 45 The photoelectron spectrum of H_2O using the helium 584 Å line; second band, expanded scale.

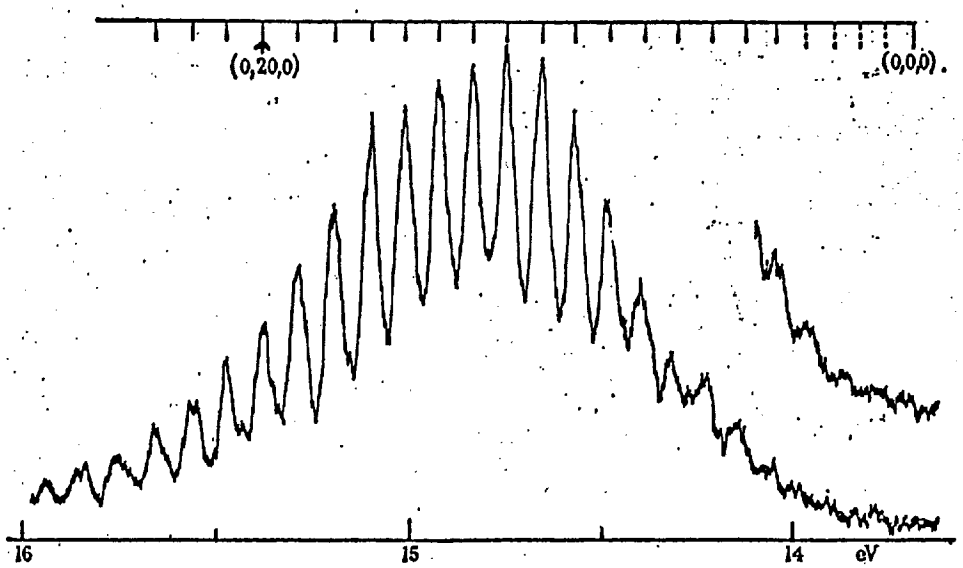

FIG. 46 The photoelectron spectrum of D_2O using the helium 584 Å line; second band, expanded scale.

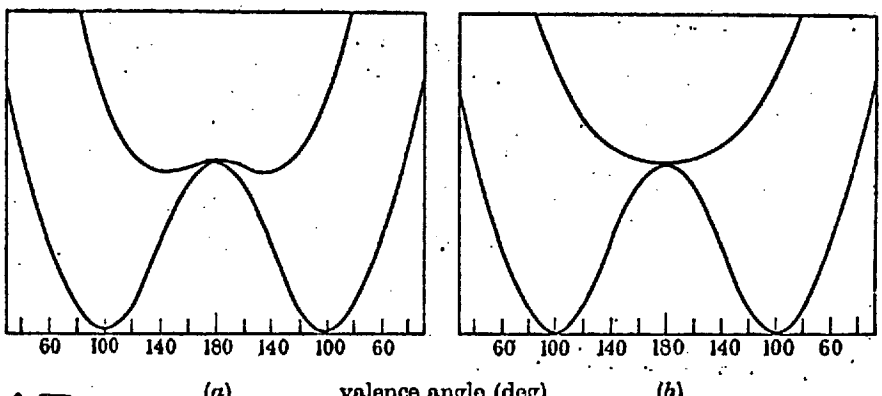

FIG. 47 Forms of the potential energy curves for NH_2 (a) for a bent excited state; (b) for a linear excited state (after Dixon).

The ion H_2O^+ is isoelectronic with the $NH_2^\cdot$ radical, the ground and first excited electronic levels of H_2O^+ being of the same symmetry species as those of $NH_2^\cdot$. The ultraviolet absorption spectrum corresponding to the transition

$$NH_2\ (\tilde{A}) \longleftarrow NH_2\ (\tilde{X})$$

$$^2A_1 \qquad\qquad ^2B_1$$

has been examined in detail by Dressler and Ramsey[145]. Both states arise from strong Renner splitting of the doubly degenerate $^2\Pi_u$ level, applicable to a linear molecule, into $^2B_1$ and $^2A_1$ states. Dixon[146] has shown the most stable conformation of NH_2 in its upper state, $^2A_1$, to be slightly bent (Figure 47). This non-linearity causes considerable complexity in the region of the first vibrational levels since sub-levels with odd and even values of K no longer fall into degenerate groups. In the second band of the photoelectron spectrum of H_2O and D_2O, a similar situation appears to arise, with the position of the 0 - 0 level being rather indeterminate, an apparent "smearing out" of the first few vibrational levels, and an alteration in width of the rest. The slight divergence of the later members of the series is characteristic of a potential function containing a quartic term.

The well defined peaks for $H_2O^+\ (\tilde{A})$ $(v' > 5)$ fit the expression

$$T(cm^{-1}) = T_0 + 890\ (v' + 1) + 6(v' + 1)^2$$

whilst

$$T(cms^{-1}) = 9,650 + 597\ (v' + 1) + 11.5(v' + 1)^2$$

is fitted by the $^{2}\Sigma^{+}$ levels in the case of NH_2[146].

The energies of the higher vibrational components of this band in H_2O and D_2O fitted curves which could be extrapolated towards a common origin near 13·7 eV. No peaks which could be associated with this progression could be found at a lower ionisation potential. The presence of traces of CO_2 (I.P. 13·78 eV) made accurate assignment of features between 13·70 and 13·80 eV difficult. T_0 for $H_2O^+ \tilde{A} \leftarrow \tilde{X}$ is thus approximately 1·1 eV compared with 1·196 eV for $NH_2^+ \tilde{A} \leftarrow \tilde{X}$.

We conclude that this state of the ion is probably slightly non-linear, involving a strong Renner effect, in a similar manner to that in NH_2. The deviation from linearity is probably less than is the case for NH_2.

We place the adiabatic ionisation potentials at $\simeq$ 13·7 eV for both H_2O and D_2O, the first clearly measurable peaks being 13·89(7) eV for H_2O, (Fig. 45 Inset) and 13.988 for D_2O (Fig. 46 Inset).

Third Band (Adiabatic Ionisation Potentials 17·22 eV for H_2O 17·26 eV for D_2O).

This (Figures 48 and 49) is markedly more complex in form than the other two bands, and consists of peaks exhibiting varying degrees of broadening.

Broadening can indicate an unstable ionic state having a short life-time. The Appearance Potential of ^{+}OH is 18·1 eV[136,140], but no upward break in the ionisation efficiency curve for H_2O^+ is observed at this value, showing that the ^{+}OH ions are formed directly by removal of a $^{1}b_2$ electron. Fiquet - Fayard and Guyon[147] suggest that the $^{2}B_2$

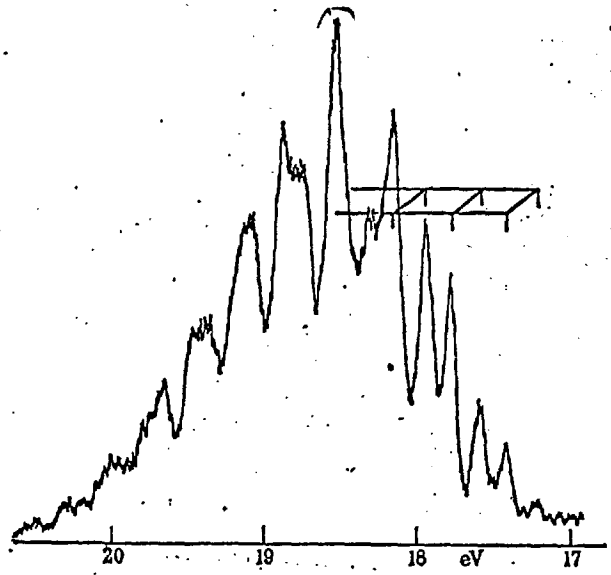

FIG. 48 The photoelectron spectrum of H_2O using the helium 584 Å line; third band, expanded scale.

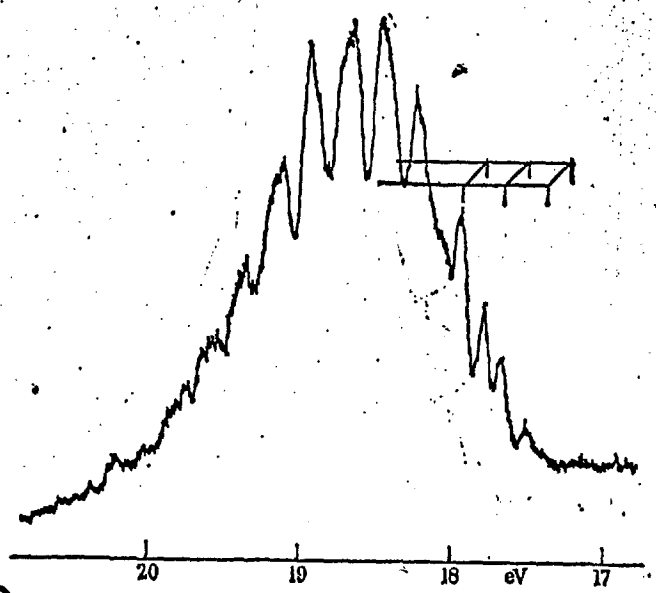

FIG. 49 The photoelectron spectrum of D_2O using the helium 584 Å line; third band, expanded scale.

state of the H_2O^+ ion is completely pre-dissociated by curve crossing with the $^4A''$ repulsive state to give ^+OH.

$$H_2O\ ^1A_1 \longrightarrow H_2O^+\ ^2B_2 \longrightarrow H\ ^2\Sigma g + OH^+\ ^3\Sigma^-$$

short life time

Our results support this. It explains why the first few peaks in the band are somewhat sharper than the rest, only these vibrational levels apparently being below the crossing point with $^4A''$ state.

Vibrational analysis of the band is made difficult by its complexity and supposedly dissociative broadening. A possible series of doublets can be picked out, (·37(0) eV and ·20(0) eV for H_2O^+, ·27(0) eV and ·15(0) eV for D_2O^+) corresponding to modes of vibration with frequencies 2990 ± 100 cm^{-1}, 1610 ± 100 cm^{-1} for H_2O and 2170 ± 100 cm^{-1}, 1210 ± 100 cm^{-1} for D_2O, the reduction in frequency for D_2O^+ compared to H_2O^+ being about what would be expected. The frequencies 2,990 cm^{-1}, 2,170 cm^{-1} probably correspond to mode ν_1, and frequencies 1,610 cm^{-1} and 1,210 cm^{-1} to bending mode ν_2. The decrease in ν_1 and slight increase in ν_2 compared with the frequencies in H_2O and D_2O are consistent with the removal of an electron from an orbital having O - H bonding character and H - H anti-bonding character, as is implied by the results of the calculations of Ellison anf Shull for the $\psi\ 1b_2$ orbital of water.

Definite assignment of the adiabatic ionisation potentials is again difficult since there may be one or two vibrational levels of such low intensity as to have been undetected. We place the 0- 0 transitions at 17·20 eV for H_2O and 17·24 eV for D_2O.

Momigny et al[148] have recently interpreted the H_2O photoelectron spectra of Blake and Carver[52] as providing evidence of the failure of photoelectron spectroscopy to detect all ionic states because of the low photoionisation cross-sections of some ionising transitions (σ levels) at impacting energies in excess of the threshold value. In their paper Blake and Carver show two spectra of water, under very low resolution, using incident radiation of 584 Å and 690 Å (via a monochromator). These spectra are reproduced in figure 50 and the 584 Å spectrum may be compared with figure 39 and figure 51 where the spectrum has been recorded using the alternative recording method of accelerating the ejected electrons to a fixed K.E. (Section 3. 1.c.). Blake and Carver correctly identify the $^2B_1$ and $^2A_1$ states of the ion, but erroneously consider the $^2B_2$ state to lie at 16·34 eV and to be obscured in the spectrum by the $^2A_1$ state peak. The true $^2B_2$ state, which is clearly represented by a large peak in their 584 Å spectrum, they leave unassigned.

The persistence of attempts to place the $^2B_2$ state at approximately 16·5 eV is due to features in Henning's[149] original U.V. absorption spectrum of H_2O. This work was done in 1932. Henning tentatively suggested an I.P. at 16·5 eV as he considered that a continuum absorption started at this value. There was no evidence of a Rydberg series leading to this continuum, and anyway Henning attributed the continuum to the 2nd I.P. of water, completely missing the true 2nd I.P. at 13·7 eV. Breaks in electron efficiency curves have sometimes been quoted in support of Henning's supposed I.P. at 16·5 eV.

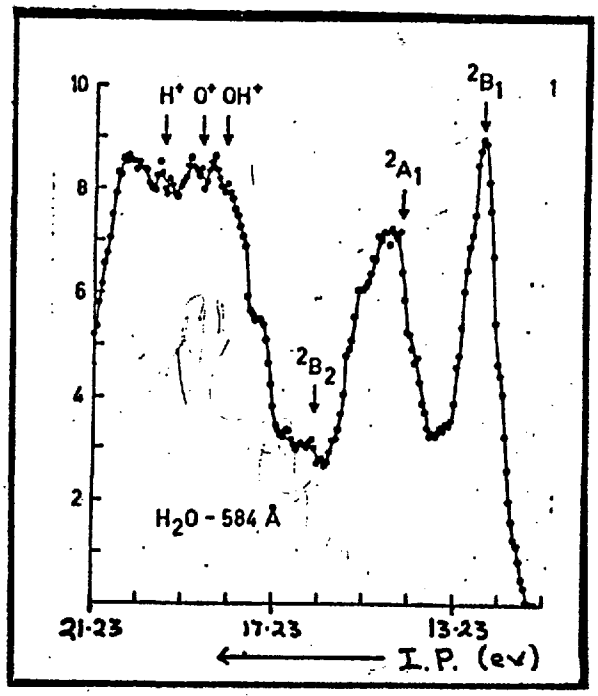

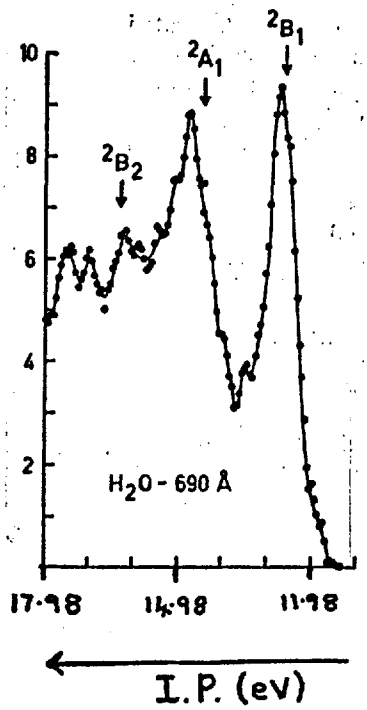

FIG. 50

LOW RESOLUTION PHOTOELECTRON SPECTRUM OF H_2O - (after Blake and Carver[52])

FIG 51 — H_2O — alternative sweep system

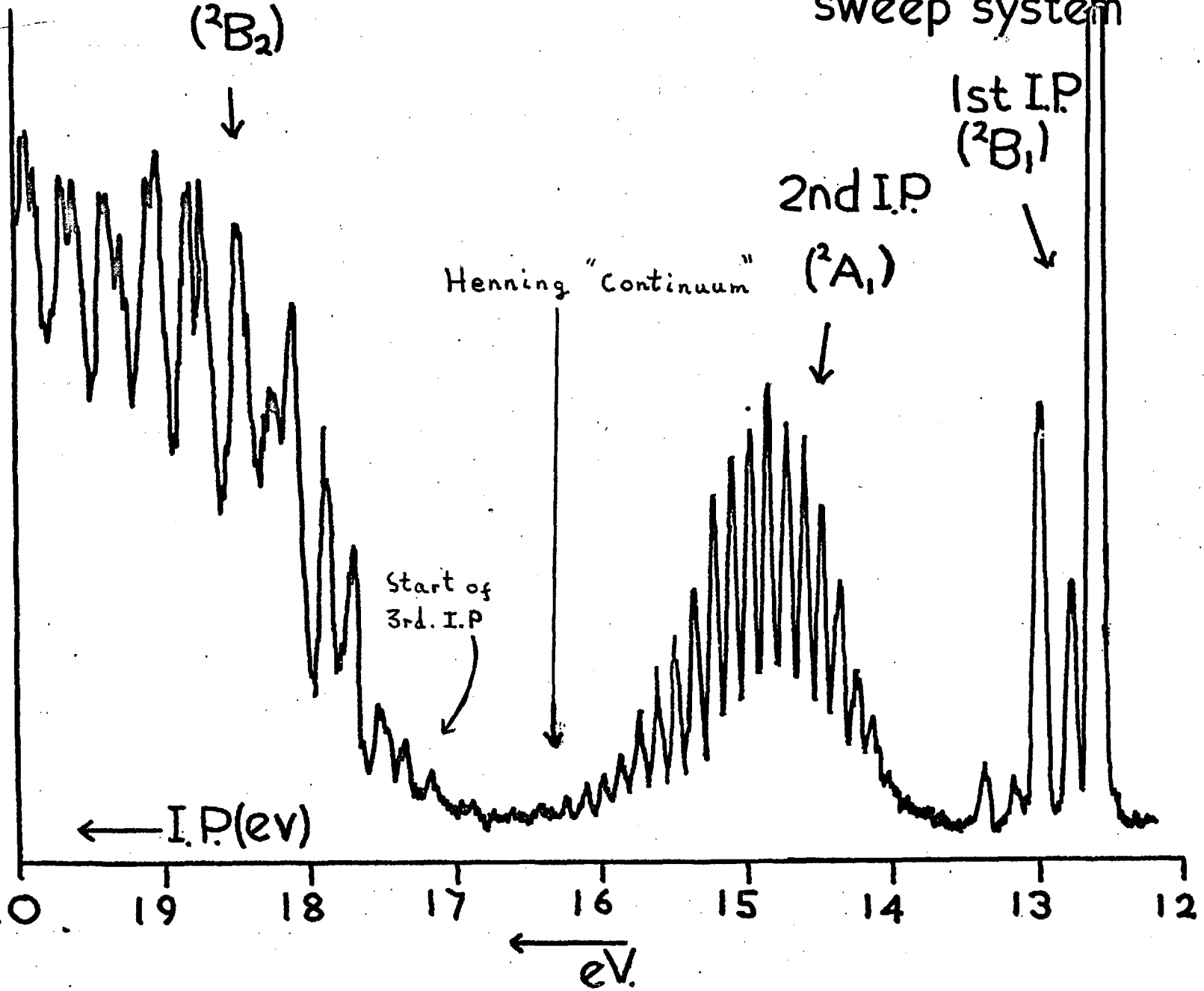

Though a break can be observed near this value, it is almost certainly due to autoionisation, and a break near the correct 3rd I.P. can also be observed. No structure due to inner ionisation potentials can be observed in the high resolution photon impact efficiency curves of Dibeler et al[140].

Thus there is no real evidence for an I.P. at 16·5 eV, and the use of Blake and Carver's spectra by Momigny et al to demonstrate that photoelectron spectroscopy has in the case of water "missed" an I.P. is totally incorrect since an I.P. does not exist at that value.

The original conclusion that the three I.P's of H_2O at 12·62 eV ($^2B_1$), 13·7 eV ($^2A_1$) and 17·2 eV ($^2B_2$) is not therefore in any way in question, and as has been shown by the band by band analysis, this interpretation is in accord with the theoretical calculations[138], and with the experimental interpretations by other authors[147].

The small differences in the features of Blake and Carver's spectrum at 584 Å and 690 Å near 16·5 eV, though hardly discernable from random fluctuations have at least two rational explanations.

The first is that there may be a "normal" autoionisation level at 690 Å (see Section 2. 4.a. Page 35) which enhances the population of vibrationally excited states of the $^2A_1$ level, and the second is the possibility of "fluorescent ionisation" (see Section 2. 4.a. Page 35).

5. 2. H_2CO and D_2CO

5. 2.1. The Photoelectron Spectra of H_2CO and D_2CO

The photoelectron spectrum of formaldehyde (figure 52) exhibits four bands, indicating four orbitals of energy greater than -21·2 eV. The values of the four adiabatic ionisation potentials deduced from these bands are 10·88(4) eV, 14·09(5) eV, 15·85(4) eV, and 16·25(4) eV. It is possible that the last value does not represent the fourth adiabatic ionisation potential since this band is overlapped by the intense peaks of the third band. The corresponding vertical ionisation potentials (measured from band maxima) are 10·88(4) eV, 14·38(8) eV, 16·00(9) eV, and 16·78 eV. Earlier work on a low resolution spectrometer[150] had indicated that there might be a fifth band present corresponding to an ionisation potential of approximately 20·5 eV.

The first ionisation potential is in close agreement with the spectroscopic value of 10·88 eV[41] and the electron impact value of 10·87 ± 0·01 eV[151]. Sugden and Price[152] detected breaks in the electron impact ionisation efficiency curve for H_2CO at 11·8 eV and 13·1 eV, and associated these with the second and third ionisation potentials. From the present results it is clear that neither of these values can be true ionisation potentials, and from the photoionisation efficiency results given in section 5.2.2. & 3 it seems that the 13·1 eV break is due to an autoionisation process. Formaldehyde-d_2 gives a spectrum whose overall form is similar to that of formaldehyde, but with differences in the vibrational fine structure, particularly in the third band (fig.59). The adiabatic ionisation potentials are 10·90(4) eV, 14.09(5) eV, and

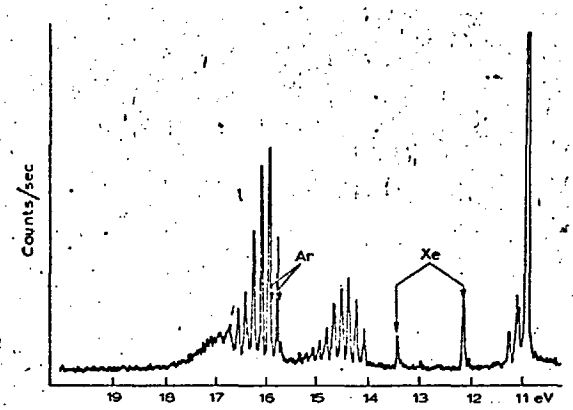

FIG. 52

Helium 584 Å photoelectron spectrum of formaldehyde.

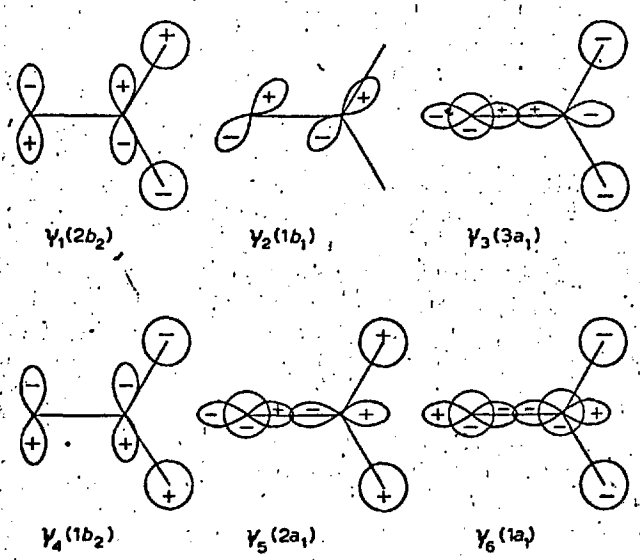

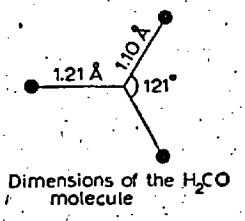

FIG. 53

. Schematic description of the filled molecular orbitals of formaldehyde. ψ_1, oxygen non-bonding, weakly CH_2 bonding, weakly C–O pseudo-π antibonding; ψ_2, strongly C–O π bonding; ψ_3, mainly CH_2 bonding, weakly C–O bonding; ψ_4, pseudo-π H–C–O bonding; ψ_5, strongly CH_2 bonding; weakly C–O antibonding; ψ_6, Strongly C–O σ-bonding, strongly C–H antibonding.

TABLE XII

CALCULATED EIGENVALUES OF THE MOLECULAR ORBITALS OF FORMALDEHYDE (eV)

	ψ_1	ψ_2	ψ_3	ψ_4	ψ_5	ψ_6
Goodfriend et al.[153], 1960	11.53	15.08	19.25	22.10	21.94	38.73
Foster and Boys[154], 1960	10.50	12.80	15.55	18.38	22.80	37.35
Peters[155], 1963	10.4	12.8	15.5	18.5	23	37
Carrol et al.[156]	10.9	15.3	14.4	16.7	20.9	30.9
	11.0	13.2	14.5	16.6	21.0	30.9
Newton and Palke[157]	10.76	13.54	16.16	18.40	22.62	38.10

15·84(6) eV. The region of the fourth band which corresponds to the adiabatic potential is completely obscured by the third band.

Calculated eigenvalues for the molecular orbitals involved, which are illustrated schematically in figure 53, have varied widely as the methods of computation improved. A summary of recent calculations of the eigenvalues is given in Table XII.

Each band in the spectrum shows a different vibrational fine structure.

First Band : (Adiabatic ionisation potential Formaldehyde, 10·88(4) eV; Formaldehyde-d_2, 10.90(4) eV)

Figures 54 and 55 show the region of the spectrum for the ion in its ground electronic state. Several vibrational modes are clearly discernable, and it appears that all three totally symmetric vibrational modes, ν_1, ν_2, and ν_3, are weakly excited. The frequencies of these vibrational modes are shown in TableXIII. The similarities of the vibrational freqencies of the ion, in comparison withthose of the molecule in its ground state, demonstrate clearly that an essentially non-bonding electron has been removed with little resultant change in molecular dimensions. Supporting evidence is supplied by the fact that the various vibrational states of the ion are only relatively weakly excited..

Second Band: Adiabatic ionisation potential; Formaldehyde 14·09(5) eV Formaldehyde-d_2 14·09(5) eV)

The second band (figures 56 and 57) appears to consist of a series

TABLE XIII

FREQUENCIES OF VIBRATIONAL MODES EXCITED IN THE GROUND IONIC STATE OF H_2CO AND D_2CO COMPARED WITH EQUIVALENT VALUES IN THE GROUND MOLECULAR STATE (cm^{-1}).

		ν_1 (C-H stretch)	ν_2 (C-O stretch)	ν_3 (C-H deformation)
GROUND IONIC STATE (from photo-electron spectrum)	H_2CO^+	2560 ± 50	1590 ± 50	1210 ± 50
	D_2CO^+	1910 ± 50	1560 ± 50	870 50
	H_2CO^+/D_2CO^+	1.34	1.02	1.39
GROUND MOLECULAR STATE (Ref. 8a)	H_2CO	2780	1744	1503
	D_2CO	2056	1700	1106
	H_2CO/D_2CO	1.35	1.03	1.36

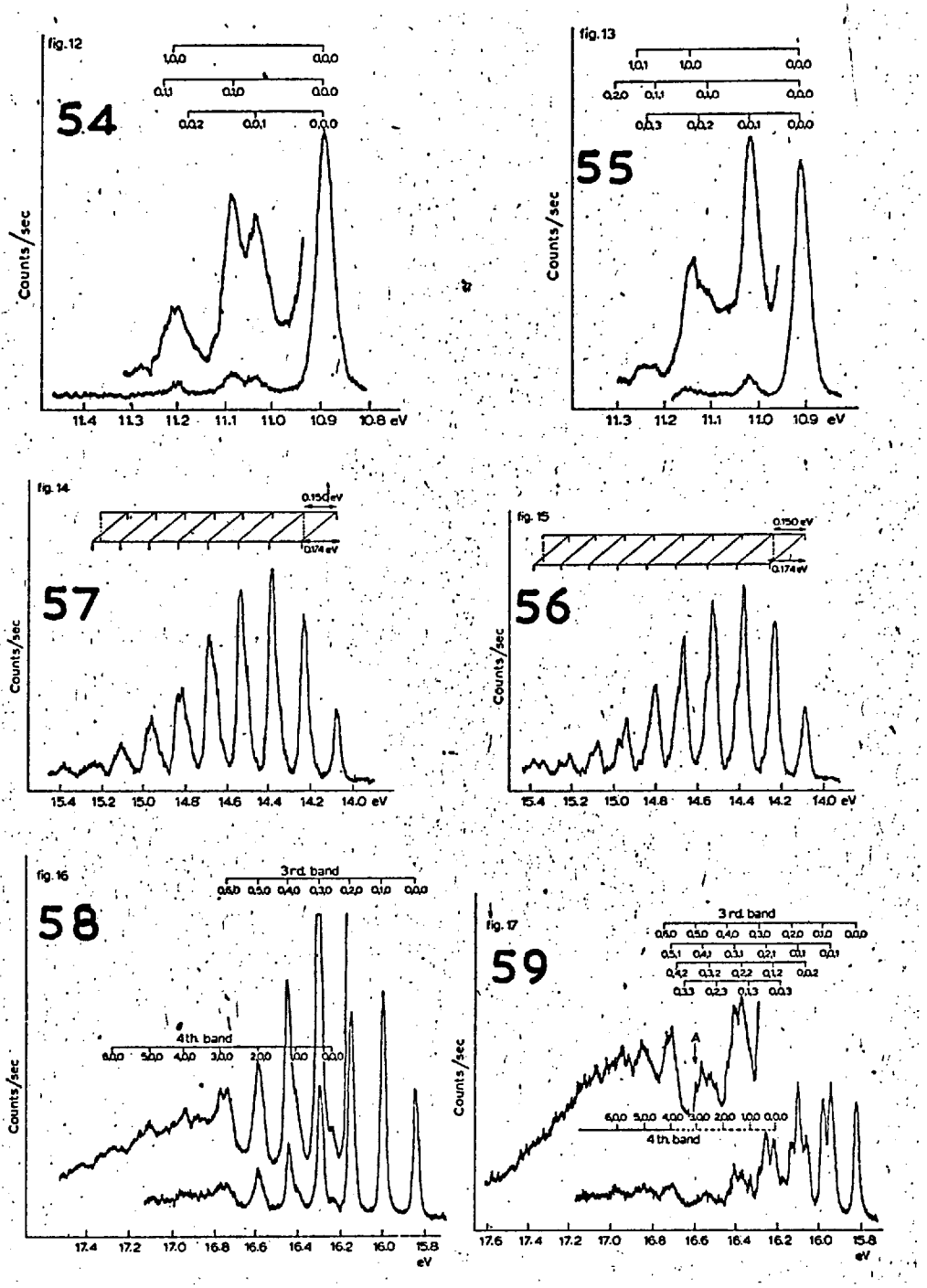

FIG. 54, 56, 58 — PHOTOELECTRON SPECTRUM OF H_2CO - expanded energy scale.

55, 57, 59 — PHOTOELECTRON SPECTRUM OF D_2CO - expanded energy scale.

of doublets. The main series of peaks converges slightly, the spacing of the first two peaks in formaldehyde being 0·150 eV. The doublet spacing is 0·174 eV. This band was originally interpreted[158] as involving the excitation of the C-O stretching vibration ν_2 (main series) with frequency 1210 ± 50 cm^{-1} and one quantum of the C-H stretching mode ν_1 (subsidiary peaks) with frequency 1400 ± 50 cm^{-1}.

At first sight the spectrum of formaldehyde-d_2 seemed to support this assignment, with the main series being unchanged indicating an essentially unchanged frequency for ν_2, but with the doublet spacing, and hence the frequency ν_1, being reduced to approximately 0·120 eV. It was therefore concluded that this state of the ion was produced by the removal of a C-O π-bonding electron (orbital ψ_2) in agreement with the theoretical molecular orbital calculations, since only the C-O stretching mode was strongly excited.

Subsequent detailed analysis of the expanded scale spectrum shown in figures 56 and 57 revealed, however, that this interpretation of the formaldehyde-d_2 spectrum was incorrect. In fact the peak spacings seem to be identical with those in formaldehyde, only the intensity distribution having changed. In formaldehyde-d_2 the "subsidiary" peaks become the more intense. This result is difficult to explain, since there should only be one vibrational mode, ν_2, which is not reduced in frequency on deuteration. It may be that the band is more complex than it appears, with either more than two vibrational modes excited, or some form of vibrational resonance present.

Third Band (Adiabatic Ionisation Potential Formaldehyde 15·85(4) eV; Formaldehyde-d_2 15·84(6) eV)

The third band in the spectrum of formaldehyde (figure 58) consists of a single, slightly converging series of narrow peaks whose spacing (0·158 eV) corresponds to a vibrational frequency of 1270 ± 50 cm^{-1}. Examination of the third band in formaldehyde-d_2 (figure 59) shows this simplicity to be the result of an equality of frequencies for two vibrational modes. On deuteration the frequency of one mode (ν_2) remains unchanged at 1270 ± 50 cm^{-1} while the other is reduced to 935 ± 50 cm^{-1}. The latter frequency obviously relates to a C-H mode, since the reduction on deuteration (1·36 : 1) is exactly that expected on theoretical grounds.

It can be either the C-H stretching mode ν_1 (molecular value 2780 cm^{-1} for formaldehyde) or the deformation mode ν_3 (molecular value 1500 cm^{-1} for formaldehyde). ν_3 would seem to be the more likely since the reduction required for it to be ν_1 is rather large. Since both vibrational modes are excited equally strongly in this state of the ion, and both are reduced in frequency compared with those in the molecular state, we conclude that the ion most probably results from the removal of an electron from an orbital involving bonding over the whole molecule, namely ψ_4. If the C-H mode involved is not ν_3 but ν_1, then it could be possible that the orbital concerned is ψ_3, since removal of an electron from the strongly CH_2 bonding orbital would be expected to produce a large reduction in frequency compared with that in the molecular ground state. However it is considered

unlikely that the C-O stretching mode would be excited so strongly on removal of an electron from an orbital not concerned with C-O bonding.

Fourth Band (Adiabatic ionisation potential: Formaldehyde 16·25(4) eV Formaldehyde-d_2, Unknown)

The fourth band starts under the third band, and for formaldehyde (figure 58) the first peak that can be observed is at 16·25(4) eV. This is taken to be the value for the adiabatic ionisation potential, but it is possible that a very small earlier peak might go undetected.

The mean spacing of the peaks (0·175 eV) corresponds to a vibrational frequency of 1400 ± 50 cm^{-1}, and the band becomes complex at higher energy. In formaldehyde-d_2 (figure 59) the only features which can be picked out from the band are three peaks at 16·74 eV, 16·86 eV, and 16·99 eV, having a separation (ca. 0·126 eV) corresponding to a vibrational frequency of approximately 990 cm^{-1}. The reduction in frequency (1/1.41) is about what would be expected on deuteration if a C-H vibrational mode were involved, and if the series is extrapolated to lower ionisation energies it is found that a peak would be positioned almost co-incident with the adiabatic ionisation peak in formaldehyde at 16·24 eV. It is a little surprising that the fourth peak in this supposed series (position A, figure 59) is not evident.

It is considered likely that this state of the ion results from the removal of an electron from orbital ψ_3, strongly CH_2 bonding; mode ν_1 being excited with the expected great reduction in frequency. The complexity of the band towards higher ionisation energy appears to

be due to peak broadening which is probably indicative of the ion having a short life time in this state. Potential energy curve crossing to another state may be involved.

From the photoelectron spectra results it is concluded that the order of orbital energies in the formaldehyde molecule is most probably:-

$$\Psi_1 \quad \Psi_2 \quad \Psi_4 \quad \Psi_3$$

and that the next orbital has an energy of less than -21.21 eV. This differs from the order resulting from most of the M.O. calculations, in that Ψ_3 and Ψ_4 are reversed.

5. 2.2. The T O F Mass Spectra of H_2CO and D_2CO

Little work has been published on the mass spectrometry of formaldehyde, and none at all using photon impact. Reed[159] and Reed and Brand[160] have measured the I Ps of H_2CO and HCO, and the Appearance Potentials of HCO^+ from H_2CO and CO^+ from HCO by electron impact spectrometry. The deuterated compounds were also studied. Their results are shown in Table XIV, together with a later determination[161] of the A.P. of CHO^+ from H_2CO by electron impact.

Graphs of the relative abundances of fragment ions to molecular ions versus energy of the incident photon beam, obtained using the T O F M S are shown in figures 60 and 61. The results for D_2CO are the more reliable as resolution between the component mass peaks of the spectrum was nearly complete, whereas for H_2CO it was very poor. The estimated

TABLE XIV

MASS SPECTROMETRIC DATA FOR H_2CO, D_2CO, AND HCO•

	I.P. (eV.)		A.P. (eV.)			I.P.(eV)	A.P.(eV)	D(H—HCO) (eV.)	
	H_2CO	D_2CO	HCO^+	DCO^+	CO^+	HCO^+	CO^+	calculated from equ. 1	calculated from equ. 2
Reed (1956)	10.87	10.88	13.10	13.10	——	9.87	15.22	$\leqslant$ 3.22	$\geqslant$ 3.34
Pritchard and Harrison (1968)	—	—	12.55	—	—	—	—	$\leqslant$ 2.55	——
Present Results	$\leqslant$ 10.98	$\leqslant$10.98	11.4–12.7	11.4–12.7	$\triangleq$ 15.5	——	—	$\leqslant$ 2.7—1,5	——

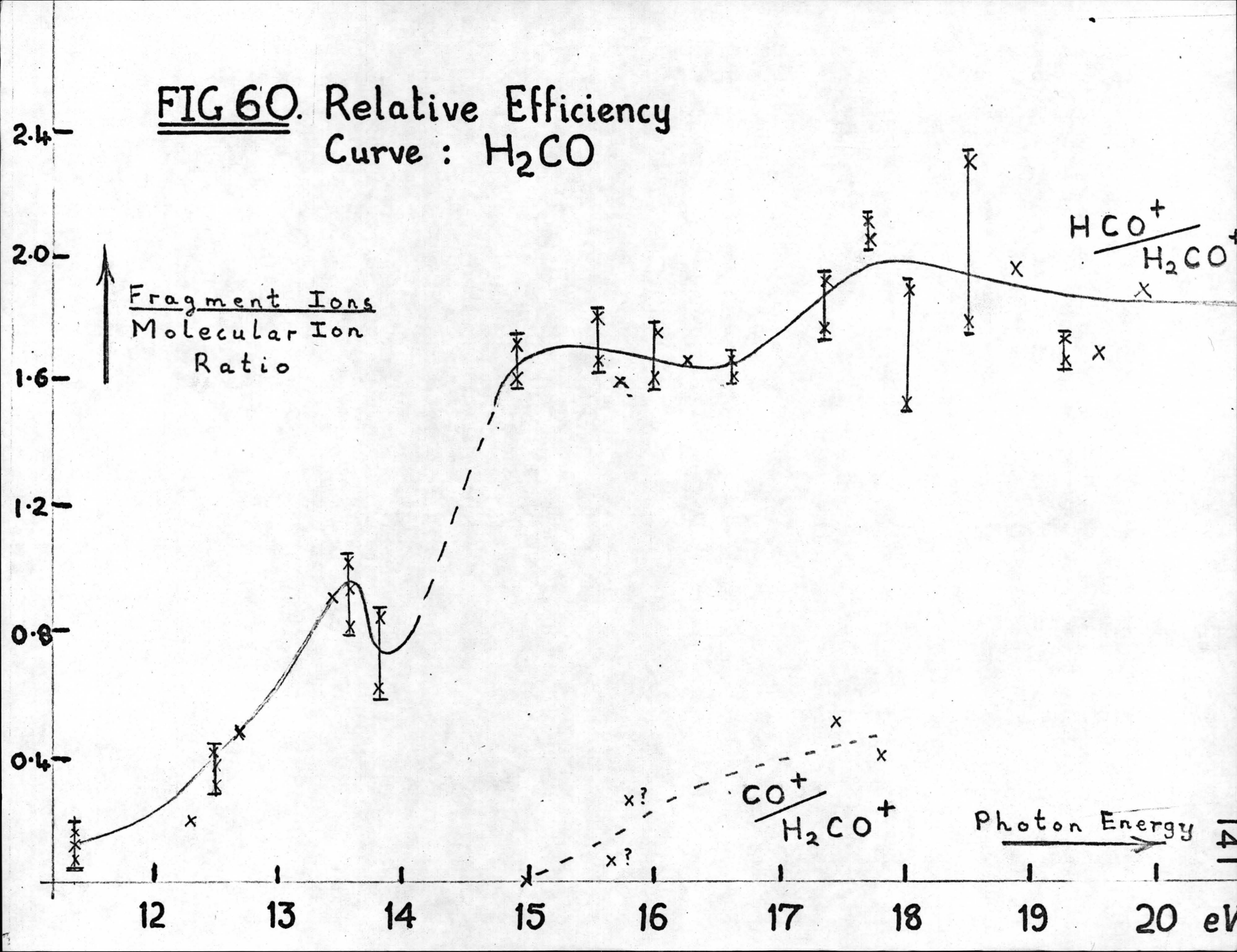
FIG 60. Relative Efficiency Curve : H_2CO
Fragment Ions / Molecular Ion Ratio
2·4
2·0
1·6
1·2
0·8
0·4
HCO^+ / H_2CO^+
CO^+ / H_2CO^+
Photon Energy
12
13
14
15
16
17
18
19
20
eV

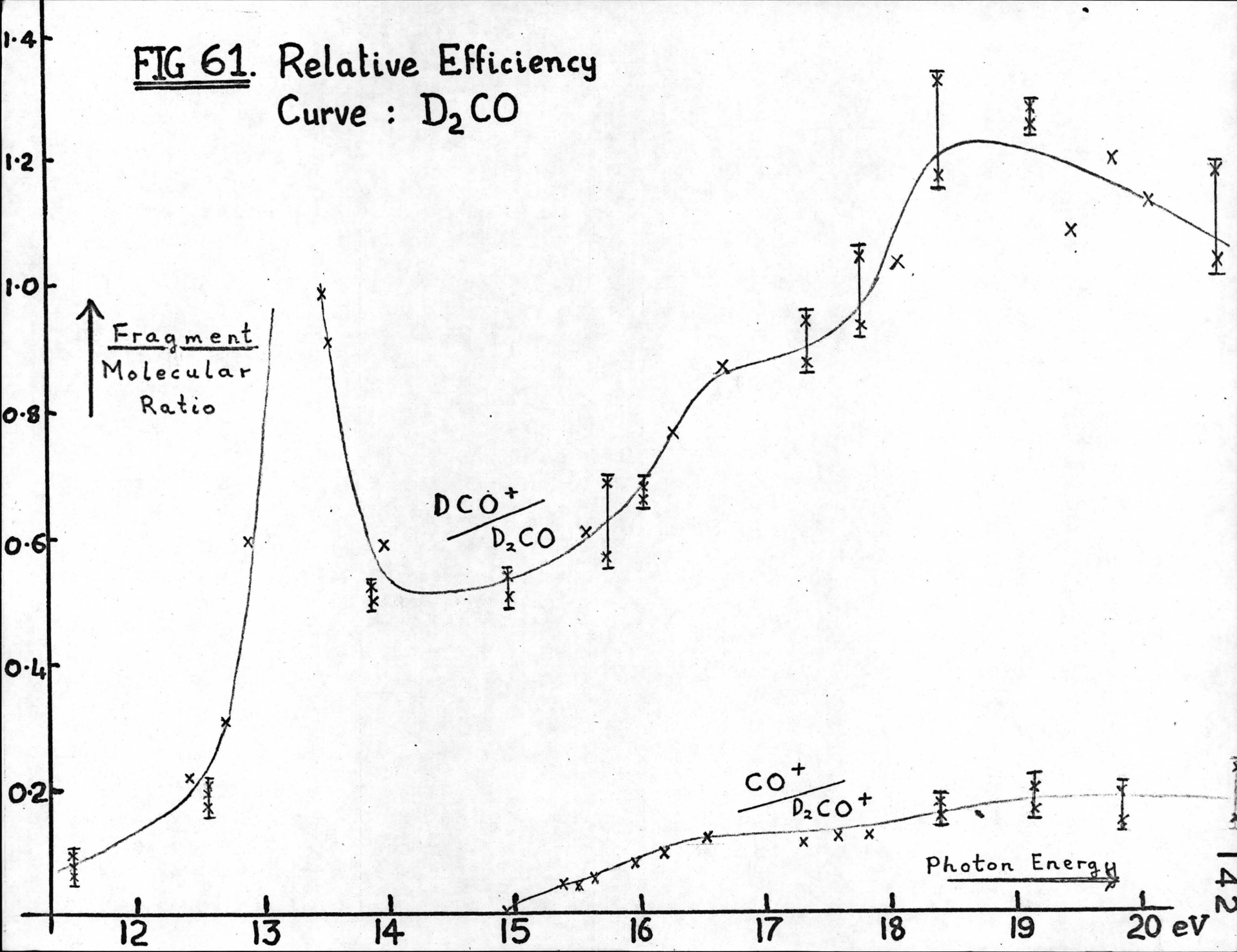
FIG 61. Relative Efficiency Curve : D_2CO
Fragment Molecular Ratio
DCO^+ / D_2CO
CO^+ / D_2CO^+
Photon Energy
1·4
1·2
1·0
0·8
0·6
0·4
0·2
12
13
14
15
16
17
18
19
20 eV

appearance potentials are indicated in table XIV. They are only of moderate value since a background mass spectrum (from the light source gases) had to be subtracted from the observed spectrum, making accurate determination of appearance potentials difficult.

The striking difference between the two ion curves is the greater fragment/molecular ion ratio for H_2CO above an ionising energy of approximately 13·5 eV. Undoubtedly some of the difference could be due to error introduced owing to the poor resolution in the H_2CO spectrum, and the co-incidence of the mass peak of D_2CO^+ with that of O_2^+ when an oxygen light source was used. These factors would seem unable to account completely for the discrepancy, which must therefore be assumed to be a genuine effect. No explanation can be offered for such a large difference, though theoretically [147,162], one might expect a few percent difference between the relative abundances from deuterated and normal compound, due to competition between autoionisation and decomposition into neutral fragments from super excited states of the molecule. The relative extent to which these two processes occur would have some slight isotope effect.

5. 2.3. Some Estimates of Bond Energies, and Some Possible Dissociation Processes.

Now $A P \; CHO^+ \geqslant I P \; CHO + D(H - CHO)$

Reed used this equation to calculate $D(H - CHO)$

$13{\cdot}10 \geqslant 9{\cdot}88 + D(H - CHO)$

$\therefore D(H - CHO) \leqslant 3{\cdot}22 \pm {\cdot}4$ eV 1

This was compared by Reed to a value of 3·21 ± ·01 eV found using independent data on H_2 [8a], CH_4 [163], and CH_3COH [159]. The data on CH_4 and CH_3COH comes from early electron impact work, and cannot be very accurate; and the combination of the three sets of data to find D(H - CHO) is likely to be even less so.

Reed similarly calculated D(H - CO) using I P CO = 14·01 eV [8c]

$$\underline{\underline{D(H - CO) \leqslant 1{\cdot}21 \text{ eV}}} \quad \ldots\ldots\ldots\ldots\ldots\ldots\ldots \quad 2$$

Taking $\Delta H\ (H_2CO \longrightarrow 2H + CO) = 4{\cdot}55$ eV [8c].

We have $\underline{\underline{D(H - CHO)}} = 4{\cdot}55 - \leqslant 1{\cdot}21$ eV

$$\underline{\underline{\geqslant 3{\cdot}34 \text{ eV}}} \quad \ldots\ldots\ldots\ldots\ldots\ldots \quad 3$$

(1) and (3) agree within experimental error and so Reed assumed that the values :-

$$D(H - CO) \simeq 1{\cdot}21 \text{ eV}$$

$$D(H - HCO) \simeq 3{\cdot}3 \text{ eV}$$

were correct.

The more recent value of A.P CHO^+ from H_2CO (see Table XIV) reduced D(H - CHO) found from equation (1) to $\leqslant$ 2·55 eV.

The present results from the T O F M S indicate that the A P of CHO^+ is certainly as low as 12·66 eV, and possibly as low as 11·4 eV. This would give a value of D(H - HCO) $\leqslant$ 1·5 eV from equation (1).

Values as low as ·607 eV, [164] and 1·04 eV [165] have been suggested for D(H - CO) from photochemical studies. Use of these values in equation (2) increases D(H - CHO) to $\geqslant$ 3·51 eV or $\geqslant$ 3·94 eV.

Thus the discrepancy between the two calculations becomes large, and

it is clear that present estimates of A.P CO^+ and I.P. HCO^+ from HCO, and A.P. HCO^+ from H_2CO are not nearly accurate enough to be relied on.

Figure 62 shows schematically a potential energy diagram for the molecular ionic states found from photoelectron spectroscopy. The zeroth vibrational levels are marked and also the energy levels to which the vibrational modes can be populated by direct ionisation. Also marked are the experimental appearance and ionisation potentials.

For the ground ionic state only a few vibrational levels are populated and it is obvious that fragmentation to yield HCO^+ cannot occur by direct ionisation unless the A P of HCO^+ is as low as 11·4 eV. If this were so, small amounts of HCO^+ might be expected but for the fact that only symmetric modes of vibration (ν_1, ν_2, ν_3, ^{8c}) are excited, none of which could lead to the formation of H· and HCO^+ at a dissociation limit.

Dissociation must take place via the antisymmetric CH_2 group stretching mode ν_5 (b_2)

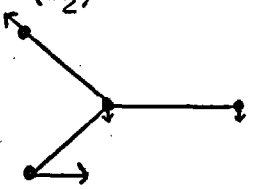

ν_5 (b_2)

Reed recognised this but assumed that the process occurred by direct population of the vibrational mode, ν_5, to a dissociation level of 13·1 eV.

$$H_2CO\ (X^1A_1) \longrightarrow H_2CO^+\ (X^2B_1) \longrightarrow CHO^+\ (X^1\Sigma^+) + H\ (^2S_{\frac{1}{2}})$$

above 10·88eV above 13·1eV

FIG 62

SCHEMATIC POTENTIAL ENERGY DIAGRAM FOR H_2CO^+, SHOWING APPEARANCE POTENTIALS AND VIBRATIONAL IONIC LEVELS POPULATED BY DIRECT FRANCK -CONDON TRANSITIONS.

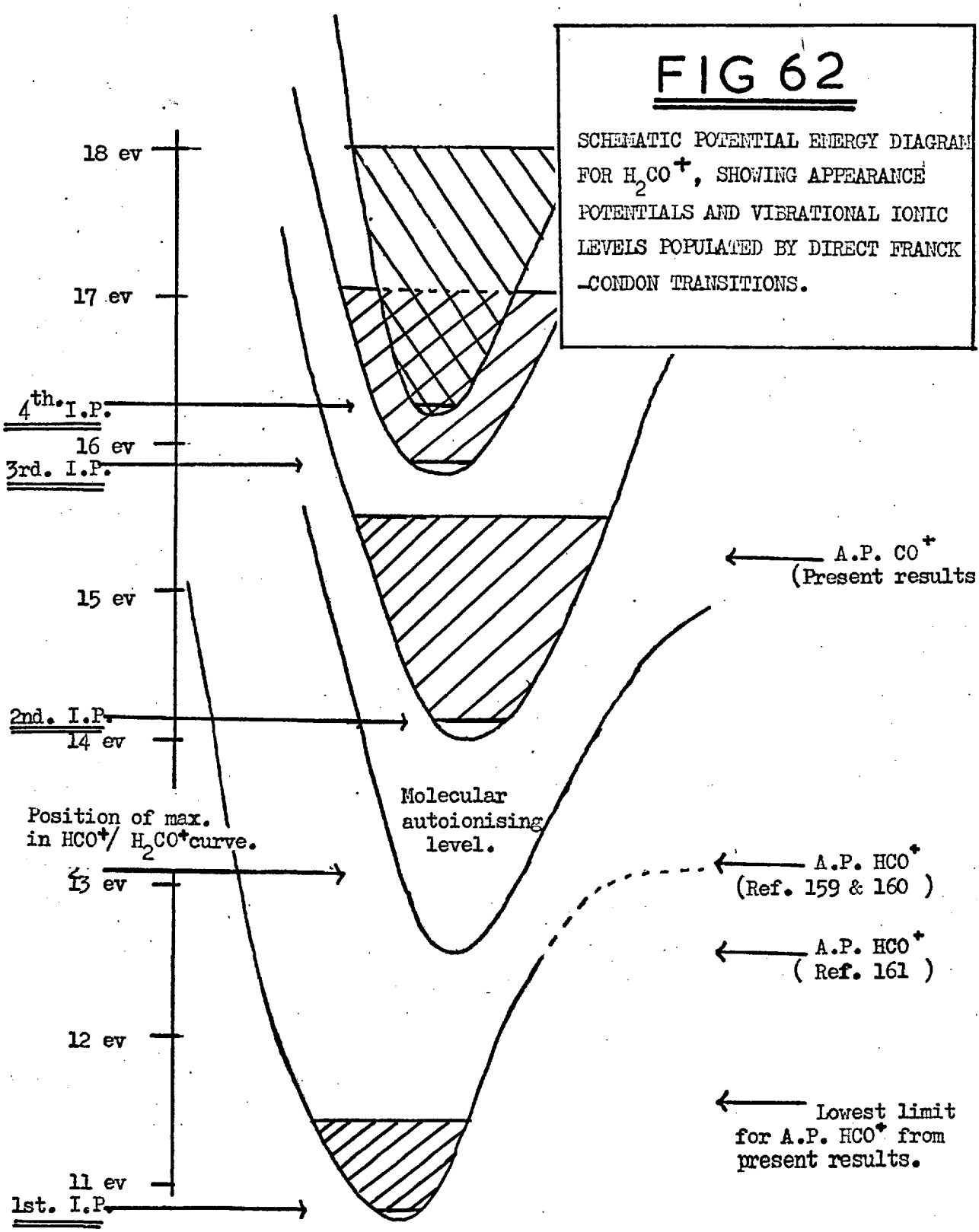

What is obvious now, from the DCO^+/D_2CO and HCO^+/H_2CO^+ curves of figures 60 and 61, and the break observed in the electron impact total ionisation curves,[152] is that the A P of HCO^+ quoted by Reed at 13·1 eV represents a dissociative autoionising level yielding HCO^+ fragment ions.

Lorquet,[166] in a theoretical discussion, showed that ν_5 would be the favoured vibration for dissociation, if it is assumed that dissociation occurred from the ground ionic state only, the required vibrational energy being obtained by radiationless transitions from excited ionic states to the ground state.

A very large number of curve crossings between states is necessary for this to be the sole means of fragmentation, and it is thought likely that dissociations from discrete excited ionic states do occur to some degree. In support of this the DCO^+/D_2CO^+ curve shows not only the autoionising level at 13·1 eV, but also signs of step functions over the energy region covered by the 2nd, 3rd, and 4th bands in the photoelectron spectrum.

Curve crossings out of these ionic levels could occur to yield HCO^+, and also CO^+ (A.P $\simeq$ 15·5 eV)

The A.P of CO^+ from D_2CO and H_2CO is interesting in that from

$$A.P\ CO^+ \geqslant I\ P\ CO + D(H - CHO)$$

one obtains $D(H - CHO) \leqslant 1{\cdot}5$ eV which is consistent with the value calculated from equation (1) using the lowest suggested A P of HCO^+ from H_2CO (present results).

Much more work on the mass spectrometery of H_2CO and HCO is

required before experimental estimates of bond strengths can be treated with confidence. High resolution photon impact efficiency curves for molecule ions and all fragments would be invaluable.

5. 3. N_2O, COS, CS_2, and CO_2

5. 3. 1. Photoelectron Spectra of the compounds.

These compounds have already been extensively studied by photoelectron spectroscopy[167-169,182,183], without complete resolution of the fine structure. In this section the spectra and the vibrational analysis of each compound are given, together with comparisons to existing data. The values of all the present experimental vibrational frequencies are collected in table XV and the experimental F-C factors in table XVI. A full discussion of the results and their implications is given in section 5. 3. 2.

5. 3. 1. (a) Nitrous Oxide, N_2O (Figures 63 and 64)

Four bands can be seen in the spectrum, each showing vibrational fine structure.

First Band (Figure 64A) :-

This band has an intense 0',0,0, peak at an I.P. of 12. 89(3) ev which is in good agreement with the value of 12.90 ev given by May and Turner[169] and those found from Rydberg series limits[170], and the photo-ionisation results of Dibeler and Walker[81] . The width of this peak at half height is 40 mv ± 5 mv, which is compatible with a spin-orbit splitting of ca. 20 mv. This is in agreement with the value of 18 mv obtained by Callomon[8c] from the emission spectrum of nitrous oxide, and indicates that the value of 40 mv given by Tanaka[170] is erroneous.

Three peaks corresponding to vibrationally excited states of the ion can be discerned, whereas no structure was visible in the original work[168,167], giving vibrational intervals of 1140 cm^{-1} ± 50 cm^{-1} and 1750 cm^{-1} ± 50 cm^{-1}. The ground state molecular frequencies of modes ν_1 and ν_2 are 1285 cm^{-1} and 2224 cm^{-1} [8c], and for the ground ionic state 1126 cm^{-1} and 1736 cm^{-1} are quoted from emission work[95] . We conclude therefore that

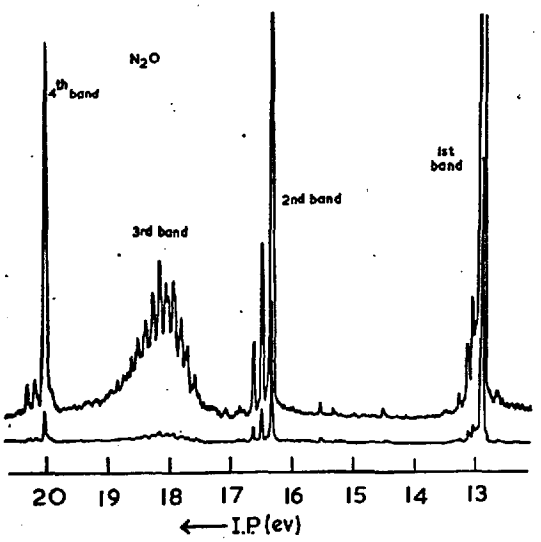

NITROUS OXIDE

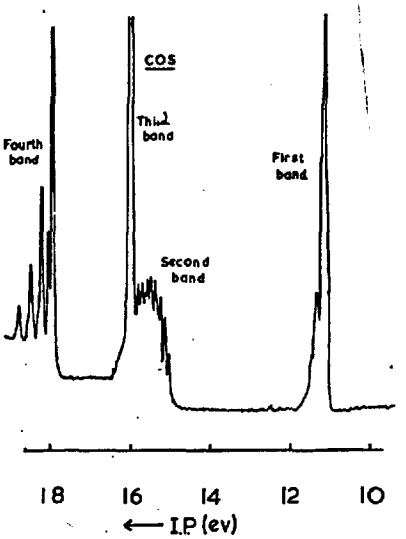

CARBONYL SULPHIDE

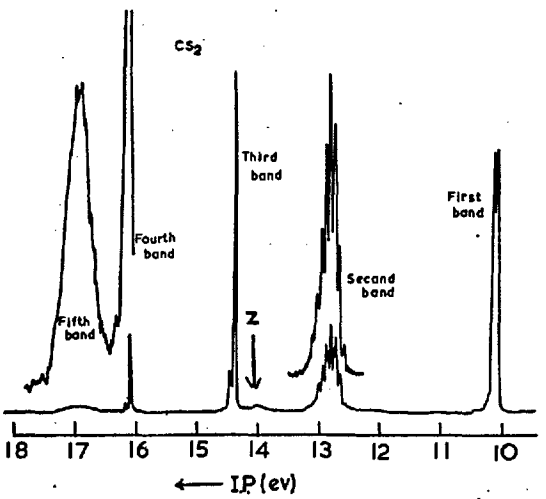

CARBON DISULPHIDE

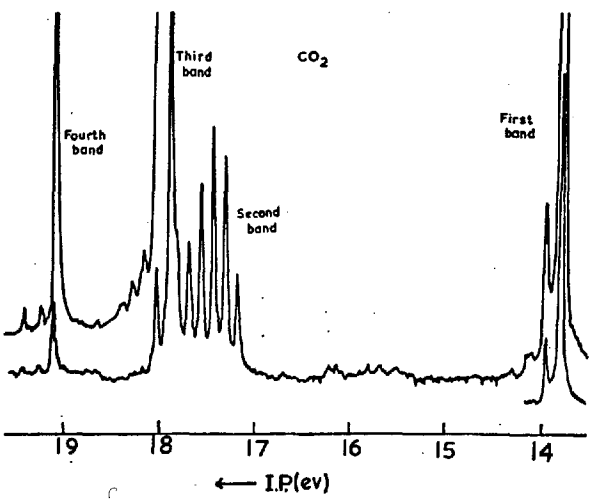

CARBON DIOXIDE

FIG. 63

PHOTOELECTRON SPECTA OF THE TRIATOMIC GASES — N_2O, COS, CS_2, CO_2

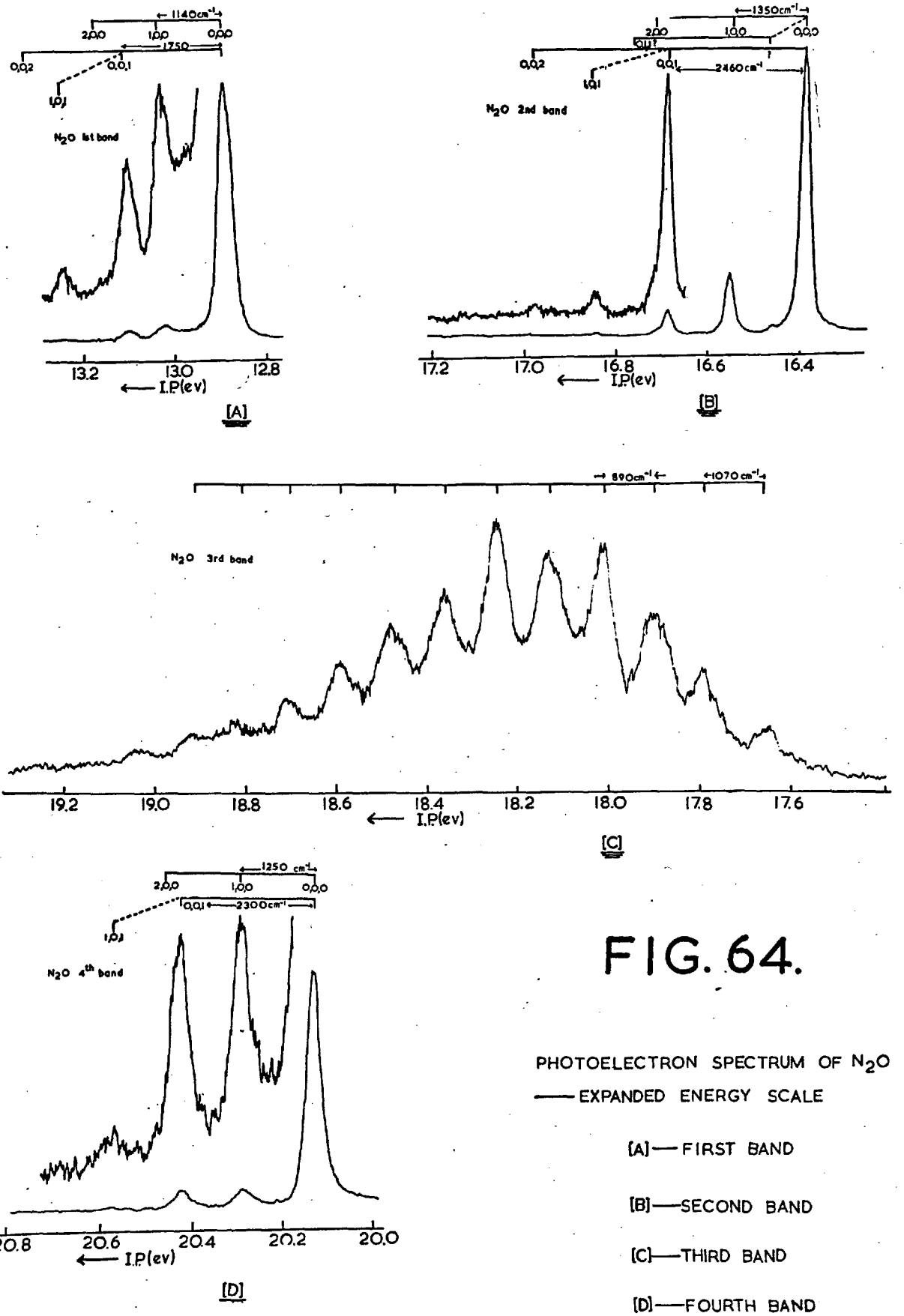

FIG. 64.

PHOTOELECTRON SPECTRUM OF N_2O

—— EXPANDED ENERGY SCALE

[A]—FIRST BAND

[B]—SECOND BAND

[C]—THIRD BAND

[D]—FOURTH BAND

modes ν_1 and ν_3 are excited in the photoelectron spectrum. Carette[76] has recently reported breaks in the electron impact efficiency curve of nitrous oxide corresponding to vibrational fine structure, though Dibeler and Walker[81] observe none on their photoionisation efficiency curve. The breaks observed are at .16 ev, .32 ev, .48 ev, and .56 ev above the N_2O^+ threshold. Though those at .16 ev (1300 cm^{-1}) and at .48 ev. (3875 cm^{-1}) probably correspond to excitations of one quanta of ν_1, and one quanta of ν_3, the others are harder to account for, and are certainly not observed in the photoelectron spectrum.

Second Band (Figure 64B) :-

Again an intense 0,0,0, peak is observed, together with well resolved associated vibrational structure spreading over at least .75 ev. The value of the I.P. 16.38(9) ev, is in close agreement with Tanaka's Rydberg series limit[170] of 16.39 ev. This excited state of the ion has also been observed recently by charge exchange experiments using A^+ and Kr^+,[171] by studying the emission spectrum of N_2O^+ excited by electric discharge[95] , and by electron impact[76].

Analysis of the vibrational structure (see figure 64B) indicates that ν_1 and ν_3 are excited with the frequencies given in table XV, which agree closely with values found from emission[95] , and the value of ν_1 found from a Rydberg series[170] converging at 16.5 ev. A simple series in ν_1 with a frequency of 1130 cm^{-1} was originally proposed by May and Turner from the low resolution spectrum. There is a small peak at 600 cm^{-1} separation from the 0,0,0, peak. Though this is in agreement with the frequency of ν_2[8c], the excitation of one quantum of ν_2 is forbidden by the selection rules (see section 5. 3. 2.(a)).

Third Band (Figure 64C) :-

This band consists of a long series of broad peaks spread over about 1 ev, with a somewhat irregular peak width, and intensity pattern. The adiabatic I. P. is 17. 65(0) ev and the vertical 18.23(6) ev. This state of the ion has

not been observed by any other technique.

The vibrational structure is complex, and almost certainly does not consist of a simple series in ν_1, of frequency 900 cm^{-1} as was originally thought[168]. The overall shape of the band is similar to that of the second band of COS (vide infra) where two vibrational modes are strongly excited, but attempts to apply a similar analysis here were not successful.

Fourth Band (fig. 64D)

The fourth band exhibits an intense 0,0,0 peak at an ionisation potential of 20.11(3) eV in good agreement with existing measurents[168,170]. No vibrational structure is reported in absorption[170], but weakly excited vibrational levels can be observed in the photoelectron spectrum. In Turner and May's paper[168], there was some doubt as to whether both ν_1 and ν_3 modes were excited, or whether the series consisted only of ν_1. There can be little doubt now that both modes are involved with frequencies 1280 cm^{-1} (ν_1) and 2300 cm^{-1} (ν_3) - see fig. 64D.

5. 3. 1. (b) Carbonyl Sulphide, COS (Figures 63 & 65)

Four bands in the spectrum (fig. 63) can be distinguished and the overall form is similar to that of CO_2. Vibrational structure is associated with each band.

First Band (fig. 65A)

The peaks are clearly split into their doublet components $^2\Pi_{3/2}$ and $^2\Pi_{1/2}$, giving adiabatic I.P.'s of 11.18(9) eV and 11.23(3) eV, and a spin-orbit splitting value of 44 mV ± 5 mV. These values are in close agreement with the results of Matsunga and Watanabe[172] who found values of 11.18 and 11.22 eV from a Rydberg absorption limit, and total photoionisation efficiency curves, and with the same values found by Dibeler and Walker from their photoionisation mass spectrometric studies. May and Turner[168]

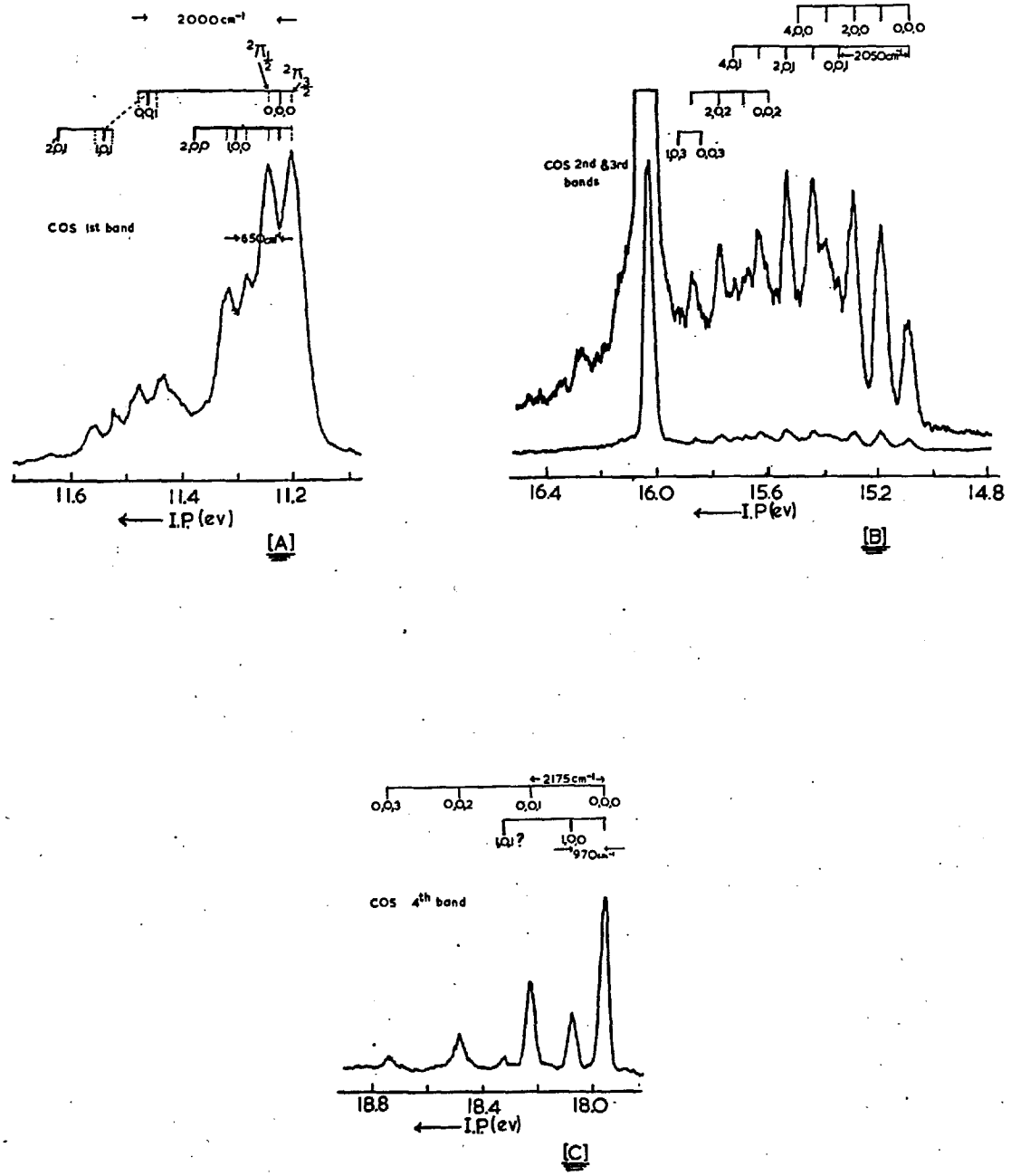

FIG. 65.

PHOTOELECTRON SPECTRUM OF COS

—— EXPANDED ENERGY SCALE

[A]—FIRST BAND

[B] SECOND AND THIRD BANDS

[C] FOURTH BAND

were unable to resolve either the spin orbit doublet or any vibrational structure in this band.

Analysis of the associated fine structure indicates two ion vibrational modes ν_3 of frequency 2000 ± 50 cm^{-1} and ν_1 of frequency 650 ± 50 cm^{-1}. The value of ν_3 is in agreement with that found by Leach[173] from the emission spectrum of COS^+ but a value for ν_1 has not previously been established, though an unassigned frequency of 610 cm^{-1} was observed in Matsunga and Watanabe's[172] absorption spectrum.

Second Band (fig. 65B)

This band consists of a long series of peaks (cf. N_2O, third band) spreading over ca. 1 eV , giving an adiabatic I.P. of 15.08(0) eV and the vertical I.P. of 15.52(8) eV. The values originally given by May and Turner[168] were 15.0 and 15.6 eV, and no vibrational structure was resolved. This I.P. has not been observed in absorption but has been identified in the emission spectrum[173] of COS^+, though it was assigned to another electronic state of the ion (see section 5. 3. 2. (a))

The vibrational structure is complex and is considered to consist of a series in ν_3 (2050 cm^{-1}) and one in ν_1 (790 cm^{-1}), together with some combination bands. This is the first time that values for the frequencies of the vibrational modes in this state of the inn have been obtained.

Third Band (Fig. 65B)

The very intense 0,0,0, peak of the third band interrupts the second band at an I.P. of 16.04(2) eV. This is in excellent agreement with the previous estimates of this I.P.[168,170] . This state of the ion has also been identified by Penning ionisation[70]. Only very weak vibrational structure is associated with the band, and since it is superimposed on the tail of the second band an analysis is not feasible.

Fourth Band (Figure 65C) :-

The 0,0,0, peak of the fourth band yields an I. P. of 17.96(0) ev which compares with the value of 18.00 ev found by Turner and May[168], and 17.93 ev from the Rydberg series limit of Tanaka et al.[170] where no associated vibrational structure was observed. The higher members of the vibrational series appear in the photoelectron spectrum.with moderate intensity and lead to estimates of 970 cm^{-1} for the frequency of ν_1, and 2175 cm^{-1} for ν_3. This clears up the earlier doubts[168], caused by incomplete resolution, as to whether both these vibrational modes were being excited.

The 1,0,1, peak is an uncertain assignment.. It is considered that a strong coupling between ν_1 and ν_3 must be involved, such that the frequency is not correctly represented by the frequency of the 1,0,0, peak plus the frequency of the 0,0,1, peak.

In previous work on the photoelectron spectrum of COS, a possible fifth band at ca. 20 ev had been observed[167,168]. With the constant electron bandwidth method of detection it is possible to observe features in this region of the spectrum with greater intensity, and it becomes obvious that peaks observed at ca. 20.3 ev are due to ionisation by the hydrogen Lyman β Line emitted in small amounts by impurity in the light source, and are a "replica" of the first band in the spectrum.

5. 3. 1. (c) Carbon Disulphide, CS_2 (Figures 63 and 66)

The spectrum exhibits at least five bands, with the possibility of a sixth (marked Z on the figure 63). Vibrational structure is well resolved on four of the bands.

First Band (Figure 66A)

This band consists of an intense 0,0,0, doublet peak, giving I.Ps of 10.06(8) ev and 10.12(2) ev for the two components, and very little, if any,

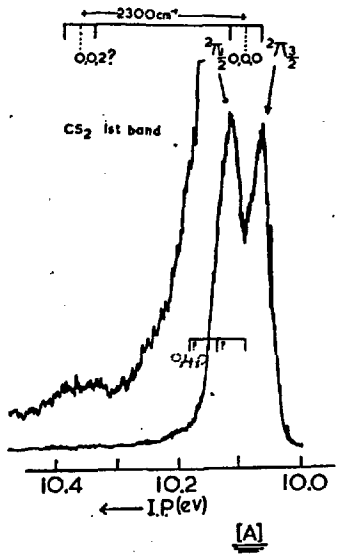

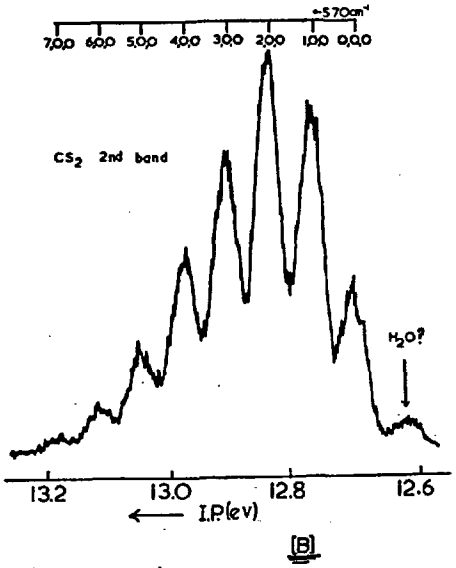

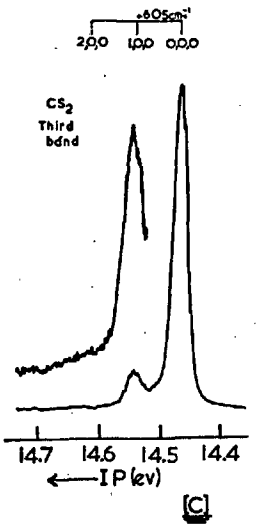

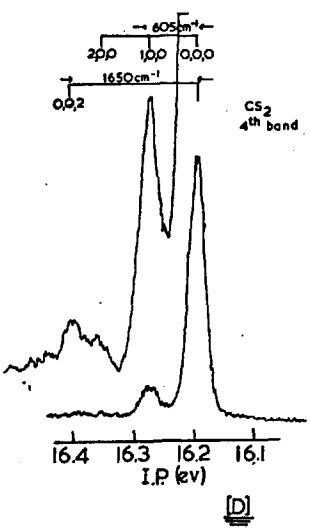

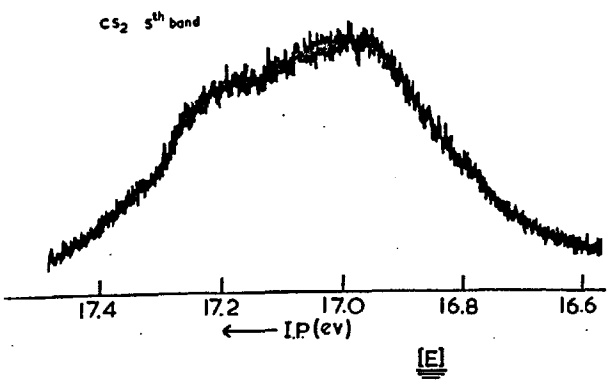

FIG. 66

PHOTOELECTRON SPECTRUM OF CS_2

——EXPANDED ENERGY SCALE

[A]—FIRST BAND

[B]—SECOND BAND

[C]—THIRD BAND

[D]—FOURTH BAND

[E]—FIFTH BAND

associated vibrational structure. These values are in agreement with the Rydberg series limits of 10.07(6) eV and 10.13(0) eV of Tanaka et al, the unresolved doublet value of 10.11 eV from the photoelectron spectrum of May and Turner,[168] and the photoionisation mass spectrometric values[81] of 10.05(9) and 10.11(2) eV. The doublet nature of this state of the ion has also been observed in emission.[95,173]

A very weak peak at separation 2340 cms^{-1} (290 mv) from the 0,0,0, peak may correspond to the 0,0,2, excitation, which places a value of 1170 cms^{-1} on the frequency of ν_3. It is also just possible that excitations involving the bending mode ν_2 are involved (See Section 5.3.2.(b).).

Second Band (figure 66B).

The second band consists of a series of peaks spreading over approximately 1 eV. The vertical ionisation potential is 12.83(8) eV, and the 0,0,0, peak is taken to be the one at 12.69(4) eV. Thus the band is interpreted as a simple vibrational series in ν_1, which has a frequency of 565 cms^{-1} $\pm$ 50 cms^{-1}. This ionisation potential has been observed only by photoelectron spectroscopy, and previous studies[167,168] failed to resolve the associated vibrational structure.

The persistence of a peak at 12.60(7) eV is somewhat worrying, for although it falls exactly at the ionisation potential of water, it could not be removed by physical or chemical means.

Third Band (figure 66C).

A very weak broad band centred at approximately 14.1 eV (figure 63) has been found. It was apparent also in May and Turner's spectrum[168] but was not mentioned in the text, and in the absence of any suitable interpretation must be regarded as an impurity band.

The intense peak at 14.47(8) eV is taken as the 0,0,0, component of

the third I.P.. This is in agreement with values found from Rydberg series limits[170], emission spectra[94], and charge exchange with A^+ and Kr^+,[171] as well as May and Turner's original photoelectron spectrum value of 14. 49 ev.[168]

One or possibly two vibrationally excited states of the ion are observable (see Fig. 66C) giving a vibrational frequency for ν_1 of 605 cm^{-1} ± 50 cm^{-1}. No structure was resolved in previous photoelectron spectra[167,168], but Tanaka et al[170] estimated that ν_1 was of the order 500 - 600 cm^{-1} from a Rydberg series.

Fourth Band (fig. 66D)

Like the third band this consists of an intense 0,0,0, peak and very little accompanying vibrational excitation. The I.P. is 16.19(6) eV in agreement with the Rydberg limit of 16.18 eV[170], and the earlier photoelectron value of 16.19 eV[168].

The vibrational spacings indicate a frequency of 605 cm^{-1} ± 50 cm^{-1}, taken to be mode ν_1, and possibly one of 1650 cm^{-1} ± 50 cm^{-1}. This latter value is near that of ν_3 in its ground molecular state (1530 cm^{-1} [8c]), however owing to the selection rules (see section 5. 3. 2. (a)) the excitation of one quantum of ν_3 is forbidden, and the only other possibilities are $2\nu_3$ with the frequency of ν_3 greatly reduced to 805 cm^{-1} (cf. CO_2 and discussion in section 5. 3. 2 (a)), or that the peak is an impurity. No values of vibrational frequencies associated with this state of the ion have previously been recorded.

Fifth Band (fig. 66E)

This band, which is broad and featureless, is centred at 17.1 eV and spreads over ca. 1.2 eV. There may be a slight suggestion of a "double hump" (see fig. 66C).

As with COS, it has previously been suggested that there might be a

further I.P. of less than 21.23 eV. Tanaka et al [170] recorded a weak series limit at 19.51 eV, and it also seems possible that some weak genuine structure might exist in the photoelectron spectrum at about this value [168]. On careful examination of this region using the present apparatus, two "replicas" of the first band were observed at 19.3 eV and 21.0 eV. These are just the values expected for ionisation by Lyman β (12.07 eV) and Lyman α (10.27 eV) impurity lines in the light source, and it is concluded that no genuine I.P. exists between the fifth band and 21.2 eV.

5. 3. 2. (d) Carbon Dioxide, CO_2 (figs. 63 & 67)

The ionic states of CO_2 have been the subject of extensive spectroscopic studies by many people [27, 76, 93, 169, 174, 111], and rather more is already known about the excited electronic states than for the preceding three compounds.

The photoelectron spectrum (fig. 63) shows four bands, each with resolved vibrational structure. The second and third bands overlap as in COS and the spectrum is very similar to that of COS, with all spectral features some 2 eV to higher ionisation energies.

First Band (fig. 67A)

The band consists of a strong 0,0,0, peak giving an adiabatic I.P. of 13.78(8) eV, and two weak vibrational overtone peaks. The half-width of the main peak, 40mV, is compatible with a spin orbit splitting of 22mV obtained from the Rydberg series limits [170] of 13.76(5) eV and 13.78(7) eV for the doublet components of this state of the ion. A value of 20 mV was indicated by Mrozowski's [93] original work on the emission spectrum of CO_2^+.

Two vibrational modes are excited, ν_1 and ν_3, and it so happens that the frequency of ν_3 (2840 ± 50 cm^{-1}) is close to the value of ν_1 (2420 cm^{-1}). Thus the very broad flat-topped peak centred at 14.09 eV consists of these two components. The frequency of ν_1 is confirmed by Tanaka et al [170] in their

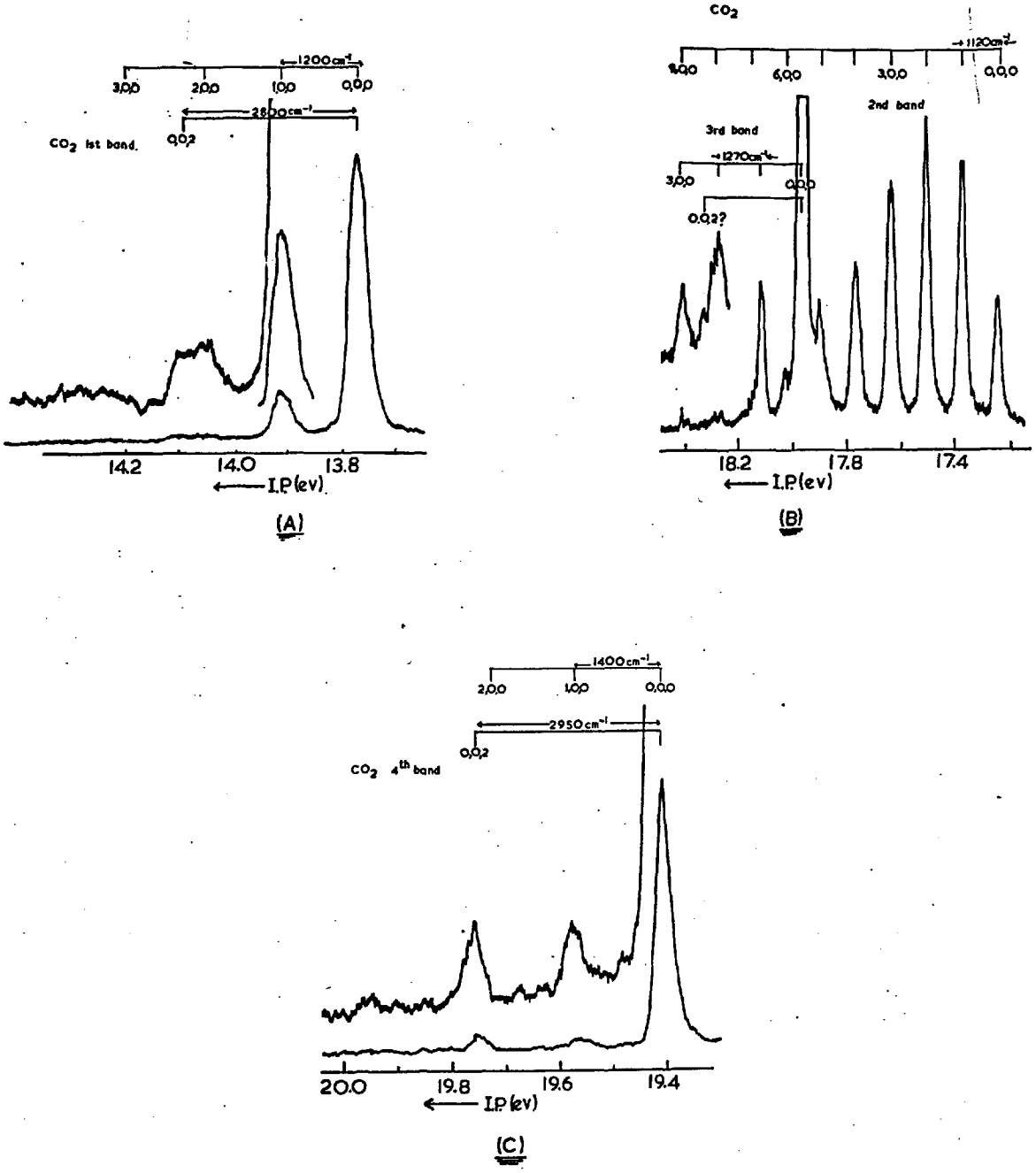

FIG. 67.

THE PHOTOELECTRON SPECTRUM OF CO_2
—EXPANDED ENERGY SCALE
(A)— FIRST BAND
(B)— SECOND AND THIRD BANDS
(C)— FOURTH BAND

Rydberg series work (1260 cm^{-1}), Dibeler and Walker's[81] mass spectrometric value (1250 cm^{-1}), and Mrozowski's[93] early work on the emission spectrum. The frequency of ν_3 is in agreement with Johns'[175] assignment of 1469 cm^{-1}, but disagrees with Mrozowski's tentative assignment of 2305 cm^{-1}. The frequencies of these modes, and the experimental F-C factors have come in for some discussion recently[169] in relation to the theoretical calculations of Sharp and Rosenstock[27]. This is dealt with in section 5.3.2. (b).

Carette[76] claims to have resolved vibrational fine structure on his electron impact efficiency curves for CO_2. The breaks come at 1290 cm^{-1} (.16ev), 2580 cm^{-1} (.32ev), 3870 cm^{-1} (.48ev), and 6210 cm^{-1} (.77ev) above threshold. The break at 1290 cm^{-1} undoubtedly corresponds to excitation of one quantum of ν_1, and that at 2580 cm^{-1} the average of $2\nu_1$ and $1\nu_3$, but the remaining breaks in Carette's curve cannot be correlated with anything in the photoelectron spectrum. It should be noted that the sharpness of the breaks in the efficiency curve would seem to indicate much larger F-C factors for the vibrationally excited states than are found from the photoelectron spectrum.

Second Band (Figure 67B)

The second band consists of a fully resolved simple series of peaks. The adiabatic I.P. is 17.32(3) ev in agreement with the value of 17.31 ev found from emission[93], and the resolved doublet values of 17.312ev and 17.323ev found in absorption[40].

The vibrational spacing indicates a frequency of 1100 cm^{-1} ± 50 cm^{-1} for the mode excited, ν_1. May and Turner were able to resolve this series quite well in their original spectrum[168] and an average spacing of 1050 cm^{-1} was found for the first five members. Ogawa and Tanaka[40] obtained Rydberg series converging to the first seven vibrational levels of this state of the ion, giving a frequency for ν_1 of 1120 cm^{-1} and Mrozowski[93] arrived at a similar value from the emission

spectrum of CO_2 . The assignment of this ionic state as $^2\pi_u$ was unambiguous in each case. (See also section 5.3.2.(a) and reference 175). There is no suggestion that this state is $^2\Sigma_u^+$ as reported by Collin and Natalis[183]. The assignment of the equivalent photoelectron bands in N_2O, COS, and CS_2 (i.e. the ones involving a long vibrational series) is also without question $^2\pi_u$.

The vertical I.P. corresponds to the 2,0,0, component in the photoelectron spectrum series, at an IP. of 17.59(5) ev. Ogawa and Tanaka considered the 3,0,0, component to be the most intense.

Third Band (Figure 67B) :-

An intense peak at 18.08(2) ev, interrupting the second band after the 5,0,0, component, is in close agreement with the Rydberg limit[40] of 18.07(6) ev. Associated with it is a peak at 18.23(5) ev, which is the 1,0,0, component of the third band (cf Rydberg limit at 18.23 ev) giving a frequency for ν_1 of 1270 cm^{-1}.

Weak peaks to higher energies, are at positions such that they may belong to the second band or third band series (see Figure 67B). This yields a value of 1400 cm^{-1} for ν_3. (A very weak peak at ~ 18.3 ev may represent the 0,0,2 vibration)

Fourth Band (Figure 67C) :-

The fourth band consists of a strong 0,0,0, peak at 19.40(0) ev (cf Rydberg limit at 19.38 ev[170]), and two vibrational peaks. Several more extremely weak peaks may also be present. It seems likely that ν_1 and ν_3 are being excited with frequencies of 1390 cm^{-1} and 1470 cm^{-1}, the two peaks being the 1,0,0, and 0,0,2 vibrational components. The very large reduction in the frequency of ν_3, compared to that of the ground state of the molecule, is discussed in section 5.3.2.(a) together with similar effects noticed in CS_2.

In the low resolution spectrum of May and Turner[168], it was not clear exactly which modes were being excited. A vibrational frequency of 1370 cm^{-1} was

TABLE XV

VIBRATIONAL FREQUENCIES OF EACH IONIC STATE OF THE TRIATOMIC MOLECULES

Compound	Electronic State	Photoelectron Band	Adiabatic Ionisation Potential (ev)	Vib. Frequencies- This Work. cm^{-1}			Vib. Frequencies— Turner & May [168]			Vib. Frequencies-Other Techniques		
				ν_1 [a] (cm^{-1})	ν_2 [b] (cm^{-1})	ν_3 [c] (cm^{-1})	ν_1 [a] (cm^{-1})	ν_2 [b] (cm^{-1})	ν_3 [c] (cm^{-1})	ν_1 [a] (cm^{-1})	ν_2 [b] (cm^{-1})	ν_3 [c] (cm^{-1})
N_2O^+	$\tilde{X}\,^2\Pi$	1st.	12.89(3)	1140	—	1750	—	—	—	1126 [8c]	461	1737
	$\tilde{A}\,^2\Sigma^+$	2nd.	16.38(9)	1350	600 ?	2460	1130	—	—	1345 [8c]	614 [8c]	2451 [8c]
	$\tilde{B}\,^2\Pi$	3rd.	17.65	900?	—	—	884	—	—	—	—	—
	$\tilde{C}\,^2\Sigma^+$	4th.	20.11(3)	1280	—	2300	1285	—	—	—	—	—
N_2O	Ground State									1285 [8c]	589 [8c]	2224 [8c]
COS^+	$\tilde{X}\,^2\Pi$	1st	11.18(9), 11.23(3)	650	—	2000	—	—	—	610 ? [172]	—	2069 [8c]
	$\tilde{A}\,^2\Pi$	2nd.	15.08(0)	790	—	2050	—	—	—	—	—	—
	$\tilde{B}\,^2\Sigma^+$	3rd.	16.04(2)	—	—	—	—	—	—	—	—	—
	$\tilde{C}\,^2\Sigma^+$	4th.	17.96(0)	970	410 ?	2175						
COS	Ground State									859 [8c]	520 [8c]	2062 [8c]
CS_2^+	$\tilde{X}\,^2\Pi_g$	1st.	10.06(8), 10.12(2)	—	—	1170 ?	—	—	—	624 [8c]	205 [8c]	—
	$\tilde{A}\,^2\Pi_u$	2nd.	12.69(4)	565	—	—	—	—	—	—	—	—
	$\tilde{B}\,^2\Sigma_u^+$	3rd.	14.47(8)	605	—	—	—	—	—	500—600 [170]	—	—
	$\tilde{C}\,^2\Sigma_u^+$	4th.	16.19(6)	605	—	805 ?	—	—	—	—	—	—
	$\tilde{D}\,^2\Sigma_u^+$	5th.	17.0 d	—	—	—	—	—	—	—	—	—
CS_2	Ground State									658 [8c]	397 [8c]	1533 [8c]
CO_2^+	$\tilde{X}\,^2\Pi g$	1st.	13.78(8)	1210	—	1420	—	—	—	1250 [170]	531 [174]	1469 [8c]
	$\tilde{A}\,^2\Pi_u$	2nd.	17.32(3)	1100	—	—	1050	—	—	1131 [8c]	560	2731 [8c]
	$\tilde{B}\,^2\Sigma_u^+$	3rd.	18.08(2)	1270	—	—	1210	—	—	1275 [40]	—	—
	$\tilde{C}\,^2\Sigma_g^+$	4th.	19.40(0)	1390	—	1470	1370	—	1370?	—	—	—
CO_2										1388 [8c]	667 [8c]	2349 [8c]

a — symmetrical stretching frequency

b — bending mode

c — unsymmetric stretching frequency

d — vertical I.P.

TABLE XVI

VIBRATIONAL FRANCK-CONDON FACTORS IN EACH STATE OF THE ION

Compound	Electronic State of ion	Vibrational Component $\nu_1\nu_2\nu_3$	Experimental Franck-Condon Factors			Calculated F-C Factors [27]
			This* Work	Spohr & Puttkamer [55]	Fluorescence [180]	
N_2O	$\tilde{X}\,^2\Pi$	000	.91	1.0		
		100	.05	-		
		001	.03	-		
		(200)	.01	-		
		101	.01	-		
	$\tilde{A}\,^2\Sigma^+$	000	.749	.82	.7	
		(010)	(.002)	-	-	
		100	.164	.12	.2	
		001	.073	.06	.1	
		101	.008	-	-	
		002	.004	-	-	
	$\tilde{B}\,^2\Pi$	000	.023			
		?	.057			
		?	.086			
		?	.127			
		?	.124			
		?	.151			
		?	.111			
		?	.095			
		?	.075			
		?	.050			
		?	.036			
		?	.027			
		?	.018			
		?	.011			
	$\tilde{C}\,^2\Sigma^+$	000	.78			
		100	.08			
		001	.11			
		101	.02			
		200	.01			
COS	$\tilde{X}\,^2\Pi$	000	.48			
		100	.28			
		(200)	(.08)			
		001	.12			
		101	.06			
	$\tilde{A}\,^2\Pi$	000	.04			
		100	.08			
		200	.10			
		001	.06			
		300	.07			

		101	.10			
		400	.06			
		201	.10			
		(002)	–			
		301	.08			
	Overlapping 3rd band	102	.06			
		401	.06			
		202	.08			
	$\tilde{B}\ ^2\Sigma^+$	000	.95			
	$\tilde{C}\ ^2\Sigma^+$	000	.48			
		100	.15			
		001	.24			
		002	.09			
		003	.02			
CS_2	$\tilde{X}\ ^2\Pi_g$	000	1			
		(020)	(.05)			
		(040)	(.025)			
	$\tilde{A}\ ^2\Pi_u$	000	.105			
		100	.216			
		200	.252			
		300	.189			
		400	.124			
		500	.070			
		600	.031			
		700	.012			
	$\tilde{B}\ ^2\Sigma_u^+$	000	.89			
		100	.10			
		200	.01			
	$\tilde{C}\ ^2\Sigma_g^+$	000	.92			
		100	.08			
		002	?			
CO_2	$\tilde{X}\ ^2\Pi_g$	000	.812	.82		.89
		100	.149	.18		.11
		200	.021	–		.01
		002	.017	–		–
	$\tilde{A}\ ^2\Pi_u$	000	.082	.08	.15	
		100	.180	.18	.24	
		200	.275	.20	.26	
		300	.180	.22	.20	
		400	.125	.15	.13	
	Overlapping 3rd band	500	.094	.12	–	
		600	.043	.04	–	
		700	.021	–	–	

$\hat{B}\,^2\Sigma_u^+$	000	.848	.9
	100	.126	.1
	(200)	.017	–
	(300)	.010	–
$\hat{C}\,^2\Sigma_g^+$	000	.91	
	100	.04	
	002	.05	

* Estimated accuracy varies from peak to peak ± .01 in the more favourable cases.

proposed for ν_1. An identical frequency was proposed for ν_3, with the assumption that it was being excited in units of two quanta. The possibility that only ν_1 was being excited with an irregular F-C intensity could not be excluded from a study of the low resolution spectrum.

5. 3. 2. Discussion of Results

5. 3. 2. (a) The Electronic Structure of the Compounds, and the Bonding Characteristics of the Orbitals involved

The electronic assignment of each ionic state of the compounds and also their vibrational parameters are given in Table XV.

Mulliken[176] in 1935 described the structure of CO_2 in its ground molecular state as being :

$$(1s_o)^2\,(1s_o)^2\,(1s_c)^2\quad \underset{\text{O—C—O}}{(s_o+s_c+s_o,\,\sigma_g)^2}\,\underset{\text{O}\leftrightarrow\text{O}}{(s_o-s_o,\,\sigma_u)^2}\,\underset{\text{O—C—O}}{(\sigma_o+s_c+\sigma_o,\,\sigma_g)^2}$$

$$\underset{\text{O—C—O}}{(\sigma_o+\sigma_c+\sigma_o,\,\sigma_u)^2}\,\underset{\text{O—C—O}}{(\pi_o+\pi_c+\pi_o,\,\pi_u)^4}\,\underset{\text{O}\leftrightarrow\text{O}}{(\pi_o-\pi_o,\,\pi_g)^4}$$

He simplified the valence shell notation to :-

$$\underset{\text{(a) O: O:}}{(\sigma_g)^2\,(\sigma_u)^2}\quad \underset{\text{(b) O-C-O O-C-O}}{(\sigma_g)^2\,(\sigma_u)^2}\quad \underset{\text{O-C-O}}{(\pi_u)^4}\,\underset{\text{O:}}{(\pi_g)^4}\quad \ldots\ldots\ldots\ldots\ {}^1\Sigma_g^+$$

Thus the $(\pi g)^4$ orbital is regarded as being virtually non-bonding, as there is very little overlap, and the $(s_o+s_c+s_o,\sigma g)^2$ and $(s_o-s_o,\sigma g)^2$ orbitals are considered also to be non-bonding and resemble atomic orbitals. They may be written as $(2s_0)^2$, $(2s_0)^2$ and regarded as "inner" oxygen atomic orbitals.

An analagous configuration can be written for CS_2, and similar ones for COS and N_2O except that the "g" and "u" notation no longer applies. Removal

of an electron in turn from the π_g, π_u, σ_u, ... orbitals will leave the ion in the electronic states :

$$\tilde{X}\ ^2\pi_g\ ,\quad \tilde{A}\ ^2\pi_u,\quad \tilde{B}\ ^2\Sigma_u^+,\quad \tilde{C}\ ^2\Sigma_g^+$$

each of these states corresponding to an ionization potential observed in the photoelectron spectrum. The two important questions are :

(1) Are the original orbital energy levels correctly ordered in the Mulliken description ?

(2) How far can one distinguish between the σ orbitals of type (a) and (b) ?

Three main theoretical calculations concerning the molecular orbital energy levels of CO_2 have been carried out since Mulliken's original semi-empirical formulation of the electronic structure. The calculated energy levels are shown in Table XVII together with the ionization potentials found in the present work.

Mulligan[32] found the orbital order to be :

$$\underbrace{(\sigma_g)^2\ (\sigma_u)^2}_{(a)}\quad (\sigma_g)^2\quad (\pi_u)^4\quad \underbrace{(\sigma_u)^2}_{(b)}\quad (\pi_g)^4$$

His results indicated that type (a) orbitals could not be considered as only $2s_O$ type. Large amounts of oxygen p_z and carbon orbital mixing indicated that these levels were strongly bonding. Similarly (b) type orbitals also have strong s-p (O) mixing which renders them less bonding than Mulliken indicated.

The general features of Mulligan's results were borne out by the later calculations of McLean[10], and Pyerimhoff et al[33]. Both calculations placed the σ_u and π_u orbitals close together and Pyerimhoff's results indicated that the (a) type orbitals had greater bonding character than the (b) type.

Now Mrozowski[93] identified the $\tilde{A}\ ^2\pi_u \rightarrow \tilde{X}\ ^2\pi_g$ transition in the emission spectrum of CO_2^+ as having an energy of 3.535 eV. The second ionisation potential

of carbon dioxide is 3.535 eV greater than the first (see section 5. 3. 2) thus there is no doubt that the second band in the photoelectron spectrum relates to the $^2\pi_u$ ionic state. That the π_u orbital is strongly bonding is borne out by the the shape of the band, a long vibrational series being excited with frequency of ν_1 reduced compared to that in the ground state of the molecule.

The valence shell configuration for carbon dioxide can thus be written :

$$(\sigma_g)^2 \ (\sigma_u)^2 \ (\sigma_g)^2 \ (\sigma_u)^2 \ (\pi_u)^4 \ (\pi_g)^4$$

provided Koopmans' theorem holds. The non-bonding character of the π_g orbital is evident from the photoelectron spectrum since the Franck-Condon factor of the 0,0,0, vibrational level approaches 1. A similar situation exists for the $\tilde{B}\ ^2\Sigma_u^+$ and $\tilde{C}\ ^2\Sigma_g^+$ states of CO_2^+ indicating that the $(\sigma_g)^2$ and $(\sigma_u)^2$ orbitals are also very nearly non-bonding. This implies that a large amount of s-p oxygen orbital mixing occurs in these orbitals, in agreement with the calculations of Mulligan[32].

Thus it becomes clear that the original Mulliken description of (a) and (b) type σ orbitals is not applicable. Both types involve s-p oxygen mixing, with the result that the (a) type become strongly bonding and the (b) type nearly non-bonding.

The same valence shell configuration can be adopted for CS_2, and for COS. For CS_2, Callomon[94] has identified the $^1\Sigma_u^+ \rightarrow \tilde{X}\ ^2\Pi_g$ transition in emission, the energy difference between the two states being identical with the energy separation between third and first ionisation potentials. This confirms that the third ionisation potential relates to the removal of a σ_u electron. His analysis also suggested, correctly, that the $^2\pi_u$ level lay between the ground level and the $^1\Sigma_u^+$ level.

The fifth band in the photoelectron spectrum of carbon disulphide is interesting and can be accounted for in several different fashions. In keeping with the proposed orbital configuration it could correspond to the removal of an

electron from the strongly bonding orbital $(6u)^2$. The complete lack of fine structure must then be explained by invoking either very small unresolvable vibrational spacings, curve crossing of potential surfaces resulting in a short life time for this state of the ion ($^1\Sigma_u^+$), or by considering that the ionisation observed in the spectrum is taking place to the level of the continuum in the potential energy surface of the ion. If this latter is the case it would imply that the minimum of the potential well i s at a much lower ionisation potential, probably below the fourth ionisation potential. A further possibility is that the peak represents an ionisation to a repulsive excited state of an otherwise stable electronic configuration. This type of transition is improbable since a two photon process would be required to achieve it, and it has not yet been observed in photoelectron spectroscopy.

No theoretical calculations have been carried out as yet concerning the orbital energy levels of carbon disulphide.

The $^2\Pi_i \rightarrow \tilde{X}^2\Pi_i$ transition has been identified in the emission spectrum of COS^+ by Leach[173] and the energy separation, 3.85 eV, confirms that the second ionisation potential relates to the Πu orbital.

Clementi[177] has performed an SCF M.O. calculation on COS, and the order of orbital energies he arrived at (Table XVII) is the same as for the CO_2 calculations - the $(\pi_u)^4$ and $(6_u)^2$ orbital order being reversed compared to the experimental order. Assuming Koopmans' theorem to be correct, the σ orbital energies are approximately 3 eV too high with respect to those of the π orbitals. Though this could arise from the method of calculation it may point to the dangers of attempting exact equation of ionisation potentials with orbital energies. Electronic reorientation energies, ignored in the Koopmans' theorem approximation, are assumed to be similar for all electronic states but differences may exist between the reorientation energies after σ electron and π electron removal.

The bonding characteristics for the orbitals as found experimentally agree well with Clementi's description, the less non-bonding character of the π_g orbital compared to the other molecules studied being reflected in in the stronger transitions to the vibrationally excited components of the $^2\pi_g$ ground state of the ion.

The experimental order of the ionic states of N_2O^+ is different from that of the other molecules, corresponding to a valence shell configuration of

$$(\sigma)^2 \ (\sigma)^2 \ (\sigma)^2 \ (\pi)^4 \ (\sigma)^2 \ (\pi)^4$$

This order is borne out by the emission spectrum of N_2O^+ [95], where the energy of the $^2\Sigma^+ \rightarrow \tilde{X}\,^2\pi_i$ transition equals the difference between the second and first ionisation potentials, not the third and first as in CS_2.

The bonding characteristics of the individual orbitals are similar to those in the other molecules, though the highest σ orbital (2nd. I.P.) would seem to be somewhat anti-bonding since the vibrational frequency of ν_1 in this $^2\Sigma^+$ ionic state is slightly increased compared to that in the ground state of the molecule. (Table XV). Similarly Callomon's [95] measurements on the rotational constant indicated a 3.3% contraction in bond length on removal of a σ electron from this orbital.

The exact nature of the bonding characteristics of the highest filled orbital, π_g, in this series, has come under some discussion [178,94]. The removal of a π_g electron leaves the bond length virtually unchanged for CS_2^+ and N_2O^+ and causes an increase of 0.015 Å in CO_2^+ [8c]. The vibrational frequencies of ν_1 (Table XV) are all reduced by various small amounts. This reduction in and also the increase in bond length for CO_2^+ would seem to suggest that the π_g orbital possesses slight bonding character, even though all the molecular orbital calculations indicate that the orbital should possess some slight anti-bonding character. Mulliken [178] explained this by including some C, 3d σ

character in the orbital. Callomon [94] on the other hand claimed that this was not necessary since the reduced nuclear screening effect of removing an electron could outweigh the antibonding effect. Hence bond lengths could still increase and the vibrational stretching frequency, ν_1, decrease on removing a nominally anti-bonding electron.

The changes in the vibrational frequencies of ν_3 found in this work are not so easily accounted for.

Electronic transitions starting from the ground vibrational state are subject to the following well-known selection rules [179]:

(1) The final state may have any number of quanta of a vibrational mode which is symmetric to all symmetry species in the molecule.

(2) Only zero or an even number of quanta of a mode which is anti-symmetric to a symmetry species is allowed.

This implies that for CS_2 and CO_2 ν_2 and ν_3 can only appear in double quanta, while for N_2O and COS ν_3 may appear in single quanta, but ν_2 should still appear in double quanta.

On this basis there is a rather striking difference between the changes in frequency of ν_3 on ionisation of the symmetric molecules CO_2 and CS_2, and the unsymmetric molecules N_2O and COS. Both in the $\tilde{X}\,^2\Pi_g$ and $\tilde{C}\,^2\Sigma_g^+$ states of CO_2 and CS_2 ν_3 has undergone a drastic reduction in frequency compared to the ground state of the molecule (Table XV). For COS and N_2O the $\tilde{C}\,^2\Sigma^+$ state actually produces a slight increase in the frequency of ν_3, while in the $\tilde{X}\,^2\Pi$ state a small decrease in ν_3 occurs for COS and a moderate one for N_2O . The frequency changes in N_2O and COS are not incompatible with mainly non-bonding orbitals having some bonding or anti-bonding character, but the drastic reductions for CO_2 and CS_2 are not at all what would be expected. At present we have no explanation for this pronounced difference between the two pairs.

TABLE XVII

EXPERIMENTAL IONISATION POTENTIALS AND CALCULATED ORBITAL ENERGIES

Compound	Orbital	State of Ion	Experimental I.P. (eV)*	Calculated Orbital Energies Ref. 32	Ref. 10	Ref. 33	Ref. 177
CO_2	π_g	$\tilde{X}\ ^2\Pi_g$	13.8	11.5	12.0	14.7	
	π_u	$\tilde{A}\ ^2\Pi_u$	17.6[a]	19	18.7	20.2	
	6_u	$\tilde{B}\ ^2\Sigma_u^+$	18.1	17.9	17.1	19.6	
	6_g	$\tilde{C}\ ^2\Sigma_g^+$	19.4	19.5	19.7	21.4	
	6_u	$\tilde{D}\ ^2\Sigma_u^+$	—	≃42	39.2	41.1	
	6_g	$\tilde{E}\ ^2\Sigma_g^+$	—	≃45	41.1	42.7	
COS	$\pi_{\blacksquare}$	$\tilde{X}\ ^2\Pi_g$	11.2				9.4
	$\pi_{\blacksquare}$	$\tilde{A}\ ^2\Pi_u$	15.5[a]				17.5
	$6_{\blacksquare}$	$\tilde{B}\ ^2\Sigma_u^+$	16.0				15.0
	$6_{\blacksquare}$	$\tilde{C}\ ^2\Sigma_g^+$	18.0				19.7
	$6_{\blacksquare}$	$\tilde{D}\ ^2\Sigma_u^+$	—				≫21
	$6_{\blacksquare}$	$\tilde{E}\ ^2\Sigma_g^+$	—				≫21

* This work

[a] Vertical Potential

5.3.2.(b). Vibrational Franck-Condon Factors.

Sharp and Rosenstock[27] have given a general technique for calculating F-C factors for most transitions in polyatomic molecules in the harmonic oscillator approximation. The input data required are the geometry and the vibrational frequencies of the initial and final states.

This has been applied to the $^1\Sigma_g^+ CO_2 \rightarrow \tilde{X}\,^2\Pi_g\ CO_2^+$ and the $^1\Sigma_g^+ \rightarrow \tilde{A}\,^2\Pi_u\ CO_2^+$ ionising transitions, and also to the corresponding transitions in CS_2. Both are assumed to be linear states.

The calculated F-C factors are compared with our experimental values in Table XVI. Spohr and Puttkamer[55] have recently estimated some of the F-C factors of these compounds by photoelectron spectroscopy, and more accurate values for the $\tilde{A}^2\Sigma^+$ state of N_2O^+ have been obtained from fluorescence measurements[180,181]. These values are also included in table XVI.

In fact erroneous values for some of the vibrational frequencies were used by Sharp and Rosenstock. The most serious error was the use of 2305 cm^{-1} for ν_3 in $\tilde{X}\,^2\Pi_g\ CO_2^+$. This was the value given by Mrozowski[93], but Johns[175] has since shown the correct value to be 1469 cm^{-1} in agreement with our work. Inghram[169] et al, who have recently studied the first band of the photoelectron spectrum of CO_2, estimated that the use of the correct value of ν_3 would increase the value of the F-C factor for the 0,0,2, excitation to a magnitude similar to that of the 2,0,0, excitation. They were unable to identify the former excitation, owing to lack of resolution which did not allow them to separate the 2,0,0, & 0,0,2, components. In our spectrum it can clearly be seen that the peak at 14.1 ev is a double one, and that the two components do indeed have similar intensities.

Koryoshkin[174] in 1966 completely re-analysed Mrozowski's original $\tilde{A}\,^2\Pi_u \rightarrow \tilde{X}\,^2\Pi_g$ emission band. The $v_1 = 1$ level in the $\tilde{X}\,^2\Pi_{\frac{1}{2}} CO_2^+$ state is split

into two sublevels and Mrozowski had ascribed this to a strong perturbation effect. Koryoshkin showed that the suggested perturbation could not account for the observed spectrum if the ion were linear. A bond angle of $168^{\circ} \pm 3^{\circ}$ and bond length $r_{CO} = 1.1830$ Å fitted perfectly with the observed spectrum.

The calculated Franck-Condon factors for the $\tilde{A}\,^2\Pi_u$ state of CO_2^+ rest on tentative assignments of ν_2 and ν_3.[9a] It can be seen from Table XVI that agreement with experimental values is good, and in particular the prediction that only mode ν_1 is excited, is supported.

For carbon disulphide only the Franck-Condon factors for the $^1\Sigma_g^+ \rightarrow \tilde{X}\,^2\Pi_g$ transition have been calculated. The prediction that mode ν_2 may be excited cannot be proved or disproved since the vibrational separation of the 0,2,0, mode from the 0,0,0 peak would be too small to be resolved (see fig. 66B).

5.3.2. (c) The Nature of the Fragmentation Processes Occurring

No direct information on the fragmentation processes can be obtained from photoelectron spectroscopy. However from the study of the population of vibrationally excited states, and of peak broadening which may indicate short lifetimes some knowledge is available. Careful correlation of the spectra with the photoionisation efficiency curves of molecular ions and fragment ions, and the relevant absorption and fluorescence data is also useful. Dibeler and Walker[81] have obtained photoionisation efficiency curves for all the molecular and fragment ions concerned in this series of compounds.

N_2O

For N_2O the ionisation threshold of N_2O^+ appears as a sharp step at 12.88(6) eV. No further steps in the curve are evident owing to superimposition of much autoionising structure. The appearance potential for NO^+ is 15.01 eV, and that of N_2^+ is 17.3 eV. Further thresholds in the NO^+ curve are clearly evident at 16.53 eV and 17.74 eV.

Figure 68 shows schematically a potential energy diagram for the

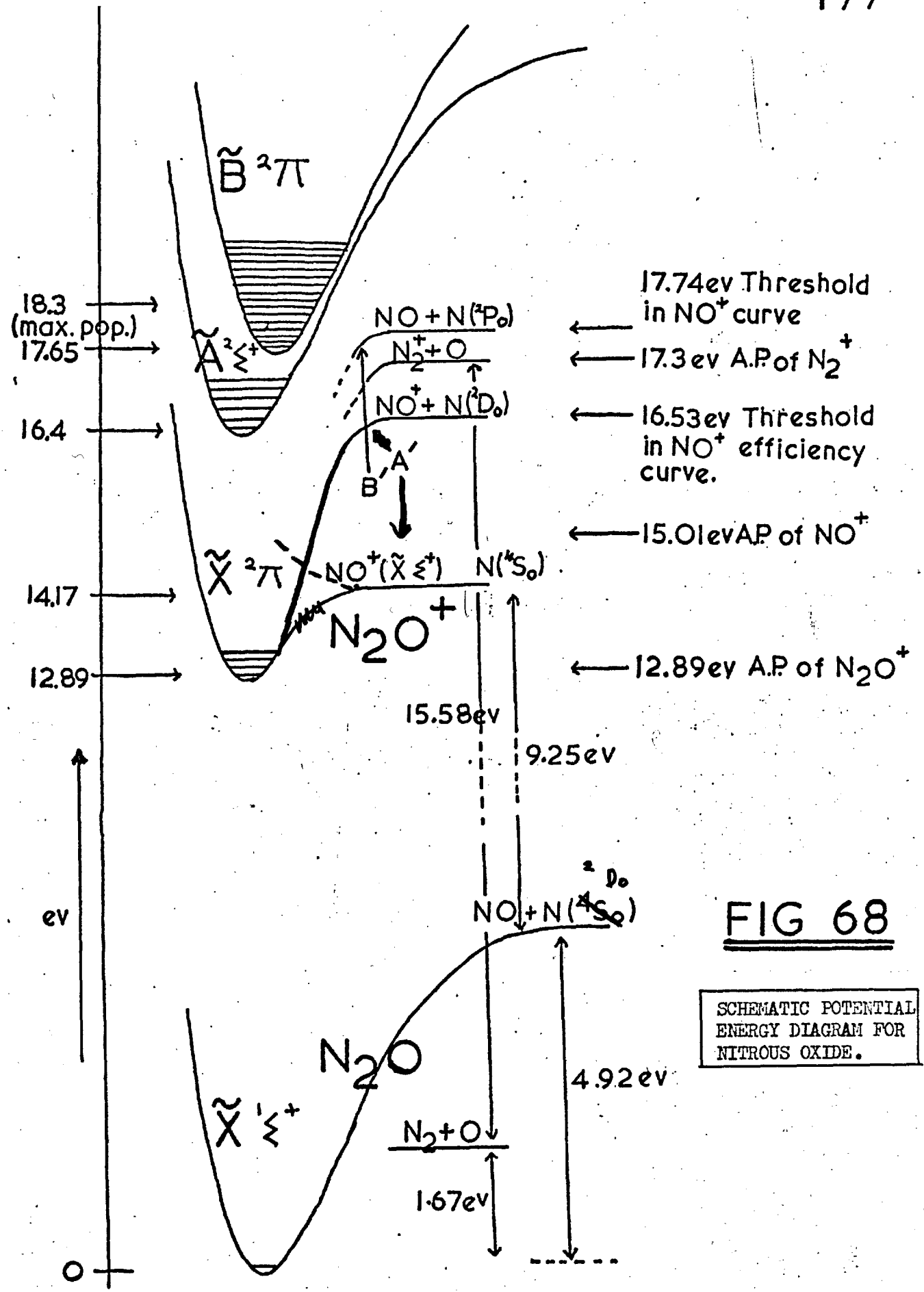

FIG 68

SCHEMATIC POTENTIAL ENERGY DIAGRAM FOR NITROUS OXIDE.

molecular ionic states found from photoelectron spectroscopy. The zeroth vibrational levels are marked and also those which can be populated by direct ionisation. No convergence of vibrational levels is observed and only a few levels are populated indicating that the ionising dissociation limits are to much higher energies. Also marked are Dibeler and Walker's [81] appearance potentials, thermochemical dissociation limits in the ground molecular state, and some dissociation limits in the ionic state estimated from known ionisation potentials and spectral data.

~~The first striking feature is the large reduction in the bond dissociation energy of $D(N-NO)^+$ compared to $D(N-NO)$. This is perhaps not too surprising since NO^+ is more stable to dissociation than NO~~. The second point is that the appearance potentials are all coincident with the thermochemical dissociation limits, within experimental error, except in the case of the first threshold of NO^+ which is 0.84 eV above the limit for the process :

$$N_2O + h\nu \longrightarrow NO^+(X\ ^1\Sigma^+) + N(\ ^4S^o\ )$$

Now direct ionisation to states (A') and (B') are not observed in the photoelectron spectrum, and it is thought that a two photon process would be required to reach them directly. Also it is obvious that photoionisation cannot produce ion fragmentation by direct transitions to any of the ionic states observed, since population at the dissociation limits does not occur. Why then do Dibeler and Walker's results show appearance potentials close to dissociation limits, even of states which require two photon excitation? One recognised path of fragmentation is by potential energy surface crossing out of the directly populated electronic states of the ion [28,147]. This can result in short lifetimes of the populated ionic levels involved, causing broadening of the vibrational peaks in the photoelectron spectrum[39] . No significant broadening is observed in our spectrum, and no populated levels exist in the region of two of the appearance potentials (15.01 and 17.3 eV - see fig. 68). The alternative explanation

is that curve crossing out of many populated excited molecular levels (stable or repulsive) into the appropriate ionising dissociation continua occurs. A combination of the two processes can probably account for all the observed results.

Cook et al[181] have obtained efficiency curves for the dissociation and ionisation continua of N_2O and have also studied the fluorescence from excited states. In the ionisation curve steps corresponding to the first and second I.P. were observed, with an additional "hump", centred at 840Å (14.8ev), superimposed on the flat continuum inbetween. The dissociation continuum shows a similar feature and because of this it is considered likely that the dissociation continuum is crossing with the ionisation continuum (see Figure 69). The dissociation process involved would appear to be :-

$$N_2O \longrightarrow N_2 (C\ ^3\Pi_u) + O (^3P) \quad .....12.7ev$$

since in the fluorescence spectrum a peak also appears at 840Å, of radiation 3200-3900Å, which can be ascribed to the process :-

$$N_2 (C\ ^3\Pi_u) \longrightarrow N_2 (B\ ^3\Pi_g)$$

Superimposed on the fluoresence continuum are peaks corresponding to the III and IV Rydberg adsorption series of Tanaka[170](leading to the second I.P.) which indicates that molecules excited to the upper states of these series pre-dissociate into $N_2 (C\ ^3\Pi_u) + O (^3P)$, and $N_2 (C\ ^3\Pi_u)$ then radiates as above (see figure 69). However there is no peak corresponding to the $v' = 0$, $n = 3$ member of series III, although this band has strong ionisation and absorption coefficients. This implies that the potential surface of the dissociation state crosses between the $v' = 0$ and $v' = 1$ levels of the $n = 3$ Rydberg state of series III. This is indicated in the schematic representation of the $n = 3$ Rydberg state in figure 69. Also included are the ground state molecular and ionic ($\tilde{X}\ ^2\Pi_g$) potential curves. Thus it can be seen that all three excited states are interacting.

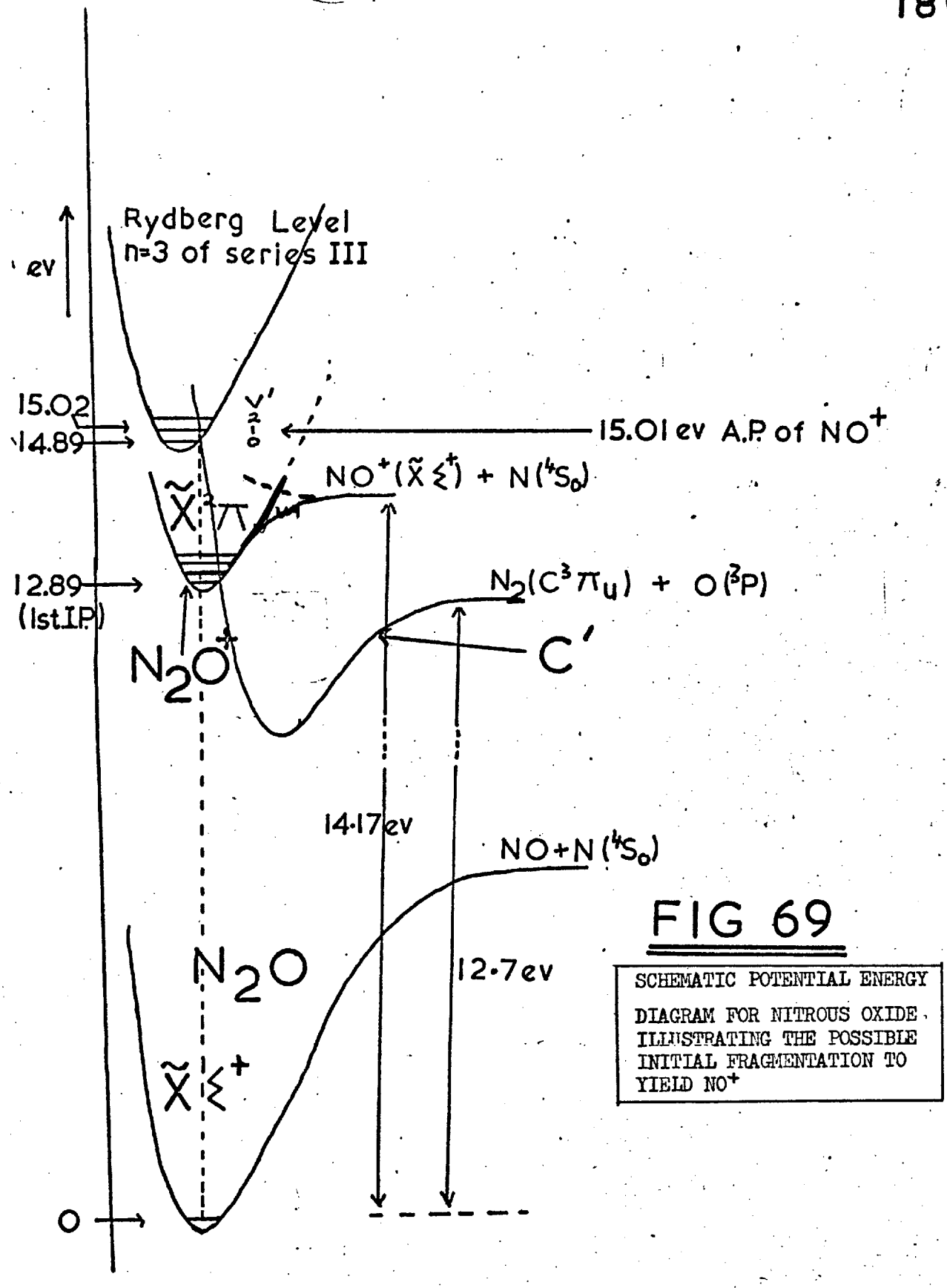

FIG 69

SCHEMATIC POTENTIAL ENERGY DIAGRAM FOR NITROUS OXIDE ILLUSTRATING THE POSSIBLE INITIAL FRAGMENTATION TO YIELD NO^+

Dibeler and Walker's appearance potential of NO^+ at 15.01 eV is coincident with the $v' = 1$ level of the $n = 3$ Rydberg series III. A feasible mechanism for the initial formation of fragment NO^+ ($X\ ^1\Sigma^+$) would therefore seem to be excitation to dissociative state C' followed by preionisation to the continuum of the ionic state $NO^+(\tilde{X}\ ^1\Sigma^+) + N(^4S)$, supplemented by additional transitions to Rydberg level $n = 3$ of series III with curve crossing above the $v' = 0$ level into state C'.

The two higher NO^+ thresholds at 16.53 eV and 17.74 eV are also represented by breaks in the N_2O dissociation continuum of Cook et al. This agreement probably indicates that curve crossings out of dissociation continua similar to those above are occurring. The coincidence of these two thresholds with the second and third ionisation potentials of N_2O (see figure 68) indicates that curve crossing out of the populated $\tilde{A}\ ^2\Sigma^+$ and $B\ ^2\Pi$ states of N_2O probably also plays a major part in the fragmentation process, possibly via a dissociation continuum.

$\underline{CO_2}$

For CO_2^+, the photoionisation efficiency curve shows the threshold at 13.775 eV, but the only other recognisable features are auto-ionisation levels. The appearance potential of O^+ is 19.10 eV. As in N_2O this is very close to the ionising limit,

$$CO_2 + h\nu \longrightarrow CO + O^+ + e$$

$$D(OC\text{-}O) = 5.47 \text{ eV}$$

$$\text{I.P. } O^\bullet = \underline{13.63 \text{ eV}}$$

$$\text{Dissociation Limit} = 19.10 \text{ eV}$$

From our photoelectron spectrum it is again obvious that the electronic states of the ion are not populated near the dissociation limits and so fragmentation is not possible by direct ionisation for CO_2 either. Rosenstock and Sharp[27] have already pointed this out for the $\tilde{X}\ ^2\Pi_g$ and $\tilde{A}\ ^2\Pi_u$ states of CO_2^+ from their theoretical Franck-Condon calculations. Thus the mechanisms for fragmentation must be similar to those of N_2O.

The rising edge of the threshold of CO^+ covers the range 19.1 - 19.6 eV[81] and the strong 0,0,0 peak of the $\tilde{C}\ ^2\Sigma_g^+$ CO_2^+ state is at 19.4 eV in the photoelectron spectrum. In the electron impact ionisation efficiency curves, without mass analysis, Carette[76] detected breaks in the curve corresponding to the $\tilde{X}\ ^2\Pi_g$ (13.75 eV), $\tilde{B}\ ^2\Sigma_u^+$ (17.35 eV) and $\tilde{C}\ ^2\Sigma_g^+$ (19.35 eV) states of the ion. If the autoionising fine structure is removed from Dibeler and Walker's CO_2^+ photon impact curve, it is possible that a step may occur at 17.35 eV corresponding to the $\tilde{B}\ ^2\Sigma_u^+$ level, but the curve is flat and featureless at 19.35 eV. Thus though the total ionisation efficiency increases at 19.35 eV, it yields no extra CO_2^+ but only O^+, even though this is at the zeroth vibrational level of an ionic state of CO_2^+ which is populated by direct ionisation. This is evidence for fragmentation being caused by curve crossing out of the directly populated state into an ionising dissociation continuum.

Cook et al. have studied the dissociation and ionisation continua, but in this case no strong conclusions can be drawn. Fluorescence corresponding to $\tilde{A}\ ^2\Pi_u \rightarrow \tilde{X}\ ^2\Pi_g$ CO_2^+ is observed, and possibly also the $\tilde{B}\ ^2\Sigma_u^+ \rightarrow \tilde{X}\ ^2\Pi_g$ CO_2^+ transition.

$\underline{CS_2}$

The photoionisation efficiency curve for CS_2 has its threshold at 10.06 eV. The second ionisation potential is not visible but there is a

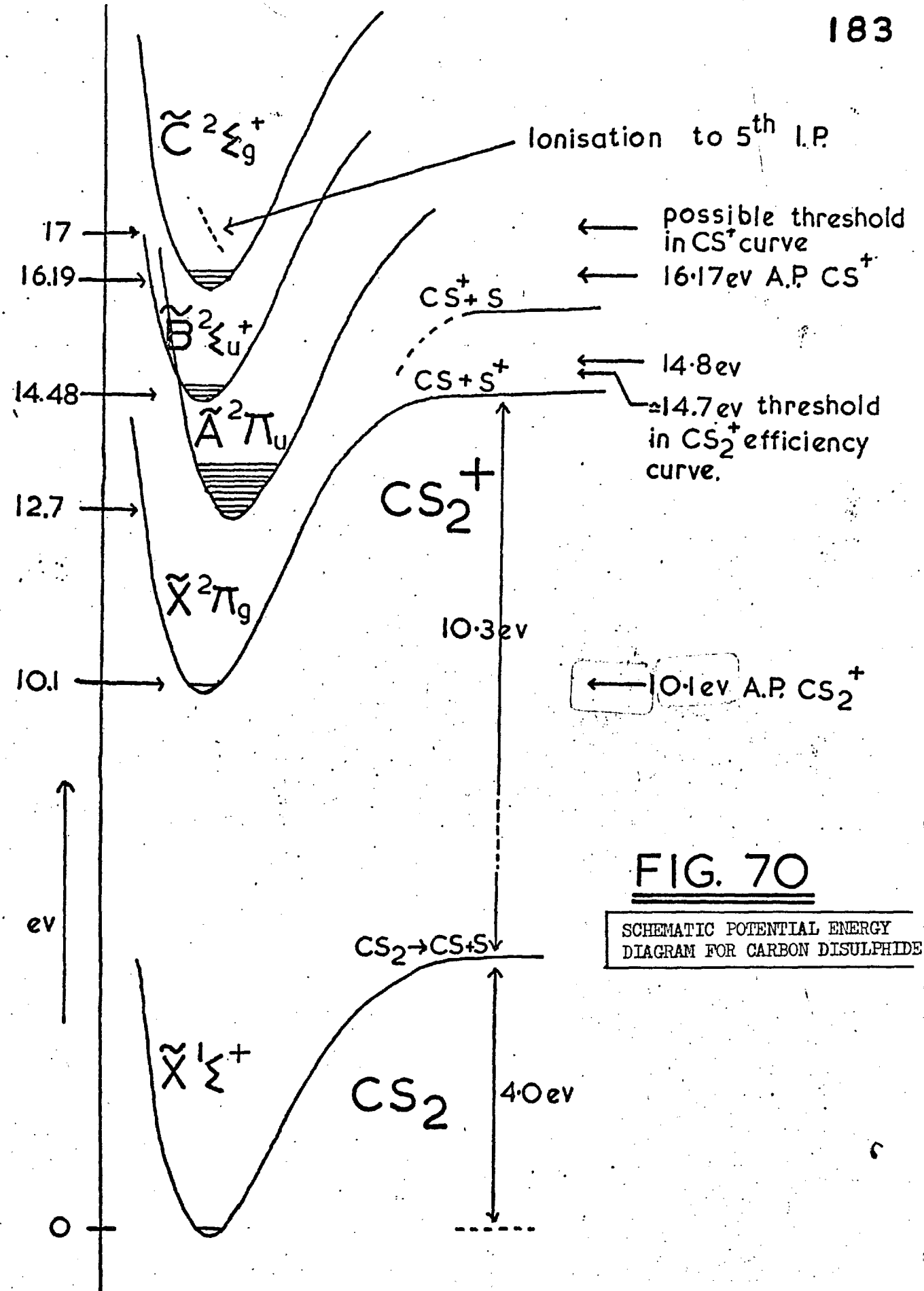

FIG. 70

SCHEMATIC POTENTIAL ENERGY DIAGRAM FOR CARBON DISULPHIDE

large step at 14.7 eV, close to the third ionisation potential (14.48 eV). The appearance potential of S^+ is 14.8 eV, and that of CS^+ 16.16 eV. Once again these values are close to calculated ionic dissociation limits. Figure 70 is a potential energy diagram showing all the relevant features. The threshold of S^+ is probably due to curve crossing out of the populated levels of $\tilde{B}\,^2\Sigma_u^+$ CS_2^+ through to the ionisation continuum of the ground state $\tilde{X}\,^2\Pi_g$, plus help from any molecular levels (stable or dissociative), which are accessible and can cross into the $\tilde{X}\,^2\Pi_g$ CS_2^+ state.

The appearance potential of CS^+ is nearly coincident with the fourth ionisation potential ($\tilde{C}\,^2\Sigma_g^+$ CS_2^+). It is a very sharp onset and implies that CS^+ must be formed by curve crossing out of the populated $\tilde{C}\,^2\Sigma_g^+$ state. No associated peak broadening is noticed in the photoelectron spectrum however.

The fifth band in the photoelectron spectrum is the only one observed in the compounds studied where fragmentation by direct ionisation may be occurring. However there are several other possibilities for this band, as mentioned in section 5.3.2.(a). The only feature of significance in the photoionisation efficiency curves of CS_2 is a small increase in the CS^+ yield.

COS

Only the threshold value of 11.18 eV is significant on the COS^+ efficiency curve, the remaining structure being largely obscured by auto-ionising peaks. The appearance potential of S^+, 13.65 eV, is only 0.13 eV above the ionic dissociation limit for the $\tilde{X}\,^2\Pi$ COS^+ state, though it can be seen from the photoelectron spectrum that the vibrational levels of this state are not populated above 11.6 eV. Fragmentation by direct ionisation cannot therefore occur. No other directly populated states exist in this region either, so curve crossing out of one of them must be excluded also. Thus fragmentation must occur via transitions to molecular excited levels,

followed by curve crossing, autoionisation, etc. The number of S^+ ions produced at threshold is very small, and the efficiency curve rises steeply on passing through the region occupied by the directly populated $\tilde{A}\ ^2\Pi\ COS^+$ and $\tilde{B}\ ^2\Sigma^+\ COS^+$ states. Curve crossing out of these states could account for this.

In this section it has been shown low fragmentation by direct ionisation to the dissociation limits of the electronic states is always impossible (with the possible exception of the fifth band of CS_2), and yet how the appearance potentials of fragments always occur near recognisable dissociation limits. We conclude therefore that for these molecules at least, there exists a sufficient density of accessible potential surfaces such that curve crossing to the ground ionic state at, or near, the dissociation limit is always possible, and that often a similar situation occurs near higher dissociation limits. The types and numbers of crossings involved are numerous, and the combined effect is often to produce a fragment threshold which approaches a step-function.

5.3.3. T.O.F. Mass Spectroscopy of N_2O

Efficiency curves for N_2O^+ and fragment ions NO^+, O^+, N_2^+, N^+, were constructed using suitable ionising lines from Oxygen and Nitrogen in the vacuum monochromator light source. At the time this work was done the only published photon impact mass spectrometric data on N_2O was that of Weissler et al[80]. Since then the high resolution efficiency curves of Dibeler et al[81] extensively referred to in section 5.3.2.(c), have been published. The T.O.F.M.S efficiency curves are shown in figure 71, and may be compared to the original curves of Weissler et al, and the curves of Dibeler et al shown in figure 72. As can be seen, the high resolution curves show much fine structure, presumed

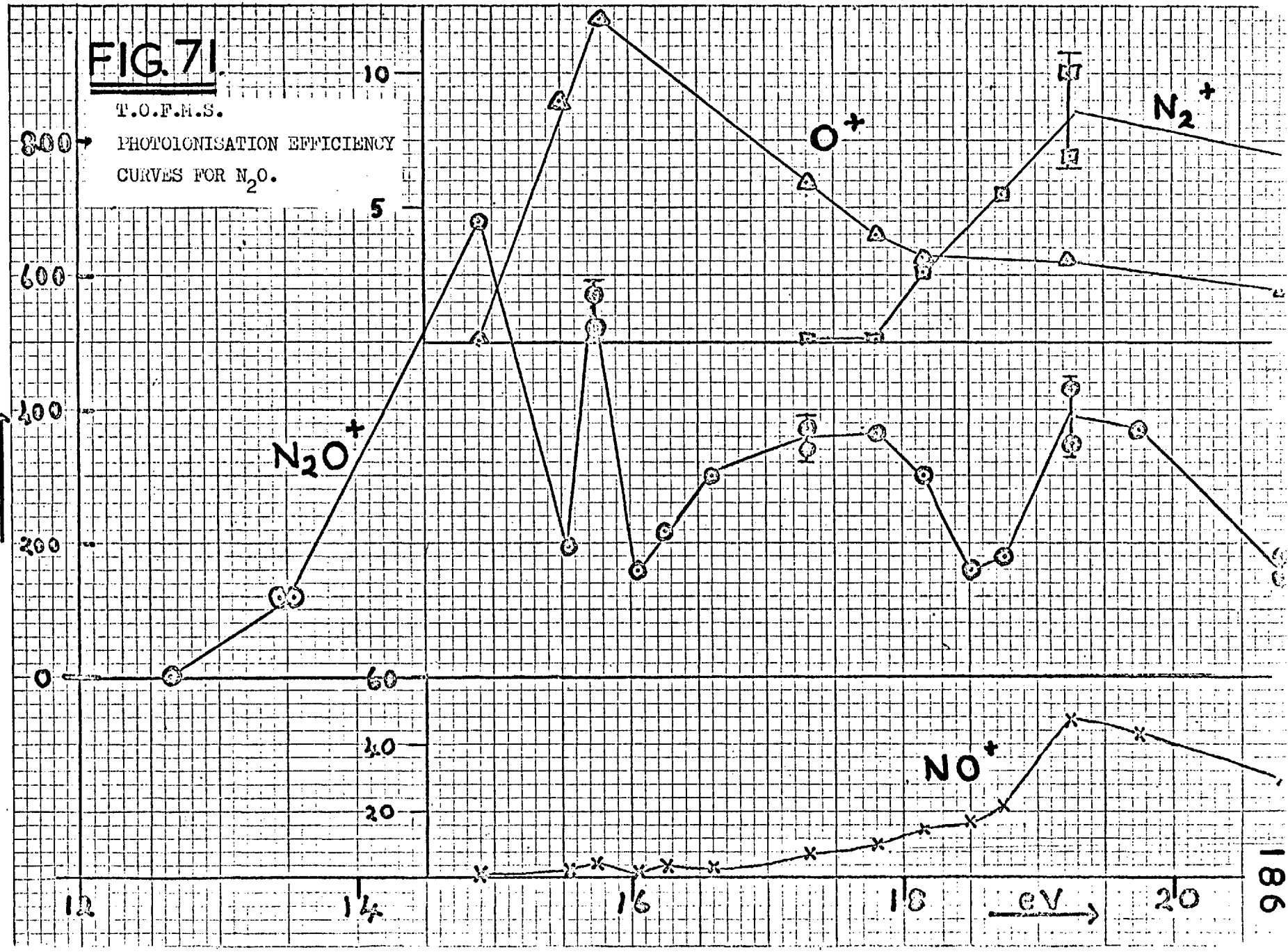
FIG. 71.
T.O.F.M.S.
PHOTOIONISATION EFFICIENCY CURVES FOR N_2O.
I/P - ARB. UNITS
800
600
400
200
0
10
5
60
40
20
O^+
N_2^+
N_2O^+
NO^+
12
14
16
18
eV
20

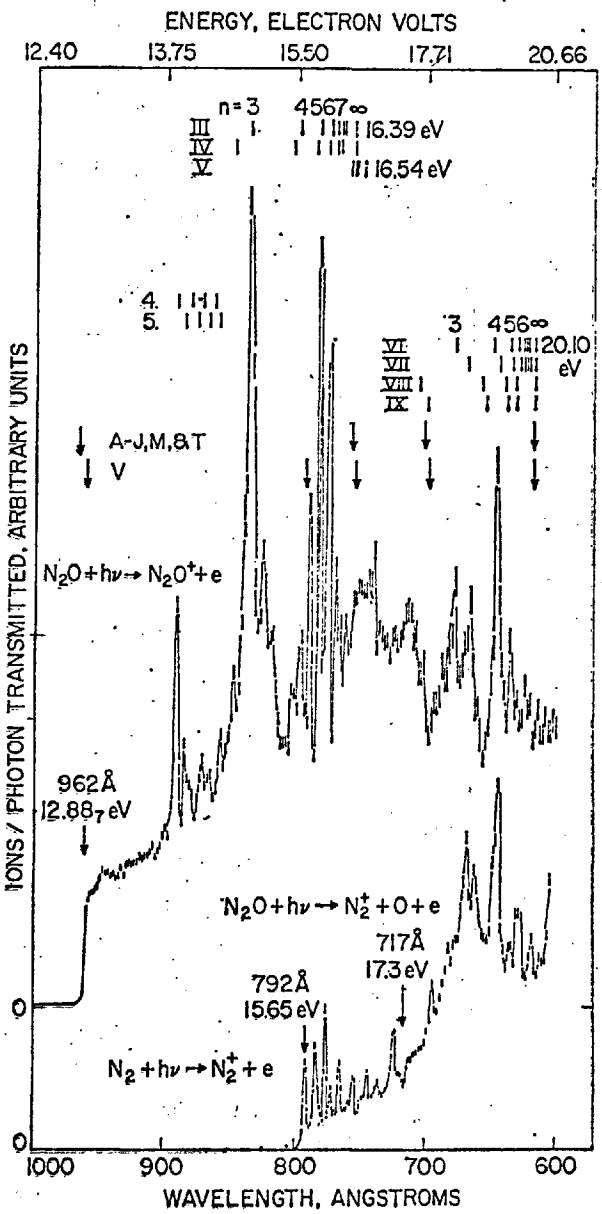

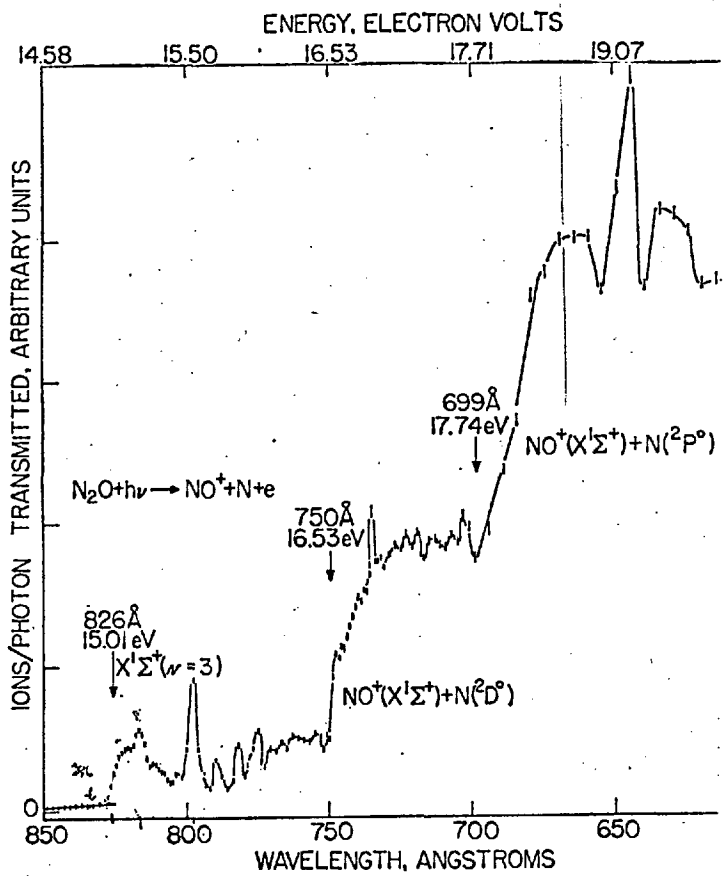

(a)

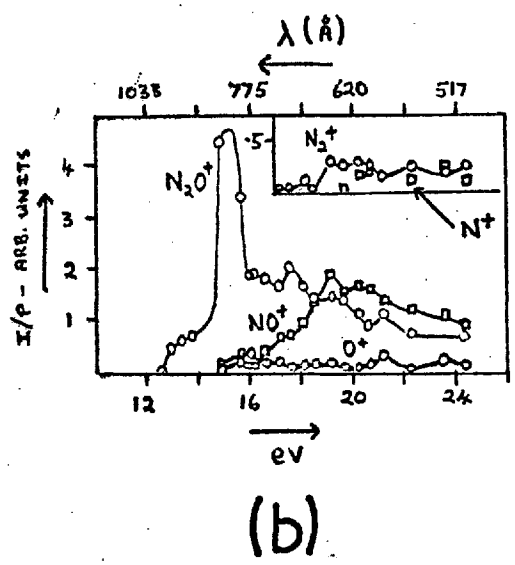

(b)

FIG. 72. — PHOTOIONISATION EFFICIENCY CURVES FOR N_2O AND FRAGMENT IONS.

(a) — after Dibeler and Walker[81]

(b) — after Weissler et al.[80]

to be due to autoionisation, which is not apparent in the other curves. For the T.OF.M.S. curves, the low intensity of all the fragment ions and the presence of background peaks (from the light source gases), make precise measurements very difficult, and an accuracy of no greater than 25% is claimed for the fragment ions.

An interesting point is the great difference between the ratio of abundances of ions found in the three experiments. The general trends can be seen from figures 71 and 72, and the following specific comparisons are available.

	Impacting Energy	Relative Abundance				
		N_2O^+	NO^+	N_2^+	N^+	O^+
Present results	599 Å	1.0	.17	.05	.03	.01
Weissler et al.[180]	600 Å	1.0	1.7	.3	.2	.2
Dibeler et al.[81]	548 Å	1.0	.59	.16	.03	.02

There is some evidence for a metastable state of N_2O^+ . Begun and Landau[184], reported the metastable process :-

$$N^{15}N^{14}O^+ \longrightarrow N^{14}O^+$$
$$(m) \quad \gamma_{1/2} \simeq 2\mu\text{sec.}$$

from the observation of a metastable peak in a conventional mass spectrometer. Newton and Scimanna[185] in later work estimated that $\gamma_{\frac{1}{2}} = .2$ sec. and that the K.E. released on dissociation was ca. 1ev.

This metastable state could be the $\tilde{A}\,^2\Sigma^+$ state of the ion, which is dissociating by radiationless transition to ground state and curve crossing to the [redacted] state, the thermochemical limit of which lies at 2.2 ev lower energy. (see figure 68), or The additional excess energy released by the process (2.2 - 1 ev.) might appear in the form of a vibrationally excited state of the NO ion. The 0–4 vibrational interval of $NO^+(X\,^1\Sigma^+)$ is 1.16 ev.[186] If this hypothesis is correct, then the metastable

N_2O^+ should be observed only at an ionising energy greater than 16.39 ev. An accurate study of the appearance potential of the metastable, and the K.E. released in its dissociation would help to resolve this point.

The ten-fold difference between the ratio N_2O^+/NO^+ observed by Weissler et al, and in the present results, may be partly accounted for by the presence a metastable species of N_2O^+. In Weissler's conventional mass spectrometer, the N_2O^+ ions may have remained in the ion source for as long as 6 μsec. where as in the TOFMS they were ejected after a delay of approximately 1.5 μsecs. Further work using a TOFMS and varying the delay before ion ejection might indicate whether residence time is a factor in the N_2O^+/NO^+ ratio.

Fig. 73 shows the portion of a typical spectrum of N_2O covering the 28 - 32 a.m.u. region. It can clearly be seen that the NO^+ peak is broadened considerably. Calculations show that the broadening is compatible with the NO^+ ion possessing approximately 0.5 eV K.E. and more accurate measurements should be able to establish this value more precisely. As mentioned in section 5.3.2.(c) the A.P. of NO^+ is 0.84 eV above the thermochemical limit of the $\tilde{X}^2\Pi\ N_2O^+$ state, and for the fragmentation process at the A.P. of NO^+ suggested in section 5.3.2.(c), K.E. of the resulting fragments would be expected. The partition of kinetic energy between fragments is inversely proportional to their masses, and so NO^+ should possess ca. 0.3 eV kinetic energy.

Again, more work on the kinetic energy distribution of NO^+ over an impacting energy range would be helpful in sorting out the dissociation processes occuring.

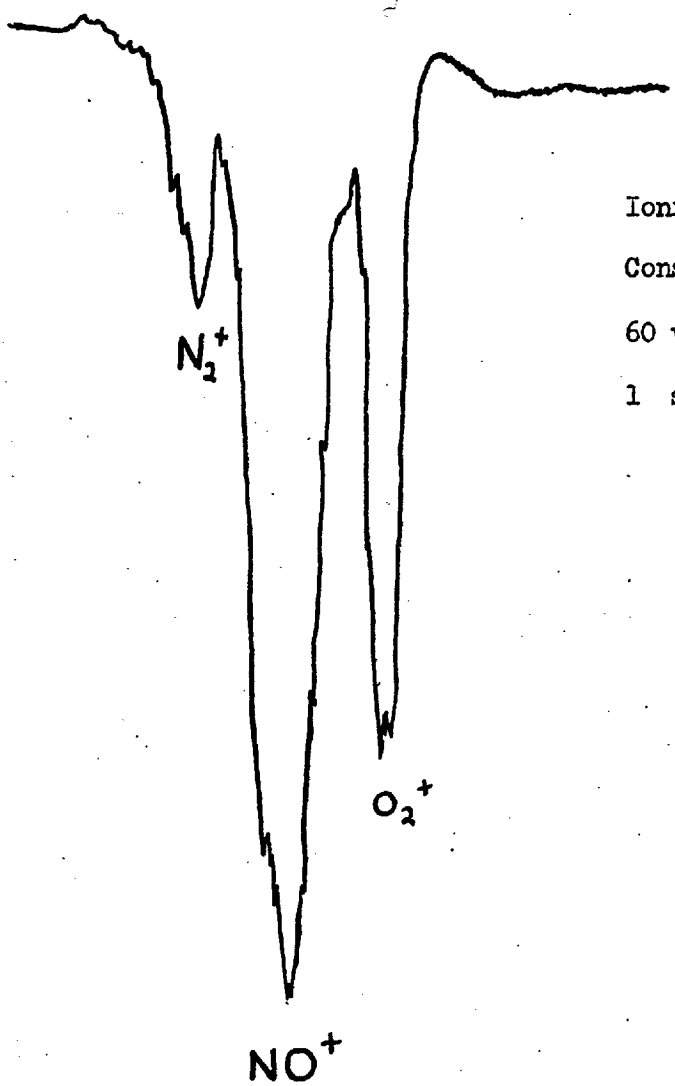

Ionising Line, Oxygen _644Å

Constant Energy Conditions ——

60 volts, 3 μsec. accelerating pulse,

1 sec. delay time.

FIG 73 —— T.O.F.M.S. SPECTRUM (28-32 a.m.u. region)

FOR NITROUS OXIDE, N_2O

5. 4. - Formamide, N - methyl formamide, N - N dimethyl formamide.

Special importance is attached to the understanding of the electronic structure and electronic spectrum of the amide group, since polypeptides may be considered as weakly coupled amide residues, their optical properties being closely related to those of the monomeric amide unit.[187]

It was originally thought that the lower-lying electronic transitions of the amide group involved a terminal π^* level only, and assignments of the bands observed in the U.V. spectrum were based upon semi-empirical theories in the π approximation.

Recently, however, Robin et Al,[187] reported the presence of a low-lying transition not previously observed in amide spectra.

This band falls in the 2000 Å region between the transitions ascribed to $n \longrightarrow \pi^*$ ($>$ 2000 Å) and $\pi \longrightarrow \pi^*$ ($<$ 2000 Å). A similar band is also observed in the U.V. spectra of various acids and acyl fluorides. It was thought that the transition might be to a σ^* level, and in an attempt to verify this a full scale all-electron Roothaan S C F - M O calculation was performed on formamide.

As was expected the calculations indicated a low lying σ^* orbital, which was of the Rydberg type. The four possibilities for a Rydberg transition were :-

$n \longrightarrow 3s$, $\qquad n \longrightarrow 3p_\sigma$

$\pi \longrightarrow 3s$, $\qquad \pi \longrightarrow 3p_\sigma$

and the calculations gave $n \longrightarrow 3s$ (5·8 eV) as the one of lowest energy. If this Rydberg transition corresponds to the observed new transition in the U.V. spectra of formamides, then it implies that the

lowest I.P of formamide involves removal of an electron from the non-bonding sigma orbital (very largely oxygen centred).

Now the first ionisation potential may be simply taken as the negative of the highest occupied orbital as calculated by the S.C.F. procedure (Koopmans' Theorem). This neglects the effects of the re-orientation energy on ionisation, and the difference between the correlation energy of the neutral and ionised states.

The S.C.F. calculations indicate that for formic acid and formyl fluoride the highest filled orbital is the non-bonding σ orbital, n, and hence by Koopmans' Theorem the first I.P. relates to the removal of an electron from this orbital. But the calculations place the π orbital above n for formamide.

Re-orientation energy can be accounted for by calculating the I.P s by computing the total S.C.F. energy of the positive ion, and subtracting this from the total energy of the neutral molecule. When calculated in this manner the 1st I.P s of all three compounds involve the n orbital, with ionisation from the π orbital being at least 1 eV more energetic.

Thus there is little doubt that for acids and acyl fluorides the 1st I.P involves ionisation from the n orbital, and the new transition observed in the U.V. spectrum is an $n \longrightarrow \sigma^*$ transition. From the calculations the origin of the 1st I.P. of formamide is undecided, but the strong similarity of the U.V. spectrum to those of the acids and acyl fluorides suggests that the 1st I.P. here also relates to the n orbital. Robin's calculations[188] gave the first and second I.P s by the two methods as :-

Koopmans' Theorem	1st. I.P	11·32 eV	——	π
	2nd I.P.	11·86 eV	——	n
Re-orientation allowed calculation	1st I.P.	8·80 eV	——	n
	2nd I.P	9·74 eV	——	π

The photoelectron spectra of formamide, N - methyl formamide, and N - N dimethyl formamide have been examined in an attempt to positively identify to which orbitals the 1st and 2nd I.P s of formamide relate.

The spectra are shown in figures 76, 74, 75, and the observed I.P s and vibrational structure are indicated also. Obviously the two bands corresponding to the 1st and 2 nd I.P s overlap and appear to change their relative positions in the spectrum on going from formamide, through N - methyl formamide to N - N dimethyl formamide.

The vibrational interval of approximately 1,600 cms $^{-1}$ associated with one of the bands, and which seems to appear in all three compounds, is very probably the O - C - N antisymmetric stretching mode which in the neutral molecule has a frequency of $\simeq$ 1,680 cms^{-1} [190], and consists largely of the C - O stretching mode.

The second band in Formamide (figure 74) has a vibrational spacing of approximately 600 cms^{-1} associated with it. The excited mode could be the O - C - N deformation mode ($\simeq$ 600 cm^{-1} in the molecule [190,191]), or one of the several modes involving the NH_2 group which have been assigned to different frequencies by different authors [191,192,193]. Whichever mode is involved, the band shape changes markedly on going to the methyl compounds.

The simplest explanation is that the band with the simple C - O

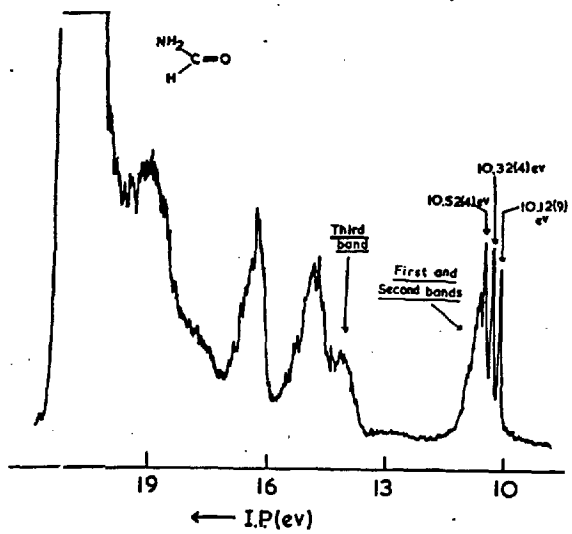

PHOTOELECTRON SPECTRUM OF FORMAMIDE

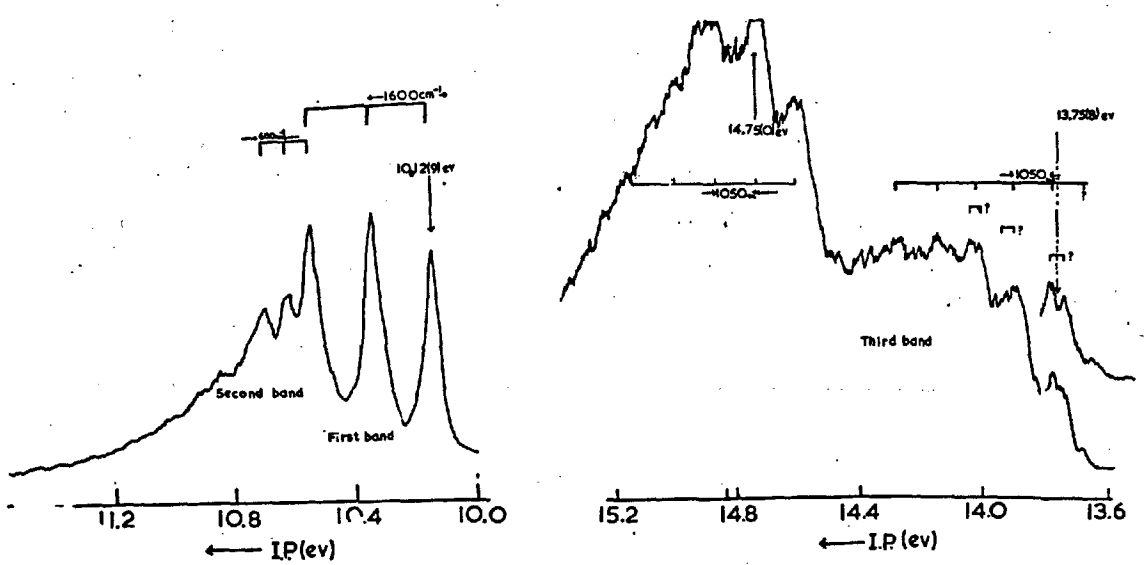

FIG 74

PHOTOELECTRON SPECTRUM OF FORMAMIDE

—— EXPANDED ENERGY SCALE

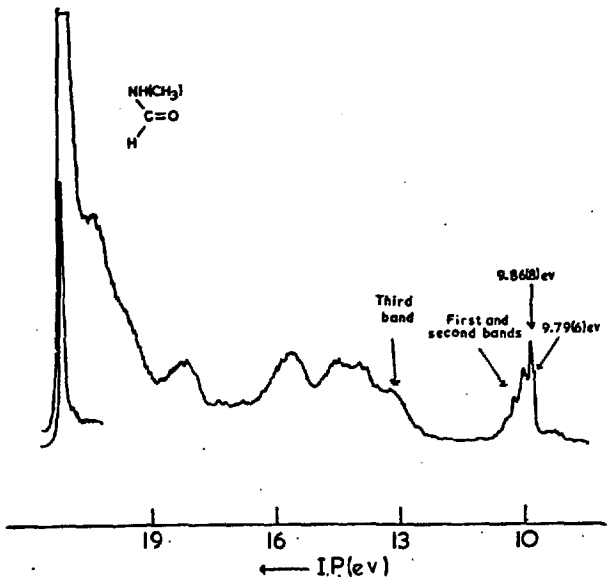

PHOTOELECTRON SPECTRUM OF
N-METHYL FORMAMIDE

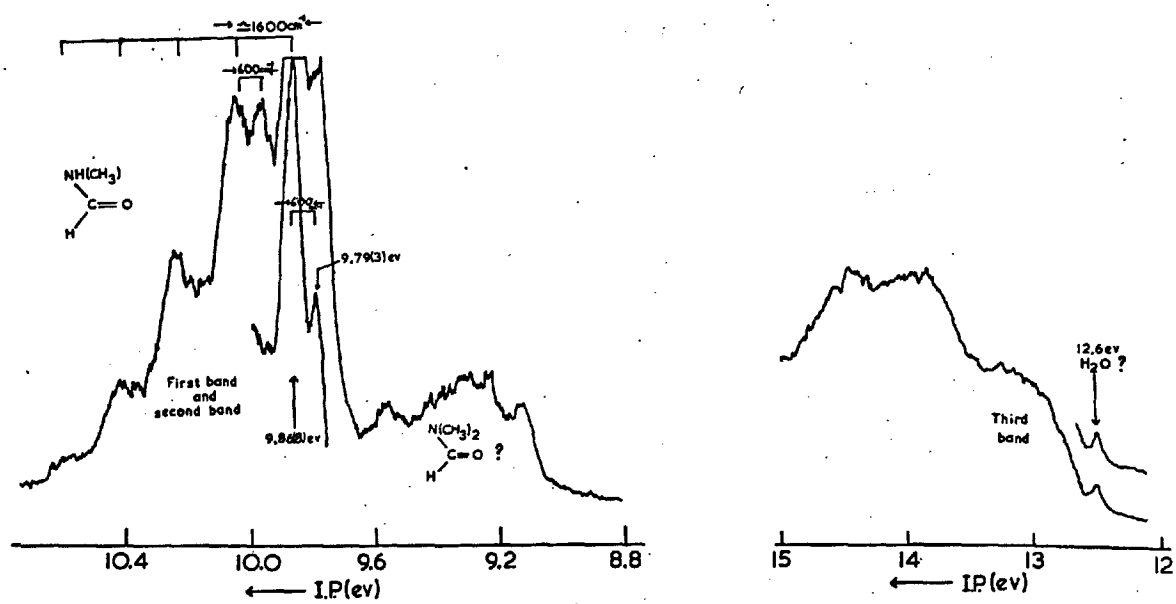

FIG 75 PHOTOELECTRON SPECTRUM OF N-METHYL FORMAMIDE
—— EXPANDED ENERGY SCALE

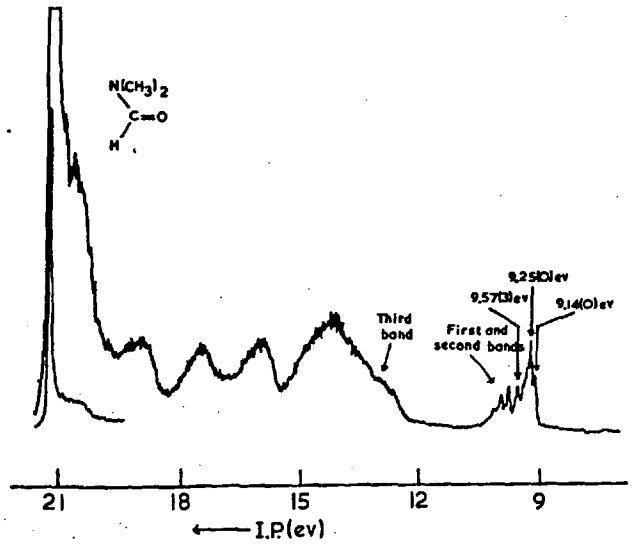

PHOTOELECTRON SPECTRUM OF

N-N-DIMETHYL FORMAMIDE

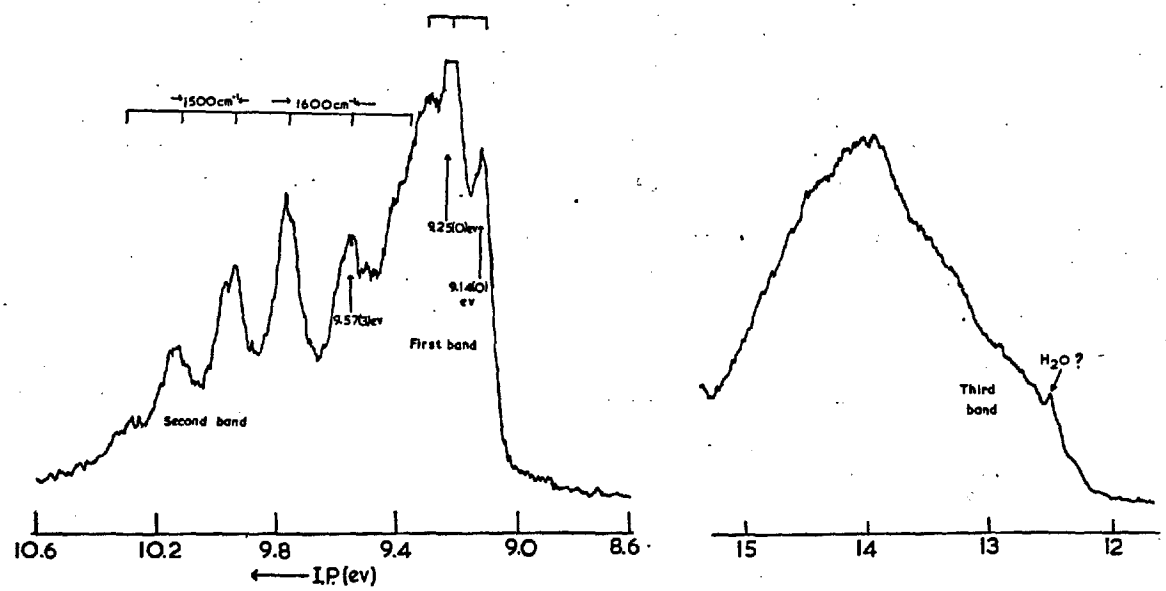

FIG 76

PHOTOELECTRON SPECTRUM OF

N-N-DIMETHYL FORMAMIDE

——EXPANDED ENERGY SCALE

vibration associated with it relates to the removal of an electron from the n orbital (oxygen non-bonding σ), and the one changing with the introduction of the methyl groups relates to the π orbital (which covers the N, C, and O atoms according to Robin's calculations).

If this explanation is correct, it can be deduced that the 1st I.P. of formamide does relate to the n orbital and that the new band observed in the U.V. spectrum by Robin et Al , is due to an $n \longrightarrow \sigma^*$ transition.

The experimental values of the 1st and 2nd I.P's of formamide are, from the photoelectron spectrum :-

1st I.P (n) = 10·13 eV

2nd I.P (π) $\leqslant$ 10·51 eV —— The position of the start of this band is not unambiguously established.

That these are both higher than the calculated values (re-orientation energy allowed), is readily explainable as being due to the larger correlation error in the calculated ground state energy, due to its having one more electron pair than the doublet ions. The calculated values seem to have over-allowed for the difference in re-orientation energy between the 1st I.P and the 2nd I.P., in that the calculated I.P s are ·96 eV apart, whereas the experimental difference is $\leqslant$ ·38 eV.

Assuming the interpretation of the origin of the first two photo-electron bands to be correct, the introduction of methyl groups onto the nitrogen atom is seen to be exerting the expected hyperconjugative effect of pushing the π orbital to higher energy, with a much less effect on the n orbital, thus reversing the origin of the 1st and 2nd

I.P s (see figure 77).

The third band in the photoelectron spectra of the compounds can reasonably be ascribed to the removal of an electron from the second highest filled π level, the introduction of methyl groups in the N - methyl and N - N dimethyl compounds again exerting the expected hyperconjugative effect (figure 77).

Nothing definite can be derived from the other bands in the spectrum, the vibrational spacings could correspond to any number of modes, but it does seem that peaks due to ionisation from the methyl orbital are showing up in the 14 - 15 eV region in the N - methyl and N - N dimethyl spectra. This is in the energy region where ionisation from methyl orbitals often occurs (see for example ref. 62).

There are two points of difficulty about the interpretation of the photoelectron spectrum given above. The first is the appearance of the weak band at lower energy than the proposed 1st. I.P. in N - methyl formamide. This is probably an N - N dimethyl impurity, and a spectrum of a clean gas chromatographed sample should eliminate this band. The second factor is that the 3rd band in N — N dimethyl formamide (assigned to the second π level) appears to be much more intense than in the other two compounds.

The photoelectron spectroscopy results have prompted Robin[194] to re-examine the optical spectra of these compounds, and he has now been able to find nearly identical F - C profiles in some of the bands. Correlation between the two types of spectra is in progress.

FIG. 77

SCHEMATIC ENERGY LEVEL DIAGRAM SHOWING THE I.P.s OF THE AMIDES CONCERNED, AND THE ORBITALS TO WHICH THEY RELATE

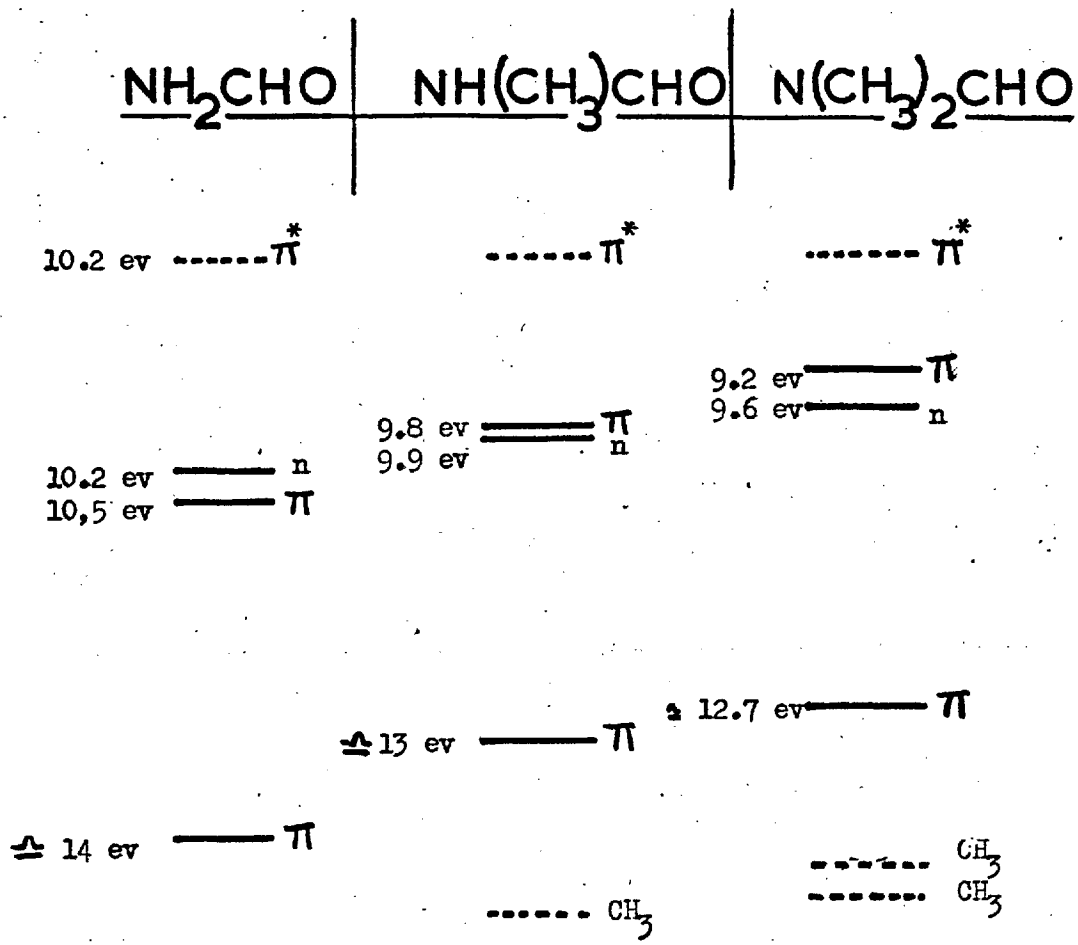

5.5. Preliminary TOFMS Study of Acetone

Molecular ions, formed in an initial ionisation process possess kinetic energy (thermal energy) according to the equation :-

$$\text{K.E.} = \tfrac{1}{2} mv^2 = \tfrac{1}{2} kT$$

at 300° K $kT \simeq 0.025$ eV

at 600° K $kT \simeq 0.05$ eV

Therefore v, the velocity, is inversely proportional to $\sqrt{m}$, the mass of the ion.

On fragmentation, if no excess energy is released in the process, the thermal energy will be partitioned between the fragments in accordance with the laws of conservation of momentum and of energy. Thus,

$$mv = m_1 v + m_2 v$$

$$\tfrac{1}{2} mv^2 = \tfrac{1}{2} m_1 v^2 + \tfrac{1}{2} m_2 v^2$$

where m_1 and m_2 are the masses of the fragment particles. In a collision free system the fragment particles will continue to travel with the velocity, v, of the original molecular ion. Under such conditions loss of ions should only occur by collision with the physical components of the spectrometer as the ions migrate thermally from the ionisation region.

Assuming a Maxwell-Boltzmann energy distribution and neglecting charge repulsion, it can be shown[118,189] that the number of ions remaining in region, length, l, (one dimensional treatment) after time t is given by

$$N_t = N_0 \frac{2}{\sqrt{\pi}} \int_0^{\alpha_0} e^{-\alpha^2} d\alpha - \frac{1 - e^{-\alpha_0^2}}{\alpha_0 \sqrt{\pi}}$$

where N_0 is the number of ions initially present in length l

$$\alpha_0 = \left(\frac{m}{2kT}\right)^{\frac{1}{2}} \frac{l}{t}$$

$$\alpha = \left(\frac{m}{2kT}\right)^{\frac{1}{2}} v$$

In three dimensional form the equation becomes a product of three one dimensional cases given by the above equation.

In the TOFMS the only significant loss of ions should be to the repeller plate, distance $l = 3$ mm from the ionising beam, and so the one dimensional equation may be used. Hourieh[118] solved this equation for several molecules (ketones and aldehydes) as a function of t, over the range t = 0 sec to 15μsec. The results were expressed as the decrease in abundance of ions detectable over that time range. These were compared to the decays in the experimental ion peak strengths observed in the TOFMS over the same time range.

There seem to be two major faults in Hourieh's use of the above equation to calculate a theoretical decay curve. The first is that he did not allow for the fact that in the apparatus ions are only "lost" to detection by migration in one direction, to the repeller plate, whereas the theoretical equation includes losses in the opposite direction also. Allowing for this the corrected equation would be :

$$\frac{N_t}{N_0} = \frac{1}{2} + \frac{1}{\sqrt{\pi}} \int_0^{\alpha_0} e^{-\alpha^2} d\alpha - \frac{1 - e^{-\alpha_0^2}}{2\alpha_0\sqrt{\pi}}$$

and the general effect of the correction is that the theoretical rate of decay is less than that calculated by Hourieh.

The second error is that in calculating theoretical curves for fragment ions Hourieh assumed that for a fragment

$$\tfrac{1}{2} m_1 v'^2 = kT$$

whereas as has been shown above, in a collision free region if no excess K.E. is liberated the fragment particles continue with the velocity, v, of the

parent ion, and so have exactly the same theoretical decay curves of the parent ion.

If excess energy is released in the dissociation process, the energy will be partitioned between the fragments in inverse proportion to their masses (conservation of momentum). Thus

$$\frac{KE_1}{KE_2} = \frac{m_2}{m_1} = \frac{m_1 v_1^2}{m_2 v_2}$$

$$\frac{v_1}{v_2} = \frac{m_2}{m_1}$$

and the smaller the fragment the greater will be the velocity it has, and the faster its rate of loss from the ionisation region.

In theory one should be able to calculate the kinetic energy liberated in a decomposition process from the difference between the theoretical decay curve (thermal migration) and the experimentally found curve.

For fragment ions Hourieh [118] found agreement between his experimental and calculated decay curves (in which the rate of loss was overestimated by a factor o at least 2), but found the behaviour of the molecular ion peak to be anomalous and in complete disagreement with theory. In general the molecular ion peak showed an increase in intensity as the time of residence of the ions in the ion source was increased, a decrease only commencing after at least 6 μ sec. The observed values for $CH_3COCH_3^+$ and its CH_3CO^+ fragment are shown in Table XVIII together with the corrected theoretical values. Figure 78 shows the results in graphical form.

Several possible explanations were advanced by Hourieh for the phenomenon.

(1) The tail of a strong fragment peak overlaps that of the parent (see figure 29 for acetone) and part of the increase of the latter might result from interference between the two.

TABLE XVIII

CHANGE OF THE RELATIVE ABUNDANCE OF IONS FROM ACETONE WITH RESIDENCE TIME IN IONISATION REGION* (14.89 ev impacting energy)

Residence time in ionisation region (μ sec)	Ion Peak at m/e			
	43 a.m.u. (CH_3CO) EXP.	43 a.m.u. (CH_3CO) CALC.	58 a.m.u. (CH_3COCH_3) EXP.	58 a.m.u. (CH_3COCH_3) CALC.
0	10	10	4.0	4.0 (arbitary value)
1	—	9.74	—	3.88
2	—	9.44	—	3.78
3	—	9.17	—	3.67
4	9.33	8.89	6.0	3.56
5	9.0	8.62	6.0	3.45
6	8.0	8.36	6.0	3.34
7	7.33	8.10	6.0	3.24
8	6.33	7.87	5.75	3.11
9	5.66	7.66	5.5	3.06
10	—	7.47	—	2.99
11	4.66	7.30	5.25	2.92
12	—	7.15	—	2.88
13	3.66	7.01	5.0	2.8
14	—	6.89	—	2.76
15	3.0	6.78	4.8	2.72

* After Hourieh, Ref. 118

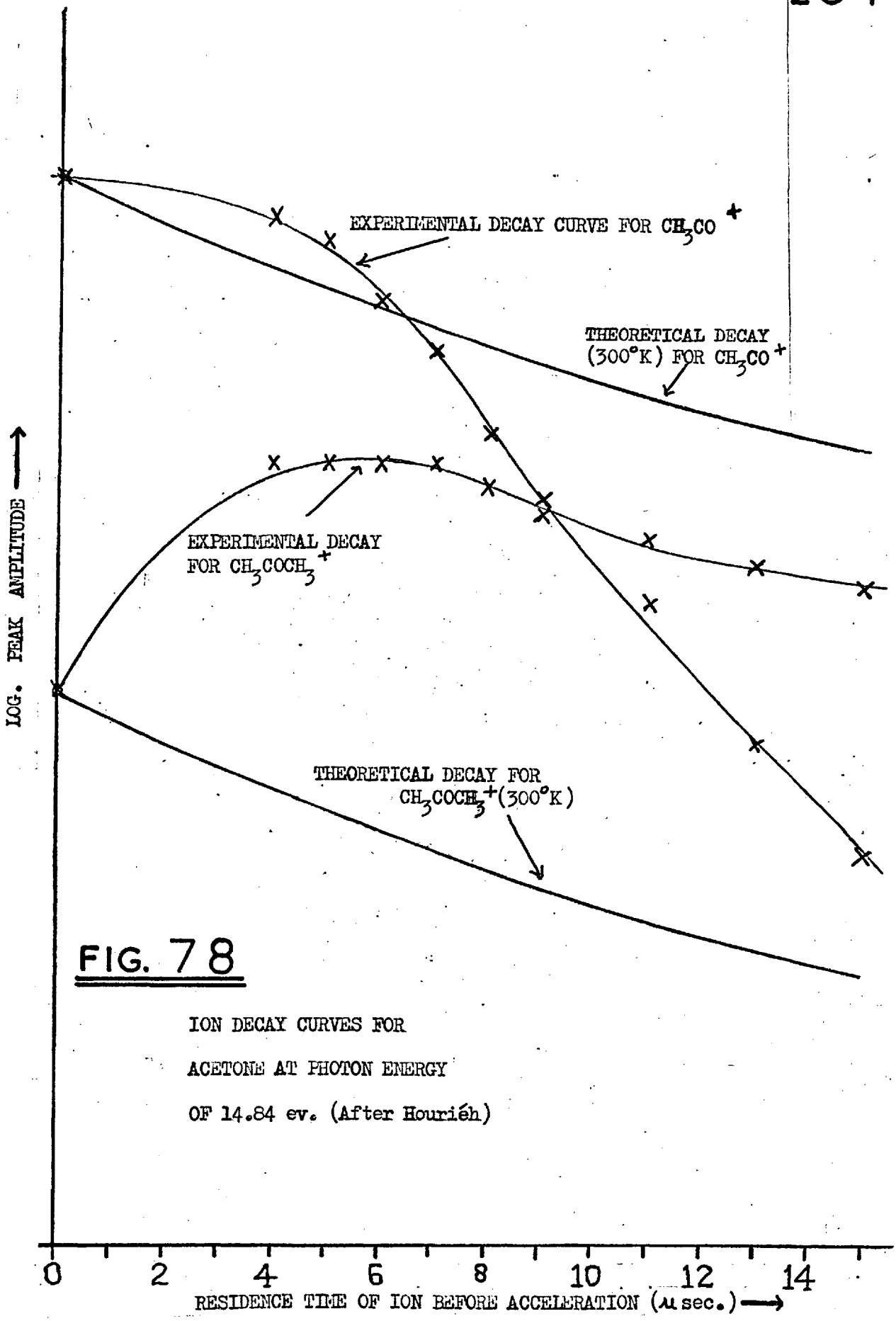

FIG. 78

ION DECAY CURVES FOR ACETONE AT PHOTON ENERGY OF 14.84 ev. (After Houriéh)

(2) A time delay focusing effect could be in operation.

(3) A slow autoionisation process could be in operation.

$$AB + h\nu \longrightarrow AB^{*} \xrightarrow[\text{slow}]{} AB + e$$

In the present work a preliminary study on CH_3COCH_3 was made both with the T.O.F.M.S. in its original form and then its reconstructed form, in an attempt to find out more about the anomalous behaviour of the $CH_3COCH_3^+$ ion. Figure 79 shows the decay curves found for a photon imact value of 14.84 ev with the original form of the spectrometer. As can be seen the anomalous effect is even more pronounced than that found by Hourieh. Under the present operating conditions of much higher resolution and sensitivity, together with the more accurate recording technique, it was found that the anomalous behaviour no longer occurred. The experimental results are indicated in figure 80.

Two conclusions are possible. The first is that in the case of CH_3COCH_3 at least, the anomalous behaviour was entirely due to instrumental effects. The poor resolution of the CH_3CO^+ and $CH_3COCH_3^+$ ions (see figure 29) using the original version of the apparatus meant that the small $CH_3COCH_3^+$ peak rode on the much larger CH_3CO^+ peak as a "tail", and so the behaviour of the two peaks was inter-related. Any change in the peak shape of the CH_3CO^+ signal would affect the height of the $CH_3COCH_3^+$ peak. The poor shape of the accelerating pulse (section 3.5.B.) caused broadening of peaks at high masses. A time delay re-focusing effect could possibly re-focus broadened peaks. Finally the actual detection and recording system involved pulse shaping of an integrated spectrum. The spectrum was produced by collecting charge on a plate (see section 3.3.B.b.), and could be non-linear for two possible reasons. The response of the pre-amplifie might be non-linear, though this is considered unlikely. Secondly, charge was maintained at the capacitor detector for a considerable length of time, unlike wit

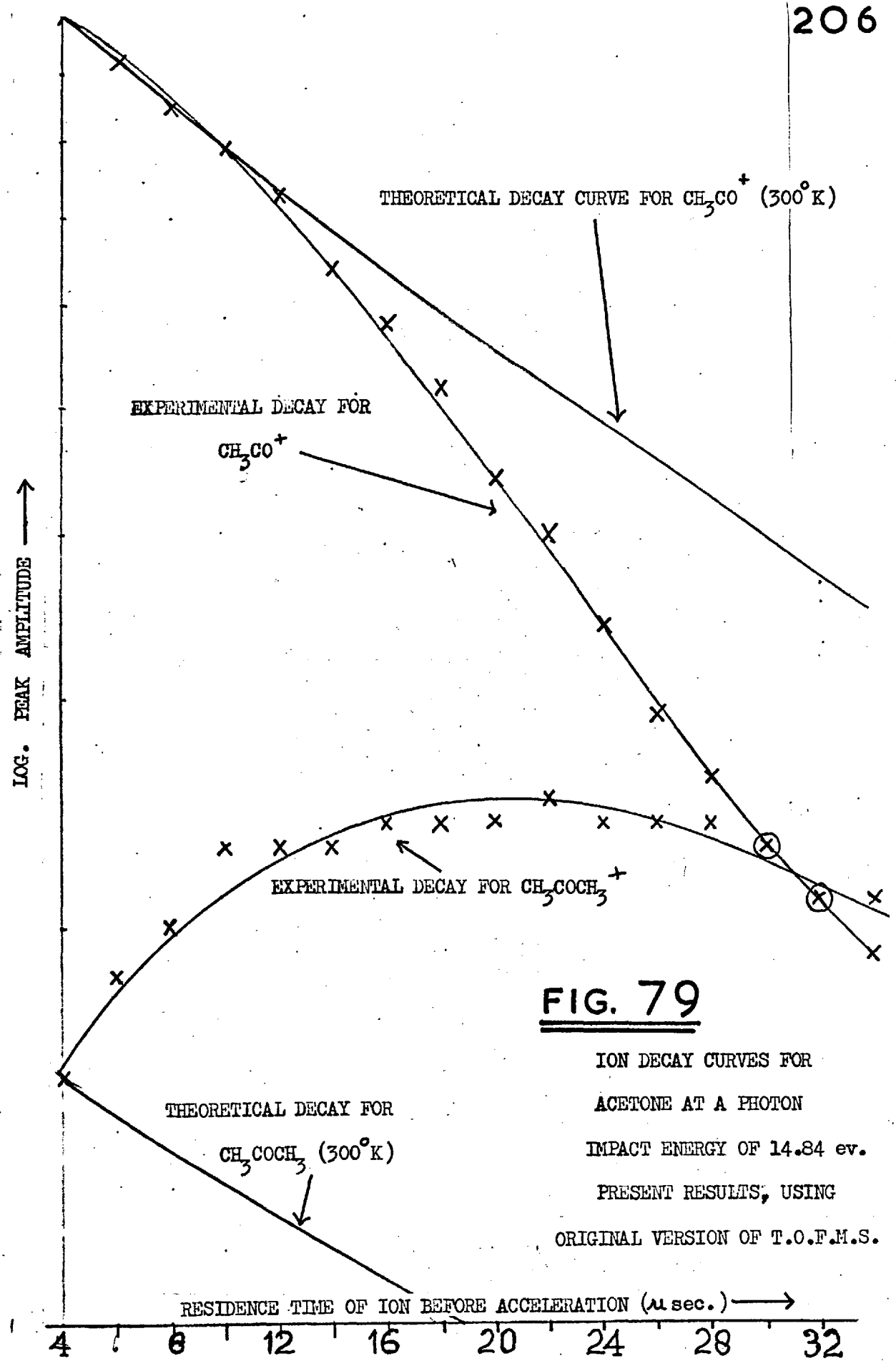

FIG. 79

ION DECAY CURVES FOR ACETONE AT A PHOTON IMPACT ENERGY OF 14.84 ev. PRESENT RESULTS, USING ORIGINAL VERSION OF T.O.F.M.S.

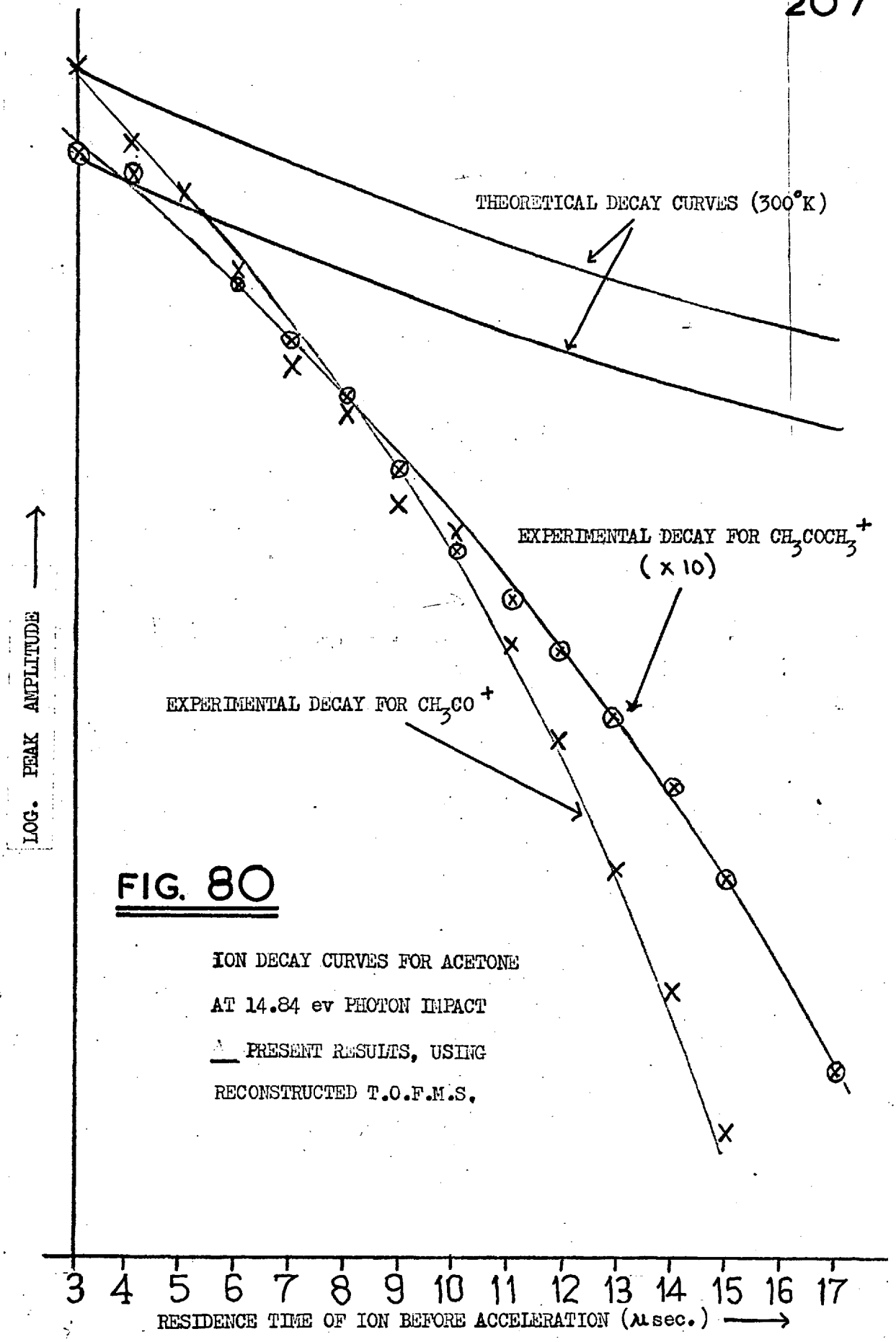

FIG. 80

ION DECAY CURVES FOR ACETONE
AT 14.84 ev PHOTON IMPACT
⊗ PRESENT RESULTS, USING
RECONSTRUCTED T.O.F.M.S.

the electron multiplier system and at the high pressures used and correspondingly large ion currents, it might have been possible for secondary effects in the vicinity of the detector to modify the much smaller molecular ion signal arriving just after the large fragment ion signal. Further work on acetone at different ionising energies, and on some of the other compounds studied by Hourieh, is required to establish whether this explanation is valid in all the anomalous cases observed.

The second possibility is that a pressure effect is in operation. Hourieh did most of his work with acetone vapour at 3 microns pressure, and claimed that peak intensities were linear with pressure up to 7 microns. The dimensions of the spectrometer are such that a pressure of 3 microns is sufficiently low for a collision free process (flight path $\triangleq$ twice mean free path) but the present work on the reconstructed spectrometer has been done at ca. 3 microns pressure (pressures of $> 1\mu$ are not feasible because of the multiplier detection system). It may be that at the higher pressure collision processes were occuring such that CH_3COCH_3 molecules were able to gain sufficient energy to ionise :

$$CH_3COCH_3^* \longrightarrow CH_3CO^+ + CH_3$$

The fact that the experimental decay curves (figure 80) have greater slope than the calculated theoretical curve cannot be taken as indicating the presence of excess kinetic energy. Obviously there is no mechanism whereby molecular ions can be formed with excess kinetic energy. Wahrhaftig[189] in a similar experiment on propane using electron impact found also that the theoretical rate of ion decay did not account for all the experimental ion loss. More significant is the greater rate of loss of CH_3CO^+ ions compared to $CH_3COCH_3^+$ molecular ions. This would seem to indicate that a small amount of kinetic energy has been released in the fragmentation process.

BIBLIOGRAPHY

1. L. B.Loeb, "Basic Processes in gaseous Electronics". Chapter 9 University of California Press, Berkeley, California, 1955.
2. M. Zelikoff, "The Threshold of Space", Pergamon Press, Oxford, 1957.
3. R. A. Craig, "The Upper Atmosphere", Academic Press, N.Y.& London 1965.
4. J. A. Ratcliffe, "Physics of the Upper Atmosphere", Academic Press, N.Y. & London 1960.
5. G.P. Kuiper, Ed., "Solar Systems", Vol 2. Univ. of Chicago Press, Chicago, 1954.
6. R. Tousey, Applied Optics, 1 679 (1967).
7. G. Herzberg, Proc. Roy. Soc., 234 516 (1956), 248 309 (1958).
8. G. Herzberg, "Molecular Spectra and Molecular Structure."
   (a) Vol. I (b) Vol. II (c) Vol. III
   D. Van Nostrand Co. New York.
9. T. Koopmans, Physica, 1 104 (1934).
10. A. D. McLean, J. Chem. Phys., 32 1595 (1960).
11. H. Basch, M.B.Robin, and N. A. Kuebler, J.Chem. Phys., 47 1201 (1967).
12. Idem. Ibid. In the press.
13. K. Siegbahn et al, "Electron Spectroscopy for Chemical Analysis." 1967 Univ. Uppsala. Sweden.
14. L. C. Jones and L. W. Taylor, Anal. Chem., 27 228 (1955).
15. W. A. Noyes and P.A. Leighton, "The Photochemistry of Gases." Reinhold Publishing Corporation N. Y. 1941.
16. G. H. Dunn and L. J. Kieffer, Phys. Rev. 132 2109 (1963).
17. P. Lenard, Ann. Phys., 1 486 (1900), 3 298 (1900).

18. A. L. Hughes, Proc. Camb. Phil. Soc., 15 483 (1910).

19. V. Schumann — A series of his papers is listed in ref. 20.

20. T. Lymann "The Spectroscopy of the extreme Ultraviolet."
Longman Green and co. London. 1928.

21. F. L. Mohler and P. D. Foote, Phys. Rev. 26 195 (1925).

22. Idem and R. L. Chenault, Phys. Rev. 27 37 (1926).

23. F. L. Mohler , C. Boeckner, and W. W. Coblentz, Science 69 479 (1929).

24. G. L. Weissler, "Handbuch der Physik." Ed. Flügge, Springer Verlag,
Berlin, 1956. Vol XXI p304—382.

25. J. A. R. Samson, Applied Optics, 6 403 (1967).

27. T. E. Sharp and H. M. Rosenstock, J. Chem. Phys. 41 3453 (1964).

28. M. Halmann and I. Laulicht, J. Chem. Phys. 43 1503 (1965).

28. H. J. Lempka, T. R. Passmore, and W. C. Price, Proc. Roy.Soc. A 304 53 (1968).

29. F. Elder and C. F. Giese, R. Steiner, and M. G. Inghram,
J. Chem. Phys. 36 3292 (1962).

30. F. H. Field and J. L. Franklin, "Electron Impact Phenomena and the
properties of Gaseous Ions." Academic Press, N. Y. 1957.

31. R. S. Mulliken, Rev. Mod. Phys. 2 60 (1930)., 2 506 (1930). 4 † (1932).

32. J. F. Mulligan, J. Chem. Phys. 19 347 (1951).

33. S. D. Peyerimhoff, R. J. Buenker, and J. L. Whitten, J. Chem. Phys. 46 1707 1967

34. W. E. Palke, and W. N. Lipscomb, J. Am. Chem. Soc. 88 2384 (1966).

35. U. Kaldor and I. Shavitt, J. Chem. Phys. 48 191 (1968).

36. J. W. Moskowitz, ibid 43 60 (1965).

37. D. Peters, Trans. Farad. Soc. 59 1121 (1963).

38. R. Botter, V. H. Dibeler, J. A. Walker, and H. M. Rosenstock,
J. Chem. Phys. 44 1271 (1966).

39. C. R. Brundle and D. W. Turner, Proc. Roy. Soc. In the press.

40. M. Ogawa and Y. Tanaka, Can. J. Phys. 40 879 (1962)

41. W. C. Price, Chem. Rev. 1947 41 257.

42. P. G. Wilkinson, J. Mol. Spec. 6 1 (1961).

43. G. R. Cook, P. H. Metzger, and M. Ogawa, J. Chem. Phys. 44 2935 (1966).

44. idem J. Opt. Soc. Am. 58 129 (1968).

45. K. Watanabe, J. Chem. Phys. 26 542 (1957).

46. W. C. Price, R. Brailsford, P. V. Harris, and R. G. Ridley, Spectrochim Acta, 14 45 (1959).

47. F. I. Vilesov, B. L. Kurbatov, and A. N. Terenin, Sov. Phys. Dokl. 6 490 (1961), 6 883 (1962).

48. D. W.Turner and M. I. Al-Joboury, J. Chem. Phys. 37 3007 (1962).

49. R.I. Schoen, J. Chem. Phys. 40 1830 (1964).

50. F. J. Comes, and H. J. Saltzer, Z. Nat. 19a 1230 (1964).

51. J. A. R. Samson and R. B. Cairns, J. Opt. Soc. Am. 56 552 (1966).

52. A. J. Blake and J. H. Carver, J. Chem. Phys. 47 1038 (1967).

53. K. Siegbahn et al, Chem Phys. Lett. 1 613 (1968).

54. J. H.D. Eland and C. J. Danby, J. Mass Spec. and Ion Phys. 1 111 (1968).

55. R. Spohr and E. Von Puttkamer, Z. Nat. 22A 705 (1967).

56. B. Brehm and E. Von Puttkamer, Int. Conf. of Mass Spect. Sept. 1967 Berlin.

57. D. W. Turner "Advances in Mass Spectrometry" Vol. 4 p755 1968.

58. idem Nature 213 795 (1967).

59. idem "Physical Methods in Advanced Inorganic Chemistry." p74 1968

60. W. C. Price, Endevour, 26 75 (1967).

61. A. D. Baker, D. P. May, and D. W. Turner, J. Chem. Soc. B. 822 (1968).

62. A. D. Baker, Ph. D. Thesis Univ. of London. 1968.

63. W. C. Price, Private Communication.

64. J. A. R. Samson, Private Communication.

65. J. Cooper and R. N. Zare, J. Chem. Phys. 48 942 (1968).

66. J. L. Hall and M. N. Siegel, ibid 48 943 (1968).

67. J. Berkowitz and H. Ehrhardt, Phys. Lett. 21 531 (1966).

68. idem & T. Tekaat Z. Phys. 200 69 (1967).

69. V. Cermak, Inter. Mass Spectrometry Conf. Berlin, Sept. 1967.

70. idem J. Chem. Phys. 44 3781 (1966).

71. E. Lindholm, Z. Nat. 9A 535 (1954).

72. E. Lindholm, I. Szabo, and P. Wilmenius, Arkiv. f. Fysik. 25 30 (1963).

73. J. D. Morrison, "Electron Molecule and Photon Molecule Collisions." Douzième Conseil de Chemie, Bruxelles, 1962. p397-466, Interscience Publishers.

74. L. J. Kieffer and G. H. Dunn, Rev. Mod. Phys. 38 1 (1968).

75. S. Geltmann, Phys. Rev. 102 171 (1956).

76. J. D. Carrette, Can. J. Phys. 45 2931 (1967).

77. C. A. McDowell, "Methods of Experimental Physics" Acad. Press. N. Y. 1962

78. E. Iassettre, in B. Jonsson & E. Lindholm, Chem. Phys. Lett. 1 501 (1967)

79. H. Hurzeler, H. G. Inghram, and J. D. Morrison, J. Chem. Phys. 28 76 (1958), 27 313 (1958).

80. G. L. Weissler, J. A. R. Samson, M. Ogawa, and G. R. Cook, J. Opt. Soc. Am. 49 338 (1959).

81. V. H. Dibeler and J. A. Walker, Inter. Conf. Mass Spect. Berlin 1967.

82. V. H. Dibeler, R. M. Reese, and M. Krauss, J. Chem. Phys. 42 2045 (1965).

83. R. Botter, J. A. Walker, and H. M. Rosenstock, J. Chem. Phys. 45 1298 (1966)

84. W. Chupka, M. F. Russell and K. Refaey, J . Chem. Phys. 48 1518 (1968).

85. B. Brehm, Z. Nat. 21a 196 (1966).

86. A. J. C. Nicholson , J. Chem. Phys. 39 954 (1963).

87. R. I. Schoen, Ibid 37 2032 (1962).

88. J. E. Collin, Proc. Nato Adv. Study Inst. Glasgow. 1964.

89. D. L. Judge, A. L. Morse, andG. L. Weissler, Bull. Am. Phys. Soc. 10 739, (1965), 10 1210 (1965).

90. G. R. Cook, P. H. Metzger, and M. Ogawa, Can. J. Chem. 43 1706 (1965); 45 203 (1967).

91. K. D. Beyer & K.H. Welger Z.Nat. 19A 19 (1964)

92. K. H. Becker & K.H. Welger, ibid 20A 442 (1965)

93. S.Mrozowski Phys. Rev. 72 691 (1947) & refs. cited therein.

94. J.H. Calloman Proc. Roy. Soc. A 244 220 (1958)

95. idem Proc. Chem. Soc. 313 (1959)

96. M.Horani & S.Leach Compt. Rend. 247 2196 (1959)

97. H.D.Hagstrum Rev. Mod. Phys. 23 185 (1951)

98. W.W. Lozier Phys. Rev. 36 1285 (1930)

99. R.Taubert 'Adv. Mass. Spectr.' Ed. Waldren 1959, p.489

100. F.Mohler, V.H. Dibeler & R.M. Reese J. Chem. Phys. 22 394 (1954)

101. A.Hustrulid, P.Kusch, & J. Tate Phys. Rev. 54, 1037 (1938)

102. H.Hagstrom & J.Tate ibid 59 354 (1941)

103. K.E.McCulloh & H.M.Rosenstock J. Chem. Phys. 48 2084 (1968)

104. W.Chupka ibid 30 191 (1959)

105. H. M. Rosenstock and M. Krauss, "Current Status of the Statistical Theory of Mass Spectra." Adv. Mass Spectrometry 2 251 (1962).

106. J.Mohan & H.Stanton J. Chem. Phys. 37 2654 (1962)

107. D. Rapp & D.D. Briglia ibid 42 4081 (1965)

108. W.Bleakney Phys. Rev. 35 1180 (1930)

109. J.H. Green & K.R. Ryan Proc. Roy. Soc. A 286 178 (1965)

110. K.E. McCulloh, T.E. Sharp, & H.M.Rosenstock J.Chem. Phys. 42 3501 (1965)

111. J.E. Collin "Extrait de s Mémoires de la Société Royale des Sciences de Liège, 5th Series, Vol 14, No1, p. 61.

112. O. Klemperer, " Electron Optics." 2nd. Ed. Cambridge University Press. 1953.

113. D. W. Turner, Proc. Roy. Soc. 1968. In the press.

114. W. E. Stephens, Bull. Am. Phys. Soc. 21 No 2 p22 (1946).

115. A. E. Cameron and D. F. Eggers, J. Rev. Sci. Instr. 19 605 (1948).

116. H. S. Katzenstein and S. S. Friedland, ibid 26 324 (1955).

117. W. C. Wiley and I. H. McLaren, ibid 26 1150 (1955).

118. M. A. Hourieh, Ph. D. Thesis, 1965 Univ. London.

119. R. G. W. Norrish and G. Porter, Nature, 164 658 (1949)

120. W. D. McGrath, Proc. Roy. Soc. A 242 265 (1957).

121. W. R. S. Garton, Proc. 5th Int. Conf. Ionisation Phenomena in Gases. Ed. H. Maeker Vol. II 1962

122. J. M. L. Janssen, Phillips Tech. Rev. 12 52 (1950).

123. I. G. McQueen, Electonic Eng. 24 436 (1952).

124. I. A. D. Lewis and F. H. Wells, " Millimicrosecond Pulse Techniques." p 208 McGraw Hill, 1954.

125. C. H. Hertz and E. Moller, Rev. Sci. Instr. 29 611 (1958).

126. R. Sugarman, ibid.. 28 933 (1957).

127. W. Lochte-Holtgrees, and C.E. Bawn, Trans. Farad. Soc. 28 698 (1932)

128. J. A. R. Samson and H. Liebl, Rev. Sci. Instr. 33 1340 (1962).

129. R. L. Kelly, " A Table of Emission Lines in the Vacuum Ultraviolet." UCRL 5612 Univ. Calif. Lawrence Rad. Lab. 1960.

130. C. E. Moore, " Atomic Energy Levels " Nat. Bur. Stand. Circular 467 Vols I II And III 1949.

131. R .W. Ditchburn, Proc. Roy. Soc. A229 44 (1955).

132. W. C. Walker, J. A. R. Samson and S. Rustgi, J. Opt. Am. Soc. 48 71 (1958)

133. W. C. Price and T. M. Sugden, Trans. Farad. Soc. 44 108 (1948)

134. D. C. Frost and C. A. McDowell, Can. J. Chem. 36 39 (1958).

135. W. C. Price, J. Chem. Phys. 4 147 (1959).

136. M. Cottin, J. Chem. Phys. 56 1024 (1959).

137. M. I. Al-Joboury, and D. W. Turner, J. Chem. Soc. B373 (1967).

138. F. O. Ellison and H. Shull, J. Chem. Phys. 23 2348 (1955).

139. R. Botter and H. M. Rosenstock, International Conf. Mass Spectroscopy, Berlin. 1967.

140. V. H. Dibeler, J. A. Walker and H. M. Rosenstock, J. Res. Nat. Bur. Stand. 70A 459 (1966).

141. S. Bell, J. Mol. Spec. 16 205 (1965).

142. W. C. Johns, Can. J. Phys. 41 209 (1963).

143. M. Krauss, J. Res. Nat. Bur. Stand. 68A 635 (1964).

144. R. Botter and H. M. Rosenstock, Private communication - to be published.

145. K.Dressler and D. A. Ramsey, Phil. Trans. Roy. Soc. 241A 553 (1959).

146. R. N. Dixon, Mol. Phys. 9 359 (1965).

147. F. Fiquet-Fayard and P. Guyon, Mol. Phys. 11 17 (1966).

148. J.Momigny, C. Goffart, and L. D'Or, Int. J. Mass Spec. and Ion Phys. 1 53 (1968).

149. H. J. Henning, Ann. Phys. 13 599 (1932).

150. D. W. Turner and D. P. May, unpublished work.

151. K. Higasi, I. Omura, and H. Baba, Nature 178 652 (1956).

152. T. M. Sugden and W. C. Price, Trans. Farad. Soc. 44 116 (1948).

153. P. J. Goodfriend, F. W. Biss, and A. B. Duncan, Rev. Mod. Phys. 32 307 (1960).

154. J. M. Foster and F. M. Boys, Rev. Mod. Phys. 32 303 (1960).

155. D. Peters, Trans. Farad. Soc. 59 1121 (1963).

156. D. G. Carrol and L. G. Vanquickenborn, and S. P. McGlynn, J. Chem. Phys. 44 2779 (1966).

157. M. D. Newton and E. W. Palke, J. Chem Phys. 45 2329 (1966).

158. C. R. Brundle and D. W. Turner, Chem. Commun. (London), 314 (1967).

159. R. L. Reed, Trans. Farad. Soc. 52 1195 (1956).

160. idem ibid 54 478 (1958).

161. H. Pritchard and A. G. Harrison, J. Chem. Phys. 48 2827 (1968).

162. H. M. Rosenstock, private communication - "Theory of Mass Spectra-A General Review."

163. C. A. McDowell and J.W. Warren, Discus. Farad. Soc. 10 55 (1951).

164. J. G. Calvert and E. W. R. Steacie, J. Chem. Phys. 19 176 (1951).

165. R. Klein and L. J. Schoen, J. Chem. Phys. 24 1094 (1956), 29 953 (1958)

166. J. C. Lorquet, Mol. Phys. 10 489 (1965-66).

167. M. I. Al-Joboury, D. P. May, and D. W. Turner, J. Chem. Soc. 6350 (1965)

168. D. W. Turner and D. P. May, J. Chem. Phys. 46 1156 (1967).

169. D. Villarejo, R Stockbauer, and M. G. Inghram, J. Chem. Phys. 48 3342 (1968

170. Y. Tanaka, A. S. Jursa, andF. J. Leblanc, J. Chem. Phys. 32 1199 (1960).

171. M. Haugh, T. G. Slanger, and K. D. Bates ibid 44 838 (1966).

172. F. M. Matsunga and K. Watanabe, ibid 46 4457 (1967).

173. S. Leach, J. Chim. Phys. 61 1493 (1964).

174. V. A. Koryoshkin, Dokl. Akad. Nauk. S. S. S. R. 167 1035 (1966).

175. W. C. Johns, Can. J. Phys. 42 1004 (1964).

176. R. S. Mulliken, J. Chem. Phys. 3 720 (1935).

177. E. Clementi, ibid 36 750 (1962).

178. R. S. Mulliken, Rev. Mod. Phys. 14 204 (1942).

179. G. Herzberg and G. Teller, Z. Physik. Chem. B.21 410 (1933).

180. G. R. Cook, P. H. Metzger, and M. Ogawa, J. Opt. Soc. Am. 58 129 (1968).

181. idem J. Chem. Phys. 44 2935 (1966).

182. J. H. D. Eland and C. J. Danby, J. Mass Spect. and Ion Phys. 1 111 (1968).

183. J. E. Collin and P. Natalis, J. Mass. Spect. and Ion Phys. 1 121 (1968).

184. G. M. Begun and L. Landau, J. Chem. Phys. 35 547 (1961).

185. A. S. Newton and A. F. Sciamanna, ibid 44 4327 (1966).

186. D. P. May, Ph.D. Thesis, University of London 1966

187. H. Basch, M. B. Robin, and N. A. Kuebler, J. Chem. Phys. In the Press.

188. idem ibid 47 1201 (1967)

189. A. L. Wahrhaftig, "Advances in Mass Spectrometry" Ed. J. D. Waldron p 274.

190. J. C. Evans, J. Chem. Phys. 22 1228 (1954).

191. I. Suzaki, Bull. Chem. Soc. Japan, 33 1359 (1960).

192. P. G. Puranic, Proc. India Acad. Sci. A56 115 (1960).

193. C. C. Costain and J. M. Dowling, J. Chem. Phys. 32 158 (1960).

194 M. B. Robin - Private communication.